R-08-18

Neutron data experiments for transmutation

Annual Report 2006/2007

J Blomgren, P Andersson, R Bevilacqua, L Nilsson,
S Pomp, V Simutkin, A Öhrn, M Österlund
Department of Neutron Research, Uppsala University

October 2007

ISSN 1402-3091
SKB Rapport R-08-18

Neutron data experiments for transmutation

Annual Report 2006/2007

J Blomgren, P Andersson, R Bevilacqua, L Nilsson,
S Pomp, V Simutkin, A Öhrn, M Österlund
Department of Neutron Research, Uppsala University

October 2007

This report concerns a study which was conducted for SKB. The conclusions and viewpoints presented in the report are those of the authors and do not necessarily coincide with those of the client.

A pdf version of this document can be downloaded from www.skb.se.

Summary

The project NEXT, Neutron data Experiments for Transmutation, is performed within the nuclear reactions group of the Department of Neutron Research, Uppsala University. The activities of the group are directed towards experimental studies of nuclear reaction probabilities of importance for various applications, like transmutation of nuclear waste, biomedical effects and electronics reliability. The experimental work is primarily undertaken at the The Svedberg Laboratory (TSL) in Uppsala, where the group is operating two world-unique instruments, MEDLEY and SCANDAL.

Highlights from the past year:

- The TSL neutron beam facility and the MEDLEY detector system have been upgraded.
- Funding for a major upgrade of the SCANDAL facility has been approved, and practical work has been initiated.
- Three new PhD students have been accepted.
- The Uppsala group contributed the largest number of accepted publications (12) at the International Conference on Nuclear Data for Science and Technology, Nice, France, April 22–27, 2007.
- The EU project CANDIDE (Coordination Action on Nuclear Data for Industrial Development in Europe), coordinated by Jan Blomgren, started January 1, 2007.
- The EU project EFNUDAT (European Facilities for Nuclear Data research), partly coordinated by Jan Blomgren, started November 1, 2006.
- Nuclear power education has reached all-time high at Uppsala University. A contract with KSU (Nuclear Training and Safety Centre) on financing the increased volume of teaching for industry needs has been signed.

Sammanfattning

Projektet NEXT, NeutrondataEXperiment för Transmutation, bedrivs inom kärnreaktionsgruppen vid institutionen för neutronforskning, Uppsala universitet. Gruppens verksamhet är inriktad mot experimentella studier av kärnfysikaliska reaktionssannolikheter för olika tillämpningsområden, som transmutation av kärnavfall, biomedicinska effekter och tillförlitlighet hos elektronik. Den experimentella verksamheten bedrivs huvudsakligen vid The Svedberglaboratoriet (TSL) i Uppsala, där gruppen driver två världsunika instrument, MEDLEY och SCANDAL.

Höjdpunkter från det gångna verksamhetsåret:

- TSLs neutronstråleanläggning och experimentuppställningen MEDLEY har uppgraderats.
- Finansiering för en omfattande uppgradering av experimentuppställningen SCANDAL har beviljats, och praktiskt arbete har inletts.
- Tre nya doktorander har antagits.
- Uppsala bidrog med flest publikationer (12) vid den internationella kärndatakonferensen i Nice, Frankrike, 22–27 april 2007.
- EU-projektet CANDIDE (Coordination Action on Nuclear Data for Industrial Development in Europe), koordinerat av Jan Blomgren, startade 1 january 2007.
- EU-projektet EFNUDAT (European Facilities for Nuclear Data research), delvis koordinerat av Jan Blomgren, startade 1 november 2006.
- Kärnkraftutbildning har nått sin största volym någonsin vid Uppsala universitet. Ett kontrakt med KSU (Kärnkraftsäkerhet och Utbildning AB) om finansiering av den ökade volymen har undertecknats.

Contents

1	**Background**	7
1.1	The NEXT project	7
2	**Introduction**	9
2.1	Why accelerator-driven transmutation?	9
2.2	Nuclear data for transmutation	10
2.3	Previous Uppsala activities in the field	11
2.4	International outlook	12
2.5	Scientific scope of NEXT	12
2.6	Outlook	13
3	**Experimental setup and techniques**	15
3.1	The TSL neutron beam facility	15
3.2	The MEDLEY setup	15
3.3	The SCANDAL setup	15
4	**Recent results**	19
4.1	Elastic scattering	19
4.2	(n,xlcp) reactions	19
4.3	(n,xn') reactions	20
4.4	Fission	20
5	**International activities**	21
5.1	Collaborations	21
5.2	Meetings and conferences	21
6	**Administrative matters**	23
6.1	Staff and students	23
6.2	Reference group	23
References		25

Appendices on CD

I M Sarsour, T Peterson, M Planinic, S E Vigdor, C Allgower, B Bergenwall, J Blomgren, T Hossbach, W W Jacobs, C Johansson, J Klug, A V Klyachko, P Nadel-Turonski, L Nilsson, N Olsson, S Pomp, J Rapaport, T Rinckel, E J Stephenson, U Tippawan, S W Wissink, Y Zhou. Measurement of the Absolute Differential Cross Section for *np* Elastic Scattering at 194 MeV, Phys. Rev. C. 74 (2006) 044003.

II P Mermod, J Blomgren, C Johansson, A Öhrn, M Österlund, S Pomp, B Bergenwall, J Klug, L Nilsson, N Olsson, U Tippawan, P Nadel-Turonski, O Jonsson, A V Prokofiev, P-U Renberg, Y Maeda, H Sakai, A Tamii, K Amos, R Crespo, A. Moro. 95 MeV neutron scattering on hydrogen, deuterium, carbon and oxygen, Phys. Rev. C. 74 (2006) 054002.

III J Blomgren. Education for the nuclear power industry – Swedish perspective (in Russian), Atomic Strategy 2 (2007) 28 (invited).

IV J Blomgren, F Moons, P De Regge, J Safieh. European Nuclear Education Network (in Russian), Atomic Strategy 2 (2007) 26 (invited).

V Y Maeda, T Kawabata, K Suda, H Sakai, K Fujita, K Hatanaka, H Okamura, Y Sakemi, Y Shimizu, Y Tameshige, A Tamii, M B Greenfield, M Hatano, H Kuboki, T Saito, M Sasano, K Yako, J Kamiya, J Rapaport, K Sekiguchi, T Wakasa, J Blomgren, P Mermod, A Öhrn, M Österlund, H Witala, J Golak, R Skibinski, A Deltuva, A C Fonseca, P U Sauer, W Glöckle, H Kamada, A Nogga. Differential cross section and analyzing power measurements for *nd* elastic scattering at 248 MeV, Phys. Rev. C. 76 (2007) 014004.

VI Yu Murin, Yu Babain, M Chubarov, Yu Tuboltsev, V Pljuschev, M Zubkov, P Nomokonov, A Voronin, M Merkin, V Kondratiev, N Olsson, J Blomgren, L Westerberg, C Ekström, A Kolozhvari, H Persson, B Jakobsson, P Goloubev, Ch Bargholtz, L Gerén, P-E Tegnér, I Zartova, A Budzanowski, B Czech, I Skwirczynska. A Setup for Inverse Kinematics Study of Single Event Effects Relevant Nuclear Reactions at Nuclear Storage Ring CELSIUS, Nucl. Instr. Meth. A578 (2007) 385.

VII J Blomgren. Biomedical aspects of high-energy neutrons, NEMEA-3, Neutron Measurements, Evaluations and Applications, Proceedings of the enlargement workshop, Borovets, Bulgaria, October 25–28, 2006 (invited). EUR Report 22794 EN, Luxembourg: Office for Official Publications of the European Communities, ISBN 978-92-79-06158-5, European Communities, 2007, p. 7.

VIII J Blomgren, H Schuhmacher. Tenth International Symposium on Neutron Dosimetry, accepted for publication in Japanese Journal of Health Physics (invited).

IX A Öhrn, J Blomgren, P Andersson, A Atac ,C Johansson, J Klug, P Mermod, S Pomp, P Wolniewicz, M Österlund, L Nilsson, B Bergenwall, K Elmgren, N Olsson, U Tippawan, S. Dangtip, P Phansuke, P Nadel-Turonski, O Jonsson, A V Prokofiev, P-U Renberg, V Blideanu, C Le Brun, J F Lecolley, F R Lecolley, M Louvel, N Marie-Noury, C Schweitzer, Ph Eudes, F Haddad, C Lebrun, E Bauge, J P Delaroche, M Girod, X Ledoux, K Amos, S Karataglidis, R Crespo, W Haider. Elastic neutron scattering of 96 MeV neutrons from iron, yttrium and lead, accepted for publication in Phys. Rev. C.

X J Blomgren. Three-body forces in nuclei, XVII International School on Nuclear Physics, Neutron Physics and Applications, Varna, Bulgaria, September 24–30, 2007 (invited).

XI P Mermod, J Blomgren, C Johansson, J Klug, L Nilsson, N Olsson, S Pomp, U Tippawan, A Öhrn, M Österlund, B Bergenwall, P Nadel-Turonski, O Jonsson, A V Prokofiev, P-U Renberg, Y Maeda, H Sakai, A Tamii. Three-body force effects in neutron-deuteron scattering at 95 MeV, 11th International Conference on Meson-Nucleon Physics and the Structure of the Nucleon (MENU 2007), September 10–14, 2007, Forschungzentrum Juelich, Germany (invited).

XII J Blomgren, E Bauge, D Cano Ott, S Czifrus, K Dahlbacka, I Goncalves, E Gonzalez, H Henriksson, R Jacqmin, A Koning, D. Lecarpentier, E Malambu, A Mengoni, R Mills, A Plompen, G Rimpault, V Stary, C Trakas, P Vaz, C Zimmerman. CANDIDE – Coordination Action on Nuclear Data for Industrial Development in Europe, 4th Workshop on Neutron Measurements, Evaluations and Applications – Nuclear data needs for Generation IV and accelerator driven systems, Prague, Czech Republic, October 16–18, 2007 (accepted).

XIII J Blomgren, K Chtioui. A proposal for an integral neutron data experiment in the 100–200 MeV region, 4th Workshop on Neutron Measurements, Evaluations and Applications – Nuclear data needs for Generation IV and accelerator driven systems, Prague, Czech Republic, October 16–18, 2007 (accepted).

XIV J Herczeg (chair). Summary record of the 18th meeting of the executive group of the nuclear science committee, Paris, May 13–15, 2007.

XV J Blomgren, S Pomp, J-C Bourselier, M Österlund, A Prokofiev, A Koning. Mono-energy neutron testing of single event effects.

1 Background

1.1 The NEXT project

The present project, Neutron data Experiments for Transmutation (NEXT), supported as a research task agreement by Statens Kärnkraftinspektion (SKI), Svensk Kärnbränslehantering AB (SKB) and Ringhalsverket AB, started 2006-07-01. The primary objective from the supporting organizations is to promote research and research education of relevance for development of the national competence within nuclear energy.

The aim of the project is in short to:

- promote development of the competence within nuclear physics and nuclear technology by supporting licenciate and PhD students,
- advance the international research front regarding fundamental nuclear data within the presently highlighted research area accelerator-driven transmutation,
- strengthen the Swedish influence within the mentioned research area by expanding the international contact network,
- provide a platform for Swedish participation in relevant EU projects,
- monitor the international development for the supporting organizations,
- constitute a basis for Swedish participation in the nuclear data activities at IAEA and OECD/NEA.

The project is operated by the Department of Neutron Research (INF) at Uppsala University, and is utilizing the unique neutron beam facility at the The Svedberg Laboratory (TSL) at Uppsala University.

In this document, we give a status report after the first year (2006-07-01–2007-06-30) of the project.

2 Introduction

2.1 Why accelerator-driven transmutation?

During the operation of a commercial nuclear power reactor, energy is released due to fission of uranium and heavier elements, with U-235 being the most important nuclide. Fission results in the creation of a large number of elements roughly half the mass and atomic number of uranium. Essentially all these new elements are radioactive, most of them with short half-lives. Immediately after irradiation in a reactor, spent nuclear fuel would be lethally harmful to be close to, and therefore the handling of spent nuclear fuel is carried out with great precaution.

The radioactivity gets reduced over time. Of the elements created in large quantities, Sr-90 and Cs-137 have the longest half-lives, in both cases around 30 years. This means that the radioactivity is reduced by a factor 1,000 in about 300 years, after which the remaining radioactivity due to fission products is so small that it does no longer pose a significant risk.

In parallel with the fission processes in a reactor, heavier elements than uranium (i.e. trans-uranium elements) are being created via neutron capture reactions followed by beta decay. At outtake of spent nuclear fuel, most of the initial U-235 has been spent. Instead, the spent fuel contains a few percent of trans-uranium (TRU) elements, with plutonium being by far the most abundant.

Many of these TRUs are long-lived alpha emitters. This means that they pose essentially no risk as long as they are outside the body, but can be highly radiotoxic after intake. This means that two strategies have evolved concerning the handling of spent nuclear fuel:

- Wait for natural decay, and reduce the possibility for intake during the decay time.
- Convert the material via nuclear reactions to short-lived elements.

The first strategy leads to geological disposal. A number of countries are preparing for geological disposal, Sweden being one of the countries with the most advanced plans. The second strategy, often called transmutation, has some attractive features in principle, but suffers from a far less mature technology. This is manifested by the fact that no country is presently relying on transmutation as a main strategy.

It is, however, known already that in principle it is possible to incinerate these long-lived TRU elements via neutron-induced fission. A fraction of these elements can be treated with thermal neutrons, which makes transmutation in present-day reactors possible. It is, however, clear that fission induced by fast neutrons is a pre-requisite for a significant reduction of the long-term radiotoxicity. This points towards reactors of a type that presently exist only as research facilities. Thus, the challenge today is not to prove the underlying physics for transmutation, but to convert a research technology into industrial-scale operation.

Fast reactors can be of two types: critical and sub-critical. Critical reactors operate on self-sustaining nuclear chain reactions. In fission, 2–4 neutrons are released, which in turn can induce new fission reactions. Hence, a critical reactor needs no external input of neutrons. All TRUs are, however, not suitable as fuels in critical reactors. This is because of the role of delayed neutrons.

After fission, most of the neutrons are released immediately. In commercial reactors, the average time from one fission reaction until a released neutron induces a new fission reaction is of the order of less than 0.1 ms. This means that if only slightly more than one neutron per fission induces another fission reaction, the neutron flux will increase very rapidly, with the power increasing correspondingly rapidly. If this were the whole story, critical reactors could not operate. Nature, however, provides a solution to this dilemma: delayed neutrons.

A small fraction of the neutrons, typically around 0.5%, are not released directly after fission, but after beta decay of fission products. This means that they are emitted in up to about a minute after fission, with 15 seconds as average time in present commercial reactors. Although being a small fraction, they extend the average time between fissions significantly, making the time required for a change of the power in the reaction moving from the millisecond scale to seconds, given that the reactor is operated close to exact criticality.

It turns out, however, that for most of the TRU elements the fraction of delayed neutrons is smaller than for U-235, making incineration in critical reactors more difficult. In the case of americium, the fraction is very small, making a critical reactor loaded with a large fraction of americium practically impossible to control. Here sub-critical systems have a cutting edge. If the reactor is under-critical, delayed neutrons are not required for stability. The price to pay is that neutrons have to be externally produced and fed into the core to keep the system running.

The presently leading technology for driving an undercritical reactor is proton-induced spallation of heavy elements. If a 1 GeV proton beam hits a lead target, about 20 neutrons per incident proton are released. If this is placed at the centre of a reactor, the emitted neutrons can induce chain reactions in the surrounding core, and the power released is proportional to the proton beam power.

There is consensus that successful implementation of transmutation requires partitioning of the spent nuclear fuel before installation into a sub-critical reactor. The fission products produced in the critical reactor need to be separated, and only the actinides should be transmuted. Therefore, this entire research field is commonly referred to as partitioning and transmutation (P&T).

It should be stressed that even optimally successful operation of P&T does not alleviate the need for geological storage. Still the fission products need to be stored, and it is likely that some losses in the handling of actinides are unavoidable, leading to some storage needs also of actinides. P&T could possible change the requirements on the geological storage, but not remove the need completely.

2.2 Nuclear data for transmutation

Nuclear data research has been carried out for a long time resulting in nuclear data libraries utilized in development and optimization of thermal reactors. In an accelerator-driven system (ADS) there are some notable differences compared to critical reactors /Blomgren 2002, 2004/:

- Proton-induced neutron production.
- Neutrons at much higher energies than in critical reactors.

To meet the corresponding nuclear data demands, the EU-sponsored project HINDAS (High and Intermediate energy Nuclear Data for Accelerator-driven Systems) was carried out during 2000-03. HINDAS was a joint European effort, which gathered essentially all European competence on nuclear data for transmutation in the 20–2,000 MeV range /Koning et al. 2002/. The program was designed to obtain a maximal improvement in high-energy nuclear data knowledge for transmutation. It was conceived that this goal could only be achieved with a well-balanced combination of basic cross section measurements, nuclear model simulations and data evaluations. The work was focused on three elements, iron, lead and uranium, selected to give a representative coverage of typical materials for construction, target and core, respectively, especially relevant to ADS, as well as a wide coverage of the periodic table of elements.

In total, 16 universities or laboratories participated, whereof 6 had experimental facilities. This means that HINDAS involved essentially all relevant European laboratories in its energy range. This distribution and coordination of experiments at many laboratories made the work very efficient. What is noteworthy is that HINDAS involved many partners and even laboratories that had previously not been involved at all in activities on nuclear data for applications. Thus, HINDAS has contributed to a widening of the field of applied nuclear physics.

The work was divided into two main energy domains, 20–200 MeV and 200–2,000 MeV. This division into two energy ranges is natural, since there appears to be a transition region around 200 MeV for the theoretical models. Below this energy the theoretical calculations have to include direct interactions, as well as pre-equilibrium, fission and statistical models, whereas at higher energies the intra-nuclear cascade model, together with fission and evaporation models, has to be considered. As a coincidence, the experimental facilities and the measurement techniques are also different below and above about 200 MeV. Within each energy domain, the experimental work was structured according to type of particles produced. This means that for each energy range, there were work packages on production of light ions, neutrons and residues, respectively.

Notably, fission was not explicitly included in HINDAS, simply because a large majority of all fission studies were undertaken within ISTC (International Science and Technology center), i.e. in collaborative efforts between former weapons scientists of the former Soviet Union and civil European researchers.

The HINDAS project resulted in a wealth of new knowledge, and has been considered a raw model for international collaboration in the realm of nuclear data.

2.3 Previous Uppsala activities in the field

Uppsala took a very active part in HINDAS, was coordinating one work package and provided the most frequently used experimental facility, TSL. Connected to HINDAS, the Uppsala group ran two projects preceding NEXT, KAT (1998–2002) and NATT (2002–2006) with similar structure and scope as NEXT.

Quickly summarizing the achievements during the last ten years, it can be concluded that the Uppsala group has advanced the research frontier significantly on neutron-induced nuclear reactions of ADS relevance. Analysis and documentation has been finalized of previously performed measurements of elastic neutron scattering on five nuclei ranging from carbon to lead at 96 MeV /Klug et al. 2003, Appendix II, Appendix IX/. The precision in the results surpasses all previous data by at least an order of magnitude. These measurements represent the highest energy in neutron scattering where the ground state has been resolved. The results show that all previous theory work has underestimated the probability for neutron scattering at the present energy by 0–30%.

A new method for measurements of absolute probabilities for neutron-induced nuclear reactions with experimental techniques only has been developed /Klug et al. 2003/. Previously, only two such methods have been known.

Compelling evidence of the existence of three-body forces in nuclei has been obtained (appendix II). The first publication on these matters from the group /Mermod et al. 2004/ turned out to qualify on the top-ten downloading list of Physics Letters B, one of the very most prestigious journals in subatomic physics.

Production of light ions from iron, lead and uranium has been studied in collaboration with a number of French research institutes /Blideanu et al. 2004/, and studies of the same reactions on carbon, oxygen and silicon have been undertaken by the local group /Tippawan et al. 2004, 2006/. These data have provided valuable benchmarking of present state-of-the-art theory models.

Fission has been studied in collaboration with a number of Russian research institutes. In these studies, the Uppsala contribution has primarily been limited to providing the beam and auxiliary equipment.

Another important result of the KAT and NATT projects is that five PhD theses with data from TSL have been successfully defended.

2.4 International outlook

During the last decade, the leading research on nuclear data for ADS has been undertaken in Europe including Russia. There is a striking imbalance around the World on nuclear data for ADS. Europe, including Russia, dominates heavily. The other large nuclear energy countries, i.e. USA and Japan, have only limited research in this field, in spite of previously having hosted important activities.

In the fifth EU framework program (FP5), a large fraction of the P&T research was devoted to nuclear data. Two large projects, HINDAS and NTOF were financed by the EC. As outlined above, HINDAS resulted in a wealth of new nuclear data and advanced the frontier significantly. NTOF was primarily focused on the low-energy range and dominated by activities at CERN, Geneva, Switzerland, where a spallation neutron source was developed. The agenda comprised mostly capture and fission cross-section measurements in the eV to keV neutron energy range. The development of the facility was significantly delayed compared with the original time table, and therefore the project was extended. At present, the facility is operational with parameters close to the specifications, and the first results have been presented.

In FP6, a notable shift in focus on European nuclear data research for ADS has taken place. With the successful completion of the HINDAS project, it was concluded that the nuclear data requirements had to a large degree been fulfilled, and therefore the EUROTRANS project was focused on other problem areas. Still, however, a work package on nuclear data was included, but at a lower ambition level than in FP5.

In parallel with the EU activities, ISTC has financed important activities on nuclear data for transmutation. It should be especially pointed out that our present knowledge of fission cross sections above 20 MeV is heavily dominated by ISTC-supported data. From a Swedish perspective, it is noteworthy that a significant fraction of these results has been produced by Russian groups working at TSL.

2.5 Scientific scope of NEXT

In the 20–200 MeV range, the most important remaining data requests from the ADS community are:

- Neutron-induced light-ion production at around 200 MeV. Up to now, high-quality data up to 100 MeV are available.
- Neutron-induced fission in the 20–200 MeV range. Data on total fission cross sections are available. What is requested now are other types of information, like distributions in angle, mass and energy of the fission products. Moreover, most data sets are relative measurements, implying that accurate calibration of the cross section scale for one or a few fission reactions would be very advantageous.
- Neutron elastic scattering at around 200 MeV. Up to now, high-quality data up to 100 MeV are available.
- Neutron inelastic scattering in the 100–200 MeV range. Up to now, high-quality data up to 30 MeV are available, and one single data set at 65 MeV has been published.

The NEXT project was originally designed to address the first two items above, with one PhD student working on each of the two topics. After NEXT was initiated, a large grant for instrument upgrade was provided by VR, allowing the third issue also to be addressed. As a consequence, a third PhD student has been recruited.

In the present FP6 project EUROTRANS (2004-08), UU participates with a joint Swedish-French experiment on neutron inelastic scattering, for which a world-unique experimental equipment has been developed. Thus, the fourth item is also dealt with, outside NEXT. It should

be mentioned that KAT and NATT were originally intended to be focused on elastic scattering, and a measurement techniques was adopted that was not considered suitable for inelastic scattering studies. It has been shown recently, however, that the existing data from the SCANDAL setup can in fact be analyzed to extract also inelastic scattering cross sections.

As outlined above, several ISTC projects have been carried out at TSL in close collaboration with the INF group. This has matured to involve joint experimental work also at other facilities. A joint fission experiment in Louvain-la-Neuve, Belgium was initiated in May 2007, and several experiment campaigns are foreseen, in which the NEXT PhD students participate. In particular, for the fission-oriented student, this offers a valuable opportunity for quality improvement.

2.6 Outlook

As described above, in the realm of ADS, two classes of nuclear data are clearly discernable, above and below 20 MeV. Above 20 MeV, no previous nuclear energy applications have been developed, and consequently the database is meagre. During the last decade, the situation on proton- and neutron-induced production of charged particles has improved considerably, and presently the situation is satisfactory for the demands as long as the aim is to build a demonstrator or prototype system. If a future full-scale ADS plant for large-scale incineration were to be built, the situation would, however, probably need to be revisited due to the higher demands of a production facility.

Concerning neutron-induced nuclear reactions at around 200 MeV, there is still room for considerable improvement. The present upgrades at TSL are dictated to fill these demands. It can be foreseen that a 5–10 year experimental campaign is required to reach a situation resembling the present situation at 100 MeV.

Up to now, all experimental activities have been focused on cross section measurements. The natural next step would be to carry out integral experiments, i.e. an experiment where the quality of the entire data library is assessed. This could for instance be measurements of neutron transmission through large blocks of various materials. Only one such experiment has been performed worldwide /Nakashima et al. 1996/. TSL is well suited for such experiments, and it is conceivable that such integral experiments could be important in FP7.

At lower energies, the nuclear data situation is fundamentally different. The development of critical reactors has motivated large efforts in data production and therefore the present work is dedicated to filling important gaps in the literature. In general, the nuclear data status is satisfactory for uranium and plutonium, whilst there is room for improvement on the minor actinides (neptunium, americium and curium). At present and in the near future, the activities on americium dominate. This is due to two factors. First, americium is the nucleus that has the largest deficiencies in the nuclear data bases and second, it is probably the element where incineration in ADS is best motivated.

Nuclear data activities at lower energies could be expected to grow in a near future, because of the interest in Gen-IV reactor systems. The nuclear data required for development of Gen-IV are more or less identical with those needed for ADS.

If realization of a full-scale ADS or Gen-IV system would be carried out, another nuclear data activity might be motivated. The nuclear data on the most important elements, i.e. uranium and plutonium, were often produced thirty years ago or more. It is not unlikely that some of the key nuclear data in the adopted databases suffer from systematic errors. This might motivate some of these data to be revisited, taking advantage of the development of novel experimental techniques in the recent years.

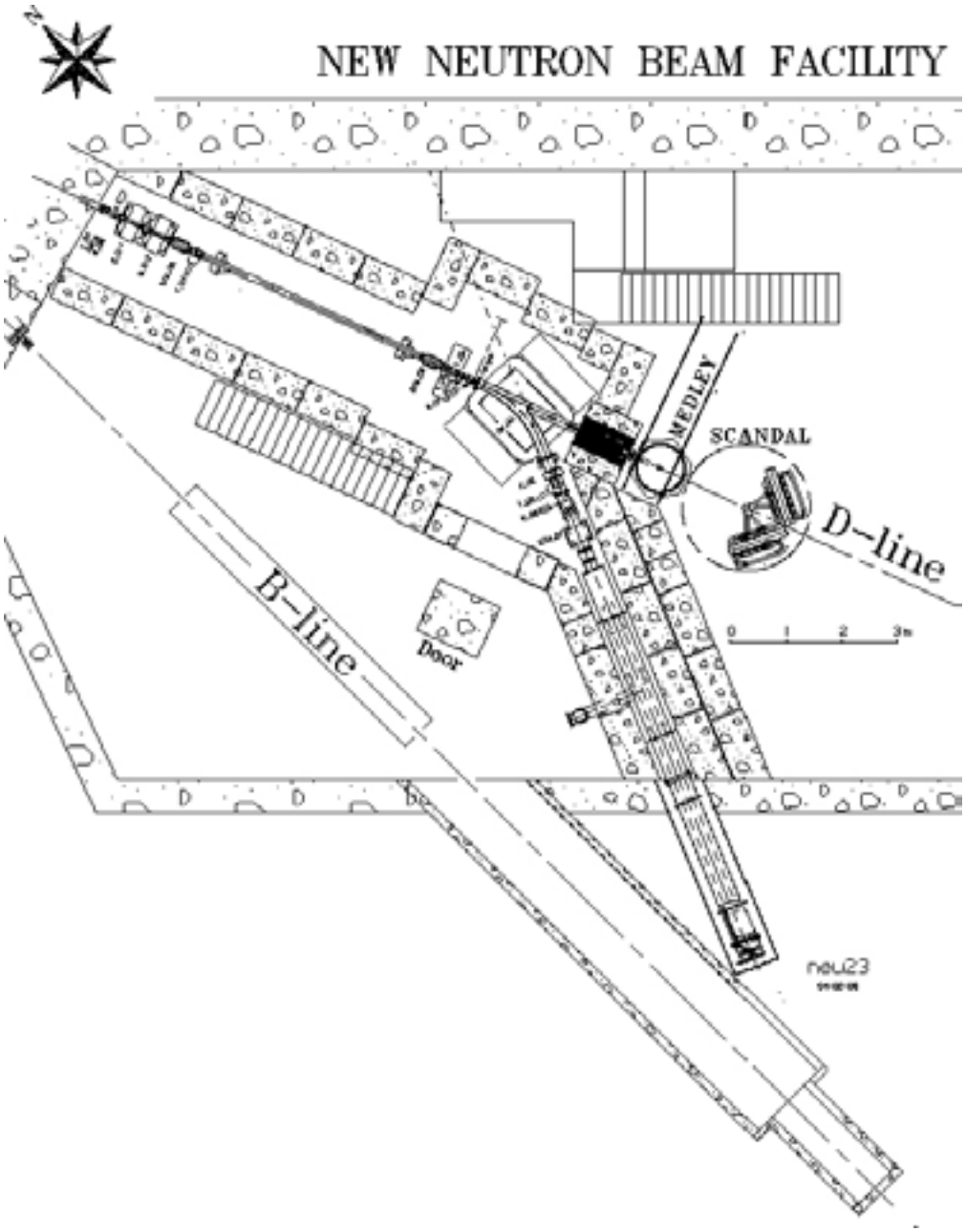

Figure 2-1. *The TSL neutron beam facility.*

3 Experimental setup and techniques

3.1 The TSL neutron beam facility

At TSL, quasi-monoenergetic neutrons are produced by the reaction ^{7}Li(p,n)^{7}Be in a ^{7}Li target bombarded by 50–180 MeV protons from the cyclotron, as is illustrated in Figure 2-1. After the target, the proton beam is bent by a dipole magnet into a concrete tunnel, where it is stopped in a well-shielded Faraday cup, used to measure the proton beam current. A narrow neutron beam is formed in the forward direction by a collimator with a total thickness of about one metre.

The energy spectrum of the neutron beam consists of a high-energy peak, having approximately the same energy as the incident proton beam, and a low-energy tail. About half of all neutrons appear in the high-energy peak, while the rest are roughly equally distributed in energy, from the maximum energy and down to zero. The low-energy tail of the neutron beam can be reduced using time-of-flight (TOF) techniques over the distance between the neutron source and the reaction target.

The relative neutron beam intensity is monitored by integrating the charge of the primary proton beam, as well as by using thin film breakdown counters, placed in the neutron beam, measuring the number of neutron-induced fissions in ^{238}U.

Two multi-purpose experimental setups are semi-permanently installed at the neutron beam line, namely MEDLEY and SCANDAL. These were described in detail in the annual report 1999/2000 of the previous KAT project, and only a brief presentation is given here.

3.2 The MEDLEY setup

The MEDLEY detector array /Dangtip et al. 2000/, shown in Figure 3-1, has been designed for measurements of neutron-induced light-ion production cross sections of relevance for applications within ADS and fast-neutron cancer therapy and related dosimetry. It consists of eight particle telescopes, installed at emission angles of 20–160 degrees with 20 degrees separation, in a 1 m diameter scattering chamber, positioned directly after the last neutron collimator. All the telescopes are fixed on a turnable plate at the bottom of the chamber, which can be rotated without breaking the vacuum.

Each telescope is a ΔE–ΔE–E detector combination, where the ΔE detectors are silicon surface barrier detectors and the E detector is an inorganic CsI(Tl) crystal. Detectors of various thicknesses are being used, with different combinations depending on the application. ΔE-ΔE or ΔE-E techniques are used to identify light charged particles (p, d, t, 3He, α). The chosen design gives a sufficient dynamic range to distinguish all charged particles from a few MeV up to 175 MeV, being the maximum energy of the facility.

3.3 The SCANDAL setup

The SCANDAL setup /Klug et al. 2002/ is primarily intended for studies of elastic neutron scattering, i.e. (n,n) reactions. Neutron detection is accomplished via conversion to protons by the H(n,p) reaction. In addition, (n,xp) reactions in nuclei can be studied by direct detection of protons. This feature is also used for calibration, and the setup has therefore been designed for a quick and simple change from one mode to the other.

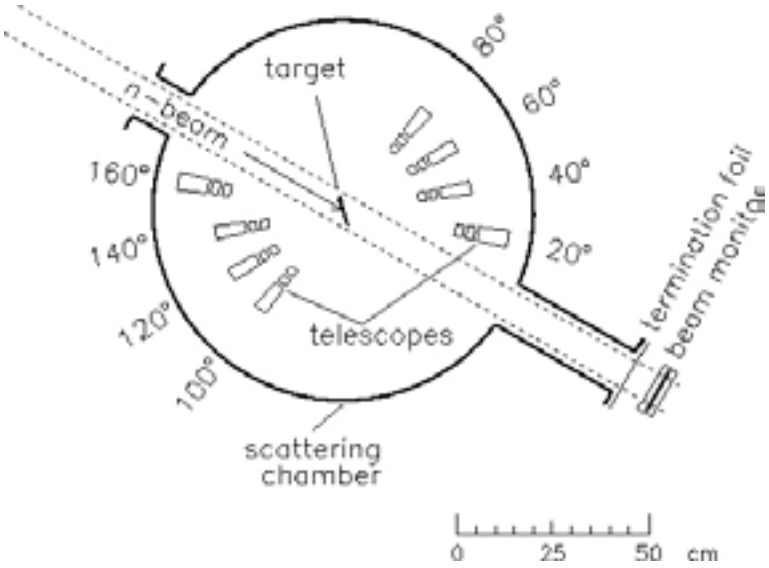

Figure 3-1. *The MEDLEY setup.*

The device is illustrated in Figure 3-2. It consists of two identical systems, in most cases located on each side of the neutron beam. The design allows the neutron beam to pass through the drift chambers of the right-side setup, making low-background measurements close to zero degrees feasible.

In neutron detection mode, each arm consists of a 2 mm thick veto scintillator for fast charged-particle rejection, a neutron-to-proton converter which is a 10 mm thick plastic scintillator, a 2 mm thick plastic scintillator for triggering, two drift chambers for proton tracking, a 2 mm thick ΔE plastic scintillator, which is also part of the trigger, and an array of 12 large CsI detectors for energy determination. The trigger is provided by a coincidence of the two trigger scintillators, vetoed by the front scintillator. The compact geometry allows a large solid angle for protons emitted from the converter. Recoil protons are selected using the ΔE and E information from the plastic scintillators and the CsI detectors, respectively. The energy resolution is about 3.7 MeV (FWHM), which is sufficient to resolve elastic and inelastic scattering in several nuclei. The angular resolution is calculated to be about 1.4 degrees (rms) when using a cylindrical scattering sample of 5 cm diameter.

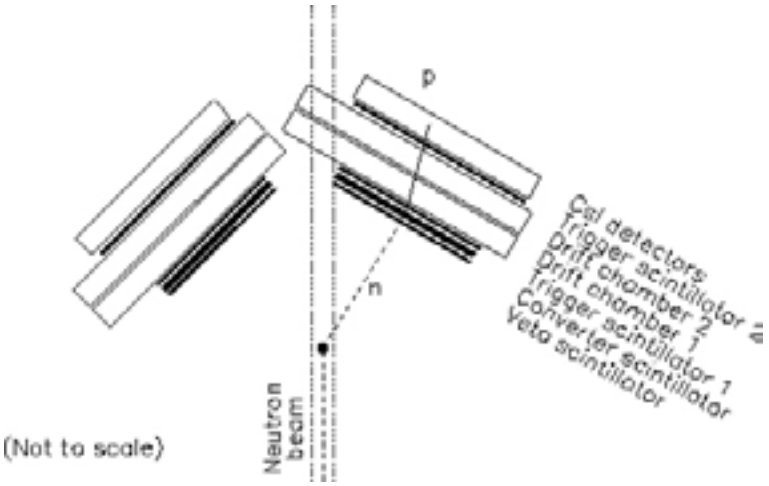

Figure 3-2. *The SCANDAL setup.*

When SCANDAL is used for (n,xp) studies, the veto and converter scintillators are removed. A multitarget arrangement can be used to increase the target content without impairing the energy resolution, which is typically 3.0 MeV (FWHM). This multitarget box allows up to seven targets to be mounted simultaneously, interspaced with multi-wire proportional counters (MWPC). In this way it is possible to determine in which target layer the reaction took place, and corrections for energy loss in the subsequent targets can be applied. In addition, different target materials can be studied simultaneously, thus facilitating absolute cross section normalization by filling a few of the multitarget slots with CH2 targets. The first two slots are normally kept empty, and used to identify charged particles contaminating the neutron beam.

4 Recent results

4.1 Elastic scattering

New experimental data on elastic scattering of 96 MeV neutrons from iron and yttrium (appendix IX) have recently been accepted for publication (see Figure 4-1). The previously published data on lead have been extended, as a new method has been developed to obtain more information from data, namely to increase the number of angular bins at the most forward angles. The results are compared with modern optical model predictions, based on phenomenology and microscopic nuclear theory, and are in general in good agreement with the model predictions.

These nuclei are all of interest from ADS point of view, since they represent construction material (iron), fuel cladding (zirconium, replaced by yttrium) and target/coolant (lead). The choice of yttrium might need a clarification. For physics interpretation, it is advantageous to have a mono-isotopic target. Zirconium has five isotopes, none accounting for more than about 50% of the abundance, while yttrium is naturally mono-isotopic.

4.2 (n,xlcp) reactions

In parallel with the other experiments mentioned above and below, data have been taken with the MEDLEY setup on light-ion production reactions. During the last years, results on oxygen, silicon, iron, lead and uranium have been published. Preliminary carbon data have been presented at an international conference. During the last year, most activities have been on facility upgrade, aiming at a large measurement campaign during late autumn 2007.

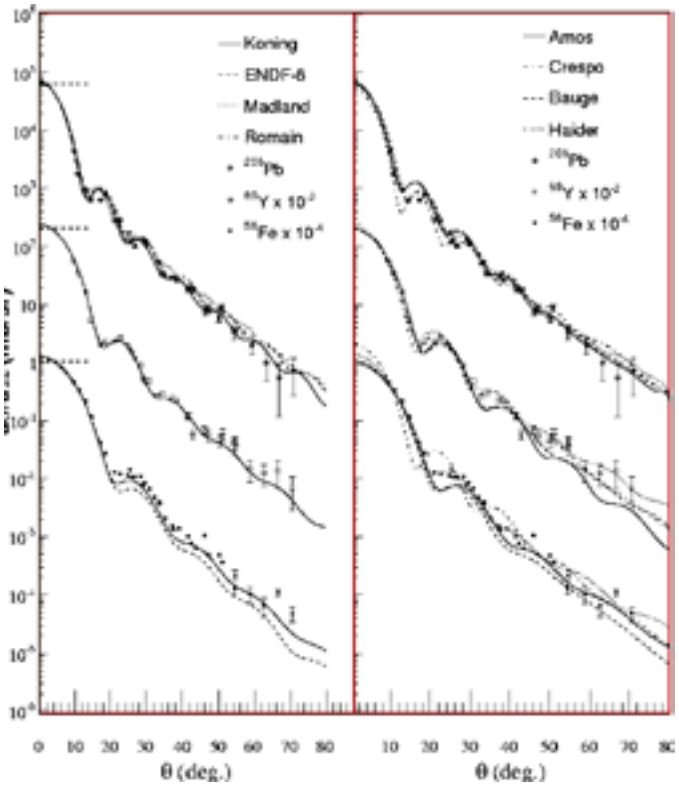

Figure 4-1. *Neutron elastic scattering cross sections on iron, yttrium and lead at 95 MeV. The lines refer to various theory predictions.*

4.3 (n,xn') reactions

We have a collaboration project with a group from Caen, France, on (n,xn') reactions. For these studies, a modified SCANDAL converter (CLODIA) has been designed and built in Caen. A large experiment on lead and iron targets was conducted in August 2004. This experiment is our deliverable in the EU 6th FWP EUROTRANS. Preliminary data were presented at the International Conference on Nuclear Data for Science and Technology (ND2007) April 22–27, Nice, France.

A method to extend the analysis of previously obtained data has been developed, resulting in the spectra shown in Figure 4-2.

4.4 Fission

We are working on the development of a setup for fission studies, based on MEDLEY in a revised geometric configuration. The setup has been tested and found to meet the specifications, and first experiments are in progress. One interesting feature of the new setup is that it allows a precise determination of the absolute cross section by measuring *np* scattering simultaneously. This is important, since only one previous experiment on high-energy fission has been performed with a reasonably good control of the absolute scale. Preliminary results have been presented at international conferences.

In addition, we have a long-term collaboration with a fission experiment group at Khlopin Radium Institute (KRI) in St. Petersburg, Russia. This collaboration continues with additional experiments at TSL as well as in Louvain-la-Neuve, Belgium.

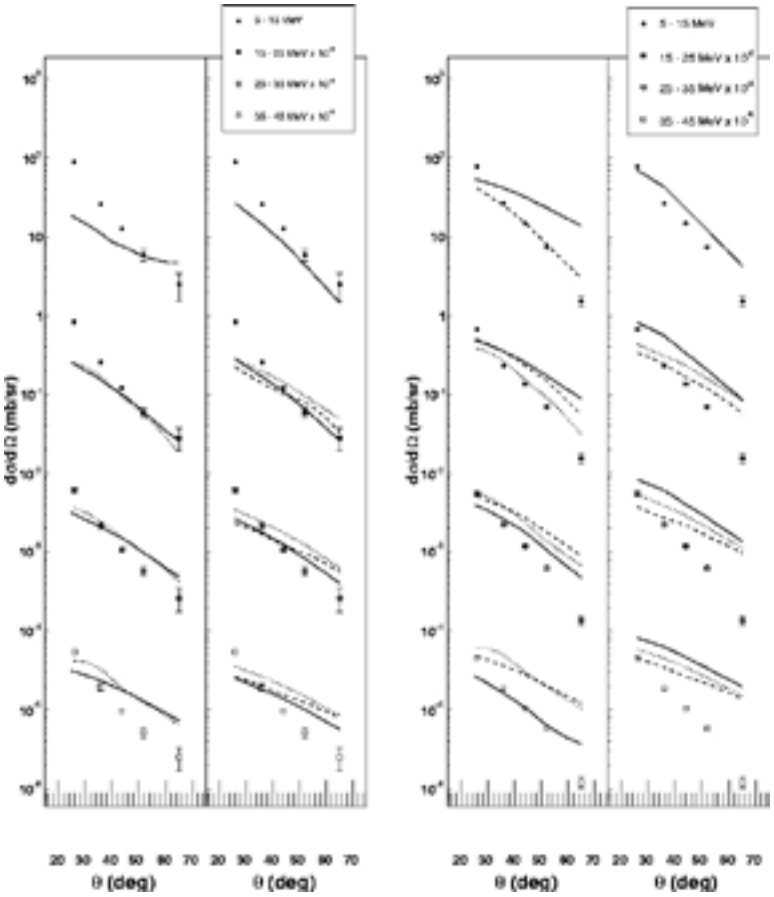

Figure 4-2. *Neutron inelastic scattering cross sections on iron at 95 MeV. The lines refer to various theory predictions.*

5 International activities

5.1 Collaborations

During 2005, the 6th EU framework program EUROTRANS started. Our group and our long-term collaborators from LPC Caen, France, have merged our activities in EUROTRANS, and we have a joint deliverable concerning (n,xn') reactions (see above).

Two new EU projects have started during the present project year. The four-year project EFNUDAT (European Facilities for Nuclear Data Measurements) aims at establishing a joint European infrastructure for nuclear data measurements by networking existing facilities. The role of INF is to provide access to The Svedberg Laboratory to other European users, and to coordinate the networking activities, i.e. organize workshops and training courses, as well as exchange programmes of technical staff. The total EU support is 2.4 M Euro, whereof 311,000 Euro is coordinated by UU/INF. The project involves 10 partners with 9 facilities in 7 countries.

INF is coordinating the two-year EU project CANDIDE (Coordination Action on Nuclear Data for Industrial Development in Europe) (appendix XII). The project aims at enhancing the European collaboration on nuclear data for nuclear waste management. This will be accomplished via networking activities (workshops, training of young professionals in the nuclear power industry) and via an assessment of the status and needs of present and future nuclear data. The project involves 15 partners from 11 countries, spanning from very large business corporations (e.g. Electricité de France and Areva) to research centres and universities. The role of INF is to coordinate the entire project, to lead the development of a school for young professionals in the field, and to contribute experience in high-energy neutron experiments in the assessment. The total EU support to the project is 779,000 Euro.

5.2 Meetings and conferences

During the last year, the entire group participated in the International Conference on Nuclear Data for Science and Technology (ND2007) April 22–27, Nice, France. Uppsala contributed 12 papers, which was the largest number of any organization.

Jan Blomgren is Swedish representative in the OECD/NEA Nuclear Science Committee (NSC) and its Executive Group. Minutes from the annual meeting is found in appendix XIV.

6 Administrative matters

6.1 Staff and students

During the project year, Jan Blomgren has been project leader, active on a 20% basis within the project. His other major activities are teaching and duties as director of studies, both at INF and the Swedish Nuclear Technology Center (SKC). Assistant professor (forskarassistent) Stephan Pomp has worked essentially full time within the project with research and student supervision. Associate professor (universitetslektor) Michael Österlund is involved in part-time research within the group. Leif Nilsson, retired professor, has been employed on about 10% time for student supervision.

Two PhD students are directly connected to and financed by the present project, Vasily Simutkin and Riccardo Bevilacqua. Simutkin's thesis work is primarily on fission and Bevilacqua is working with light-ion production reactions. In addition, Pernilla Andersson has been working with upgrading the SCANDAL setup during the present year, and will begin PhD studies on elastic scattering early 2008.

From the previous NATT project, Angelica Öhrn (born Hildebrand) is in the final stage of her PhD studies. She will defend her thesis on neutron scattering February 29, 2008, with Dr. Bob Haight, Los Alamos National Laboratory, USA, as faculty opponent.

6.2 Reference group

The reference group consists of Fred Karlsson (SKB), Benny Sundström (SKI), and Fredrik Winge (BKAB). The progress of the work has continuously been communicated to the reference group members by short, written, quarterly reports.

References

Blideanu V, Lecolley F R, Lecolley J F, Lefort T, Marie N, Atac A, Ban G, Bergenwall B, Blomgren J, Dangtip S, Elmgren K, Eudes Ph, Foucher Y, Guertin A, Haddad F, Hildebrand A, Johansson C, Jonsson O, Kerveno M, Kirchner T, Klug J, Le Brun Ch, Lebrun C, Louvel M, Nadel-Turonski P, Nilsson L, Olsson N, Pomp S, Prokofiev A V, Renberg P-U, Rivière G, Slypen I, Stuttgé L, Tippawan U, Österlund M, 2004. Nucleon-induced reactions at intermediate energies: New data at 96 MeV and theoretical status, Phys. Rev. C 70, 014607.

Blomgren J, 2002. Experimental activities at high energies, Proceedings from an international symposium on Accelerator Driven Systems for Energy production and Waste Incineration: Physics, Design and Related Nuclear Data, Trieste, 2002, p. 327. (Invited talk)

Blomgren J, 2004. Nuclear data for accelerator-driven systems – Experiments above 20 MeV, Proceedings from EU enlargement workshop on Neutron Measurements and Evaluations for Applications, Bucharest, Romania, October 20–23, 2004 (invited).

Dangtip S, Atac A, Bergenwall B, Blomgren J, Elmgren K, Johansson C, Klug J, Olsson N, Alm Carlsson G, Söderberg J, Jonsson O, Nilsson L, Renberg P-U, Nadel-Turonski P, Le Brun C, Lecolley F-R, Lecolley J-F, Varignon C, Eudes Ph, Haddad F, Kerveno M, Kirchner T, Lebrun C, 2000. A facility for measurements of nuclear cross sections for fast neutron cancer therapy, Nucl. Instr. Meth. A452, 484.

Klug J, Blomgren J, Atac A, Bergenwall B, Dangtip S, Elmgren K, Johansson C, Olsson N, Rahm J, Jonsson O, Nilsson L, Renberg P-U, Nadel-Turonski P, Ringbom A, Oberstedt A, Tovesson F, Le Brun C, Lecolley J-F, Lecolley F-R, Louvel M, Marie N, Schweitzer C, Varignon C, Eudes Ph, Haddad F, Kerveno M, Kirchner T, Lebrun C, Stuttgé L, Slypen I, Prokofiev A, Smirnov A, Michel R, Neumann S, Herpers U, 2002. SCANDAL – A facility for elastic neutron scattering studies in the 50–130 MeV range, Nucl. Instr. Meth. A489, 282.

Klug J, Blomgren J, Atac A, Bergenwall B, Hildebrand A, Johansson C, Mermod P, Nilsson L, Pomp S, Tippawan U, Elmgren K, Olsson N, Jonsson O, Prokofiev A V, Renberg P-U, Nadel-Turonski P, Dangtip S, Phansuke P, Österlund M, Le Brun C, Lecolley J-F, Lecolley F-R, Louvel M, Marie-Noury N, Schweitzer C, Eudes Ph, Haddad F, Lebrun C, Koning A J, Ledoux X, 2003. Elastic neutron scattering at 96 MeV from ^{12}C and ^{208}Pb, Phys. Rev. C. 68 064605.

Koning A, Beijers H, Benlliure J, Bersillon O, Blomgren J, Cugnon J, Duijvestijn M, Eudes Ph, Filges D, Haddad F, Hilaire S, Lebrun C, Lecolley F-R, Leray S, Meulders J-P, Michel R, Neef R-D, Nolte R, Olsson N, Ostendorf E, Ramström E, Schmidt K-H, Schuhmacher H, Slypen I, Synal H-A, Weinreich R, 2002. In Proceedings of Int. Conf. on Nuclear Data for Science and Technology, Tsukuba, Japan (2001); J. Nucl. Sci. Tech., Suppl. 2, 1161.

Mermod P, Blomgren J, Bergenwall B, Hildebrand A, Johansson C, Klug J, Nilsson L, Olsson N, Österlund M, Pomp S, Tippawan U, Jonsson O, Prokofiev A V, Renberg P-U, Nadel-Turonski P, Maeda Y, Sakai H, Tamii A, 2004. Phys. Lett. B 597, 243.

Nakashima H, Nakao N, Tanaka S, Nakamura T, Shin K, Tanaka S, Takada H, Meigo S, Nakane Y, Sakamoto Y, Baba M, 1996. J. Nucl. Sci. Eng. 124, 243.

Tippawan U, Pomp S, Atac A, Bergenwall B, Blomgren J, Dangtip S, Hildebrand A, Johansson C, Klug J, Mermod P, Nilsson L, Österlund M, Olsson N, Elmgren K, Jonsson O, Prokofiev A V, Renberg P-U, Nadel-Turonski P, Corcalciuc V, Watanabe Y, Koning A, 2004. Light-Ion Production in the Interaction of 96 MeV Neutrons with Silicon, Phys. Rev. C 69, 064609.

Tippawan U, Pomp S, Atac A, Bergenwall B, Blomgren J, Dangtip S, Hildebrand A, Johansson C, Klug J, Mermod P, Nilsson L, Österlund M, Olsson N, Elmgren K, Jonsson O, Prokofiev A V, Renberg P-U, Nadel-Turonski P, Corcalciuc V, Koning A, 2006. Light-Ion Production in the Interaction of 96 MeV Neutrons with Oxygen, Phys. Rev. C 73 (2006) 034611.

Measurement of the absolute differential cross section for *np* elastic scattering at 194 MeV

M. Sarsour,[1,*] T. Peterson,[1,†] M. Planinic,[1,‡] S. E. Vigdor,[1] C. Allgower,[1] B. Bergenwall,[2] J. Blomgren,[2] T. Hossbach,[1] W. W. Jacobs,[1] C. Johansson,[2] J. Klug,[2] A. V. Klyachko,[1] P. Nadel-Turonski,[2,§] L. Nilsson,[2] N. Olsson,[2] S. Pomp,[2] J. Rapaport,[3] T. Rinckel,[1] E. J. Stephenson,[1] U. Tippawan,[2,4] S. W. Wissink,[1] and Y. Zhou[1]

[1]*Indiana University Cyclotron Facility, Indiana University, Bloomington, Indiana 47401, USA*

[2]*Uppsala University, Uppsala, Sweden*

[3]*Ohio University, Athens, Ohio 45701, USA*

[4]*Chiang Mai University, Chiang Mai, Thailand*

(Received 15 February 2006; published 25 October 2006)

A tagged medium-energy neutron beam was used in a precise measurement of the absolute differential cross section for *np* backscattering. The results resolve significant discrepancies within the *np* database concerning the angular dependence in this regime. The experiment has determined the absolute normalization with ±1.5% uncertainty, suitable to verify constraints of supposedly comparable precision that arise from the rest of the database in partial wave analyses. The analysis procedures, especially those associated with the evaluation of systematic errors in the experiment, are described in detail so that systematic uncertainties may be included in a reasonable way in subsequent partial wave analysis fits incorporating the present results.

DOI: 10.1103/PhysRevC.74.044003 PACS number(s): 13.75.Cs, 21.30.−x, 25.10.+s

I. INTRODUCTION

Theoretical treatments and applications of the nucleon-nucleon (*NN*) force at low and intermediate energies have progressed considerably in sophistication through the past decade. Partial wave analyses and potential model fits to the *NN* scattering database have incorporated explicit allowance for breaking of isospin (I) symmetry, e.g., by removing constraints that previously required equal $I = 1$ phase shifts for the *pp* and *np* systems, and have been used to constrain the pion-nucleon-nucleon coupling constant [1]. Effective field theory approaches [2] have become competitive with more traditional meson-exchange models of the interaction, in terms of the quality of fit provided to the database and the number of adjustable parameters employed, while holding out the promise of providing internally consistent two- and three-nucleon forces from the same theory. Striking success has been achieved in *ab initio* calculations of the structure of light nuclei [3] by combining phenomenological three-nucleon forces with *NN* interactions taken without modification from fits to the *NN* scattering database. An important aspect in these advances has been the approach toward consensus on which measurements should be included in an *NN* database to which conventional χ^2 optimization techniques can be sensibly applied. The rejection of specific, allegedly flawed, experiments from the database has not been without controversy. In the present article, we report detailed results from a new *np* scattering experiment addressing one of the most prominent of these controversies.

Discrepancies among different experiments have led to a drastic pruning of cross section measurements for intermediate-energy *np* scattering. For example, the partial wave analysis (PWA) of the *np* database carried out with the code SAID [4] rejects more than 40% of all measured cross sections in the range 100–300 MeV in neutron laboratory kinetic energy. The rejected fraction is even larger in the Nijmegen PWA [5,6], especially so for scattering at center-of-mass angles beyond 90°. The rejected data include nearly all of the most recent experiments carried out by groups at Uppsala [7] and Freiburg [8,9]. The problems are illustrated in Fig. 1 by the comparison of data from these two groups with earlier Los Alamos measurements [10] that dominate the medium-energy back-angle cross section data retained in the database. Clear differences among these data sets are seen in the shape of the angular distribution. Other differences, reflecting the general experimental difficulty in determining the absolute scale for neutron-induced cross sections, are masked in the figure by renormalization factors that were applied in the partial wave analyses. Removal of the Uppsala and Freiburg data, which exhibit fairly similar angular dependences, begs the question of whether the χ^2 criterion used to reject them [4–6,11] may subtly bias the PWA results toward agreement with older measurements that might have had their own unrecognized systematic errors.

The *np* back-angle cross section discrepancies have been highlighted in debates concerning the value and extraction methods for the charged πNN coupling constant f_c^2 (in the notation of pseudovector formulations of the interaction, or equivalently $g^2_{\pi^\pm}/4\pi$ in pseudoscalar formulations) [12,13]. *np* scattering PWAs appear to determine this basic parameter of the *NN* force well: e.g., the Nijmegen analysis [5] yields $f_c^2 = 0.0748 \pm 0.0003$ (equivalent to $g^2_{\pi^\pm}/4\pi = 13.54 \pm 0.05$), and the authors claim that the constraints are imposed by the entire database, with no particularly enhanced sensitivity to any specific observable [5]. In contrast, Ericson *et al.* have extracted a significantly higher coupling constant, consistent

*Present address: Dept. of Physics, Texas A & M University, College Station, TX 77843, USA.

†Present address: Dept. of Radiology and Radiological Sciences, Vanderbilt University, Nashville, TN 37235, USA.

‡Present address: Dept. of Physics, University of Zagreb, Zagreb, Croatia.

§Present address: Dept. of Physics, George Washington University, Washington, DC 20052, USA.

 ©2006 The American Physical Society

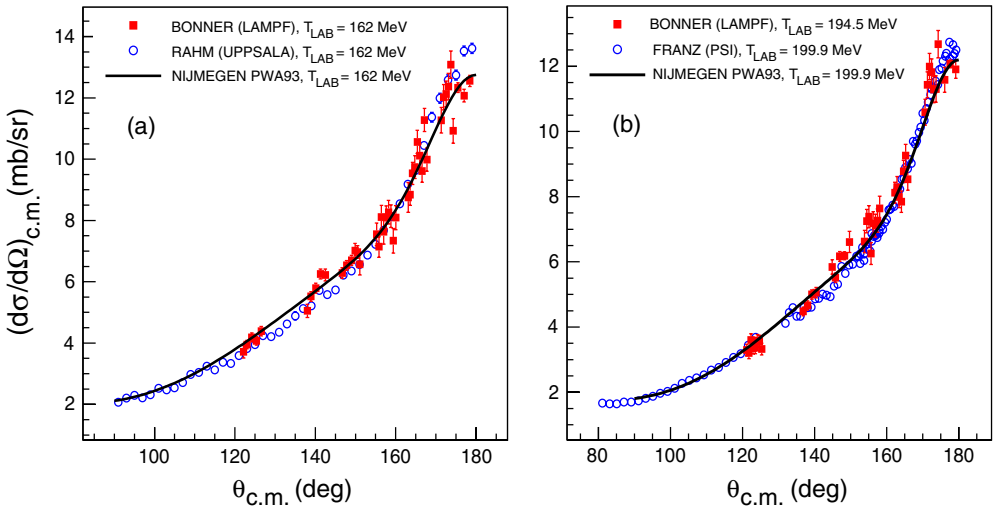

FIG. 1. (Color) Comparison of previous *np* scattering differential cross section measurements (a) from Uppsala [7] and Los Alamos [10] and (b) from PSI [9] and Los Alamos [10] near 200 MeV. The Los Alamos data in each case are represented by solid squares and the other data by open circles. The experimental results are compared to the Nijmegen PWA93 [5] partial wave analysis solution evaluated at appropriate energies. The Los Alamos data were renormalized by factors of 1.092 in (a) and 1.078 in (b) to bring them into agreement with the PWA. The relative cross sections reported in [9] were similarly normalized here, while the reported absolute cross section scale for the Uppsala data was retained.

with older "textbook" values ($g_\pi^2/4\pi \approx 14.4$), by applying controversial pole extrapolation techniques to the Uppsala back-angle *np* scattering cross sections alone [12]. While much debate has centered on the rigor of the pole extrapolation method [13–15], it is clear that the discrepancy in coupling constant values arises in large part [16] from the cross section discrepancies between the Uppsala measurements and the "accepted" database. An experimental resolution of these discrepancies is highly desirable, especially if a new experiment can also pin down the absolute cross section scale. Bugg and Machleidt have pointed out [11] that the largest uncertainty in their determination of f_c^2 is associated with the normalization of *np* differential cross sections, which are often allowed to float from the claimed normalization in individual experiments by 10% or more in PWAs. In contrast, the Nijmegen group claims [6] that, despite sizable normalization uncertainties in existing elastic scattering data, precise total cross section measurements fix the *np* absolute cross section scale to $\pm 0.5\%$ accuracy. This claim could also be checked by a new experiment that provides good experimental precision on absolute differential cross sections.

In the present article we report detailed results from such a new experiment, designed to resolve these *np* back-angle cross section discrepancies. The experiment employed techniques completely independent of those used in other medium-energy measurements, in order to provide tight control over systematic errors. A tagged neutron beam [17] centered around 194 MeV kinetic energy bombarded carefully matched, large-volume CH_2 and C targets, which permitted accurate subtraction of backgrounds from quasifree scattering and other sources. The bombarding energy range was chosen to match approximately that used in earlier high-precision *np* scattering polarization measurements from the Indiana University Cyclotron Facility (IUCF) [18–20]. Recoil protons from *np* scattering were identified in a detector array of sufficient angular coverage to measure the differential cross section at all c.m. angles beyond 90° simultaneously.

The tagging allows accurate determination of the absolute scattering probability for the analyzed subset of all neutrons incident on a secondary target, but it also offers a host of other, less obvious, advantages important to a precise experiment: (1) accurate relative normalization of data taken with CH_2 vs C targets; (2) event-by-event determination of neutron energy, impact point, and incidence angle on the secondary target, with the latter measurement being especially important for cross section measurements very near 180° c.m. scattering angle; (3) three-dimensional location of background sources displaced from the secondary target [17]; (4) precise measurement of the detector acceptance for *np* scattering events; and (5) methods to tag *np* scattering event subsamples that should yield identical cross section results but different sensitivity to various sources of systematic error. The tagging was thus essential to the entire approach of the experiment; no *extra* work was required to extract *absolute* cross sections and thereby to provide an important calibration standard for medium-energy neutron-induced reactions.

The basic results of this experiment have recently been reported briefly [21]. In the present article we provide more detail on the comparison of results to PWAs, on the data analysis procedures, and on the evaluation and characterization of systematic uncertainties. Such details are important for resolving the sort of discrepancies that have plagued the *np* database. Partial wave analyses should, in principle, incorporate experimental systematic as well as statistical errors in optimizing fits to data from a wide variety of experiments. To do so, they must have access to clear delineations of which errors affect only the overall normalization, which have angle dependence, and, in the latter case, what the degree

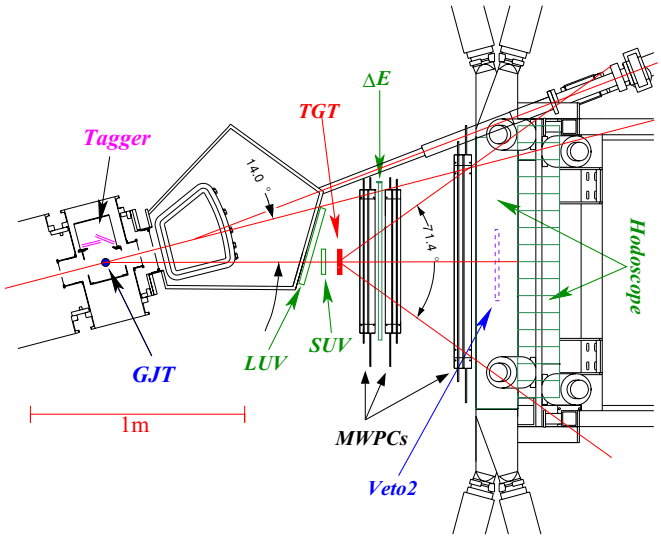

FIG. 2. (Color online) Top view of the *np* scattering experiment setup.

of correlation is among errors at different angles. Overall systematic uncertainties in the absolute cross sections reported here average $\pm 1.6\%$, with a slight angle dependence detailed herein. Statistical uncertainties in the measurements are in the range $\pm(1-3)\%$ in each of 15 angle bins.

II. DETAILS OF THE EXPERIMENT

The experiment was carried out in the IUCF Cooler Ring [22], with apparatus (see Fig. 2) installed in a ring section where the primary stored proton beam was bent by 6°. A primary electron-cooled unpolarized proton beam of 202.5 MeV kinetic energy and typical circulating current of 1–2 mA was stored in the ring. Neutrons of 185–197 MeV were produced via the charge-exchange reaction $p + d \rightarrow n + 2p$ when the proton beam passed through a windowless internal deuterium gas jet target (GJT) of typical thickness $\approx 3 \times 10^{15}$ atoms/cm^2. The ultrathin target permitted detection of the two associated low-energy recoil protons from the production reaction in double-sided silicon strip detectors (DSSDs) comprising the "tagger." Measurements of energy, arrival time, and two-dimensional position for both recoil protons in the tagger, when combined with the precise knowledge of cooled primary proton beam direction and energy, allowed four-momentum determination for each tagged neutron on an event-by-event basis. During the measurement periods, the stored proton beam was operated in "coasting" mode, with rf bunching turned off to minimize the ratio of accidental to real two-proton coincidences in the tagger. The proton beam energy was then maintained by velocity matching (induced naturally by mutual electromagnetic interactions) to the collinear electron beam in the beam cooling section of the ring.

Details of the layout, design, and performance of the tagger detectors and of the forward detector array used to view *np* scattering events from the secondary target are provided in Ref. [17]. Here, we summarize the salient features briefly. The tagger included an array of four 6.4×6.4 cm^2 DSSDs with 480 μm readout pitch in two orthogonal (x', y') directions, each followed by a silicon pad ("backing") detector (BD) of the same area. The DSSDs were positioned about 10 cm away from the center of the gas jet production target. Each DSSD had 128 x' and 128 y' readout channels. Readout was accomplished with front-end application-specific integrated circuits (ASICs) that provided both timing and energy information [17]. The timing signals provided to external electronics consisted of the logical OR over groups of 32 adjacent channels of leading-edge discriminator signals based on fast shaped and amplified analog signals generated in the ASICs. The timing signals available from $4x' \times 4y'$ logical pixels for each DSSD permitted operation of the tagger in a self-triggering mode, where the time-consuming digitization of slow pulse height signals from all 1024 DSSD channels could be initiated by logic based solely on the tagger hit pattern, as reconstructed from the fast timing signals. This self-triggering was critical to the determination of precise absolute cross sections, because it allowed acquisition of data to count directly the flux of tagged neutrons that did not interact in the secondary target or in any of the forward detectors.

Only recoil protons that stopped either in the DSSDs ($E_p \lesssim 7$ MeV) or BDs ($E_p \lesssim 11$ MeV) were considered in the data analysis, because for these the tagger provided a measurement of total kinetic energy with good resolution. By combining these energy measurements with position measurements for both recoil protons, we were able to determine the energy and angle of each tagged neutron, within their broad distributions, with respective resolutions of $\sigma_E \approx 60$ keV and $\sigma_{\text{angle}} \approx 2$ mrad. As part of this determination, we reconstructed the longitudinal origin (z_{vertex}) of each produced neutron within the extended GJT density profile with a resolution of ≈ 2 mm, by comparing neutron momentum magnitudes inferred by applying energy conservation (independent of vertex position) vs vector momentum conservation (dependent on vertex position) to the tagger information for the two recoil protons. Similar resolution was obtained for the transverse coordinates at which each tagged neutron impinged upon a secondary scattering target (TGT in Fig. 2) positioned 1.1 m downstream of the GJT.

Two solid secondary targets were used during the production running: a $20 \times 20 \times 2.5$ cm^3 slab of ultra-high-molecular-weight polyethylene (CH_2) containing 1.99×10^{23} hydrogen atoms/cm^2 and a graphite target of known density machined to have identical transverse dimensions and the same number of carbon atoms per unit area. Each target thickness was determined to $\pm 0.4\%$ by weighing. Data were collected in 18-h cycles, comprising 6 h of running with the CH_2 target, followed by 6 h with C, and 6 h more with CH_2. The frequent interchange of the targets facilitated accurate background subtractions. Both targets intercepted neutrons over an approximate production angle range of $14° \pm 5°$, and cuts were generally placed on the tagger information during data analysis to confine attention to tagged neutrons that would hit the secondary target. Such tagged neutrons were produced at a typical rate of $\sim 200\,\text{s}^{-1}$, leading to typical free *np* backscattering (angle-integrated) rates $\sim 1\,\text{s}^{-1}$ from the CH_2 target.

Protons emerging from the secondary target were detected in a forward array of plastic scintillators for triggering and

energy information, and a set of (three-plane) multiwire proportional chambers (MWPCs) for tracking, as indicated in Fig. 2. The plastic scintillators included large upstream veto (LUV) and small upstream veto (SUV) counters to reject charged particles produced upstream of the secondary target. The ΔE scintillator was separated from the secondary target by a MWPC to permit easy discrimination against *np* scattering events initiated in that scintillator. The rear hodoscope comprised 20 plastic scintillator bars [23] of sufficient thickness (20 cm) to stop 200 MeV protons and give 15%–20% detection efficiency for 100–200 MeV neutrons. All forward detectors were rectangular in transverse profile, with the rear MWPC and hodoscope spanning a considerably larger vertical than horizontal acceptance. The entire forward array provided essentially 100% (>50%) geometric acceptance for *np* scattering events initiated at the CH_2 target for angles $\theta_{\text{c.m.}} \gtrsim 130^\circ$ ($\theta_{\text{c.m.}} \gtrsim 90^\circ$). For c.m. angles forward of 90° the large size and significant neutron detection efficiency of the hodoscope provided a small efficiency for detecting forward-scattered neutrons in coincidence with larger-angle protons that fired at least the first two MWPCs.

The tagger and forward detector array were designed to facilitate a kinematically complete double-scattering experiment with a first target giving negligible energy loss. With the same apparatus, a similar measurement of *pp* scattering was possible simultaneously. For this purpose one could use the tagger to detect a single large-angle recoil deuteron instead of two recoil protons to tag a secondary proton beam via *pd* elastic scattering in the GJT. By requiring a coincidence between a single hit in the tagger and a signal from the small upstream veto scintillator (SUV in Fig. 2), we could define a secondary proton beam of transverse dimensions very similar to those of the tagged neutron beam. Another scintillator (Veto2) placed just in front of the rear hodoscope allowed us to distinguish, at trigger level, between protons from *pd* elastic scattering that traversed the forward array without further nuclear interactions and protons that scattered out of this secondary beam in material following SUV. In the present article, we discuss only the former group, as their yield provides an accurate relative normalization of runs taken with the CH_2 vs C targets.

The triggered events of interest for the present analysis were recorded in four mutually exclusive event streams, three for tagged neutron candidates (consistent with two distinct tagger hits and no accompanying signals from LUV or SUV) and one for tagged proton candidates (consistent with a single tagger hit in prompt coincidence with both LUV and SUV). The trigger logic defined these event streams as follows: (1) tagged neutrons with no rear hodoscope coincidence, providing a prescaled (by a factor of 20) sample for neutron flux monitoring; (2) *np* scattering candidates for which a tagged neutron was in coincidence with signals from both the ΔE scintillator and the rear hodoscope; (3) tagged neutrons in coincidence with the hodoscope but *not* with the ΔE scintillator, a sample used for evaluating the neutron detection efficiency of the hodoscope [17]; and (4) tagged protons in coincidence with both the ΔE and Veto2 scintillators, providing a prescaled (by a factor of 10) sample including *pd* elastic scattering events from the GJT, used to cross-normalize C and CH_2 secondary target runs. The total flux of tagged neutrons intercepting the secondary target was determined from a sum over event streams (1) + (2) + (3), while comparative analyses of the three streams facilitated crosschecks to calibrate the system [17] and aid understanding of potential systematic errors.

III. DATA ANALYSIS

A. Cuts and conditions on tagged neutron beam properties

The general philosophy of the data analysis was to define properties of the tagged neutron beam by identical cuts applied to event streams (1)–(3), so that associated systematic uncertainties would cancel in the yield ratios from which the absolute *np* scattering cross section is extracted. Among these common cuts, described in more detail below, were ones to remove BD noise contributions correlated among the four quadrants of the tagger, to identify the recoil particles detected in the tagger, and to divide the tagged neutron events into subsamples for subsequent analysis. Additional cuts defined a fiducial range for the tagged neutron's predicted transverse coordinates at the secondary target ($|x_{\text{tag}}| <$ 9.5 cm and $|y_{\text{tag}}| < 9.5$ cm) and selected prompt tagger two-particle coincidences ($|t_{p1} - t_{p2} - 30\,\text{ns}| \leqslant 70$ ns, where $t_{p1}(t_{p2})$ is the arrival time of the recoil proton with the larger (smaller) DSSD energy deposition). Software cuts applied to event stream (2) alone to identify free *np* scattering events were kept to a minimum to avoid complicated systematic errors. We relied instead on the accuracy of the background subtractions, which could be verified to high precision. Before application of cuts, additional MWPC requirements were added in software to amplify the hardware definitions of the various triggers. Thus, at least one hit in the x plane and at least one hit in the y plane were required for each of the three MWPCs for events from stream 2.

1. Particle identification

The correlation of DSSD vs BD energy depositions was used to select two basic event classes for analysis of each of the three tagged neutron event streams: (a) "2-stop" events, where both protons associated with the neutron stopped inside the DSSD (either the same or different quadrants of the tagger); and (b) "1-punch" events, where one of the protons stopped inside a DSSD and the other punched through to the BD in a different quadrant and stopped there. These two classes, as discussed further below, differ significantly in neutron energy (E_n) and position (x_{tag}) profiles, allowing an important crosscheck on the accuracy of the tagging technique by comparing *np* cross sections extracted independently from each class. The 2-stop events were further subdivided according to whether the higher of the two recoil proton DSSD energy depositions (E_{p1}) was below or above 5.0 MeV. Protons with $E_{p1} > 5.0$ MeV range out near the exit of the DSSD, and hence possibly in dead layers at the back of the DSSD or front of the BD, making this event class subject to somewhat greater ambiguity regarding complete recoil proton energy reconstruction and accuracy of the predicted x_{tag} value for the

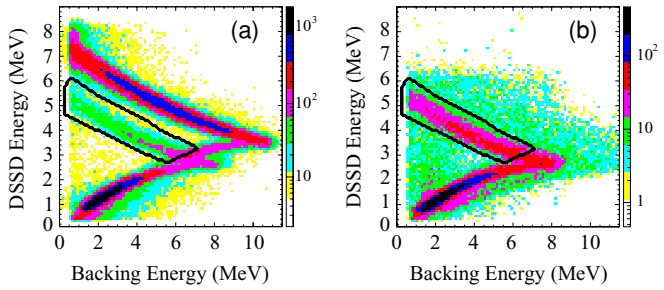

FIG. 3. (Color online) Particle identification plot for one DSSD-BD combination for (a) tagged proton candidates and (b) tagged neutron candidates. The two-dimensional gate used as part of the selection criteria for 1-punch tagged neutron events is shown in panel (b), and again in panel (a), where its location can be gauged with respect to both recoil deuterons and recoil protons that punch through the backing detector.

tagged neutron. Events where both protons punched through to the BDs, or where either punched through the BD itself, were not included in the analysis because they corresponded to E_n below the range of interest.

Figure 3 shows raw spectra for both tagged neutron candidates [event stream 1 in panel (b)] and tagged proton candidates [event stream 4 in panel (a)] of the energy deposited in a typical DSSD quadrant vs that in the companion BD when the latter is nonzero. The tagged proton events exhibit clear recoil proton (lower) and deuteron (upper) particle identification loci, while only the proton locus remains for tagged neutron events. The loci bend backward when the detected particle begins to punch through the BD. The two-dimensional gate (dark boundary) shown in each panel was used to select recoil protons that enter and stop inside the BD, e.g., to identify the 1-punch tagged neutron events. Note that the most intense region along the proton locus, corresponding to deuteron breakup events with an energetic large-angle proton, is thereby eliminated. So are events lying off the proton locus, where the backing detector response may be corrupted by noise or pileup.

Figure 4 shows the reconstructed E_n and x_{tag} distributions for the tagged neutrons in the 2-stop (for all values of E_{p1}) vs 1-punch samples. While the two samples yield overlapping distributions, it is clear that the 1-punch events correspond on average to lower-energy neutrons at larger production angles (preferentially populating the beam-right side of the secondary target).

2. *Correlated noise in the BD*

Special care was taken in the definitions of 1-punch and 2-stop events to minimize effects of substantial detector noise picked up by the large-capacitance BDs. An important source of this noise was discovered to arise from the initiation of pulse height information readout on the adjacent DSSD front-end electronics [17]. The induced noise was strongly correlated among the four BDs, as illustrated in Fig. 5. This figure reveals two uncorrelated bands parallel to the x and y axes, due to 1-punch events in one of the quadrants and low pulse height noise in the other (the pedestals for each BD appear in ADC channel ≈10). But one also observes a strong diagonal band indicative of noise correlations between the two quadrants.

Since the noise correlation pattern extends beyond a reasonable software threshold, it was necessary to use a two-dimensional gate, such as that shown in Fig. 5, to bound the noise correlation region. Candidates for valid 1-punch events were then required to: (1) surpass a threshold ADC channel (≈15) on at least one BD; (2) fall outside the noise correlation gates for all BD pairs; (3) not surpass the BD noise peak (ADC ≈70) in more than one BD; and (4) fall within the PID gate in Fig. 3 for the appropriate quadrant. These conditions and the complementary ones required for 2-stop events reduced the flux of tagged neutrons considered for subsequent analysis by removing events with BD pulse height ambiguities, but because they were applied equally to all

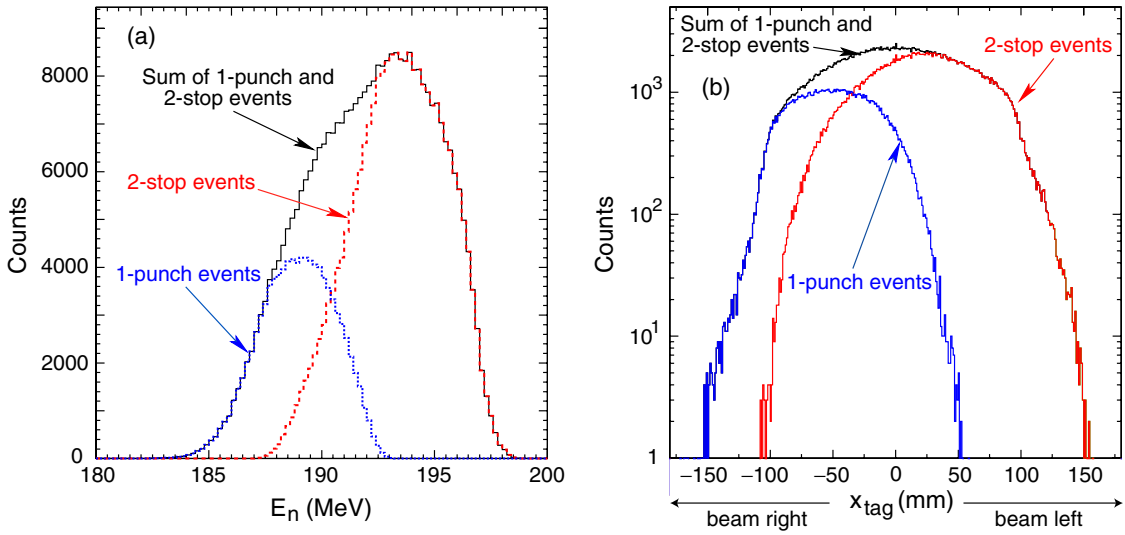

FIG. 4. (Color online) The reconstructed energy (a) and horizontal transverse coordinate (b) of tagged neutrons at the secondary target for 1-punch events, 2-stop events, and their sum (solid black line).

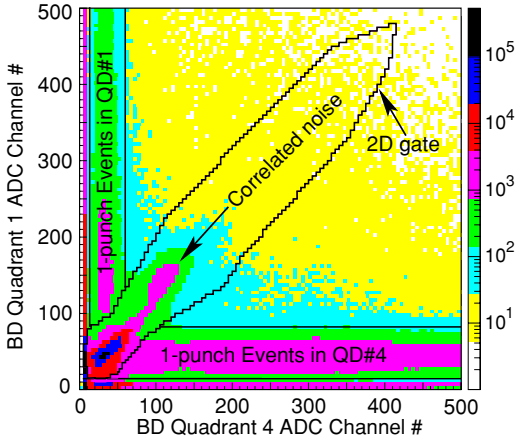

FIG. 5. (Color online) The ADC outputs of two BDs plotted against one another, revealing regions of 1-punch tagged neutron events, but also a region dominated by correlated noise in both quadrants. Events along the x and y axes, where one BD signal falls in the pedestal region, are also mostly valid 1-punch events.

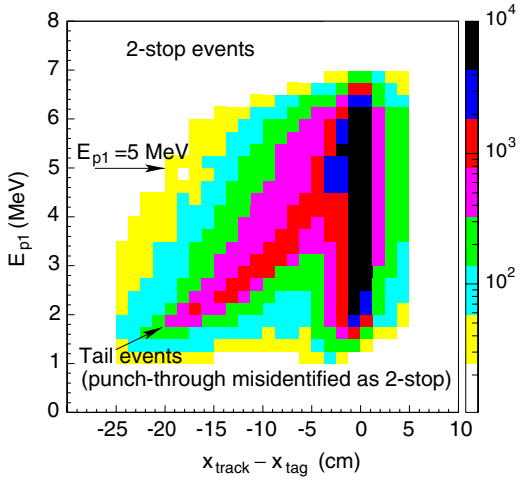

FIG. 6. (Color online) The correlation for apparent 2-stop *np* scattering candidates between the higher of the DSSD energy depositions for the two recoil protons in the tagger and the difference in predicted x coordinates at the secondary target from neutron tagging vs forward proton ray-tracing. The long correlated tail contains corrupted punch-through events for which electronic loss of backing detector energy information has led to misidentification of the event and large systematic errors in the tagging.

tagged neutron event streams they did not introduce systematic errors in the *np* cross section extraction.

B. Corrupted events subtraction

An event misidentification mechanism discovered during the data analysis was attributed to an electronics malfunction in the gating or clearing circuit for the electronics module that was used to digitize the pulse height information for all four BDs. The effect of the malfunction was to zero out valid BD energy signals for a randomly selected fraction of punch-through events. The effect was seen clearly, for example, in the *pd* elastic scattering events in stream 4, where a software gate placed on the two-body kinematic correlation between recoil deuteron DSSD energy deposition and forward proton angle could be used to select events in which the deuteron must have stopped in the BD. Roughly 3/4 of these events showed the anticipated BD pulse height, but 1/4 had $E_{\mathrm{BD}} = 0$. In the case of tagged neutrons, the corrupted events were misidentified as 2-stop events and gave systematically incorrect predictions of the tagged neutron trajectory, because some recoil proton energy was lost. However, the availability of full information for the surviving punch-through samples allowed us to emulate the effect and subtract the corrupted events accurately.

The corrupted events were easily distinguished in event stream 2 by using the MWPC tracking information. Figure 6 shows the correlation for event stream 2 between E_{p1} in the tagger and $x_{\mathrm{track}} - x_{\mathrm{tag}}$, where x_{track} denotes the transverse coordinate of the detected proton from *np* scattering at the secondary target, as reconstructed from the MWPC hits. The majority of events have $x_{\mathrm{track}} - x_{\mathrm{tag}} \approx 0$, independent of E_{p1}, as expected when both the tagging and tracking are accurate. The corrupted events populate the "tail" to the left of the most intense band, with x_{tag} exceeding x_{track} by an amount that is strongly correlated with the recoil proton energy deposition in the DSSD: the lower E_{p1}, the larger is the lost E_{BD} and the consequent error in x_{tag}. While the corrupted events could be eliminated from event stream 2 by a software gate within Fig. 6, they could not have been similarly eliminated from event streams 1 and 3, where there was no forward proton to track. Hence, it was essential to find a way to subtract these corrupted events reliably and consistently from all three tagged neutron event streams.

The corrupted events were simulated using all recorded punch-through events that survived with their BD energy information intact by reanalyzing these events after artificially setting $E_{\mathrm{BD}} = 0$ in the software before tagging reconstruction. The distribution shapes of the tail events in Fig. 6 with respect to all variables were accurately reproduced when this simulation was based on *all* events in Fig. 3(b), both inside and outside the two-dimensional gate drawn, and also including events where *both* recoil protons punched through their DSSDs. To determine the fraction of these punch-through events that was affected by the electronics malfunction, we relied on a comparison of the subsamples of our simulated events and of the apparent 2-stop events that had valid BD timing information despite having $E_{\mathrm{BD}} = 0$. Because the BD noise problems necessitated high thresholds to generate timing signals, these subsamples populate mostly the far tail in Fig. 6, corresponding to $E_{p1} \lesssim 3.5$ MeV (thus, to relatively large BD analog signals). The corrupted fraction of punch-through events was in this way determined independently for each of the three tagged neutron event streams and found to be identical for the three, within the statistical precision (typically $\approx$1%) available in matching simulated and recorded corrupted event subsamples. The fraction varied slightly with time during the production run, but averaged 23%. The success of this simulation and the persistence of the corrupted fraction across (both tagged neutron and tagged proton) event streams provide strong support for our assumption that the malfunction

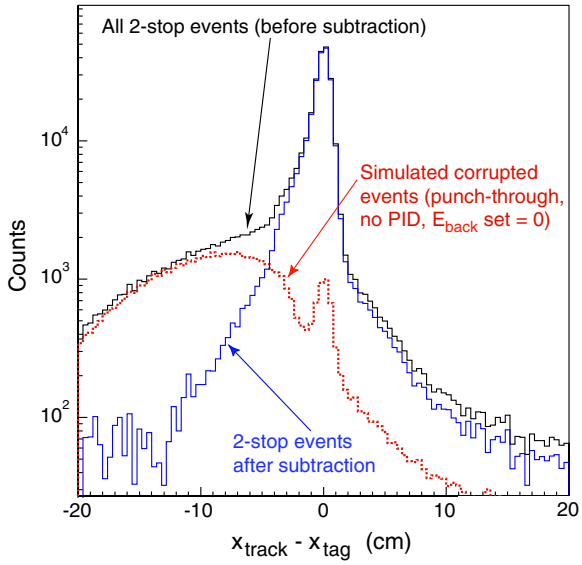

FIG. 7. (Color online) The subtraction of the simulated corrupted events removes the tail from the 2-stop event sample. The simulated spectrum has been normalized by matching to the 2-stop subsample characterized by backing detector information with valid times but zero energy.

affected a random sample of punch-through events. Because the fractional loss of 1-punch events to this corruption was independent of event stream, there was no residual systematic effect on the extracted 1-punch cross sections, but rather only a slight loss of statistical precision.

Figure 7 shows a comparison of the $x_{\rm track} - x_{\rm tag}$ spectrum for all 2-stop events in stream 2 with the simulated corrupted sample, normalized as described above via the subsample with valid BD timing signals. The subtraction eliminates essentially completely the corrupted events with $E_{p1} \lesssim 5.0$ MeV, or $x_{\rm track} - x_{\rm tag} \lesssim -5$ cm, leaving a reasonably symmetric small background (discussed further in Sec. V A5) at $|x_{\rm track} - x_{\rm tag}| > 5$ cm. We therefore assume that the subtraction is similarly successful for event streams 1 and 3, where we have no tracking information to compare, and associate a systematic error for the subtraction (see Sec. V B2) that reflects only the uncertainty in the normalization scheme for the simulated corrupted events.

For $E_{p1} > 5.0$ MeV, there is a remaining tail of small extent in the subtracted $x_{\rm track} - x_{\rm tag}$ spectrum in Fig. 7 that arises not from the electronics malfunction but rather from recoil protons that barely punch through the DSSD, while depositing insufficient energy in the BD to be distinguished from noise. Because of these events, we have separately analyzed the 2-stop samples with $E_{p1} \leqslant 5.0$ MeV and $E_{p1} > 5.0$ MeV. For the latter sample, after subtracting simulated corrupted events, we used a two-dimensional software gate on Fig. 6 to eliminate events in stream 2 that had potentially distorted $x_{\rm tag}$ information, thereby rejecting 18% of 2-stop $E_{p1} > 5.0$ MeV events (as opposed to the 23% of *all* 2-stop events in stream 2 that were affected by the corruption). The yields of 2-stop $E_{p1} > 5.0$ MeV events in streams 1 and 3 were then scaled down by the same 18% to remove the remaining events of questionable 2-stop pedigree.

The small peak at $x_{\rm track} - x_{\rm tag} \approx 0$ in the simulated background in Fig. 7 indicates that a small fraction of the punch-through event sample used in the simulation really corresponds to true 2-stop events that were misidentified by virtue of BD noise that evaded the noise cuts discussed in the preceding subsection. Subtracting this small fraction of valid 2-stop events along with the simulated corrupted events has the effect of reducing the 2-stop tagged neutron yield by ≈3% in all three event streams, with no significant consequence for the absolute *np* cross sections extracted from the 2-stop sample.

C. Background subtraction

The background events for this experiment came mostly from *np* quasifree scattering off carbon nuclei in the CH_2 target. However, there were also some prominent sources displaced from the secondary target, including: (1) protons coming directly from the gas jet production target, or from the exit flange on the Cooler beam 6° magnet chamber (see Fig. 2), that evaded the veto scintillators because of either their imperfect coverage or their electronic inefficiencies; (2) *np* scattering events induced either on scintillator edges or on the Lucite light guide for the SUV, yielding pulse heights below that veto detector's threshold; and (3) quasifree *np* scattering induced on the vertically narrow (but longitudinally thick) aluminum frame used to support the secondary target. By frequently interchanging the CH_2 target with a graphite target closely matched in transverse dimensions and in areal density of carbon nuclei, we were able to subtract the backgrounds from all sources simultaneously. The relative normalization of the CH_2 and C runs was determined from the *pd* elastic scattering yield from the GJT, as recorded in event stream 4 [17]. The background subtraction was determined to be sufficiently reliable that we could avoid imposing many kinematic cuts, with potentially significant systematic ambiguities, to define free *np* scattering events.

The accuracy of the background subtraction can be judged, for example, from Fig. 8, which presents CH_2 and C spectra, and their difference, with respect to $y_{\rm tag}$ (the vertical impact position of the neutron on the secondary target, as reconstructed from the tagger) and ΔE scintillator pulse height within a narrow *np* scattering angle range. These two particular variables have been chosen for display in the figure because the CH_2 spectra show prominent background features associated both with quasifree scattering (the long high pulse height tail in ΔE) and with other sources (the $y_{\rm tag} = -11$ cm peak from the aluminum support frame). Both sources are precisely eliminated by the background subtraction. Indeed, upper limits on the surviving remnants of these features allow us (as described in Sec. V B1) to reduce the systematic uncertainty for the background subtraction even below the level given by the precision of the measured C/CH_2 target thickness ratio (±0.6%). Comparison of the $y_{\rm tag}$ spectra for C and CH_2 in Fig. 8 also reveals another localized non-target source, near $y_{\rm tag} = 0$, that is removed by the subtraction. This appears to be localized horizontally as well, to a region near the beam-left edge of the SUV scintillator, and might reflect scattering from a small damaged region of that scintillator with reduced light collection and veto efficiency.

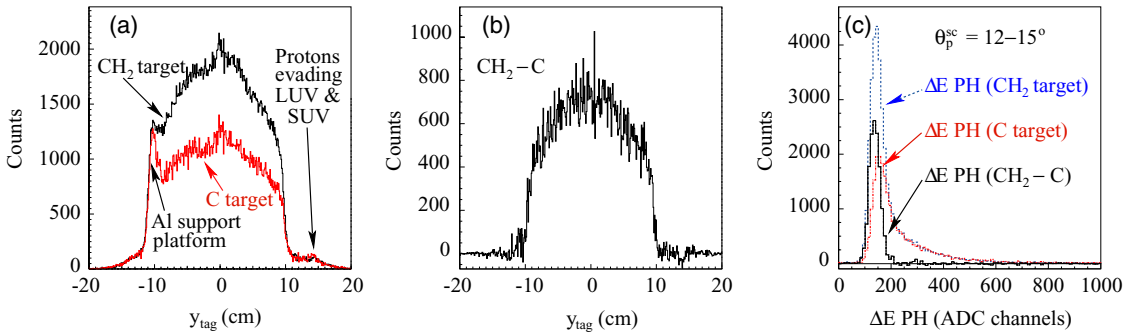

FIG. 8. (Color) Distribution of *np* scattering event candidates with respect to y_{tag} and to ΔE scintillator pulse height for the CH_2 and C targets separately and for the difference between them.

D. Free scattering cuts

Software conditions imposed only on event stream 2 to distinguish free scattering from background events have the potential to remove free scattering yield in sometimes subtle ways. They were thus used in the analysis only when they could substantially reduce the statistical uncertainties (i.e., by suppressing background to be subtracted) without introducing significant systematic uncertainties in correcting for the free scattering losses, or when such losses were judged to be inevitable to remove ambiguities in the analysis. The accuracy of the C background subtraction provided a reliable method to judge the extent of any free scattering event removal.

The most effective such cut applied was placed on the correlation of forward proton energy loss in the ΔE scintillator with the laboratory angle of the proton trajectory. The applied two-dimensional software gate is superimposed on the observed distribution of events following CH_2-C subtraction in Fig. 9. This distribution reveals that very few free scattering events were removed by this gate, but it is clear from the long tail seen in the projected unsubtracted spectrum for one angle bin in Fig. 8(c) that a substantial number of quasifree background events, leading to lower-energy outgoing protons, were successfully removed.

In contrast, we did not apply a comparable cut on the energy deposition of the forward proton in the rear hodoscope, where it generally stopped, despite an appreciable difference in the distributions of hodoscope energy between free and quasifree events. The reason for avoiding this cut is illustrated in Fig. 10: the free scattering spectrum revealed by the C subtraction exhibits a quite substantial low-energy reaction tail in addition to the well-defined full-energy peak. An unacceptably large systematic error would have been introduced by the need to correct for loss of these reaction tail events if we had imposed a cut on hodoscope energy to suppress background.

A benign cut imposed for slight background reduction placed an upper threshold on the χ^2 value obtained for a linear track fit to the reconstructed MWPC space points. The CH_2-C subtraction indicates that only $(0.2 \pm 0.1)\%$ of free scattering

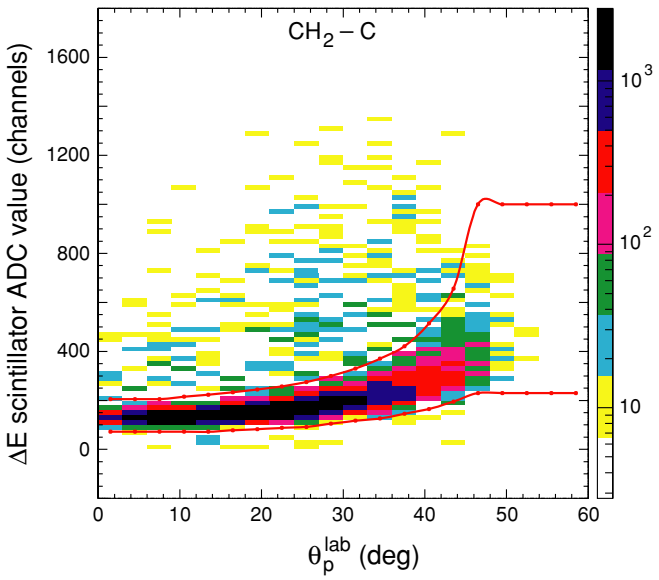

FIG. 9. (Color online) The distribution of *np* scattering candidate events after subtraction of C from CH_2 data with respect to ΔE ADC and proton lab angle. The lines show the boundaries of the gate applied to event stream 2 to select free scattering events.

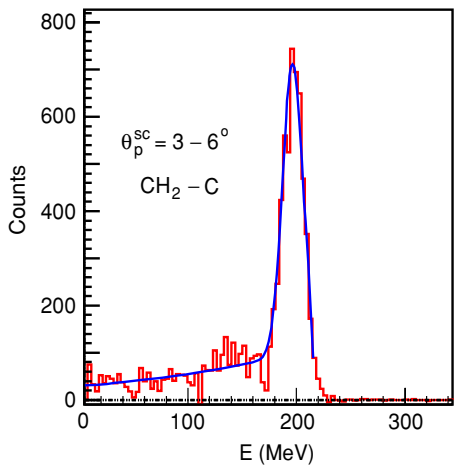

FIG. 10. (Color online) The distribution of *np* free scattering events in the scattering angle bin $\theta_p^{sc} = 3°$–$6°$ with respect to forward proton energy deposition in the rear hodoscope. The curve represents a fit with a Gaussian plus exponential tail. The tail represents valid free scattering events where the proton undergoes a nuclear reaction in the stopping scintillator.

events were removed by this condition. More serious (6.3% of total CH_2-C yield), but unavoidable, losses were introduced by cuts confining the tagging and tracking information in event stream 2 to agree within $|x_{\rm track} - x_{\rm tag}| \leqslant 2.5$ cm and $|y_{\rm track} - y_{\rm tag}| \leqslant 2.0$ cm. These limits correspond to $\pm 3\sigma$ of the narrow Gaussian resolution function that dominates these distributions in the CH_2-C spectra. Nonetheless, the cut eliminates events in long distribution tails that are affected either by tagging errors or by sequential reactions of the tagged neutron, which introduce serious ambiguities in interpretation. This cut, and its consequence for systematic uncertainties, is discussed further in Sec. V A5.

Finally, it is worth mentioning one additional cut that we chose *not* to impose. The transverse *np* vertex coordinates are, in fact, determined by the tagging and tracking with considerably better resolution than implied by the $\sigma \approx 7$–8 mm value mentioned in the preceding paragraph [17]. This latter value is dominated by the thickness of the secondary target, simply reflecting the uncertainty in precise longitudinal origin of the *np* scattering vertex. Much better information is, in principle, available by locating the vertex in three dimensions at the point of closest approach of the neutron trajectory reconstructed from the tagger and the proton trajectory reconstructed from the MWPCs. Distributions of such reconstructed secondary vertex coordinates [17] permit tagged neutron radiography of the background sources displaced from the CH_2 target. However, any cuts to remove such background sources in this manner would be affected by the strong dependence of the reconstructed vertex resolution on the proton scattering angle (vertex information clearly deteriorates as the neutron and proton trajectories approach collinearity). We decided to rely completely on the C subtraction to remove such other sources of background, in order to avoid consequent angle-dependent free scattering event losses.

E. Acceptance

The lab-frame proton scattering angle $\theta_p^{\rm sc}$ is determined for each analyzed event as the opening angle between the neutron trajectory reconstructed from the tagger and the forward proton trajectory reconstructed from the MWPCs. The geometric acceptance of the forward detector array for *np* scattering events is a function of both $\theta_p^{\rm sc}$ and the coordinates of the scattering vertex at the secondary target. Because the distribution of scattering vertex coordinates, especially of $x_{\rm tag}$ (see Fig. 4), differed among the three analyzed data subsamples (1-punch, 2-stop with $E_{p1} \leqslant 5.0$ MeV, and 2-stop with $E_{p1} > 5.0$ MeV), the acceptance had to be evaluated separately for each subsample. This was done by comparing simulated to measured distributions of events with respect to azimuthal angle $\phi_p^{\rm sc}$ within each $\theta_p^{\rm sc}$ bin, for each data subsample.

The simulations were constrained to reproduce the measured distributions of the longitudinal production vertex coordinate of the neutron within the GJT (common to all three data subsamples) and its transverse coordinates on the secondary target (separately for each subsample). Within these distributions, coordinates were generated randomly for each event, as were also $\theta_p^{\rm sc}$ (in the range 0°–75°) and $\phi_p^{\rm sc}$ (over the full azimuthal range). Generated outgoing proton trajectories were then accepted if they would yield signals above the hodoscope pulse height threshold (required in trigger) and in all three MWPCs (required in the data analysis). Forward detector location parameters were tuned slightly from their measured values to optimize the fit of the simulated to the measured $\phi_p^{\rm sc}$ distributions for all $\theta_p^{\rm sc}$ bins and for 1-punch and 2-stop samples simultaneously.

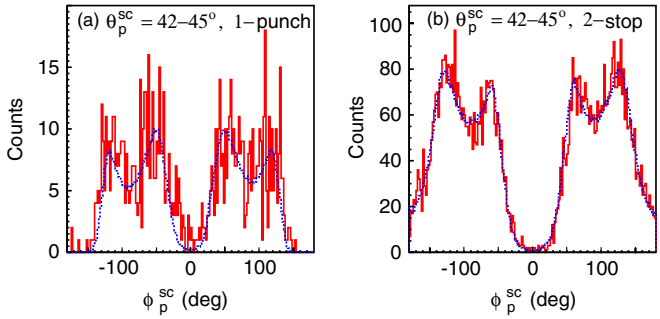

FIG. 11. (Color) Comparison of the measured (solid line with sizable statistical fluctuations) and simulated (dotted line) distributions of free (CH_2-C) *np* scattering events in the angle bin $\theta_p^{\rm sc} = 42°$–45° with respect to proton azimuthal scattering angle $\phi_p^{\rm sc}$ for the 1-punch (a) and 2-stop (b) data samples. Forward detector geometry parameters, plus a single overall normalization parameter per angle bin and data sample, were adjusted to optimize the fit simultaneously for all angle bins and both data samples.

The high quality of the fits obtained is illustrated in Fig. 11 for the 1-punch (a) and 2-stop (b, summed over all E_{p1}) samples for a single large angle bin, $\theta_p^{\rm sc} = 42°$–45°, where the observed azimuthal distributions display considerable structure. The structure reflects the rectangular shape of the hodoscope and large MWPC, projected onto $\theta - \phi$ space: e.g., the four peaks observed correspond to the four detector corners. The small changes in distribution between the 1-punch and 2-stop samples – e.g., in the relative heights of the peaks and in the extent of the dips near $\phi_p^{\rm sc} = 0°$ (beam-left side) and 180° (beam right) – arise from the shift in $x_{\rm tag}$ profiles seen in Fig. 4. These features are all reproduced very well by the simulations. For $\theta_p^{\rm sc} \leqslant 24°$, the measured and simulated ϕ distributions are essentially uniform over 2π, indicating full acceptance. Figure 12 shows the simulated acceptance for the 1-punch data sample as a function of $\theta_p^{\rm sc}$. The 0.2% shortfall from full acceptance near 0° reflects protons incident normally on the small cracks between adjacent hodoscope elements. Results presented in the next section are limited to the angle range for which the acceptance is at least 50%; at larger proton angles the uncertainty in acceptance grows rapidly.

IV. RESULTS

The absolute differential cross section for *np* backscattering was extracted independently for three data samples – 1-punch, 2-stop with $E_{p1} \leqslant 5$ MeV, and 2-stop with $E_{p1} > 5$ MeV–from

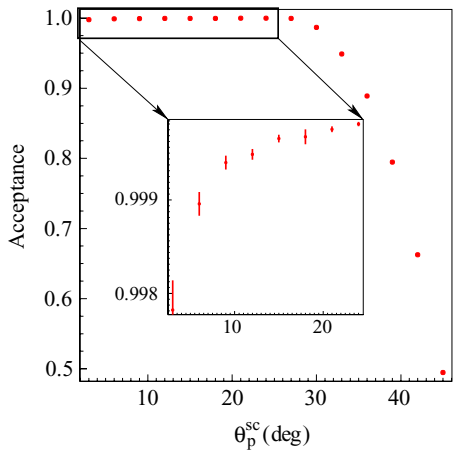

FIG. 12. (Color online) The simulated acceptance of the 1-punch data sample. The inset shows a greatly magnified vertical scale for the most forward proton scattering angles.

the yields of event streams 1, 2, and 3 as follows:

$$\left(\frac{d\sigma}{d\Omega}\right)_{\rm lab} = \frac{N_2(\theta_p^{\rm sc})\prod c_i}{(N_1+N_2+N_3)t_H|d\cos(\theta_p^{\rm sc})|a_\phi(\theta_p^{\rm sc})}, \quad (1)$$

where $N_2(\theta_p^{\rm sc})$ represents the number of free scattering events from stream 2 within a given reconstructed proton angle bin, surviving all relevant cuts and background subtractions; N_1, N_2, and N_3 in the denominator represent analogous tagged neutron yields from the mutually exclusive event streams 1 (corrected for prescaling), 2 (angle-integrated), and 3; the c_i represent small corrections, summarized in Table I with details in Sec. V, for various inefficiencies, tagged neutron losses or backgrounds, software cut and dead time differences among event streams, and resolution smearing; $t_H = (1.988 \pm 0.008) \times 10^{23}$ H atoms/cm^2 for the CH_2 target; and a_ϕ is the azimuthal acceptance determined from simulations for the given angle bin. The data were analyzed in 1 MeV wide slices of reconstructed neutron energy from 185 to 197 MeV and an effective cross section was extracted at the mean neutron energy of 194.0 ± 0.15 MeV. For this purpose, a small (always $<1\%$) cross section correction was made for the deviation of each analyzed slice from the mean energy, using the theoretical energy- and angle-dependence calculated with the Nijmegen PWA93 solution [5].

The *np* scattering angle was determined event by event with a resolution dominated by the multiple Coulomb scattering of the outgoing proton in the CH_2 target material. The rms multiple scattering angle through half the target thickness (assuming an average scattering vertex at the center plane of the target) varied from 1.0° for forward protons to 2.3° for the largest-angle protons analyzed. In contrast, the angle of the incident neutron was determined from the tagging with a typical resolution $\sigma \approx 2$ mrad [17]. To keep corrections for resolution smearing of the angular distribution small (see Sec. V D), the data were analyzed in 3° wide lab angle bins.

The cross sections for the three data subsamples, with their independently determined absolute scales, are mutually consistent in both magnitude and angular shape, within statistical uncertainties, as revealed by the comparisons in Fig. 13. The figure shows the relative difference, $((\frac{d\sigma}{d\Omega})_{\rm sampleA} - (\frac{d\sigma}{d\Omega})_{\rm sampleB})/(\frac{d\sigma}{d\Omega})_{\rm sampleB})$, between pairs of cross sections for the three data samples. The reduced χ^2 value for the comparison of each pair of samples is indicated in the legend to Fig. 13. This comparison supports the reliability of the experiment and analysis, because these samples come from complementary regions of the tagged beam spatial and energy profiles (see Fig. 4) and are subject to somewhat different systematic error concerns. We view the agreement in absolute cross section scale as a particularly significant demonstration of the accuracy of the neutron profiles reconstructed from tagging and of the subtraction procedure applied to remove corrupted events from the 2-stop sample (see Sec. III B). Cross sections extracted for different time periods within the production runs, and with different sets of cuts, are also consistent within uncertainties.

The results, averaged over all three data samples, are compared in Fig. 14 with previous experimental results at 162 MeV [7] and with the Nijmegen partial wave analysis (PWA93) at the two relevant energies [24]. The measured points are plotted at the yield-weighted centroid angle of each analyzed bin. The comparison of the present results with previous experiments and with partial wave analyses is discussed in detail in Sec. VI, after first describing the

TABLE I. Correction factors and systematic uncertainties in correction factors for the *np* cross sections.

Source	Correction factor (c_i)	Uncertainty in c_i
Accid. tagger coinc.	1.0003	$<\pm 0.001$
Non-^{2}H tagger background	1.0067 (2-stop); 1.0044 (1-punch)	± 0.002
n pos'n unc. on CH_2	1.0000	± 0.001
n atten'n before CH_2	1.005	± 0.0025
Sequential react'ns & $x_{\rm tag}(n)$ errors	1.063	± 0.010
C bkgd. subtraction	1.0000	± 0.004
H in C target	1.000	± 0.004
Corrupted event subtraction	1.000	$< \pm 0.001$
Software cut losses	1.010	± 0.005
Reaction tail losses	1.004	± 0.002
Neutron polarization effects	Angle-dependent: <1.0012 (1-punch) >0.9986 (2-stop)	± 0.001
CH_2 tgt. thickness	1.0000	± 0.004
np scattering acceptance	1.0000	$\leqslant \pm 0.001$ ($>120°$) $\rightarrow \pm 0.017$ (90°)
MWPC inefficiency	1.017	± 0.002
Trigger inefficiency	$1.002 + 0.008 \times \cos^2(\theta_p^{\rm lab})$	$\pm[0.001 + 0.004 \times \cos^2(\theta_p^{\rm lab})]$
Dead time diffs.	0.991	± 0.005
Scattering angle errors	1.000	Angle-dependent, $\leqslant \pm 0.004$
Angle resolution (mult. scattering)	Angle-dependent: 0.946 – 1.014	± 0.001–0.005
Net, typical	≈ 1.10	$\approx \pm 0.016$

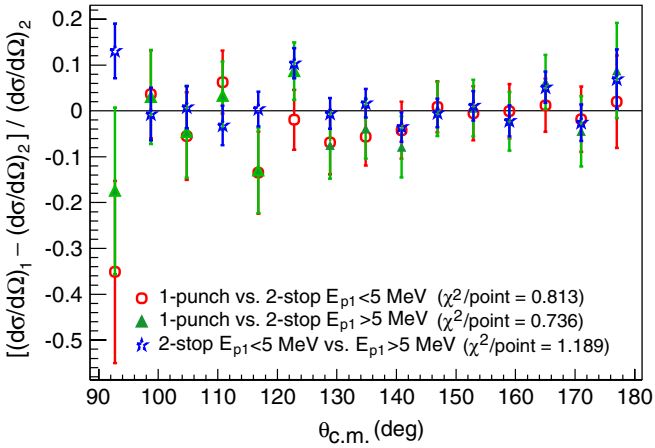

FIG. 13. (Color) The fractional differences between the absolute differential cross sections extracted for different analyzed data subsamples. The plotted error bars take into account only the independent statistical (including those from background subtractions) uncertainties for the three samples. Slightly different correction factors c_i were applied to the cross sections for different samples, as indicated in Table I, before the comparison was made.

nature and evaluation procedure for each of the systematic uncertainties included in Table I.

V. SYSTEMATIC ERRORS

Most of the individual correction factors c_i applied to the extracted cross sections, and their associated systematic uncertainties listed in Table I, have been evaluated via complementary analyses of the data. In this section we briefly describe the procedures used and error estimates for each, being careful to distinguish uncertainties that affect only the overall cross section normalization from those with appreciable angle dependence. In the latter cases, we also characterize the degree of correlation among the uncertainties at different angles to facilitate inclusion of the uncorrelated systematic errors in PWAs including the present data. For purposes of logical flow, we organize the discussion into four categories: (A) tagged neutron flux uncertainties; (B) *np* backscattering yield uncertainties; (C) target thickness, acceptance, and efficiency uncertainties; and (D) errors in determining the kinematic variables. In Sec. V E we present a summary of the angle-dependent systematic errors.

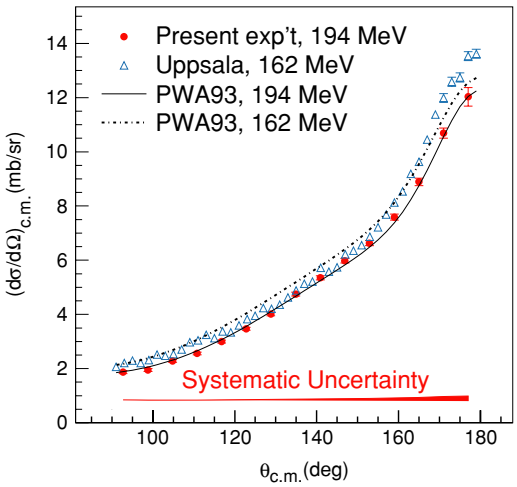

FIG. 14. (Color online) Absolute differential cross section from the present experiment compared with data from Ref. [7] and with PWA calculations at two relevant energies. The error bars on the present results are statistical, including background subtraction. The width of the shaded band at the bottom, representing the net absolute systematic uncertainty, including that in the overall normalization, is comparable to or smaller than the statistical error at each angle.

A. Tagged neutron flux uncertainties

The sources below contribute to uncertainties in extracting the angle-integrated yields $N_{1,2,3}$ in Eq. (1), dominated by the noninteracting tagged neutrons in event stream 1. All of the issues discussed in this subsection give rise to overall (angle-independent) normalization errors in the differential cross sections.

1. Accidental tagger coincidences

Accidental coincidences between two uncorrelated particles detected in the tagger contribute slightly to the apparent tagged neutron flux on the secondary target, leading to an underestimate of the cross section. The accepted events in all three event streams passed a cut on the time difference $\Delta t = (t_{p1} - t_{p2})$ between the two tagger hits, as indicated in Fig. 15. The correction factor was determined from the ratio of events in stream 1 that passed all other cuts defining the tagged neutron beam but fell within one of two displaced time windows, $|\Delta t + 110\,\text{ns}| \leqslant 70$ ns and $|\Delta t - 170\,\text{ns}| \leqslant 70$ ns, to the yield in the prompt coincidence window $|\Delta t - 30\,\text{ns}| \leqslant 70$ ns. The resulting correction factor is $c_1 = 1.0003$, with an uncertainty $< \pm 0.001$, showing that accidental coincidences were a minor issue for the experiment.

2. Tagger background from non-^{2}H sources

Additional possible background contributions to the tagged neutron flux could arise from real (correlated) two-particle coincidences in the tagger, generated by proton beam interactions with nuclei heavier than deuterium in material displaced from the GJT. This possibility was checked via runs where hydrogen gas was substituted for the deuterium in the GJT to induce similar beam "heating" without any real possibility of tagged neutron production (since the proton beam energy was far below pion production threshold for the *pp* system). A correction factor $c_2 = 1.0044 \pm 0.002\,(1.0067 \pm 0.002)$ for 1-punch (2-stop) events was determined from the ratio of accidental-subtracted tags satisfying the tagged neutron conditions with the hydrogen vs deuterium production targets. The statistical uncertainties in these ratios were considerably smaller than ± 0.002; the quoted uncertainty is intended to allow for the possibility of slight systematic differences in beam heating, hence in the rate of interactions with displaced material, between the two GJT gases.

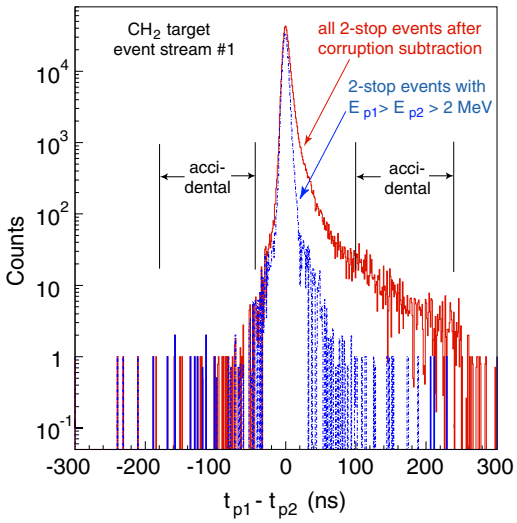

FIG. 15. (Color online) The distribution of DSSD arrival time difference between the two recoil protons for tagged neutron events, shown for all 2-stop events (following subtraction of the corrupted events as per Sec. III B) and for 2-stop events where the lower of the two DSSD energy depositions (E_{p2}) exceeds 2.0 MeV. The vertical lines indicate the prompt coincidence gate (central region between the inner two lines) imposed in the analysis, plus two displaced gates used to assess accidental coincidence background in event stream 1. The long tail seen for events with $E_{p2} \leqslant 2.0$ MeV, arising from detector noise and imperfect software corrections for time walk near the front-end discriminator threshold, leads to an overestimate of the accidental coincidence yield, but the correction and uncertainty still remain quite small.

3. *Impact position uncertainty on the* CH_2 *target*

This is the first of several error sources we consider that arise when a properly tagged neutron does not reach the CH_2 (or C) secondary target, or reaches it at a significantly different position than expected from the tagging. Because of the finite (several mm) impact position resolution from the tagger, some tagged neutrons predicted to hit the secondary target may actually miss it, while some predicted to miss the target may hit it. Especially near the target edges, where the yield of *np* scattering events drops rapidly and nonlinearly as a function of impact position, this resolution smearing can affect the extracted cross sections. In practice, however, we observe no statistically significant difference in cross section normalization between the independent event samples from the bulk of the target ($|x_{\rm tag}| \leqslant 9.0$ cm and $|y_{\rm tag}| \leqslant 9.0$ cm) and from a 5.0-mm-wide strip ($9.0 < |x_{\rm tag}| \leqslant 9.5$ cm or $9.0 < |y_{\rm tag}| \leqslant 9.5$ cm) surrounding this core. From this comparison and the fraction of all events arising near the target edges, we infer a correction factor $c_3 = 1.000 \pm 0.001$.

4. *Neutron attenuation before the* CH_2 *target*

Some tagged neutrons fail to hit the secondary target, leading to an underestimate of the extracted *np* cross section, as a result of interactions they undergo upstream of that target. Approximately 3.5% of 200 MeV neutrons will undergo an inelastic reaction of some sort in the upstream material [25], which is dominated by the 0.29-cm-thick stainless steel vacuum window at the exit of the Cooler's 6° magnet vacuum chamber, the 0.64-cm-thick LUV plastic scintillator, and the 0.64-cm-thick SUV plastic scintillator (the first two of these traversed at an incidence angle ≈14°). However, many of these "prescattering" neutrons give rise to charged products that get vetoed by LUV or SUV (and hence do not contribute to the tagged flux) or are removed by the C subtraction as apparent *np* scattering events from an upstream source. Others yield an energetic neutron or proton, not strongly deflected from the original tagged neutron trajectory, that still strikes the nearby secondary target with a chance to induce a tertiary interaction there, and so might still be considered as part of the incident flux.

We may judge the rate of such tertiary interactions from events where a forward proton emerges from the secondary target at a transverse location ($x_{\rm track}$, $y_{\rm track}$) substantially different (by much more than the tagging position resolution effect considered in Sec. V A3) from the predicted impact position of the tagged neutron ($x_{\rm tag}$, $y_{\rm tag}$). Such tertiary interactions introduce their own problems in the analysis, to be addressed separately in the next subsection. Here, we study them to place limits on the probability of larger-angle upstream scattering, which yields no chance of a tertiary scattering. In Fig. 16, we show the difference spectra for $x_{\rm track} - x_{\rm tag}$ and $y_{\rm track} - y_{\rm tag}$ for 1-punch events (to eliminate ambiguities from the corrupted 2-stop events seen in Fig. 6) after CH_2-C subtraction (to eliminate ambiguities from *np* scattering induced on material displaced from the secondary target). The narrow Gaussian resolution peaks sit atop a broad background that has important contributions from these tertiary interactions.

By fitting the background in Fig. 16 with a broad Gaussian, and assuming that the probability of initiating a scattering in the secondary target is roughly the same for the prescattered neutrons as for the bulk of the tagged neutrons, we estimate that 0.5% of tagged neutrons may be prescattered through a sufficiently large angle to cause a transverse displacement greater than 10 cm (i.e., half the target width or height) on the secondary target. We use this estimate to infer a correction factor $c_4 = 1.005 \pm 0.0025$ for tagged neutron prescattering flux losses before the CH_2 target. The ±50% uncertainty we assign to $(c_4 - 1)$ is intended to account for non-prescattering

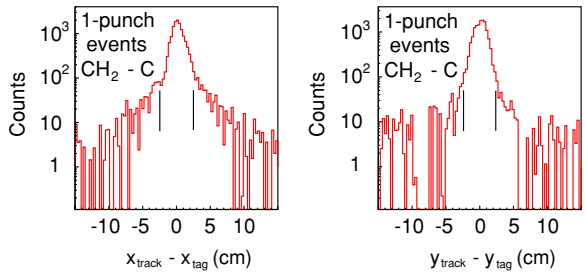

FIG. 16. (Color online) The difference distributions in x (left) and y (right) coordinates determined from tracking of the forward proton vs reconstruction of the tagged neutron, for the 1-punch data sample after CH_2-C subtraction. The vertical lines indicate the location of software gates used to remove events that may be complicated by sequential reactions or tagging errors.

origins of the background in Fig. 16 (e.g., tagging errors or sequential reactions *within* the CH_2 or tertiary scattering of a forward proton in material *following* the CH_2 target) and for possible upstream neutron interactions that elude the above analysis.

5. Sequential reactions in the secondary target or upstream material

Here we deal explicitly with the events contributing to the broad backgrounds in Fig. 16 and in the analogous distributions for 2-stop events. From the behavior of these events and the differential cross sections we extract specifically from them, we judge them to correspond primarily to valid free *np* scattering in CH_2 either following an earlier interaction of the tagged neutron or preceding a later interaction of the forward proton. The two interactions will in some cases both have taken place within the CH_2 target. Some of the background may also arise from tagging errors associated with less than complete energy collection for the recoil protons in the tagger. A more quantitative decomposition of the observed background among these sources is discussed below. Regardless of their detailed source, the events in the tail regions of Fig. 16 are distorted because we mismeasure the scattering angle and possibly the incident neutron energy for the free *np* scattering. While a small fraction of the events within the *peak* regions in Fig. 16 may also be affected by (forward) sequential reactions, we consider them to be a valid part of the analyzed sample because the agreement between tracking and tagging demonstrates that the *np* scattering angle has been measured within our experimental resolution for all these events.

The least biased way to handle the tail events in Fig. 16 is to eliminate them from the analyzed sample. This is simple enough to do for each angle bin in event stream 2, via the software cuts requiring $|x_{\rm track} - x_{\rm tag}| \leqslant 3\sigma_x$ and $|y_{\rm track} - y_{\rm tag}| \leqslant 3\sigma_y$, where $\sigma_x \approx 0.8$ cm and $\sigma_y \approx 0.7$ cm are the widths of the narrow Gaussian peaks in Fig. 16. (The widths are dominated by the longitudinal vertex uncertainty introduced by the secondary target thickness, see Sec. III C) These cuts combine to eliminate 6.3% of the event stream 2 (CH_2-C) yield, averaged over 1-punch and 2-stop samples and integrated over scattering angle. The fraction of events removed varies slowly with *np* scattering angle, increasing by an average factor of 1.2–1.3 as one goes from c.m. angles near 180° to those near 100°, thus slightly modifying the angular distribution shape of the extracted *np* differential cross section.

The fraction of events removed and its angle dependence are qualitatively consistent with expectations. Of the 3.5% of tagged neutrons that will undergo inelastic reactions upstream of the CH_2 target, we estimate that roughly 1.5% will escape being vetoed and hence will contribute to these tails. Another 2.6% of incident neutrons or outgoing protons are expected to undergo a second reaction in the CH_2, at normal incidence. However, proton postscattering grows in importance with the proton angle emerging from the primary *np* scattering, because the proton sees a thicker target at a lower energy (implying a larger reaction cross section). We thus expect roughly 5% of *np* scattering events to be removed from the peak to the tail regions in Fig. 16 via nuclear pre- and postscattering, with the fraction increasing slowly with increasing proton angle. This estimate is consistent with the 2.4% of events seen in the tails of the $y_{\rm track} - y_{\rm tag}$ distribution. The somewhat larger losses observed in the $x_{\rm track} - x_{\rm tag}$ tails suggest an additional contribution from tagger errors, which cannot depend on *np* scattering angle.

Removal of the tail events from the analyzed *np* scattering sample requires simultaneous removal of the neutron flux that leads to such compromised events. However, we have no access to analogous cuts for event streams 1 and 3, where there is no MWPC information. Hence, we introduce the (angle-independent) flux correction factor $c_5 = 1.063 \pm 0.010$ under the assumption that the events removed from event stream 2, integrated over angle, arise from the same fraction of the tagged neutron flux. (The actual correction factors applied differ for the three data samples, reflecting differences in the fraction of events removed by these cuts.) The uncertainty allows for errors in this assumption, for example, because it neglects the energy dependence of the *np* scattering probability in the CH_2 target. The uncertainty is also intended to encompass the possible exclusion of valid single-scattering *np* events in the extreme (beyond $\pm 3\sigma$) tails of the resolution profile and the possible inclusion of events (lying beneath the peaks in Fig. 16) slightly affected by sequential reactions. This is the largest single correction and systematic uncertainty we apply.

B. Uncertainties in absolute *np* backscattering yields

Analysis issues in the extraction of the free scattering yield $N_2(\theta)$ needed in Eq. (1) can lead, in principle, to angle-dependent errors. We thus specify for each case below whether the estimated uncertainty should be considered as angle dependent and as uncorrelated from angle bin to bin.

1. Uncertainties in background subtraction via the C *target*

As described in Sec. III C, we relied heavily on the CH_2-C subtraction to remove simultaneously backgrounds due to quasifree scattering from carbon nuclei in the secondary target and to reactions induced on displaced sources. The precision of the subtraction depends on that of our knowledge of the relative target thicknesses and integrated neutron flux exposures for the CH_2 vs C runs and on the stability of beam conditions between the two sets of runs. The relative normalization, taken from cleanly (kinematically) identified *pd* scattering yields measured simultaneously, is determined with quite high statistical precision but could, in principle, deviate systematically from the more relevant ratio of tagged neutron yields. The overall precision of the relative normalization was judged from the extent to which scattering events from the aluminum target platform [see Fig. 8(a)] were successfully removed by the C subtraction. We concentrate first on this background source because its yield is not sensitive to the CH_2/C target thickness ratio.

The reconstructed $y_{\rm tag}$ distributions in the vicinity of the aluminum platform peak, for both CH_2 and C targets (see Fig. 8), could be well reproduced by the sum of a Fermi distribution and a polynomial to represent the bottom target

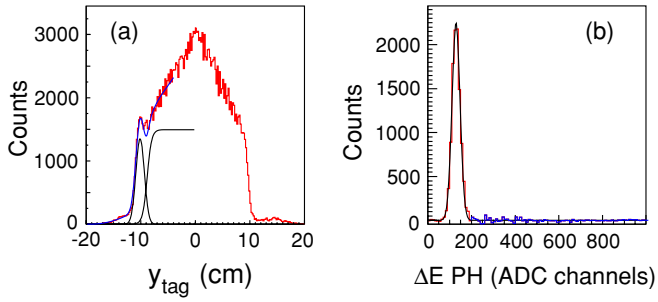

FIG. 17. (Color online) The reconstructed (a) y_{tag} spectrum for the CH_2 target before background subtraction and (b) ΔE pulse height spectrum for CH_2-C for the θ_p^{sc} bin 3°–6°. The superimposed curves in both frames represent fits used in estimating background subtraction accuracy.

edge and a Gaussian to represent the aluminum peak. The fit for the CH_2 is shown in Fig. 17(a). An analogous fit was then carried out for the C-subtracted spectrum in Fig. 8(b), fixing the positions and widths of the Gaussian and Fermi-function contributions to their common values for CH_2 and C. The ratio of events in the Gaussian peak after subtraction to that before subtraction is $(1.9 \pm 0.54) \times 10^{-3}$, providing one measure of the accuracy of the background subtraction.

An independent measure was provided for each *np* scattering angle bin by the fraction of high energy-loss tail events that survive the subtraction in ΔE pulse height spectra [see Fig. 8(c)]. The tail events were integrated by summing all counts at ΔE values more than 4σ above the center of a Gaussian fitted to the free scattering peak, as illustrated in Fig. 17(b). For the three largest θ_p^{sc} bins studied, this approach breaks down because the free scattering ΔE peak develops a substantial Landau tail and is no longer well reproduced by a Gaussian shape. But for all (12) smaller-angle bins, the ratio of tail events after to before C subtraction fluctuates about zero, with a weighted average over angle bins of $(2.97 \pm 0.24) \times 10^{-3}$. This measure is sensitive to the target thickness ratio as well as to the relative flux normalization for CH_2/C. The two measures combined do not give compelling evidence of a need for any correction and are conservatively summarized by associating with the C subtraction an angle-independent correction factor $c_6 = 1.000 \pm 0.004$.

The uncertainty estimated in this way also subsumes two other potential sources of systematic error. One is accidental coincidences between a real tagged neutron and an uncorrelated forward-going proton emerging from the GJT or the Cooler beam pipe (the most abundant sources of protons). To the extent that such coincidences passed all our cuts, they might have contributed to $N_2(\theta)$ for the CH_2 target. However, since these accidentals are independent of the presence or nature of the secondary target, they would be subtracted via the C target measurements. The second effect concerns possible proton attenuation before the hodoscope, which is required as part of the event stream 2 hardware trigger. The dominant material between secondary target and hodoscope that might have served as a source of such proton losses is the ΔE scintillator, where tertiary interactions should cause abnormal energy loss. Since the c_6 uncertainty estimate includes allowance for such abnormal pulse heights in carbon-subtracted ΔE spectra, it should also include such proton attenuation effects.

One further potential complication with the background subtraction could have arisen if there had been any appreciable hydrogen buildup on the graphite target used for the subtraction, a possibility limited by the hydrophobic nature of graphite. In this circumstance we would subtract some small fraction of the valid free scattering events and thus would introduce an effective overall normalization error in the hydrogen target thickness t_H used in Eq. (1). To estimate this effect we considered *np* scattering events forward of $\theta_{c.m.} = 90°$, where event stream 2 contained some coincidence events, with a forward-scattered neutron detected in the hodoscope and the larger-angle proton detected in the ΔE scintillator and (at least) the front two MWPCs. The angle of the proton was determined from MWPC ray-tracing, whereas that of the neutron was deduced from the hodoscope elements fired and from the position inferred from the time difference between hodoscope phototubes mounted at the two ends of each element [17]. The opening angle spectrum reconstructed for such *np* coincidence events exhibited a clear free scattering kinematic peak for the CH_2 target, but only the Fermi-smeared and acceptance-limited angular correlation characteristic of quasifree scattering for the C target (see Fig. 18). Figure 18 includes fits to the distributions for both targets based on the sum of a quadratic background and a Gaussian free scattering peak, with the peak location and width fixed for the C target to the values determined from CH_2. The fit for C is statistically consistent with no hydrogen content in the graphite target, with a 1σ limit on the hydrogen thickness of 0.4% that of the hydrogen in CH_2. We thus apply a cross section correction factor $c_7 = 1.000 \pm 0.004$ for hydrogen in the C target.

2. *Uncertainty in subtraction of corrupted events*

For the 2-stop event stream, we followed the procedure described in Sec. III B to subtract the punch-through events that had been corrupted by the electronic loss of backing detector pulse height information. There is no evidence for any systematic deviation in distribution shapes between the corrupted sample and our simulation of this sample using valid recorded punch-through events. Thus, the only uncertainty we consider is that in the normalization of the simulated sample to the corrupted events in stream 2. The normalization factors were determined from fits for the subsample of corrupted events that had valid backing detector timing signals, and the uncertainty in these normalization factors was then deduced from the change in normalization factor that caused an increase of unity in the overall χ^2 value for the fit. The effect of this normalization uncertainty on the extracted 2-stop cross sections was typically ≈0.01% and is negligible in comparison with other systematic errors. Hence, we assign a correction factor $c_8 = 1.000$ with uncertainty $< \pm 0.001$ to the subtraction of corrupted events.

3. *Losses via software cuts*

The efficiency of software cuts applied to event stream 2, but not to streams 1 and 3, was judged by comparing

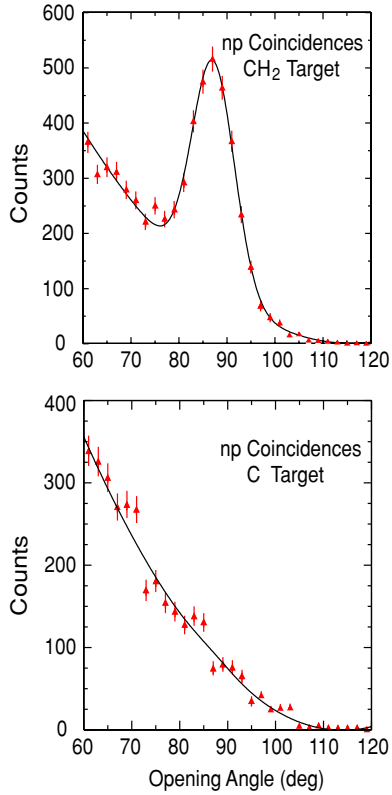

FIG. 18. (Color online) *np* scattering opening angle spectra reconstructed for events where a large-angle proton fires at least the first two MWPCs and a forward neutron appears to fire the rear scintillator hodoscope. For such coincidence events, a clear free scattering peak is seen with the CH_2 production target (upper frame), whereas no hint of such a peak is seen for the C target (lower). The solid curves are fits with a Gaussian peak superimposed on a quadratic background. The distribution shape for C reflects the quasifree *np* scattering opening-angle spectrum convoluted with the coincidence acceptance of the forward detector array.

the ratio of cross sections obtained, after CH_2-C subtraction, for all events failing vs satisfying a given cut. The most important of these cuts were on $\Delta E(\theta_p^{\rm sc})$ (see Fig. 9) and on $x_{\rm track} - x_{\rm tag}$ and $y_{\rm track} - y_{\rm tag}$. The latter cuts were already dealt with in Sec. V A5. (Another cut, on the quality of track fits, is treated together with wire chamber inefficiencies below.) The ΔE cut limits were somewhat tighter than the 4σ allowance used in estimating background subtraction accuracy (see Sec. V B1). We found the ratio of background-subtracted events failing/satisfying the ΔE cut to be 1.0%, averaged over all event streams and angles. There is no evidence for any significant angle dependence in this loss, but there are strong enough fluctuations in the losses from angle to angle or event stream to event stream that we assign a ±50% uncertainty to the losses. We thus apply a corresponding, angle-independent correction factor $c_9 = 1.010 \pm 0.005$. With this systematic uncertainty, application of the ΔE cut still reduced the overall cross section error bars slightly because the quasifree background to be subtracted decreased significantly.

4. Reaction tail losses beneath the hodoscope energy threshold

Because we did not use any software cuts on energy deposition in the rear hodoscope, we avoided the large corrections that would have been needed to account for protons lost to nuclear reactions in this hodoscope (see Fig. 10). However, if the reaction is sufficiently severe that the deposited energy falls below the hodoscope hardware threshold, then the event will have been lost in hardware to a trigger inefficiency. To estimate these potential losses, we fit the hodoscope energy spectra after CH_2-C subtraction to the sum of a Gaussian and an exponential (reaction) tail, as shown in Fig. 10. The tail was extrapolated to zero energy deposition, and the ratio of yields below to above threshold (typically set at 5–10 MeV proton energy) was thereby estimated. The loss below threshold was found to be quite consistent with 0.4% for each scattering angle bin, so that we again have applied an angle-independent correction factor $c_{10} = 1.004 \pm 0.002$.

5. Neutron polarization effects

While the stored proton beam in the Cooler was unpolarized for this experiment, the neutron production reaction selected neutrons scattered to one side of the beam (beam right) at about 14° in the laboratory frame. At this angle, the ^{2}H(p, n) charge exchange reaction that dominates our tagged beam production has a small polarization, so the beam neutrons would have been slightly polarized vertically (perpendicular to the horizontal production plane). The magnitude of this effect is $P_n^{\rm prod} \approx -0.1$, where the minus sign indicates that, for neutron production to the right of the cooled proton beam, the neutron spin points preferentially downward at the secondary target. The tagged neutron polarization can then give rise to a left-right asymmetry in *np* scattering events:

$$\varepsilon_{np}(\theta, \phi) \equiv P_n^{\rm prod} A_{np}(\theta) \cos(\phi). \tag{2}$$

Measurements and phase shift solutions at intermediate energies [24] show the *np* scattering analyzing power, A_{np}, to be a strong function of scattering angle, but with magnitude no larger than 0.12 over the angle range of interest for the present experiment. The $\cos(\phi)$ factor reflects the fact that it is only the component of the vertical neutron polarization perpendicular to the scattering plane for a given *np* event that matters.

Because the scattering yield is simply redistributed between scattering toward the left and the right, there would be no effect at all on cross sections measured with a fully left-right symmetric forward detector array. Thus, the only residual polarization effect changes the measured yield by a fraction:

$$\delta(\theta) = P_n^{\rm prod} A_{np}(\theta) \int_0^{2\pi} a(\theta, \phi) \cos(\phi) d\phi \Big/ \int_0^{2\pi} a(\theta, \phi) d\phi, \tag{3}$$

where $a(\theta, \phi)$ is the fractional detector acceptance (determined from fits such as those in Fig. 11) in the specified angle bin. The sign convention used here is that positive $\delta(\theta)$ implies that we observe a higher event stream 2 yield than we should in the corresponding $\theta_p^{\rm sc}$ bin, necessitating a correction factor $c_{11}(\theta_p^{\rm sc}) = 1.0 - \delta(\theta)$.

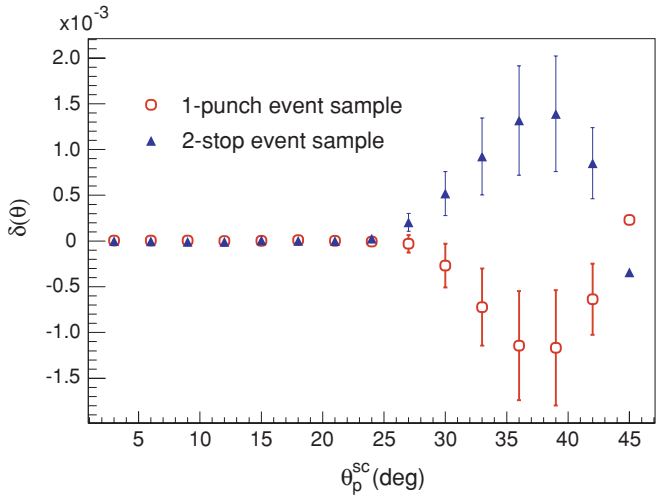

FIG. 19. (Color online) The estimated fractional cross section error introduced by neutron polarization effects for the 1-punch and 2-stop event samples, plotted as a function of *np* scattering angle.

Figure 19 shows the $\delta(\theta)$ distribution calculated for 1-punch and 2-stop data samples from Eq. (3), taking $A_{np}(\theta)$ from Nijmegen PWA93 calculations [24]. We find $\delta = 0$ for both samples at all angles $\theta_p^{\rm sc} \lesssim 25^\circ$, because the detector has full azimuthal acceptance in that region. The small corrections have opposite sign, and hence tend to cancel, for the two samples at larger angles because the 2-stop events preferentially populate the left side of the secondary target, while the 1-punch events originate mostly on the right (see Fig. 4). The latter difference is reflected in their respective $a(\theta, \phi)$ functions (see Fig. 11) used in Eq. (3).

While the *np* analyzing power and the forward detector acceptance functions are well determined in this experiment, we assign a significant uncertainty to the average tagged neutron polarization, $P_n^{\rm prod} = -0.10 \pm 0.05$, to account for contributions from production mechanisms other than charge exchange. There is correspondingly a $\pm 50\%$ uncertainty assigned to each value of $\delta(\theta)$ in Fig. 19, but these errors are completely correlated from one angle bin to another and are strongly correlated between 2-stop and 1-punch data samples. The largest net uncertainty from neutron polarization after the (separately corrected) 1-punch and 2-stop results are combined is $\pm 0.6 \times 10^{-3}$, and so we conservatively assign an angle-independent uncertainty of ± 0.001 to c_{11}.

C. Target thickness, acceptance, and efficiency errors

1. CH_2 *target thickness uncertainty*

The overall normalization uncertainty associated with t_H in Eq. (1) was determined to be $\pm 0.4\%$ (i.e., $c_{12} = 1.000 \pm 0.004$) from careful weighing of the CH_2 target used. The carbon-to-hydrogen ratio in the target was precisely constrained by the target material. The target consisted of Tivar 1000, an ultra-high-molecular-weight (6.2×10^6 u) polyethylene. Two extra hydrogen atoms per molecular chain (one on each end) cause a negligible (2×10^{-6}) deviation from the nominal 2.000 hydrogen/carbon atom ratio. Because the target only sat in a secondary neutron beam of low flux, there should not have been any appreciable deterioration in the target during the length of the run, nor was any visually evident.

2. *Acceptance uncertainty*

The acceptance uncertainty was determined independently for each angle bin by varying the most critical one or two detector geometry parameters used in the simulations (see Fig. 11) from their best-fit values until the overall χ^2 value for the simulated vs measured $\phi_p^{\rm sc}$ distribution in that angle bin increased by unity. Because the optimized values of χ^2 per degree of freedom for the different angle bins and event samples were statistically distributed about 1.14, rather than 1.00, we multiplied these acceptance changes by a uniform factor of 1.07 to arrive at final systematic uncertainties. The acceptance uncertainty is strongly angle dependent, varying from ± 0.001 at $\theta_{\rm c.m.} > 120^\circ$, where $a_\phi > 95\%$, to ± 0.017 at $\theta_{\rm c.m.} = 90^\circ$, where $a_\phi \approx 50\%$. With this evaluation method, we consider the estimated uncertainties to be largely uncorrelated from angle bin to bin.

3. *Wire chamber efficiencies*

The MWPCs were not used at all in forming a hardware trigger, but in software event reconstruction we required at least one hit registered in each of the x and y planes, for chambers 1, 2, and 3, plus a χ^2 value below an upper threshold for fitting these hits to a straight line track. Thus, the overall MWPC efficiency to use in extracting absolute cross sections is

$$\eta_{\rm MWPC} = \eta_x(1)\eta_y(1)\eta_x(2)\eta_y(2)\eta_x(3)\eta_y(3)\eta_{\rm fit\ quality}. \quad (4)$$

The efficiency of each MWPC plane was determined from tracks reconstructed without the benefit of the plane in question, based on the fraction of such tracks that produced a hit on this plane in the immediate vicinity of the reconstructed crossing point. Each of the first six factors in Eq. (4) was found to exceed 0.99 and was determined with an uncertainty $\approx \pm 5 \times 10^{-4}$. Their product is 0.985 ± 0.0013.

The factor $\eta_{\rm fit\ quality} = 0.998 \pm 0.0011$ was determined by estimating the number of free scattering events removed from the analysis by the χ^2 cut. This was done by examining ΔE spectra for individual angle bins, following carbon subtraction, for events that failed the fit quality test. The number of free scattering events (and its uncertainty) in each such spectrum was extracted by fitting Gaussian peaks of the same position and width as those used for the normal ΔE spectra, such as Fig. 17(b). There was no indication in these analyses that any of the factors in Eq. (4) varied with position on the MWPCs, or therefore with scattering angle. The overall wire chamber efficiency correction is thus an angle-independent $c_{14} = 1.0017 \pm 0.002$.

4. Trigger inefficiencies

Inefficiencies in detectors used to form the hardware trigger lead to loss of events in an unrecoverable way. Possible tagger inefficiencies do not matter here, because they lead to loss of the same fraction of events from streams 1, 2 and 3 and, hence, do not affect the cross sections determined from ratios of event yields in these streams. The two detectors used to form the hardware trigger for event stream 2, but not for stream 1, are the ΔE scintillator and the rear hodoscope. The former was viewed by four phototubes, at least three of which were required to give signals surpassing threshold in the trigger logic. In the data analysis, we were able to determine for each scattering angle bin the ratio of reconstructed free scattering events that had only three vs all four ΔE phototubes above threshold. We then estimated the ΔE trigger inefficiency under the conservative assumption that the ratio of free scattering events with two or fewer phototubes firing to those with three firing would be the same as the determined ratio of events with three to four firing. (Some illuminated locations on the scintillator lacked a direct line of sight to one or another, but never simultaneously to two, of the four phototubes.) The resulting inefficiency appears to show a systematic angle dependence, roughly represented by $0.008\cos^2(\theta_p^{\rm sc})$; i.e., the inefficiency grows as the ΔE pulse height shrinks.

We have considered two different types of potential hodoscope trigger inefficiencies. Problems in an individual hodoscope element or phototube would show up as an inefficiency localized in θ and ϕ and, therefore, as a deviation of the measured ϕ distribution for some angle bins from the simulated acceptance function. Any such localized trigger-level inefficiencies should thus be subsumed in the acceptance uncertainty calculation mentioned above.

However, an electronic inefficiency in the modules forming the hodoscope trigger logic could have caused equal fractional losses in all angle bins. A limit on this inefficiency was estimated from event stream 4 (observing tagged protons from the GJT), which included the Veto2 scintillator directly in front of the hodoscope, but not the hodoscope itself, in the trigger logic. We found that $(0.6 \pm 0.1)\%$ of these triggered events were not accompanied by hodoscope signals above threshold in both relevant phototubes, of which 0.4% have already been accounted for as reaction tail losses below threshold (see Sec. V B4).

Combining the above effects, the overall correction factor for trigger inefficiencies has been taken as $c_{15} = [1.002 + 0.008 \times \cos^2(\theta_p^{\rm sc})] \pm [0.001 + 0.004 \times \cos^2(\theta_p^{\rm sc})]$. The angle-dependent part of the uncertainty here is intended to accommodate observed fluctuations in the inferred ΔE trigger efficiency and is viewed as largely uncorrelated among different angle bins.

5. Dead time differences among event streams

Triggers in all event streams were blocked electronically at an early stage in the event trigger logic by a common busy signal reflecting electronic readout or computer processing activity in *any* of the event streams. To first order, then, the different streams should have a common dead time ($\approx$10% for typical running conditions), and the dead time should cancel in the event stream ratios from which cross sections are deduced [see Eq. (1)]. However, this cancellation is imperfect, as revealed by ratios of scaler values recording the number of tagged neutron vs tagged proton candidates before and after busy-vetoing. Typically, $\approx$1% fewer neutron tags survived the veto, and this was traced to the occurrence of bursts of electronic noise triggers from the tagger. While the loss of these noise triggers should not have directly depleted the valid sample of any event streams (i.e., (2)–(4)) that required other detectors in coincidence with the tagger, it did reduce the number of valid events recorded in the neutron flux stream (1), because all raw neutron tags, whether valid or not, contributed equally to the countdown of a (divide by 20) prescaler used for this stream. To compensate for this loss of neutron flux events, we must reduce the extracted cross sections at all angles by a factor $c_{16} = 0.991 \pm 0.005$. The uncertainty in this correction allows for possible model dependence in our interpretation of the live-time difference inferred from the scaler ratios.

D. Errors in determination of kinematic variables for *np* scattering

1. Neutron energy errors

As explained in Sec. IV, the data were analyzed in narrow neutron energy slices, with each result then being corrected slightly to extract a final overall cross section at the single mean energy of 194.0 MeV. There is an overall scale uncertainty in the tagged neutron energies that we estimate to be $\pm$150 keV, with roughly equal contributions from the energy of the stored primary proton beam in the Cooler and the energies extracted from the tagger for the low-energy recoil protons. The stored beam energy (202.46 MeV) is based on the precisely measured rf frequency (1.96502 MHz) and the Cooler circumference, which has been previously calibrated [26] to better than 1 cm out of 87 m, translating to $\pm$70 keV. In the "coasting" (rf off) mode used for data taking, the beam energy is maintained by interactions with the cooling electrons, and this may increase the beam energy uncertainty to $\approx$100 keV. The energy scale of the recoil protons is calibrated by analysis of ^{228}Th α-source spectra measured with the tagger [17], and its $\pm$100 keV uncertainty arises predominantly from thickness uncertainties for detector dead layers, combined with the quite different corrections for energy loss in the dead layers needed for protons vs the calibration α particles.

The energy scale uncertainty could be translated into a consequent cross section uncertainty as a function of angle by using Nijmegen PWA93 calculations to evaluate

$$\delta\sigma_{\rm energy}\left(\theta_p^{\rm sc}\right) = (\pm 150\,{\rm keV})\frac{\partial[d\sigma/d\Omega]\left(\theta_p^{\rm sc}\right)}{\partial E}\bigg|_{194\,{\rm MeV}}. \quad (5)$$

Although this systematic error can be angle dependent, the values at different angles would still be completely correlated, since the neutron energy scale will be off in the same direction for all angles. Hence, we prefer to not include this effect in the cross section uncertainties, but rather to quote the measured

cross sections as applying at a mean neutron energy of 194.0 ± 0.15 MeV.

2. Scattering angle errors

A systematic error $\delta\theta_p^{\rm sc}$ in determination of the centroid np scattering angle within a given analyzed bin is equivalent to an error $\delta\sigma_{\rm angle}(\theta_p^{\rm sc})$ in the measured differential cross section:

$$\delta\sigma_{\rm angle}\left(\theta_p^{\rm sc}\right) = \delta\theta_p^{\rm sc}\left.\frac{\partial[d\sigma/d\Omega]\left(\theta_p^{\rm sc}\right)}{\partial\theta_p^{\rm sc}}\right|_{194\,\rm MeV}, \qquad (6)$$

where the angular derivative of the cross section can be taken, for example, from Nijmegen PWA calculations [24]. In evaluating $\delta\theta_p^{\rm sc}$, we consider the contributions from uncertainties $\delta\theta_{\rm inc}$ in the neutron incidence angle on target deduced from the tagger and $\delta\theta_{\rm out}$ in the angle of the outgoing proton through the MWPCs:

$$\delta\theta_p^{\rm sc} = [\langle\delta\theta_{\rm inc}\rangle^2 + \langle\delta\theta_{\rm out}\rangle^2]^{1/2}, \qquad (7)$$

where the averages are evaluated over the full free scattering event sample, over the transverse coordinates $(x_{\rm tag}, y_{\rm tag})$ of the scattering origin on the secondary target, and over all scattering angles. Consistent values were extracted for the 2-stop and 1-punch samples.

The angle uncertainties were estimated within 1×1 cm^2 pixels in $(x_{\rm tag}, y_{\rm tag})$ as half the mean event-by-event difference between angles reconstructed by two different approaches. In the case of $\theta_{\rm inc}$ one method utilized tagger information only to predict the neutron trajectory, whereas the second considered instead the straight line from the neutron production vertex on the GJT, inferred from the tagger, to the intersection $(x_{\rm track}, y_{\rm track})$ of the reconstructed forward proton track with the secondary target. For $\theta_{\rm out}$ we used proton tracks reconstructed with MWPC geometry parameters that were either (i) optimized to minimize the overall χ^2 value for tracks or (ii) adjusted to increase overall χ^2 by unity. A yield-weighted average of the results over all target pixels gives $\langle\delta\theta_{\rm inc}\rangle = 1.3$ mrad and $\langle\delta\theta_{\rm out}\rangle = 0.04$ mrad.

The cross sections were not corrected for potential systematic angle errors, but we extract from Eq. (6) net systematic uncertainties of ±0.4% for $120 \leqslant \theta_{\rm c.m.} \leqslant 180^\circ$, ±0.3% for $100 \leqslant \theta_{\rm c.m.} \leqslant 120^\circ$, and ±0.1% for $90 \leqslant \theta_{\rm c.m.} \leqslant 100^\circ$. Because the extracted incidence angle differences (between the two methods described above) exhibit sizable fluctuations from one target pixel to another, or from one angle bin to another, we view these estimated uncertainties as uncorrelated from angle bin to angle bin.

3. Angle resolution smearing

Even if the centroid angle of each analyzed bin is determined accurately in the experiment, the angle resolution can lead to migration of events among bins and, hence, to a modification of the underlying angular distribution. For comparison with theoretical angular distributions, it is desirable to correct the experimental results for this smearing effect. The correction depends on the shape of the underlying angular distribution, the angle bin sizes, and the shape of the resolution profile associated with each bin. In the present case, we have excellent models for the shapes of both the underlying distribution (Nijmegen PWA93 [5,24]) and the resolution profile (a proton multiple Coulomb scattering Gaussian, neglecting single Coulomb scattering tails as these contribute to the sequential reaction tails already corrected in Sec. V A5). Furthermore, the angle bin sizes were chosen to be larger than the angle resolution width, keeping the smearing corrections small. We are thus able to make the corrections without relying on Monte Carlo simulations and their statistical limitations.

We consider protons redirected from their initial solid angle $d\Omega'$ at angles (θ', ϕ') into the observed solid angle $d\Omega_{\rm meas}$ at $(\theta_{\rm meas}, \phi_{\rm meas})$ by multiple scattering through angle

$$\Delta\theta_{\rm ms} = \cos^{-1}[\cos\theta'\,\cos\theta_{\rm meas} + \sin\theta'\sin\theta_{\rm meas}\cos\phi']. \qquad (8)$$

The redirection contributes to the measured yield whether or not the initial direction (θ', ϕ') falls within the detector acceptance. For given θ' and $\theta_{\rm meas}$, as $\phi' - \phi_{\rm meas}$ varies from 0 to π, $\Delta\theta_{\rm ms}$ varies from $|\theta' - \theta_{\rm meas}|$ to $\theta' + \theta_{\rm meas}$. The probability for multiple scattering into $d\Omega_{\rm meas}$ is taken to be a Gaussian, normalized to unit integral, of width dependent on θ' [27]:

$$P(\Delta\theta_{\rm ms})d\Omega_{\rm meas} = \frac{\exp\left[-\Delta\theta_{\rm ms}^2/2\delta\theta_{\rm rms}^2(\theta')\right]}{2\pi\,\delta\theta_{\rm rms}^2(\theta')}d\Omega_{\rm meas}, \qquad (9)$$

with rms angle [28]

$$\delta\theta_{\rm rms}(\theta') = \frac{13.6\,\text{MeV}}{T_p^{\rm lab}\left[1 + \left(1 + T_p^{\rm lab}/M_p\right)^{-1}\right]}\sqrt{\frac{0.233}{\cos\theta'}} \cdot\left[1 + 0.038\ln\left(\frac{0.233}{\cos\theta'}\right)\right], \qquad (10)$$

where $T_p^{\rm lab}$ is the lab energy in MeV of the outgoing proton, M_p is the proton mass, and 0.233 is the number of radiation lengths corresponding to half the target thickness at normal incidence. The rms angles vary from 1.0° to 2.3° over the scattering angle range covered in the experiment.

The smeared (observed) differential cross section is then given by

$$\left(\frac{d\sigma}{d\Omega}\right)_{\rm lab}^{\rm smear}(\theta_{\rm meas}) = \frac{1}{\pi}\int_0^{\pi/2}\frac{\sin\theta' d\theta'}{\delta\theta_{\rm rms}^2(\theta')}\left(\frac{d\sigma}{d\Omega'}\right)_{\rm lab}^{\rm PWA93}(\theta') \cdot\int_0^{\pi} d\phi'\exp\left[-\Delta\theta_{\rm ms}^2/2\delta\theta_{\rm rms}^2(\theta')\right]. \qquad (11)$$

In writing Eq. (11), we have made the implicit assumption that the first and subsequent scatterings occur at spatial separations that can be neglected in comparison with the distance to the solid-angle-defining detectors. This is a good approximation for the present experiment, where the target is the dominant source of the multiple scattering. The resulting correction factors, by which the observed differential cross section must be multiplied to revert to the underlying distribution, are tabulated in

TABLE II. Final differential cross section results for *np* scattering at $E_n = 194.0 \pm 0.15$ MeV, averaged over data samples.

c.m. angle (deg.)	Mult. scat. corr'n	$(d\sigma/d\Omega)_{\text{c.m.}}$ (mb/sr)	Stat. unc. (mb/sr)	Syst. unc.[a] (mb/sr)
92.7	0.946±0.005	1.87	0.06	0.03
98.8	0.975±0.003	1.95	0.05	0.02
104.8	0.989±0.001	2.28	0.05	0.02
110.8	0.995±0.001	2.56	0.05	0.02
116.8	0.998±0.001	3.00	0.05	0.02
122.8	0.999±0.001	3.47	0.06	0.02
128.8	1.000±0.001	4.01	0.06	0.02
134.9	1.001±0.001	4.75	0.07	0.03
140.9	1.001±0.001	5.35	0.08	0.03
146.9	1.000±0.001	5.98	0.08	0.04
152.9	0.999±0.001	6.63	0.10	0.04
159.0	0.998±0.001	7.59	0.11	0.05
165.0	1.000±0.001	8.89	0.14	0.06
171.0	1.007±0.001	10.69	0.19	0.07
177.0	1.014±0.001	12.03	0.34	0.08

[a]This column lists point-to-point systematic uncertainties. In addition, there is an overall cross section scale uncertainty of ±1.5%.

Table II. We assign a systematic uncertainty to the correction factor for each angle bin, ranging from ±0.001 to ±10% of the correction itself, to allow for shortcomings in our approximation that the angle resolution profile can be adequately described by multiple Coulomb scattering through half the target thickness. Different recipes for numerical evaluation of the integrals in Eq. (11) provide answers consistent to better than this estimated uncertainty. We consider these smearing correction uncertainties to be uncorrelated from point to point. The correction factor is appreciably smaller than unity for the largest outgoing proton lab angle bins, because in these cases near the differential cross section minimum more events are multiply scattered into than out of the bin.

E. Summary of angle dependence

The effect of the correction factors c_i associated with the various sources of systematic error considered in this section is cumulative, and averages 1.10, with small variations with angle and data sample, as summarized in Table I. We assume, however, that the various uncertainties are uncorrelated with one another, and we add them in quadrature to obtain final systematic error estimates. The majority of error sources we have considered are explicitly or effectively angle independent; when combined, these yield an overall absolute normalization uncertainty of ±1.5%. The uncertainties associated with our measurements of acceptance and scattering angle (both systematic angle errors and angle resolution), and with trigger inefficiencies, are considered angle dependent and uncorrelated from point to point. These sources are combined to give the net point-to-point systematic uncertainties in Table II, where we also collect our final absolute cross section measurements obtained from a weighted average over the three independently analyzed and corrected data samples (1-punch, 2-stop with $E_{p1} \leqslant 5.0$ MeV, and 2-stop with $E_{p1} > 5.0$ MeV). The final cross sections differ very slightly from those reported in Ref. [21] because of the inclusion here of the multiple scattering correction indicated in Table II. The point-to-point and normalization uncertainties combine to give an overall systematic error of ±1.6% in most angle bins.

VI. DISCUSSION

The preceding section provided a detailed catalog of the issues that must be carefully controlled to measure precise absolute cross sections with medium-energy neutron beams. To our knowledge, no previous experiments have attempted a comparable degree of control. The best existing absolute neutron-induced cross section standards at intermediate energies are from attenuation measurements of total cross sections [29], which are not suitable for calibrating neutron fluxes. It is hoped that the present results will provide a new calibration standard. The excellent agreement of our experimentally determined absolute cross section scale with that given by the Nijmegen PWA93 solution (see Fig. 14) confirms the consistency of our results with the total cross section measurements.

The level of agreement of our measurements with PWAs at $E_n = 194$ MeV is presented in more detail in Fig. 20. Here it is seen that, while the absolute cross section scale of the experimental results is in very good agreement with the Nijmegen PWA93 solution, there is a small systematic deviation in angular shape between the two: our results are higher than those of PWA93 by 2%–3% for $135 < \theta_{\text{c.m.}} < 165^\circ$ and lower by a similar amount for $100 < \theta_{\text{c.m.}} < 130^\circ$. These deviations considerably exceed our estimated

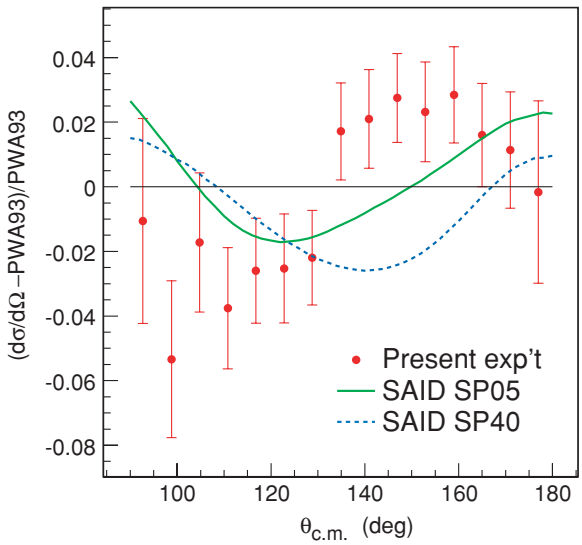

FIG. 20. (Color online) The relative differences of the present absolute *np* scattering differential cross sections and of two SAID PWA solutions [4,30] from the Nijmegen PWA93 solution [5,24], all at $E_n = 194$ MeV. The SP40 solution is from a 2003 analysis of the database from 0 – 400 MeV, while SP05 is the current SAID solution, fitted over the range 0–3.0 GeV, including the present data in the fit.

systematic uncertainty in the angle dependence. In particular, we note that the forward detector acceptance used in the former angle range is already essentially 100% (see Fig. 12), so that the extracted cross section cannot be overestimated by virtue of underestimating acceptance. Furthermore, the results for the three independently analyzed data samples agree extremely well in this angle region (see Fig. 13). We do see a possible small, statistically marginal, systematic deviation among our three data samples in Fig. 13 over the angle region from 100 to 130°, with the 1-punch cross sections falling on average a few percent below those for the two 2-stop event samples. However, even if this difference reflects a real systematic problem, it could only pull the averaged cross section down by less than 0.5% in this region, too small to account for the deviation from PWA93 in Fig. 20.

We also show in Fig. 20 the relative differential cross section differences between two recent SAID PWA solutions [4,30] and the Nijmegen PWA93. The various PWA solutions differ from one another by as much as 2%–3% also in the angle region displayed. Furthermore, we note that the SAID solution has shifted by ∼2% after inclusion of the present results in the fitted *np* database (even though that inclusion was carried out by adding our full, mostly angle-independent, systematic uncertainties in quadrature with our statistical uncertainties, thereby underweighting the present data in the fit). We conclude that the deviations between the present results and PWA93 are of the same order as the present uncertainties in the PWA solutions and most likely point to the need to refit phase shifts. We note, however, that there is a conceptual flaw in the procedures for such refitting to a database where all experiments have systematic uncertainties, but there is considerable variability in the level at which those systematic uncertainties are reported in the literature.

Finally, we address the comparison of the present results with those from the recent experiments by the Uppsala [7] and Freiburg [9] groups, both of which have been rejected from the *np* database used in the Nijmegen and SAID PWAs. As illustrated in Fig. 14 by the comparison of the two experimental results with PWA curves at the respective energies of the experiments, the present results deviate systematically from those of [7] in the steepness of the back-angle rise in cross section. These deviations are larger than the differences anticipated from the difference in neutron energy between the two experiments. There is a similar, though not quite as pronounced, systematic deviation of the present results from those of Franz *et al.* [9] shown in Fig. 1.

It is difficult to say definitively whether there might be a common problem that caused excessive cross sections near $\theta_{\mathrm{c.m.}} = 180^\circ$ in both of these earlier, completely independent and quite different, experiments [7,9]. We note only that measurements near $\theta_p^{\mathrm{sc}} = 0^\circ$, where the solid angle is vanishing, can be tricky with a secondary neutron beam of sizable angular divergence. One of the great advantages of the use of a tagged beam is that we are able in the present experiment to determine the neutron incidence angle event by event. Without such tagging information, the beam angular spread would contribute to the experimental angle resolution and thereby to migration of analyzed scattering events among proton lab angle bins. The bin migration effects in this case are more complicated than those treated in Sec. V D3, because only events that begin and end within the detector acceptance can now migrate. The acceptance for a spatially extended secondary beam depends on both incident and outgoing nucleon directions and on position of impact on the secondary target as well. In particular, the acceptance can be systematically different for the events most likely to migrate, because they preferentially populate outer regions in impact position on target, than for the events most likely to be retained within the same angle bin. Thus, the extracted cross section can suffer not only from averaging over a resolution function but also from acceptance evaluations that do not take proper account of the resolution smearing.

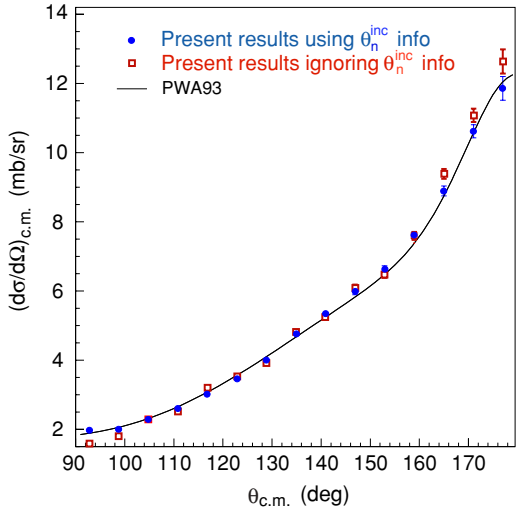

FIG. 21. (Color online) The effect on the present analysis of neglecting tagger information about the neutron incidence angle in the reconstruction of the *np* scattering angle for each event. The solid circles represent the final results (before multiple scattering corrections), while the open squares result when the scattering angle is estimated only with respect to the central neutron beam direction. Note the suppressed zero on the cross section scale.

We demonstrate these effects in Fig. 21 by comparing the present results with those we would have extracted had we chosen to ignore the neutron incidence angle information from the tagger in reconstructing the *np* scattering angle event by event. We thus bin the events in θ_p^{lab} (measured with respect to the central neutron beam direction) rather than in θ_p^{sc}. In this alternative analysis, the yield per angle bin in the numerator of Eq. (1) is altered, whereas the solid angle and acceptance functions in the denominator are not. Such neglect is seen to give rise to a systematic overestimate of the cross section at the largest angles by ∼5% and to a substantial underestimate near $\theta_{\mathrm{c.m.}} = 90^\circ$. The latter effect (opposite in sign and much larger than the effect of multiple scattering smearing summarized in Table II) can be easily understood, because the acceptance of our detector array is plunging to zero forward of $\theta_{\mathrm{c.m.}} = 90^\circ$. Here, then, events can migrate out of an analyzed bin in either direction, but can effectively migrate into the bin only from $\theta_p^{\mathrm{sc}} < \theta_p^{\mathrm{lab}}$, strongly reducing the apparent yield without an appropriate compensation in the calculated acceptance.

Similarly, near $\theta_{\text{c.m.}} = 180^\circ$ the vanishing solid angle implies that there are many more events that can migrate into a given θ_p^{lab} bin from $\theta_p^{\text{sc}} > \theta_p^{\text{lab}}$ (induced by neutrons deviating from the central beam direction) than can migrate out of the bin. When the acceptance calculation does not account for these skewed origins, the result is an overestimated cross section. The effect would differ for different experiments, depending on the angular profile of the neutron beam, including any effects from scattering off collimator edges (the present experiment used no collimators), other contributions to the angle resolution, the angle bin size used in the analysis, and the detector acceptances and acceptance evaluation procedures. The experiments in Refs. [7,9] presumably had neutron incidence angle spreads that were substantially smaller (though not as well measured) than those of the present experiment, but they also utilized considerably finer angle binning. These two differences have competing influences on the sensitivity to the beam divergence, leaving the net effect in the earlier experiments unclear without more detailed information.

VII. CONCLUSIONS

A tagged intermediate-energy neutron beam produced at the IUCF Cooler Ring has facilitated a measurement of the *np* scattering differential cross section at 194 MeV bombarding energy to an absolute precision $\approx \pm 1.5\%$ over the c.m. angular range 90°–180°. The usage of carefully matched and frequently interchanged solid CH_2 and C secondary targets permitted an accurate background subtraction, reducing reliance on kinematic cuts that might have introduced larger systematic uncertainties. The internal consistency in both magnitude and angular shape of the cross sections extracted from independent data samples characterized by substantially different neutron beam spatial and energy profiles supports the accuracy of the tagging technique. Systematic uncertainties in the measurement, affecting both the overall absolute scale of the cross sections and the angular dependence, have been carefully delineated, often via auxiliary measurements and analyses.

The present results are in reasonable agreement with the Nijmegen PWA93 calculation, over the full angular range covered, although there are systematic deviations at the 2%–3% level in the angular dependence that might be removed by minor tuning of phase shifts. In contrast, the present results deviate systematically from other recent measurements [7,9], especially in the steepness of the back-angle cross section rise. Our results thus appear to validate the omission of these earlier experiments from the database used in partial wave analyses of *np* elastic scattering, while also suggesting a conceivable experimental cause of the earlier overestimates of the cross section near $\theta_{\text{c.m.}} = 180^\circ$. As the back-angle rise is particularly influential in pole extrapolations that have occasionally been used [12,13] to extract the charged pion-nucleon-nucleon coupling constant f_c^2, the present data also bear on that coupling strength. Since our measurements at the largest angles are consistent with, or even slightly less steep than, those of the PWA93 solution, a valid pole extrapolation analysis of the present results should yield a coupling constant value no larger than that ($f_c^2 = 0.0748 \pm 0.0003$) extracted from the Nijmegen PWA [6].

ACKNOWLEDGMENTS

We thank the operations staff of the Indiana University Cyclotron Facility for providing the superior quality cooled beams and Hal Spinka and Catherine Lechanoine-Leluc for the loan of critical detector hardware needed for the successful execution of this experiment. We acknowledge the U.S. National Science Foundation's support under Grant Numbers NSF-PHY-9602872, 0100348, and 0457219.

[1] R. Machleidt and I. Slaus, J. Phys. G **27**, R69 (2001).
[2] D. R. Entem and R. Machleidt, Phys. Rev. C **68**, 041001(R) (2003).
[3] S. C. Pieper and R. B. Wiringa, Annu. Rev. Nucl. Part. Sci. **51**, 53 (2001); P. Navratil and E. W. Ormand, Phys. Rev. C **68**, 034305 (2003).
[4] http://lux2.phys.va.gwu.edu/analysis/nn_analysis.html
[5] V. G. J. Stoks, R. A. M. Klomp, M. C. M. Rentmeester, and J. J. deSwart, Phys. Rev. C **48**, 792 (1993).
[6] M. C. M. Rentmeester, R. G. E. Timmermans, and J. J. deSwart, Phys. Rev. C **64**, 034004 (2001).
[7] J. Rahm *et al.*, Phys. Rev. C **57**, 1077 (1998).
[8] W. Hürster *et al.*, Phys. Lett. **B90**, 367 (1980).
[9] J. Franz *et al.*, Phys. Scr. **T87**, 14 (2000).
[10] B. E. Bonner, J. E. Simmons, C. L. Hollas, C. R. Newsom, P. J. Riley, G. Glass, and M. Jain, Phys. Rev. Lett. **41**, 1200 (1978).
[11] D. V. Bugg and R. Machleidt, Phys. Rev. C **52**, 1203 (1995).
[12] T. E. O. Ericson *et al.*, Phys. Rev. Lett. **75**, 1046 (1995).
[13] *Proceedings of Workshop on Critical Issues in the Determination of the Pion-Nucleon Coupling Constant*, edited by J. Blomgren, Phys. Scr. **T87**, 33 (2000).
[14] M. C. M. Rentmeester, R. A. M. Klomp, and J. J. deSwart, Phys. Rev. Lett. **81**, 5253 (1998).
[15] T. E. O. Ericson *et al.*, Phys. Rev. Lett. **81**, 5254 (1998).
[16] R. A. Arndt, I. I. Strakovsky, and R. L. Workman, Phys. Rev. C **52**, 2246 (1995).
[17] T. Peterson *et al.*, Nucl. Instrum. Methods A **527**, 432 (2004).
[18] S. E. Vigdor, W. W. Jacobs, L. D. Knutson, J. Sowinski, C. Bloch, P. L. Jolivette, S. W. Wissink, R. C. Byrd, and C. Whiddon, Phys. Rev. C **46**, 410 (1992).
[19] J. Sowinski *et al.*, Phys. Lett. **199B**, 341 (1987).
[20] T. W. Bowyer, Ph.D. dissertation, Indiana University (1994, unpublished).
[21] M. Sarsour *et al.*, Phys. Rev. Lett. **94**, 082303 (2005).
[22] R. E. Pollock, Annu. Rev. Nucl. Part. Sci. **41**, 357 (1991).
[23] A. Ahmidouch *et al.*, Nucl. Instrum. Methods Phys. Res., Sec. A **326**, 538 (1993).
[24] http://nn-online.sci.kun.nl/NN/
[25] R. K. Tripathi, J. W. Wilson, and F. A. Cucinotta, NASA Technical Paper 3656 (1997) (http://hdl.handle.net/2002/13366).
[26] E. J. Stephenson *et al.*, Phys. Rev. Lett. **91**, 142302 (2003).

[27] H. A. Bethe, Phys. Rev. **89**, 1256 (1953).
[28] V. L. Highland, Nucl. Instrum. Methods **129**, 497 (1975); **161**, 171 (1979); G. R. Lynch and O. I. Dahl, Nucl. Instrum. Methods B **58**, 6 (1991).
[29] P. W. Lisowski, R. E. Shamu, G. F. Auchampaugh, N. S. P. King, M. S. Moore, G. L. Morgan, and T. S. Singleton, Phys. Rev. Lett. **49**, 255 (1982); V. Grundies, J. Franz, E. Rossle, and H. Schmitt, Phys. Lett. **B158**, 15 (1985); W. P. Abfalterer, F. B. Bateman, F. S. Dietrich, R. W. Finlay, R. C. Haight, and G. L. Morgan, Phys. Rev. C **63**, 044608 (2001).
[30] R. A. Arndt, I. I. Strakovsky, and R. L. Workman, Phys. Rev. C **62**, 034005 (2000).

International Conference on Nuclear Data for Science and Technology 2007
DOI:

95 MeV neutron scattering on hydrogen, deuterium, carbon and oxygen

P. Mermod[1], J. Blomgren[1,a], C. Johansson[1], A. Öhrn[1], M. Österlund[1], S. Pomp[1], B. Bergenwall[2], J. Klug[1], L. Nilsson[1], N. Olsson[3], U. Tippawan[4], P. Nadel-Turonski[5], O. Jonsson[6], A. Prokofiev[6], P.-U. Renberg[6], Y. Maeda[7], H. Sakai[7], A. Tamii[7], K. Amos[8], and R. Crespo[9]

[1] Department of Neutron Research, Uppsala University, Box 525, S-75120 Uppsala, Sweden
[2] Department of Nuclear and Particle physics, Uppsala University, Sweden
[3] Swedish Defence Research Agency, Stockholm, Sweden
[4] Fast Neutron Research Facility, Chiang Mai University, Thailand
[5] The George Washington University, Washington, D.C., USA
[6] The Svedberg Laboratory, Uppsala University, Sweden
[7] Department of Physics, University of Tokyo, Japan
[8] School of Physics, University of Melbourne, Australia
[9] Departamento de Fisica, Instituto Superior Técnico, Lisboa, Portugal

Abstract. Three neutron-deuteron scattering experiments at 95 MeV have been performed recently at The Svedberg Laboratory in Uppsala. Subsets of the results of these experiments have been reported in two short articles, showing clear evidence for three-nucleon force effects. In this paper, we present further discussion of the results. We obtained excellent precision in the angular range of the *nd* cross-section minimum. The data are in good agreement with Faddeev calculations using modern *NN* potentials and including 3*N* forces from a 2π-exchange model, while the calculations without 3*N* forces fail to describe the data. CHPT calculations at next-to-next-to-leading order represent an improvement compared to calculations with *NN* forces only, but still underestimate the data in the minimum region. In addition to neutron-deuteron scattering data, neutron-proton and ^{12}C(n,n) elastic scattering data have been measured for normalization purposes, and ^{16}O(n,n) data have been obtained for the first time at this energy. It was possible to extract ^{12}C(n,n') and ^{16}O(n,n') inelastic scattering cross sections to excited states below 12 MeV excitation energy. These data are shown to have a significant impact on the determination of nuclear recoil kerma coefficients.

1 Introduction

Nuclear properties and interactions can be understood *ab initio* from the basic knowledge of the nucleon-nucleon (*NN*) interaction. For this purpose, *NN* potentials, which are based on meson-exchange theories, have been developed: the most widely used ones are the Argonne AV18 potential [1], the CD-Bonn potential [2,3] and the Nijmegen potentials [4]. After proper adjustment of the free parameters, these models are able to describe very well a restricted *pp* and *np* data base below 350 MeV [5].

In three-nucleon (3*N*) systems, quantitative descriptions can be provided rigorously by using *NN* potentials in the Faddeev equations [6]. However, theoretical considerations indicate that the description of systems made of more than two nucleons is not complete if three-body forces are not taken into account : 3*N* forces can be represented by introducing a 3*N* potential in the Faddeev equations. As a first experimental evidence, the ^{3}H and ^{3}He binding energies can be reproduced model-independently taking 3*N* forces into account [7], while calculations using only *NN* interactions underestimate them by typically half an MeV [2]. The ^{4}He binding energy can also be described correctly with combined *NN* and 3*N* forces [8], indicating that the role of four-nucleon forces is not significant.

The ultimate goal of nuclear physics would be to have a single consistent theory that could describe both nucleon and nuclear properties and dynamics. Chiral symmetry breaking can be analyzed in terms of an effective field theory, chiral perturbation theory (CHPT). This model can be applied to describe consistently the interaction between pions and nucleons, as well as the pion-pion interaction. Calculations made within the CHPT framework at next-to-next-to-leading order implicitly include 3*N* forces [9,10]. Calculations at the next higher order were made recently [11,12], allowing for instance an excellent description of *NN* phase shifts.

Besides the ^{3}H and ^{3}He binding energies, a number of observables that may reveal the effects of 3*N* forces have been identified. We will concentrate our discussion to nucleon-deuteron scattering in the energy range 65−250 MeV. At these energies, significant 3*N*-force contributions are expected in the elastic scattering angular distribution [13,14] as well as for various spin-transfer observables in elastic scattering [6] and observables in the break-up process in various kinematical configurations [15,16]. In particular, for elastic nucleon-deuteron scattering, Faddeev calculations including a 3*N* potential with parameters adjusted to the triton binding energy predict that 3*N* forces affect substancially the differential cross section in the minimum region of the angular distribution [13]. Around 100 MeV, this effect is of the order of 30% in the minimum region.

Thus, a robust way to investigate 3*N* forces is to measure the proton-deuteron (*pd*) and neutron-deuteron (*nd*) elastic scattering differential cross sections. Numerous *pd* elastic scattering experiments have been performed [18–26].

[a] Corresponding author, e-mail: jan.blomgren@tsl.uu.se

A coulomb-free signal can be obtained by performing *nd* scattering experiments [27–31]. In general, for both *pd* and *nd* scattering, in the energy range 65-150 MeV the data show the expected effects of 3*N* forces in the cross-section minimum, while at higher energies, the effects tend to be too large to be accounted for by present theories. This might be due to the lack of a full relativistic treatment in the calculations [32,33]. At 95 MeV, the energy of the present work, relativistic effects are not expected to contribute significantly.

In the context of the *nd* scattering experiments, we obtained elastic scattering angular distributions for carbon and oxygen at 95 MeV. Differential cross sections for neutron inelastic scattering on carbon and oxygen to excited states below 12 MeV excitation energy could also be extracted [34]. These data are relevant for medical treatment of tumors with fast neutrons as well as in dosimetry, since the human body contains significant amounts of carbon and oxygen. Recoil nuclei from elastic and inelastic scattering are expected to account for more than 10% of the cell damage, the rest being mainly due to neutron-proton (*np*) scattering and neutron-induced emission of light ions [35,36]. The oxygen data may also be relevant for future incineration of nuclear waste in subcritical reactors fed by a proton accelerator, where the nuclear fuel might be in oxide form.

2 Results for *np* and *nd* scattering

By detecting either the scattered neutron or the recoil proton/deuteron, we were able to cover the angular range from 15 to 160 degrees in the c.m. system. By using two different detector setups, MEDLEY [37] and SCANDAL [38] in various configurations, we could keep the systematic uncertainties under control. Additionally, by measuring the *np* scattering differential cross section and, in the case where scattered neutrons were detected, also elastic scattering in carbon (i.e., the ^{12}C(n,n) reaction), the systematic error due to uncertainties in the normalization factors was minimized.

The *np* data are shown in Fig. 1. The absolute scale was adjusted to the Rahm *et al.* data [39] (filled triangles) which were in turn normalized to the well-known total *np* cross section [40]. The excellent agreement with both previous data and calculations based on *NN* potentials allows us to validate the quality of the *nd* data since the *np* and *nd* differential cross sections were measured under essentially the same conditions. Besides, the *np* data give supplementary information about the *np* angular distribution at 95 MeV (for previous data, see, e.g., Refs. [39,40]). In many experiments, neutron cross sections are measured relative to the *np* cross section [40], i.e., it is used as a cross-section standard. Neutron-proton scattering plays an important role in nuclear physics, since it can be used to validate *NN* potentials and to derive a value of the absolute strength of the strong interaction. The extensive database of *np* differential cross sections is not always consistent and, not unrelated, there are still problems with the determination of a precise value of the πNN coupling constant [5,41,42].

The *nd* results at 95 MeV in the minimum region ($80° < \theta_{c.m.} < 160°$) are shown in Fig. 2, and are compared with theoretical predictions based on Faddeev calculations [13] using the AV18 *NN* potential [1] combined with two different

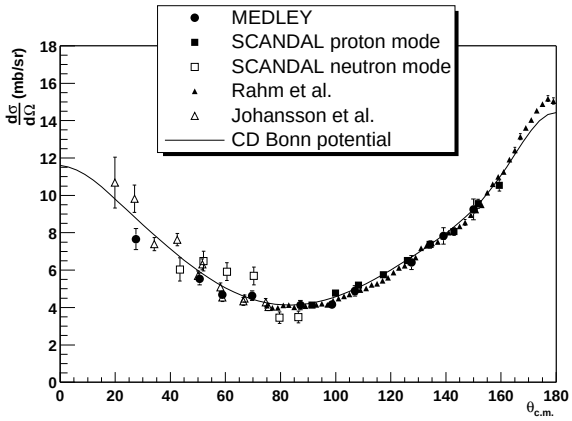

Fig. 1. The present and previous Uppsala data for *np* elastic scattering at 95 MeV. The dots and squares are the results of our *nd* experiments [28,29], and the triangles were obtained from previous *np* experiments by Rahm *et al.* [39] and Johansson *et al.* [40]. The data are compared with a calculation using the CD-Bonn *NN* potential [2].

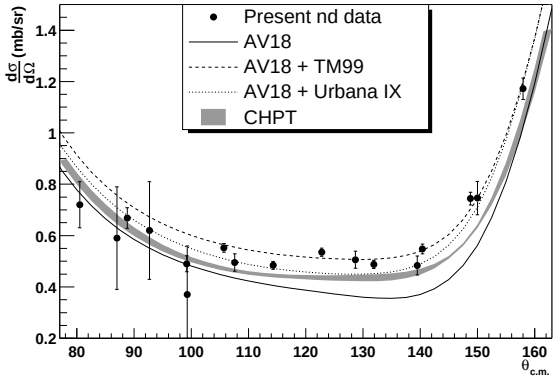

Fig. 2. The present *nd* data (filled dots) in the angular range $80° < \theta_{c.m.} < 160°$. The solid, dashed, and dotted curves were obtained from Faddeev calculations with the Argonne AV18 potential [1] without 3*N* forces, with the Tucson-Melbourne (TM99) 3*N* potential [43], and with the Urbana IX 3*N* potential [44], respectively. The gray band was obtained from chiral perturbation theory at next-to-next-to-leading order [9].

3*N* potentials (Tucson-Melbourne [43] and Urbana IX [44]), as well as predictions from CHPT [9]. It is quantitatively illustrative to compute the reduced χ^2 between our data and the calculations for the *nd* differential cross section in the minimum, i.e., all data points shown in the figure. When no 3*N* forces are included, the χ^2 is larger than 18. The best description is given by the CD-Bonn potential (version 1996) with the TM99 3*N* force, with a χ^2 of 2.1. With the AV18 potential (shown in the figure), the *nd* differential cross section is slightly better described with the TM99 3*N* potential (χ^2 = 2.3) than with the Urbana IX potential (χ^2 = 3.5). The CHPT prediction gives a χ^2 of 6.5. Note that the deviations from one may be partly due to the normalization uncertainties in the data [29,34].

3 Results for ^{12}C(n,n) and ^{16}O(n,n) scattering

Differential cross sections for elastic and inelastic neutron scattering on carbon and oxygen must be well known for a precise evaluation of the damage caused by fast neutrons in human tissue. Figs. 3 (carbon) and 4 (oxygen) illustrate how recoil kerma coefficients are obtained from the differential cross sections. The elastic neutron scattering data at 96 MeV are from Mermod *et al.* [34], Klug *et al.* [45], Salmon [46] and Osborne *et al.* [47]. The theoretical curves are predictions from the Koning and Delaroche global potential [48], the Watson global potential [49], Amos *et al.* [50], and Crespo *et al.* [51] (see Refs. [34,45] for details). In the top panels of the figures, the differential cross sections (in logarithmic scale) are plotted as functions of the neutron scattering angle in the laboratory. In the bottom panels, the distributions have been multiplied with the solid angle element $2\pi \sin\theta$ and weighed with the energy of the recoil nuclei E_R, thus illustrating the angular probability distributions for the neutrons to cause cell damage. As the solid angle vanishes at zero degrees, these distributions are no longer forward-peaked. Back-scattered neutrons transfer more energy to the nuclei than forward-scattered neutrons, and therefore the energy of the recoil nuclei increases with the neutron scattering angle. From these distributions, which peak at about 16°, we can deduce that, for elastic scattering, most of the damage is caused by neutrons scattered between 10 and 30°, but there is still a significant contribution up to 60°. With this way of plotting, the recoil kerma coefficient (and the cell damage due to elastic scattering) is proportional to the area under the distribution [34]. There are large variations among the different models, it leads to an uncertainty in the the recoil kerma coefficients of at least 10% for the theoretical calculations, while the experimental uncertainty reached with the present data is about 5%. For elastic scattering on carbon, most models are inaccurate in the region 25−35°. For oxygen, the prediction closest to the data is provided by the Koning and Delaroche potential.

For inelastic scattering on carbon and oxygen at 96 MeV to collective states up to 12 MeV excitation energy, the main contribution to the kerma from inelastic scattering is between 30 and 60°. The data obtained in this angular range (not shown in the figures) tend to be significantly underestimated (by about 50%) by the calculations [34]. Although the contribution from inelastic scattering is small compared to other processes, the disagreement between calculations and data for inelastic scattering is still responsible for a significant (about 8%) discrepancy in the recoil kerma coefficient for the sum of elastic and inelastic reactions below 12 MeV excitation energy.

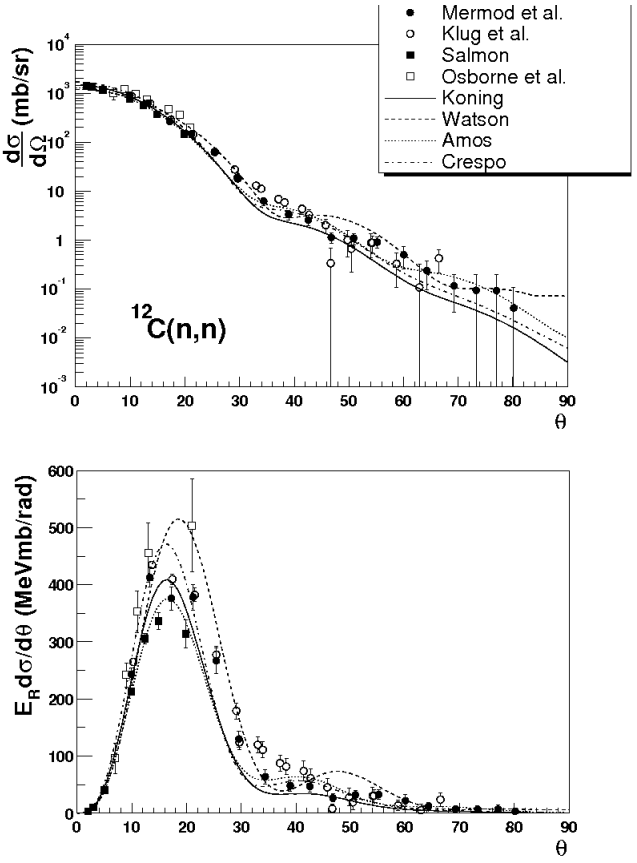

Fig. 3. Elastic neutron scattering on carbon at 96 MeV. The angle θ is the neutron scattering angle in the laboratory. The experimental data are from Refs. [34,45–47]. The elastic scattering differential cross section is shown in the top panel, and in the bottom panel, the differential cross section was multiplied with the solid angle element and with the energy of the recoil nucleus. The area under this plot is proportional to the nuclear recoil kerma coefficient for elastic scattering.

4 Conclusions

The *np* and *nd* elastic scattering differential cross sections at 95 MeV have been extensively and accurately measured. The data agree well with predictions based on *NN* and 3*N* potentials, provided that 3*N* forces are taken into account for *nd* scattering. This represents an important step to validate the approach in which *NN* and 3*N* potentials or effective field theories are used in *ab initio* models, which can be applied in systems of more than three nucleons.

As by-products of the *nd* experiments, elastic and inelastic neutron scattering differential cross sections on carbon and oxygen have been measured at 95 MeV. Experimental recoil kerma coefficients were obtained and shown to be quite sensitive to the differential cross sections in the angular range 25 – 70°. This is relevant for the evaluation of deposited doses for applications such as dosimetry and fast neutron cancer therapy.

This work was supported by the Swedish Nuclear Fuel and Waste Management Company, the Swedish Nuclear Power Inspectorate, Ringhals AB, the Swedish Defence Research Agency and the Swedish Research Council.

References

1. R.B. Wiringa, V.G.J. Stoks, and R. Schiavilla, Phys. Rev. C **51**, 38 (1995).
2. R. Machleidt, F. Sammarruca, and Y. Song, Phys. Rev. C **53**, R1483 (1996).
3. R. Machleidt, Phys. Rev. C **63**, 024001 (2001).

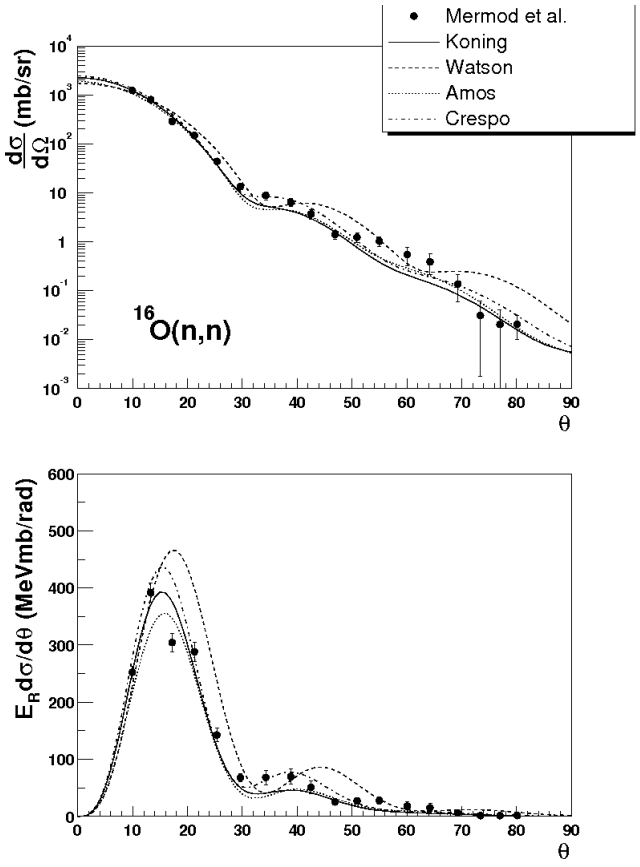

Fig. 4. Elastic neutron scattering on oxygen at 96 MeV. The angle θ is the neutron scattering angle in the laboratory. The experimental data are from Ref. [34]. The elastic scattering differential cross section is shown in the top panel, and in the bottom panel, the differential cross section was multiplied with the solid angle element and with the energy of the recoil nucleus. The area under this plot is proportional to the nuclear recoil kerma coefficient for elastic scattering.

4. V.G.J. Stoks, R.A.M. Klomp, C.P.F. Terheggen, and J.J. de Swart, Phys. Rev. C **49**, 2950 (1994).
5. R. Machleidt and I. Slaus, J. Phys. G **27**, R69 (2001).
6. W. Glöckle, H. Witała, D. Hüber, H. Kamada, and J. Golak, Phys. Rep. **274**, 107 (1996).
7. A. Nogga, A. Kievsky, H. Kamada, W. Glöckle, L.E. Marcucci, S. Rosati, and M. Viviani, Phys. Rev. C **67**, 034004 (2003).
8. A. Nogga, H. Kamada, W. Glöckle, and B.R. Barrett, Phys. Rev. C **65**, 054003 (2002).
9. E. Epelbaum, A. Nogga, W. Glöckle, H. Kamada, Ulf-G. Meissner, and H. Witała, Phys. Rev. C **66**, 064001 (2002).
10. P.F. Bedaque and U. van Kolck, Annu. Rev. of Nucl. Part. Sci. **52**, 339 (2002).
11. D.R. Entem and R. Machleidt, Phys. Rev. C **68**, 041001(R) (2003).
12. E. Epelbaum, W. Glöckle, and Ulf-G. Meissner, Nucl Phys. **A747**, 362 (2005).
13. H. Witała, W. Glöckle, D. Hüber, J. Golak, and H. Kamada, Phys. Rev. Lett. **81**, 1183 (1998).
14. S. Nemoto, K. Chmielewski, S. Oryu, and P.U. Sauer, Phys. Rev. C **58**, 2599 (1998).
15. L.D. Knutson, Phys. Rev. Lett. **73**, 3062 (1994).
16. J. Kuroś-Żołnierczuk, H. Witała, J. Golak, H. Kamada, A. Nogga, R. Skibiński, and W. Glöckle, Phys. Rev. C **66**, 024003 (2002).
17. S.A. Coon, M.D. Scadron, P.C. McNamee, B.R. Barrett, D.W.E. Blatt, and B.H.J. McKellar, Nucl. Phys. **A317**, 242 (1979); S.A. Coon and W. Glöckle, Phys. Rev. C **23**, 1790 (1981).
18. O. Chamberlain and M.O. Stern, Phys. Rev. **94**, 666 (1954).
19. H. Postma and R. Wilson, Phys. Rev. **121**, 1229 (1961).
20. K. Kuroda, A. Michalowicz, and M. Poulet, Nucl. Phys. **88**, 33 (1966).
21. G. Igo, J.C. Fong, S.L. Verbeck, M. Goitein, D.L. Hendrie, J.C. Carroll, B. McDonald, A. Stetz, and M.C. Makino, Nucl. Phys. **A195**, 33 (1972).
22. R.E. Adelberger and C.N. Brown, Phys. Rev. D **5**, 2139 (1972).
23. H. Shimizu, K. Imai, N. Tamura, K. Nisimura, K. Hatanaka, T. Saito, Y. Koike and Y. Taniguchi, Nucl. Phys. **A382**, 242 (1982).
24. H. Sakai *et al.*, Phys. Rev. Lett. **84**, 5288 (2000).
25. K. Hatanaka *et al.*, Phys. Rev. C **66**, 044002 (2002).
26. K. Ermisch *et al.*, Phys. Rev. C **68**, 051001(R) (2003).
27. H. Rühl *et al.*, Nucl. Phys. **A524**, 377 (1991).
28. P. Mermod *et al.*, Phys. Lett. B **597**, 243 (2004).
29. P. Mermod *et al.*, Phys. Rev. C **72**, 061002(R) (2005).
30. J.N. Palmieri, Nucl. Phys. **A188**, 72 (1972).
31. Y. Maeda *et al.*, submitted to Phys. Rev. C.
32. H. Witała, J. Golak, W. Glöckle, and H. Kamada, Phys. Rev. C **71**, 054001 (2005).
33. K. Sekiguchi *et al.*, Phys. Rev. Lett. **95**, 162301 (2005).
34. P. Mermod *et al.*, Phys. Rev. C **74**, 054002 (2006).
35. M.B. Chadwick, P.M. DeLuca Jr., and R.C. Haight, Radiat. Prot. Dosim. **70**, 1 (1997).
36. J. Blomgren and N. Olsson, Radiat. Prot. Dosim. **103**, 293 (2003).
37. S. Dangtip *et al.*, Nucl. Instr. Meth. **A 452**, 484 (2000).
38. J. Klug *et al.*, Nucl. Instr. Meth. **A 489**, 282 (2002).
39. J. Rahm *et al.*, Phys. Rev. C **63**, 044001 (2001).
40. C. Johansson *et al.*, Phys. Rev. C **71**, 024002 (2005).
41. J. Blomgren, N. Olsson, and J. Rahm, Phys. Scr. **T87**, 33 (2000).
42. M. Sarsour *et al.*, Phys. Rev. Lett. **94**, 082303 (2005).
43. J.L. Friar, D. Hüber and U. van Kolck, Phys. Rev. C **59**, 53 (1999); S.A. Coon and H.K. Han, Few-Body Syst. **30**, 131 (2001).
44. B.S. Pudliner, V.R. Pandharipande, J. Carlson, Steven C. Pieper, and R.B. Wiringa, Phys. Rev. C **56**, 1720 (1997).
45. J. Klug *et al.*, Phys. Rev. C **68**, 064605 (2003).
46. G.L. Salmon, Nucl. Phys. **21**, 14 (1960).
47. J.H. Osborne *et al.*, Phys. Rev. C **70**, 054613 (2004).
48. A.J. Koning and J.P. Delaroche, Nucl. Phys. **A713**, 231 (2003).
49. B.A. Watson, P.P. Singh and R.E. Segel, Phys. Rev. **182**, 977 (1969).
50. K. Amos, P.J. Dortmans, H.V. von Geramb, S. Karataglidis, and J. Raynal, Adv. Nucl. Phys. **25**, 275 (2000).
51. R. Crespo, R.C. Johnson, and J.A. Tostevin, Phys. Rev. C **46**, 279 (1992).

«Безопасный рай» вопреки власти

Ян Бломгрен,
профессор Упсальского университета (Центр ядерных технологий и кафедра нейтронных исследований), Швеция

Атом раздора

Доля «атомной» электроэнергии в Швеции составляет порядка 50%, а по ее выработке на душу населения эта страна – первая в мире. Сейчас в Швеции эксплуатируется 12 реакторов, запущенных в 1972–1985 гг. Из них 9 реакторов кипящего типа (BWR) были спроектированы в Швеции, 3 других реактора – с водой под давлением (PWR) – американские.

Использование ядерной энергии имеет политическую подоплеку во многих странах, но Швеция, по моим данным, – единственное государство, в котором правительство подало в отставку из-за разногласий в отношении ядерной отрасли (в 1978 г.)

В 1980 году был проведен референдум, предметом которого являлось будущее шведской ядерной энергетики; это событие можно назвать эхом аварии на Три-Майл-Айленде. По итогам голосования предпочтение было отдано схеме «эксплуатировать имеющиеся и не строить новые реакторы». Парламент установил срок эксплуатации реакторных установок 25 лет, и это означало: 2010 год станет последним годом функционирования шведской ядерной энергетики.

Однако с течением времени восприятие ядерной энергетики общественностью существенно улучшилось. Недавно проведенные исследования позволили установить, что подавляющее большинство населения (60–80%) согласны с эксплуатацией существующих реакторов, пока они соответствуют требованиям безопасности.

В настоящее время считается, что технически допустимый срок эксплуатации шведских ядерных энергоблоков составляет не менее 40 лет, серьезно рассматривается его продление до 60 лет. Учет этого фактора и осознание того, что вывод из эксплуатации сразу 12 энергоблоков обойдется дорого и несет в себе опасность для окружающей среды, привели к новому парламентскому решению 1997 г. об отмене остановки всех энергоблоков к 2010 году. Вместо этого было решено завершить эксплуатацию двух реакторов в течение двух лет (в качестве доказательства «серьезности» позиции парламента). Оставшиеся же 10 реакторов должны были быть остановлены через равные интервалы времени, но продолжительность этих интервалов так и не была жестко определена.

Профессор Ян Бломгрен работает на кафедре нейтронных исследований университета в Упсале. Область научных интересов – нейтронно-индуцированные ядерные реакции и их применение в энергетических технологиях, электронике, процессах трансмутации радиоактивных отходов, нейтронной терапии. Ян Бломгрен имеет порядка 170 публикаций в международных периодических изданиях и сборниках международных конференций, и выступает в роли рецензента в 5-ти международных журналах. Являясь главным руководителем образовательных программ Шведского центра ядерных технологий, на государственном уровне осуществляет координацию в сфере образования, относящегося к ядерной энергетике.

Университет Упсалы: www.uu.se/english

В связи с остановкой двух энергоблоков, решили вложить 1,5 млрд евро в модернизацию и в программы по продлению срока эксплуатации оставшихся 10-ти реакторов. Модернизация установок должна компенсировать мощность, потерянную в результате остановки двух относительно маленьких реакторов.

Все политические маневры прошедших лет привели к тому, что долгое время шведская ядерная энергетика считалась отраслью, не имеющей будущего. Редкий молодой человек ставил перед собой цель сделать карьеру в ядерной отрасли; в результате прием на ядерные инженерные специальности очень резко упал, и всего лишь несколько лет назад шведские технические высшие учебные заведения выпускали менее десятка инженеров с ядерным образованием. Из-за этого отрасль переживала тяжелые времена, связанные фактически с невозможностью обеспечить свои потребности в персонале за счет выпускников вузов. Чтобы выйти из положения, приходилось принимать инженеров других специальностей, зачастую – людей в возрасте, и переквалифицировать их для новой работы. Но в достаточно короткое время ситуация значительно изменилась. Ядерная энергетика сейчас не ассоциируется в молодежной среде с чем-то «политически некорректным», более того, на сегодняшний день в Швеции она воспринимается как некий «безопасный рай», несмотря на все разговоры политиков о закрытии реакторов в неопределенном будущем.

Оператор как вино. Требует выдержки

Шведская ядерная отрасль ежегодно принимает на работу 30–50 новых сотрудников на должности, требующие знания ядерной физики и ядерных технологий. Этих специалистов можно условно разделить на две подгруппы: (1) операторы и (2) прочие специалисты. Из их числа лишь незначительная часть (менее 10%) изучает эти предметы в университете. Подавляющее большинство имеет инженерное образование в других областях: электротехника, машиностроение, и т.п. На сегодняшний день операторы ядерных установок, как правило, имеют только среднее (high school) образование. Однако сейчас появилась тенденция к тому, чтобы вновь нанимаемые операторы имели дипломы бакалавров. Чтобы стать оператором сотрудник должен пройти многолетний карьерный путь. Это 3 (а на практике, как правило, 5) лет работы в сфере технического обеспечения АЭС и еще порядка 3-х лет обучения. Существуют две категории операторов: операторы турбин и операторы собственно реакторов. Эти сотрудники выполняют различные обязанности в БЩУ. Вначале обучаемый сотрудник получает должность оператора турбин и может продолжить обучение с целью стать оператором ядерного реактора. Учеба заключается в прохождении теоретических курсов и работе на тренажерах. Существуют соответствующие тренажеры для каждого эксплуатируемого реактора.

Наконец, существует полугодовая образовательная программа для подготовки начальников смены. Эта программа в основном сконцентрирована на вопросах организации и управления, но также включает и определенное техническое образование.

Инспекторат по надзору за ядерной энергетикой требует, чтобы штат операторов проходил дополнительное обучение, по меньшей мере, 10 дней в году, из них 5 дней уделяется отработке на тренажерах. Вполне обычная ситуация, когда человек имеет двойную специализацию, являясь, например, одновременно оператором ядерного реактора и турбины, и должен, соответственно, уделять двойную норму времени отработке на тренажерах.

Вдобавок введено обучение фундаментальным аспектам, лежащим в основе функционирования ядерного реактора. Основанием для этого стали результаты расследований причин аварий на Три-Майл-Айленде и в Чернобыле, указавшие на недостаточный уровень образованности операторов.

Кроме управления ядерным реактором существует большая категория сотрудников (не операторов), работающих над проблемами, требующими углубленных знаний о работе реактора (например, исследование процессов в активной зоне или приборное обеспечение). Они не проходят обучение на тренажерах, но должны обладать общими знаниями по физике реактора и ядерной технологии, зачастую в объеме, превышающем знания операторов.

Для удовлетворения потребности в образованных специалистах предприятия ядерной отрасли совместно основали образовательную организацию, названную «Центр ядерной безопасности и обучения персонала» (KSU). Доля участия каждого предприятия в KSU примерно соответствует доле вырабатываемой предприятием ядерной энергии. KSU не приносит прибыли в том смысле, что его владельцы платят за обучение своего же персонала. Нет и убытков. В соответствии с организацией центра, образовательные программы KSU открыты и для сторонних организаций.

KSU является собственником тренажерных центров и обеспечивает обучение практической работе. Программы, нацеленные на обучение реакторной физике, разработаны факультетом нейтронных исследований (INF) университета в Упсале. Основой этого сотрудничества является шестилетний контракт, в соответствии с которым KSU оказывает поддержку INF, и в обмен на это может требовать предоставления определенного объема образовательных услуг.

Профессорский исход

Вплоть до недавнего времени ядерное инженерное образование и ядерные исследования осуществлялись лишь в двух высших учебных заведениях: Чалмерском технологическом институте в Готенбурге и Королевском технологическом институте в Стокгольме. В Чалмерском институте есть две кафедры: реакторной физики и радиохимии (последняя занимается вопросами переработки и разделения ОЯТ). Королевский институт имеет четыре кафедры: реакторной физики, радиохимии (специализирующейся на вопросах захоронения в геологических формациях), ядерной техники и обеспечения безопасности АЭС. Профессура этих кафедр в большинстве своем уволилась несколько лет назад, примерно в один и тот же период времени, и перспективы замещения профессорско-преподавательского состава были не слишком радужными.

С целью долгосрочного укрепления и развития ядерных исследований и образования не так давно был основан Шведский центр ядерных технологий (SKC). Центр финансируется атомными станциями пропорционально доле вырабатываемой энергии, а также вестингаузским предприятием по производству ядерного топлива и Шведским инспекторатом по надзору за ядерной энергетикой (SKI).

Тот факт, что инспекторат, будучи государственным надзорным органом, принимает участие в финансировании, вероятно, требует дополнительных разъяснений. Дело в том, что согласно давней традиции, шведский инспекторат действует достаточно активно. Основная функция инспектората, предписанная ему правительством, – обеспечение радиационной безопасности. Считается, что сюда входит и поддержка образования и исследований в ядерной сфере, играющих ключевую роль в сохранении высоких стандартов безопасности. В соответствии с этим, Шведский центр ядерных технологий финансируется инспекторатом примерно на одну треть.

Центр имеет долгосрочные соглашения с тремя высшими учебными заведениями: Королевским технологическим институтом, Чалмерским технологическим институтом и университетом в Упсале. В соответствии с этими соглашениями, университеты осуществляют обучение по ядерным специальностям, за что получают финансовую поддержку от центра. Вдобавок, центр поддерживает исследовательские проекты по ядерным и сопутствующим технологиям, в которых могут принять участие ученые любого университета.

Эти соглашения по сотрудничеству позволили добиться продолжения работы всех «ядерных» кафедр, указанных выше, так как наиболее вероятно, что в противном случае объем их работы снизился бы до незначительного уровня (если вообще не до нуля). Более того, в университете Упсалы (до той поры мало связанном с ядерной энергетикой) недавно были утверждены образовательные програм-

мы по ядерным специальностям и исследования в области ядерных технологий.

Недавно центр ядерных технологий инициировал внедрение в вузы магистерских курсов по ядерным специальностям, основываясь на том, что прием в аспирантуру в шведских университетах ограничен, и это создает трудности в поддержании ядерных образовательных программ для аспирантов в каждом университете. Вместо этого были введены магистерские программы, причем реорганизованные таким образом, чтобы по ним могли обучаться студенты из любого университета страны. В практическом приложении это означает, что курсы должны быть сконцентрированы по времени, наподобие летних школ. Типичный курс, организованный таким образом, займет полную рабочую неделю. Более продолжительные курсы могут быть разбиты на несколько отдельных недель.

Такой порядок организации адаптирует курсы и для иностранных студентов. Поскольку они сжаты во времени, то по существу каждый европейский студент имеет возможность их посетить. Следует отметить, что примерно в то же время, когда Шведский центр ядерных технологий разработал новый порядок организации учебных программ, аналогичный процесс начался во всем Евросоюзе. Значительное количество европейских университетов не так давно сформировали Европейскую сеть ядерного образования (ENEN).

Один особый аспект, который необходимо учесть – это структурная взаимосвязь между высшим образованием и исследовательской деятельностью с учетом отсутствия научно-исследовательских институтов. Кроме Шведского агентства оборонных исследований в Швеции, по сути, нет исследовательских центров, соответственно, исследования по ядерным тематикам осуществляются либо силами предприятий ядерной отрасли, либо университетами.

Вследствие такой стратегии лишь незначительная часть прикладных исследований в шведских университетах финансируется за счет правительственных грантов. Бóльшая же часть финансируется за счет внешних грантов, получаемых университетами от промышленности, и ядерная энергетика не является в этом смысле исключением. Практически все исследовательские и аспирантские работы для ядерной энергетики выполняются за счет отраслевых грантов. Только высшее образование в значительной степени финансируется правительством. Предусмотренное финансирование дополнительной преподавательской деятельности по организации и проведению вышеупомянутых курсов лишь немногим больше оплаты по основной работе, и, в отсутствие других схем, преподавателю пришлось бы отрабатывать полный рабочий день за зарплату, соответствующую основному окладу. Следовательно, требуется дополнительный источник денежных ресурсов, чтобы получить необходимый преподавательский потенциал, и это возможно благодаря поддержке со стороны ядерной отрасли.

Сжатый формат привлекает

Курсы, организованные KSU – Центром ядерной безопасности и обучения персонала, – предназначены для новых сотрудников ядерной отрасли. Сжатость курсов по срокам делает их подходящими и для аспирантов. Поэтому было достигнуто соглашение между KSU и SKC (Шведским центром ядерных технологий), что при наличии вакантных мест в любой программе, проводимой KSU, могут участвовать студенты из любого шведского университета. Это привело к заметному увеличению суммарного объема читаемых курсов. Более того, сам факт прохождения курсов участниками с различными базовыми знаниями обусловливает повышенную активность студентов просто из-за необходимости преодоления профессиональных барьеров и ввиду того, что поднимаемые вопросы охватывают более широкий диапазон понятий.

Вплоть до настоящего времени такое сотрудничество практиковалось в отношении общих ядерных курсов, читаемых новому персоналу. В содержание курсов входят основы физики ядерных реакторов, термогидравлика, вопросы обеспечения радиационной безопасности. Эти дисциплины не обеспечивают глубокого погружения в предмет, и они могут быть полезны для аспирантов, работающих в областях, связанных с ядерной энергетикой, но не сфокусированных на эксплуатации реактора. Для них знания о работе реактора полезны, чтобы видеть место своей работы в общей перспективе.

Данная категория слушателей достаточно велика (по крайней мере, для Швеции), она включает около 50 аспирантов. Для специалистов, ориентированных конкретно на функционирование ядерных установок, эти курсы недостаточно фундаментальны. Пример положительного результата сотрудничества как раз в области специализированного образования: осенью 2004 г. были проведены двухнедельные курсы по вероятностному анализу безопасности, примерно половина их участников относилась к научному сообществу, а другая половина – к ядерной промышленности и надзорным органам. Этот курс осуществляется коммерческой компанией, готовой проводить обучение по мере поступления предложений. Каждая категория «студентов» была относительно маленькой, чтобы нести все расходы по обучению, но общая группа оказалась достаточно крупной, чтобы сделать стоимость обучения каждого отдельного участника реалистичной.

Недавно в качестве следующего шага было организовано сотрудничество между различными учреждениями. KSU устраивал курсы для обучения специалистов в течение нескольких лет. Но, так как сегодня эти курсы преподаются на базе университета, они доступны и для обычных студентов. Чисто по географическим причинам курсы посещаются, в основном, местными студентами, если только наличествуют свободные места. Это привело к возникновению новых аспектов обучения. Первое и основное – такой подход позволил частично внедрить ядерное образование в университет, до сих пор не занимавшийся ядерным образованием. В результате этого выделился преподавательский штат в составе пяти профессоров, и были разработаны соответствующие образовательные дисциплины. Открылись новые возможности для развития других курсов по ядерным инженерским специальностям. Второе: данные курсы быстро приобрели популярность среди студентов благодаря своему сжатому формату. Студенты особенно приветствуют то, что на занятиях присутствуют сотрудники, уже работающие в ядерной отрасли, что делает образовательный процесс более практически-ориентированным.

Маленькая страна с большим умом

Швеция – страна с маленьким населением, проживающим на относительно большой территории, что в значительной степени обуславливает сжатость курсов по времени. Подобная организация образовательного процесса достаточно хорошо подходит для интеграции в европейскую образовательную систему. Время и стоимость поездок в пределах Швеции и в пределах Европы не слишком сильно различаются; и Бельгия, к примеру, уже осуществила реорганизацию своего ядерного инженерного образования, создав похожую структуру курсов (хотя и по другим причинам). Более того, в Бельгии такая же схема утверждена и для обучения студентов. Подобная реструктуризация уже начинается и во многих странах Европы в рамках ENEN. Недавно подобный процесс по согласованию программ обучения персонала отрасли был инициирован через проект NEPTUNO.

Мы уже можем наблюдать коренные перемены образовательной системы во многих европейских странах, обусловленные болонским процессом. Задачей этого процесса является приведение образовательной системы Европы к схеме 3+2+3: 3 года бакалавриата + 2 года магистратуры + 3 года исследовательской работы и присвоение степени PhD (аналог российского кандидата наук). В данной статье проводится различие между обучением студентов по инженерным специальностям и обучением в аспирантуре с целью получения PhD, но уже через несколько лет четкое различие между этими этапами перестанет существовать. Мы приближаемся к ситуации, когда то, что сегодня является последним курсом профессионального образования студентов или первым курсом аспирантуры, превратится в один этап обучения, т.е. станет частью образовательной программы магистра. Принимая во внимание все, что обсуждалось выше, областью сосредоточения усилий ядерной образовательной структуры ENEN станет, вероятно, именно магистерское образование.

По моему мнению, рост популярности и качества ядерного инженерного образования вполне возможен и в краткосрочной перспективе. Но даже в этом случае, насколько я могу предвидеть, ядерная отрасль вряд ли сможет заполнить хотя бы половину вакантных мест инженерами и кандидатами (PhD), получившими образование именно по ядерным специальностям. Однако ядерная энергетика на сегодняшний день является полностью сформировавшейся, развитой отраслью, а во всех развитых отраслях вакантные должности зачастую занимаются людьми, имеющими некое общее техническое образование, которые затем для выполнения своих профессиональных обязанностей дообучаются по специализированным программам. Подобная ситуация уже долгое время существует в целлюлозно-бумажной, лесной, горнодобывающей промышленности и т.п. – т.е. в пресловутых развитых отраслях. По этой причине вряд ли роль дополнительного обучения персонала ядерной отрасли уменьшится, даже если университетские образовательные программы изменятся в лучшую сторону.

Швеция – настолько маленькая страна, что мы просто не можем допустить дублирование усилий. В этой статье я представил несколько примеров, как в течение последних лет удавалось достичь положительного результата при взаимодействии между различными организациями. Я не верю, что все возможности сотрудничества с целью рационального использования человеческих ресурсов были исчерпаны. Наоборот, я предвижу интенсификацию такого сотрудничества. Следует подчеркнуть, что эффективное использование живых ресурсов не является единственной выгодой, которую можно извлечь из сотрудничества, поскольку благодаря такому сотрудничеству появляется возможность улучшить и качество образования. Когда встречаются специалисты из разных областей – выявляются новые проблемы и возможности, это и обеспечивает, в большей или меньшей степени, гарантию качества образования.

Перевод Юрия Коряковского

Еропейская сеть ядерного образования (ENEN)

Ян Бломгрен,
Шведский центр ядерных технологий, факультет нейтронных исследований университета Упсалы, Швеция

Франц Мунц,
Учебный центр ядерной энергетики, Буртан, Бельгия

Питер Поль де Регг,
Национальный институт ядерной науки и техники, Сакле, Франция

Джозеф Сафье,
Комиссариат по атомной энергии, Франция; Национальный институт ядерной науки и техники, Сакле, Франция

Объединяйтесь!

Необходимость сохранения, усиления и укрепления ядерных знаний была широко осознана во всем мире буквально несколько лет назад. Среди всего прочего, в 2001 году группа экспертов официально рекомендовала Европейской Комиссии «создавать образовательные сети для поддержания ядерных знаний» [1]. Текущая ситуация такова, что в программах европейских систем высшего образования ядерная техника пока еще представлена в достаточно полной мере, хотя не всегда и не везде. Однако в соответствии с данными наблюдения, некоторые области ядерного образования находятся в критическом положении, включая такие важные с точки зрения обеспечения безопасности предметы, как реакторная физика и ядерная термогидравлика. Более того, в некоторых странах наблюдаются явные недостатки образования по дисциплинам, относящимся к конечному этапу ядерного топливного цикла, обращению с отходами и выводу ядерных объектов из эксплуатации.

Чтобы переломить это рискованное положение, европейским странам крайне важно вступать в более тесное сотрудничество для решения означенной проблемы. Координация и совершенствование в сфере ядерного образования должны иметь возможность реализации на международном уровне с целью сохранения и передачи знаний в пределах всей Европы. Это жизненно необходимо для соответствующего стандартам безопасности и экономической целесообразности проектирования, эксплуатации и демонтажа ныне существующих и будущих ядерных энергетических установок. Именно для выполнения этих задач и была сформирована ENEN – Европейская сеть ядерного образования – некоммерческая организация, чьей «родиной» можно считать Францию. Эту международную организацию можно рассматривать как шаг к созданию виртуального Европейского ядерного университета, символизирующего активное сотрудничество между национальными организациями, ответственными за ядерное образование.

ENEN предлагает своим «студентам» сертификат европейского магистра в области ядерной техники. Рассмотренная концепция ENEN совместима с планируемой гармонизированной структурой европейского высшего образования, предусматривающей степени бакалавра и магистра. При этом основной целью является достижение высокого качества ядерного образования в Европе посредством стимуляции обмена студентами и преподавателями, взаимной проверки качества предлагаемых программ, а также через тесное сотрудничество с авторитетными исследовательскими коллективами университетов и лабораторий. Разработанная программа обучения «ядерного» магистра состоит из рекомендованных курсов по общеинженерным и собственно ядерным дисциплинам, формирующим фундаментальные знания; кроме того, в ней предусмотрены углубленные курсы и практика. Некоторые углубленные курсы являются также частью программ для докторантов.

Вторую важную составляющую деятельности ENEN можно назвать продолжением профессионального развития (Continued Professional Development) для специалистов, работающих в ядерной отрасли. Содержание соответствующих учебных программ для этой группы обучаемых должно отвечать запросам промышленности и надзорных органов, поэтому требуется создание специальной организации, ответственной за оценку качества и аккредитацию программ по данному направлению.

Об авторах

Профессор **Ян Бломгрен** работает на факультете нейтронных исследований университета в Упсале. Выступает в роли рецензента в 5-ти международных журналах. Являясь главным руководителем образовательных программ Шведского центра ядерных технологий, на государственном уровне осуществляет координацию в сфере ядерного образования в Швеции.

Франц Мунц является координатором межуниверситетских программ по обучению магистров в области ядерной техники. Занимает должность научного секретаря комиссии экспертов Центра ядерных исследований SCK•CEN (Бельгия); основатель и глава лаборатории коррозии в SCK•CEN. В 1998–2006 гг. – координатор научных исследований, руководитель кандидатских (PhD) проектов в SCK•CEN. С 2006 г. – заведующий исследовательским реактором BR2.

Питер Поль де Регг с 2004 г. – генеральный секретарь ENEN. В течение 20 лет являлся ответственным лицом за планирование, управление, координацию и руководство научно-исследовательской деятельностью Центра ядерных исследований SCK•CEN (Бельгия). В 1997–2004 гг. – занимал пост главы физической, химической и приборной лаборатории МАГАТЭ в Шиберсдорфе.

Джозеф Сафье – президент ассоциации ENEN. В 1991–2002 гг. – генеральный директор реактора в Улиссе, Франция. С 1998 г. – декан факультета ядерной техники в Национальном институте ядерной науки и техники в Сакле, Франция. В настоящее время является также координатором проекта NEPTUNO.

Два в одном

В рамках 5-го научного и образовательного проекта по атомной энергии Евроатома (1998–2002) Европейская Комиссия поддержала проект по европейскому ядерному инженерному образованию, в котором приняли участие 22 университета и исследовательских центра [2]. В процессе его реализации были определены основные составляющие образования «ядерного» магистра и учреждена организация ENEN [3].

Следует особо подчеркнуть, что ENEN была создана на основе «восходящего» принципа: сеть сформирована без участия правительств стран ЕС; вообще – без какой-либо идущей сверху инициативы. Отправной точкой стало формирование коллектива активных профессоров, специализирующихся в ядерных науках и сопутствующих областях, которые увидели необходимость (и возможность) предпринять определенные усилия. Отсутствие централизованного руководства, навязанного «сверху», означает, что основные составляющие проекта утверждаются по соглашению большинства участников. Конечно, сам процесс выработки решений при этом затягивается, но по достижении соглашения его претворение в жизнь происходит без проволочек.

Поскольку ENEN не имеет полномочий по управлению деятельностью университетов, то стратегия по продвижению ядерного образования неизбежно должна основываться на доброй воле ее участников. Такое положение дел и обусловило подход, при котором основы организации университетов, входящих в ENEN, не затрагиваются. Как и прежде, студенты числятся в своих университетах и получают в них образование. Если студент сдает ряд экзаменов в соответствии с критериями ENEN, он получает сертификат, удостоверяющий присвоение ему степени европейского магистра в области ядерной техники.

В настоящее время происходят глобальные изменения образовательной системы во многих европейских странах в соответствии с **Болонским процессом**, нацеленным на гармонизацию всех систем высшего образования в европейских странах с приведением их к системе 3+2+3: первые три года обучения в вузе затрачиваются на обязательный этап с целью получения степени бакалавра. Результатом следующих 2-х лет обучения станет степень магистра, за которой следует три года исследовательской работы и степень кандидата наук (PhD).

Чтобы смягчить неразбериху в самом наименовании – «ENEN», следует сразу же сказать, что аббревиатуре ENEN исторически было приписано два различных значения. Во-первых, ENEN – это европейский проект (называвшийся «европейская ядерная инженерная сеть» (European Nuclear Engineering Network) – ENEN), чья активная фаза приходилась на 2002–2003 гг. Результатом реализации этого проекта стало создание организации «Европейская сеть ядерного образования» (European Nuclear Education Network), также с сокращением ENEN. Несмотря на то, что все участники проекта ENEN ныне являются членами сети ENEN, в нее впоследствии вошло гораздо больше членов. Собственно, изменение названия было предложено Европейской Комиссией на основании ряда причин. Ниже приведены основные составляющие проекта ENEN.

300 кредитов за магистра наук

Как упомянуто выше, была учреждена степень европейского магистра в области ядерной техники. Это введение совместимо с болонской философией высшего образования для европейских инженеров/ученых (6 полных семестров для присвоения степени бакалавра, еще 4 – для степени магистра).

Полный учебный план, который необходимо выполнить для получения степени магистра, состоит из курсов, одобренных ENEN. Степень магистра может быть присвоена студенту только после обучения в течение 10 полных семестров, или, другими словами, получения 300 т.н. **кредитов**, соответствующих инженерному образованию. Один кредит подразумевает учебную нагрузку в 30 часов, полный семестр соответствует 30 кредитам или 900 часам учебной нагрузки [4].

Как минимум два семестра, эквивалентные 60 кредитам, должны быть обязательно посвящены «ядерным» предметам, чей список состоит из ряда базовых курсов, совмещенных с факультетской учебной программой, и проекта/диссертации по специальности.

Студенты зарегистрированы в аккредитованном ENEN «материнском» вузе и могут «зарабатывать» требуемые кредиты в других университетах, входящих в ядерную сеть. «Материнский» вуз присваивает степень магистра по ядерным технологиям на основе набранного количества кредитов. ENEN от имени всех своих членов присваивает степень «европейский магистр» в области ядерной техники, если определенная доля кредитов (например, 20 или 30) получены за пределами «материнского» университета. Эти кредиты, в частности, можно получить, выполнив проект/диссертацию «за рубежом», включив также в план некоторые углубленные специализированные курсы.

Работа на сохранение

Целью ассоциации ENEN является сохранение и развитие высшего ядерного образования и профессионализма. Эта цель реализуется посредством сотрудничества между европейскими университетами, включенными в образовательные и исследовательские программы по ядерным специальностям, отраслевыми исследовательскими центрами и собственно ядерной отраслью. В настоящее время членами ENEN являются 35 университетов и 6 исследовательских центров. Опираясь на поддержку 5-й и 6-й целевых программ Европейского Сообщества, ENEN выдает сертификаты «европейского магистра» по ядерным технологиям. Были созданы и внедрены в университеты соответствующие курсы (включающие базовый, обязательный набор предметов и дисциплины, выбираемые студентом). При поддержке ядерной отрасли и международных организаций были организованы пробные «пилотные» курсы и испытания образовательных программ. ENEN вносит вклад в организацию ядерных знаний не только в рамках Европейского Союза, но и на международном уровне, сотрудничая с сетями в Азии, Канаде и США, и принимая участие в деятельности Всемирного ядерного университета (WNU).

В ENEN предусмотрено два типа членства: действительные члены, представляющие научное сообщество и имеющие легальный статус в стране Евросоюза (или в стране-кандидате на вступление в ЕС), обеспечивают высокий научный уровень образования по ядерным дисциплинам в комбинации с исследовательскими разработками, предъявляют высокие требования к приему абитуриентов и студентов; и «союзные» организации, также имеющие легальный статус в Евросоюзе и долгосрочные отношения с действительными членами в области исследований и образовательной деятельности, выразившие поддержку ENEN.

Цели ассоциации ENEN

Основные цели, определенные ENEN в отношении высшего образования, следующие:

- развить более скоординированный подход к образованию в области ядерной техники и «ядерных» наук в Европе,
- объединить европейское образование в вопросах, касающихся радиационной безопасности и защиты от атомной радиации,
- достичь оптимального сотрудничества и разделения научных ресурсов на национальном и международном уровне с учетом интересов «конечных» пользователей (атомной промышленности, законодательных органов и т.д.),
- создать и поддерживать базу ценных для Евросоюза «ядерных» знаний,
- организовать и поддерживать адекватное обеспечение человеческими ресурсами проектирования, строительства, эксплуатации и технического обслуживания в инфраструктуре ядерной отрасли (в частности для АЭС),
- поддерживать необходимый уровень опыта и профессионализма для безопасного использования ядерной энергии и применения радиации в промышленности и медицине.

Цели и структура ассоциации ENEN сформулированы в Договоре, который, в свою очередь, следует рекомендациям 5-го целевого проекта ENEN, где основная цель ENEN оговорена следующим образом: «Сохранение и дальнейшее развитие высшего ядерного образования и профессионализма в ядерной сфере». Основные цели перечислены ниже:

- выдача сертификатов ENEN европейским магистрам в области ядерной техники,
- поощрение и поддержка исследований аспирантов,
- развитие обмена студентами и преподавателями между членами ENEN,
- утверждение системы критериев для взаимного признания специалистов,
- стимуляция и укрепление отношений между университетами, исследовательскими лабораториями ядерной отрасли, промышленностью и надзорными органами,
- гарантия качества ядерного инженерного образования и исследовательских работ,
- создание стимулов и увеличение привлекательности ядерного образования для абитуриентов, студентов и молодых ученых.

Критерий качества

Работа внутри ENEN выполняется **пятью комиссиями**. Комиссия ENEN по преподаванию и науке (TAAC) сформирована для контроля эквивалентности учебных программ по ядерному образованию в университетах-членах ENEN и их координации. Комиссия по углубленным курсам и научным исследованиям (AC&RC) отвечает за связь между вузами ENEN и исследовательскими лабораториями, а также с другими подобными сетями. Пользуясь устойчивыми контактами с исследовательскими центрами, университетами и промышленностью, AC&RC утверждает темы магистерских и кандидатских (PhD) диссертаций и практики. AC&RC также оказывает студентам поддержку в перемещениях между университетами. Следующая структура – Комиссия по обучению персонала и промышленным проектам (T&IPC) определяет запросы ядерной отрасли в отношении профессиональных знаний своих специалистов и организует учебные курсы по различным предметам, представляющим интерес с точки зрения членов ENEN, надзорных органов и предприятий ядерной отрасли. Комиссия по обеспечению качества (KAC) разрабатывает и внедряет критерии качества, которые должны выполняться членами ENEN в процессе разработки и преподавания учебных курсов. KAC оценивает и контролирует, насколько текущие члены ENEN и организации-кандидаты соответствуют ряду установленных критериев. Наконец, Комиссия по управлению качеством (KMC) определяет и устраняет недостатки в областях научного знания, относящихся к ядерной отрасли.

От Европы — ко всему миру

Спустя три года с момента своего основания, ENEN выполнила множество разнообразных задач и внесла весомый и признанный вклад в области европейского высшего образования и исследовательской деятельности. Финансовая поддержка со стороны Европейской Комиссии внесла существенный вклад в реализацию всех названных достижений. Хотя в настоящее время поле деятельности ENEN и ограничено научным и инженерным ядерным образованием, ENEN планирует расширить область своих интересов и вложить усилия также в развитие «ядерных» дисциплин, таких, как защита от радиации, радиохимия, переработка РАО. В планы ENEN входит дальнейшее распространение деятельности и внедрение, помимо системы высшего образования, в область промышленности и государственных органов; с перспективой их включения в число членов ENEN.

«Стартуя» с базового и углубленного университетского образования, ENEN намеревается разработать и скоординировать учебные программы для ключевых специальностей атомной промышленности, надзорных органов и прочих областей, где применяется ионизирующее излучение; и обеспечить взаимное признание этих программ на международном уровне. ENEN собирается продолжать участие в целевых проектах ЕС, особенно в тех, что касаются высшего образования и исследований. Наконец, ENEN стремится к укреплению связей с Мировым ядерным университетом (WNU) и сетями ядерного образования в Азии, Северной Америке и прочих мировых регионах. Таким образом, ENEN в составе своих управляющих органов, комиссий и членов собирается выполнить этот комплексный план и, таким образом, внести существенный вклад в развитие ядерных знаний не только внутри Евросоюза, но и на мировом уровне.

Последние проекты ENEN

NEPTUNO

В рамках 6-го исследовательского и учебного проекта Евроатома по атомной энергии (2002–2006) Европейская Комиссия поддержала проект «Ядерная Европейская Платформа Образовательных Организаций и Университетов» («Nuclear European Platform of Training and University Organisations», NEPTUNO) [5]. В этом проекте участвуют 35 партнеров из областей промышленности, образовательных организаций, университетов и исследовательских лабораторий.

Напомним, что проект ENEN был начат с целями «сохранять, расширять и укреплять ядерные знания». Эти же цели перешли и получили дальнейшее развитие в проекте NEPTUNO. Однако если ENEN концентрирует усилия на высшем образовании, то деятельность NEPTUNO направлена на дальнейшее профессиональное развитие работающих специалистов. Актуальность проекта NEPTUNO заключается в интернационализации и глобализации атомной промышленности и атомной энергетики, из чего вытекают требования мобильности и признания квалифицированного лицензированного персонала ядерной отрасли прочими организациями. Собственно, для удовлетворения этих требований, а также с целью развития систем обучения персонала перед непосредственной работой в ядерной отрасли и был запущен проект NEPTUNO. Современные тенденции в отношении сотрудничества между обучающими, исследовательскими организациями и Высшей Школой имеют своих сторонников. Среди всего прочего, внимание уделяется переобучению инструкторов и преподавателей и модульным схемам обучения персонала, которому не требуется прохождение полного курса высшего образования. Следует учитывать отличие термина «обучение» (training), используемого в отношении деятельности NEPTUNO, от термина «образование» (education), относящегося к базовым схемам обучения в вузах. Соответственно, проект NEPTUNO ориентирован как на «тренинг» (техников, инженеров), так и на образование (магистров, PhD, докторов).

ENEN-II

Основная цель проекта ENEN-II (запущенного 1 октября 2006 г.) – закрепить результаты и достижения ассоциации ENEN и ее партнеров, реализованные в процессе выполнения проектов ENEN и NEPTUNO, и еще более расширить поле деятельности ENEN.

Проект ENEN-II ставит три основные цели:

– Укрепить позицию ENEN внедрением модульных образовательных программ, предложенных и разработанных за последние несколько лет и протестированных на проверочных курсах. Также планируется применить на практике критерии оценки курсов; выявить их эффективность, приняв к рассмотрению отзывы обучаемых лиц и организаций, являющихся их конечными «потребителями», а также других заинтересованных организаций. С другой стороны, планируется объединить и организовать в хорошо продуманную и доступную систему разрозненные веб-сайты, базы данных и информацию по учебным курсам; за основу этой информационной системы взята аналогичная схема для проекта NEPTUNO.

– Расширить деятельность ENEN за пределы университетского образования в области профессионального и профессионально-технического обучения, укрепляя, таким образом, взаимодействие и сотрудничество между университетами, исследовательскими и учебными центрами и промышленностью, с целью добиться лучшего соответствия учебных курсов требованиям промышленности и достичь взаимного признания квалификационных степеней сотрудников ядерной отрасли по всей Европе.

– Расширить деятельность ENEN и выдвинуться за пределы дисциплин, относящихся к ядерной технике (а конкретно – к проектированию, строительству и эксплуатации ядерных энергетических установок), в более широкую область, включающую защиту от атомной радиации, обращение с радиоактивными отходами, радиохимию, вывод из эксплуатации и применение ядерных технологий в промышленности.

Некоторые итоги

Итак, в конце 90-х годов внутри Европейского Сообщества была признана необходимость сохранения, развития и укрепления ядерных знаний. Организация ENEN создана с целью решения этих задач «снизу» по инициативе заинтересованных лиц. ENEN – некоммерческая организация, действующая на законных основаниях с целью сохранения и развития высшего ядерного образования. И если вначале сферой приложения усилий ENEN являлось высшее образование в области ядерной техники, то впоследствии круг интересов расширился и включил в себя также профессиональное обучение (training) специалистов ядерной отрасли и продолжает расширяться, охватывая другие «ядерные» предметы, например, радиационную безопасность.

Усилия, предпринятые в последнее время для развития ядерных знаний, катализировали формирование сетей в области как высшего ядерного образования, так и профессионального обучения. Однако до сих пор остается ключевым вопрос: удается ли привлечь больше студентов (или, вернее, больше способных студентов)? Хотя процесс все еще находится в ранней стадии развития, и обоснованные заключения делать еще рано, данные предварительных наблюдений указывают на положительный эффект в отношении как качества, так и количества студентов.

Ссылки: 1. EUR 19150 EN, «Strategic issues related to a 6th Euratom Framework Programme (2002–2006)». Scientific and Technical Committee Euratom. p. 14. **2.** ENEN. http://www.sckcen.be/ENEN. **3.** ENEN. http://www.enen-assoc.org. **4.** ECTS. http://europa.eu.int/comm/education/programmes/socrates/ects_en.html. **5.** NEPTUNO. http://www.sckcen.be/NEPTUNO

Перевод Юрия Коряковского

ФотоPRоба

Рекламное агентство «PRo Атом» объявляет о начале проведения интернет - конкурса «Фото PRоба» Ждем от вас красивых, образных, серьезных или шутливых, словом, интересных снимков. Конкурс будет проходить с 1 февраля по 1 мая 2007 года на страницах портала.

www.proatom.ru

www.infomirspb.ru

ИНФОМИР
каталоги нового поколения

Оборудование. Металлообработка.

Химическая промышленность.

Строительство.

Судостроение. Судоходство.

Энергетика. НефтеГаз.

Тираж каждого печатного каталога – 5000 экз.
Формат - А4, 300-500 страниц, в т.ч. полноцветные страницы;
Электронная версия каждого издания на сайте ИнфоМир;
Тысяча компакт-дисков – весь год на профильных выставках;
Периодичность выхода – ежегодно по каждому из 5 направлений.

ДЛЯ ТЕХ, КТО НАХОДИТ...

ООО «ИнфоМир»
197376, Санкт-Петербург, ул. Льва Толстого, 7, оф.408
тел./факс (812) 740-47-98
e-mail: mail@infomirspb.ru

Differential cross section and analyzing power measurements for $\vec{n}d$ elastic scattering at 248 MeV

Y. Maeda,[1,*] H. Sakai,[2,3] K. Fujita,[4] M. B. Greenfield,[5] K. Hatanaka,[4] M. Hatano,[2] J. Kamiya,[6] T. Kawabata,[1] H. Kuboki,[2] H. Okamura,[4] J. Rapaport,[7] T. Saito,[2] Y. Sakemi,[4,†] M. Sasano,[2] K. Sekiguchi,[3] Y. Shimizu,[4,‡] K. Suda,[1,§] Y. Tameshige,[4] A. Tamii,[4] T. Wakasa,[8] K. Yako,[2] J. Blomgren,[9] P. Mermod,[9] A. Öhrn,[9] M. Österlund,[9] H. Witała,[10] A. Deltuva,[11] A. C. Fonseca,[11] P. U. Sauer,[12] W. Glöckle,[13] J. Golak,[10] H. Kamada,[14] A. Nogga,[15] and R. Skibiński[10]

[1]*Center for Nuclear Study, The University of Tokyo, Bunkyo, Tokyo 113-0033, Japan*
[2]*Department of Physics, The University of Tokyo, Bunkyo, Tokyo 113-0033, Japan*
[3]*RIKEN, Institute of Physical and Chemical Research, Wako Saitama 351-0198, Japan*
[4]*Research Center for Nuclear Physics, Osaka University, Ibaraki, Osaka 567–0047, Japan*
[5]*International Christian University, Mitaka, Tokyo 181-8585, Japan*
[6]*Japan Atomic Energy Agency, Tokai, Ibaraki 319-1195, Japan*
[7]*Department of Physics, Ohio University, Athens, Ohio 45701, USA*
[8]*Department of Physics, Kyushu University, Higashi, Fukuoka 812-8581, Japan*
[9]*Department of Neutron Research, Uppsala University, S-75120 Uppsala, Sweden*
[10]*Institute of Physics, Jagiellonian University, PL-30059 Cracow, Poland*
[11]*Centro de Física Nuclear da Universidade de Lisboa, P-1649-003 Lisboa, Portugal*
[12]*Institut für Theoretische Physik, Universität Hannover, D-30167 Hannover, Germany*
[13]*Institut für Theoretische Physik II, Ruhr-Universität Bochum, D-44780 Bochum, Germany*
[14]*Department of Physics, Faculty of Engineering, Kyushu Institute of Technology, Kitakyushu 804-8550, Japan*
[15]*Institut für Kernphysik, Forschumgszentrum Jülich, D-52425 Jülich, Germany*

(Received 13 November 2006; published 19 July 2007)

The differential cross sections and vector analyzing powers for nd elastic scattering at $E_n = 248$ MeV were measured for 10°–180° in the center-of-mass (c.m.) system. To cover the wide angular range, the experiments were performed separately by using two different setups for forward and backward angles. The data are compared with theoretical results based on Faddeev calculations with realistic nucleon-nucleon (NN) forces such as AV18, CD Bonn, and Nijmegen I and II, and their combinations with the three-nucleon forces (3NFs), such as Tucson-Melbourne 99 (TM99), Urbana IX, and the coupled-channel potential with Δ-isobar excitation. Large discrepancies are found between the experimental cross sections and theory with only $2N$ forces for $\theta_{\mathrm{c.m.}} > 90°$. The inclusion of 3NFs brings the theoretical cross sections closer to the data but only partially explains this discrepancy. For the analyzing power, no significant improvement is found when 3NFs are included. Relativistic corrections are shown to be small for both the cross sections and the analyzing powers at this energy. For the cross sections, these effects are mostly seen in the very backward angles. Compared with the pd cross section data, quite significant differences are observed at all scattering angles that cannot be explained only by the Coulomb interaction, which is usually significant at small angles.

DOI: 10.1103/PhysRevC.76.014004 PACS number(s): 21.30.−x, 21.45.+v, 24.10.Jv, 25.40.Dn

I. INTRODUCTION

Studies of few-nucleon systems allow us to test current models of nuclear forces through comparisons of precise data and rigorous theoretical predictions. Modern NN potentials, such as AV18 [1], CD Bonn [2], and Nijmegen I, II, and 93 [3], very accurately reproduce a rich set of experimental NN data up to a laboratory energy of 350 MeV. These realistic NN interactions are, at least partially, based on the traditional meson-exchange picture.

When applied to many-body ($>2N$) systems, the NN potentials fail to predict experimental binding energies. Theoretical predictions underestimate binding energies by 0.5–1 MeV for ^{3}H and ^{3}He and by 2–4 MeV for ^{4}He [4,5]. For heavier nuclei, disagreements become larger as demonstrated by calculations using stochastic techniques [6,7]. These results indicate the necessity of the introduction of many-body interactions. The three-nucleon force (3NF) is considered to be the most important among them. Present-day 3NF models, such as the Tucson-Melbourne (TM) [8] and the Urbana IX 3NF [9], are mostly based on 2π exchange between three nucleons with the intermediate Δ-isobar excitation [10]. These forces can provide additional binding when included in the nuclear Hamiltonian. Taking appropriate parameters, one can reproduce the correct binding energies of $3N$ and $4N$ systems [4,5]. Addition of the 3NF drastically improves the description

*Department of Physics, Kyushu University, Higashi, Fukuoka 812-8581, Japan; yukie@kutl.kyushu-u.ac.jp
†Cyclotron and Radioisotope Center, Tohoku University, Sendai, Miyagi 980-8578, JAPAN
‡Center for Nuclear Study, The University of Tokyo, Bunkyo, Tokyo 113-0033, Japan
§Research Center for Nuclear Physics, Osaka University, Ibaraki, Osaka 567-0047, Japan

 ©2007 The American Physical Society

of low energy bound states of up to $A = 10$ nuclei [7]. On the other hand, nuclear forces recently derived from chiral perturbation theory (χPT) have become available for laboratory energies below 100 MeV and lead to a comparable reproduction of the $2N$ data set [11–13]. The χPT approach is expected to give more systematic understanding of nuclear forces than the traditional approach.

Elucidation of the properties of 3NFs is one of the principal topics in nuclear physics. Nucleon-deuteron (Nd) scattering is expected to be a good probe for a detailed investigation of 3NFs. Cross sections [14–20] and spin observables, such as analyzing powers [21–24], spin correlation coefficients [25], and polarization transfer coefficients [26,27] have been measured for elastic Nd scattering. Large discrepancies between these data and theoretical predictions based on exact solutions of the Faddeev equations with only modern NN forces are reported. These discrepancies are particularly significant in the angular region of the cross section minima and at energies of incoming nucleons above about 60 MeV [28]. However, concerning the differential cross sections and vector analyzing powers, the inclusion of the 2π-exchange 3NF models such as TM-3NF or Urbana IX-3NF into the calculations removes many of the discrepancies. This result clearly shows 3NF effects in the $3N$ continuum and forms a basis to test new theoretical 3NF force models. In contrast, theoretical calculations with 3NFs still have difficulties in reproducing data of some spin observables.

In Ref. [27], the precise data for the cross section and spin transfer coefficients of the ^{2}H$(\vec{p}, \vec{p})^2$H reaction at 250 MeV are reported. The large discrepancies between cross section data and theoretical calculations based on NN forces are only partially removed by including 3NFs. This contrasts with the case of 135 MeV pd elastic scattering reported in Ref. [18] where inclusion of 3NFs leads to good agreement between data and calculations. This implies that at higher energies, not only spin observables but also cross sections indicate the deficiencies of the present 3NF models. The energy dependence of the discrepancies found in Ref. [27] is similar to that observed in the total nd cross section [29,30] where inclusion of 3NFs only partially improves the agreement with the data at higher energies. In Ref. [30], it is indicated that at higher energies, corrections to the nd total cross section resulting from relativistic kinematics are comparable in magnitude to the effects of 3NF. An estimation of the magnitude of relativistic effects is required before coming to any conclusion regarding the origin of the remaining discrepancy for the cross section at 250 MeV.

In pd reactions, in addition to nuclear forces, the Coulomb interaction between two protons is present. Despite recent efforts to introduce the Coulomb interaction in the calculations of elastic pd scattering [31–34], no results were available for energies as high as 250 MeV until quite recently [35,36]. A direct comparison of nd and pd data is the simplest form for studying the importance of Coulomb effects in the three-nucleon system. To study the 3NF forces in the absence of the Coulomb interaction, we measured the ^{2}H$(\vec{n}, n)^2$H elastic reaction using a 248 MeV polarized neutron beam at the Research Center for Nuclear Physics (RCNP) of Osaka University. The cross sections and analyzing powers were measured over a wide angular range $\theta_{\mathrm{c.m.}} = 10°$–$180°$. To cover such a wide angular range, we applied two methods: detection of recoiled deuterons via a magnetic spectrometer for the backward angles, and detection of scattered neutrons via a time of flight (TOF) method for the forward angles.

The experimental details are presented in Secs. II and III. In Sec. IV we briefly describe the basics of $3N$ scattering theory and how relativistic corrections are incorporated into the Faddeev calculations. The data are compared with the theoretical predictions in Sec. V, and conclusions are given in Sec. VI.

II. EXPERIMENTAL PROCEDURE FOR BACKWARD SCATTERING

The measurements in the backward angular region ($\theta_{\mathrm{c.m.}} \geqslant 60°$) were carried out at the (n, p) facility [37] constructed in the west RCNP experimental hall. The neutron beam was produced by the ^{7}Li$(\vec{p}, \vec{n})^7$Be reaction, and it subsequently bombarded the deuteron targets. The recoiled charged particles were momentum analyzed by the large acceptance spectrometer (LAS). The elastic ^{1}H$(\vec{n}, p)n$ reaction was measured to calibrate the intensity of the neutron beam as well as the acceptance of the LAS.

A. Polarized neutron beam

The polarized proton beam was provided by the high-intensity polarized ion source (HIPIS) [38]. The beam was extracted from HIPIS and injected into the Azimuthally Varying Field (AVF) cyclotron. The radio frequency (RF) of the AVF cyclotron was 14.496 MHz with a beam-pulse period of 69.0 ns. The preaccelerated proton beam was accelerated in the Ring cyclotron up to 250 MeV. The beam was single-turn extracted and transported to the (n, p) facility through the WS course [39].

The beam polarization was monitored continuously by two beamline polarimeters BLP1 and BLP2 placed in the beamline. The beam polarization was measured using the ^{1}H$(\vec{p}, p)^1$H reaction [40]. Both polarimeters used polyethylene films as hydrogen targets. The scattered and recoiled protons were detected in coincidence by a pair of plastic scintillators placed at $\theta_{\mathrm{lab}} = 17.0°$ and $70.9°$. Four sets of detectors were placed in left, right, up, and down directions.

The asymmetry measured by the polarimeters contains contributions of the quasi-elastic $(\vec{p}, p)$ reaction from the carbon nucleus. The analyzing power for this reaction is different from the analyzing power of the free pp scattering. The effective analyzing power of the polarimeter, including hydrogen and carbon contributions at a proton energy of 250 MeV at $\theta_{\mathrm{lab}} = 17.0°$, was measured to be $A_y = 0.362 \pm 0.003$ [27]. A typical value of the proton polarization was 0.6 during this experiment.

Figure 1 shows the schematic view of the (n, p) facility. The primary proton beam was achromatically transported to a ^{7}Li target mounted in a neutron production chamber. This chamber was placed in between the pole gap of the C-shape clearing magnet [41] which was inclined by 24.05° with respect to the vertical axis, allowing the proton beam to be deflected to the beam dump in the floor.

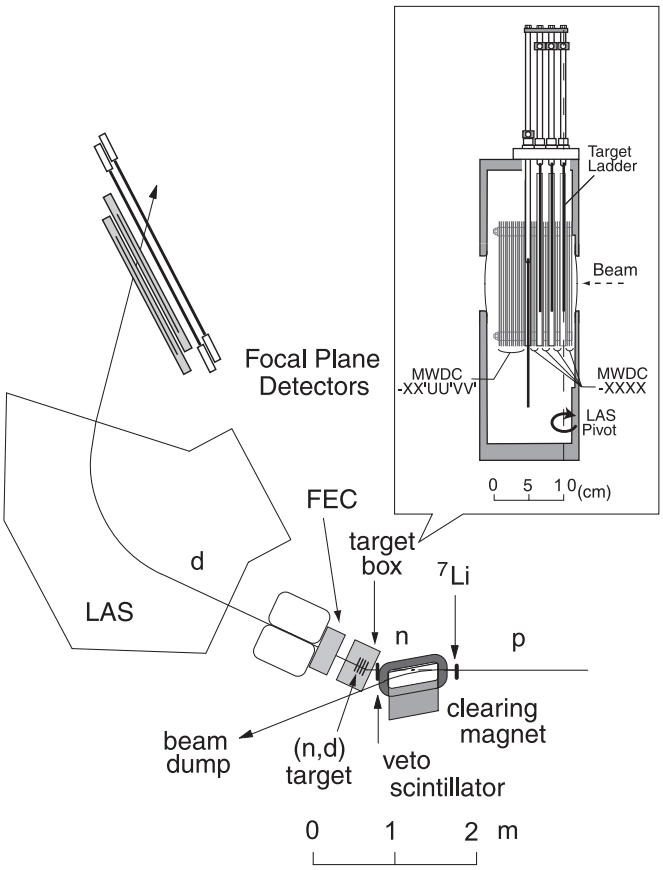

FIG. 1. Schematic view of (n, p) facility at RCNP. This facility mainly consists of a vacuum chamber for the neutron beam production, a clearing magnet for sweeping the primary beam, and a segmented target system with two MWDC boxes. The recoiled charged particles are momentum analyzed by the LAS and detected at the focal plane.

The "quasi-mono-energetic" polarized neutron beam was produced by the ^{7}Li$(\vec{p}, n)^7$Be reaction in the vacuum chamber. We selected the produced neutrons corresponding to the transitions to both the ground state and the first excited state at 0.43 MeV in ^{7}Be. The energy and spread of the neutron beam were 248 MeV and 2 MeV full width at half maximum (FWHM), respectively.

The produced neutron beam traverses the clearing magnet and passes through the vacuum window of a 10 μm-thick aramid film at the end of the vacuum chamber. The neutrons further pass through a veto counter made of 1-mm-thick plastic scintillator with a size of $40^W \times 34^H$ cm^2 which was positioned just downstream of the vacuum chamber. Signals from this counter are used to reject the events regarded as due to charged particles. The typical count rate of this veto counter is 400 kHz when a 250 nA proton beam bombards a ^{7}Li target with a 560 mg/cm^2 thickness.

The differential cross section and polarization transfer coefficient for the ^{7}Li$(\vec{p}, n)$ reaction at 0° are $\frac{d\sigma}{d\Omega}_{\rm lab} = 37.4 \pm 1.1$ mb/sr [42] and $D_{NN} = -0.28 \pm 0.05$ [43], respectively. Thus the typical intensity and polarization of the resulting neutron beam over the deuteron target area of $30^W \times 20^H$ mm^2 were estimated to be 2×10^6/s and $P_n = 0.2$, respectively.

B. Targets

The (n, p) facility is equipped with a segmented target system. The advantage of such a target system is the use of several targets, thus increasing the total target thickness while maintaining good angular resolution, yet without sacrificing energy resolution. General features of the target system are similar to those developed at TRIUMF [44]. In the present setup, we used two multiwire drift chamber (MWDC) boxes, called the target box and the front-end chamber (FEC) box, between the clearing magnet and the LAS. The target box has ten wire planes (X_1-X_2-X_3-X_4-$XX'UU'VV'$) and the FEC box has six wire planes ($YY'VV'UU'$).

The target box has four target ladders. Each target ladder is positioned behind four X_i-wire planes. Because the MWDC planes are only sensitive to charged particles, the specific target from which the recoiling particle is emitted can be identified, thus making it possible to correct for the energy loss of recoiled particles in the downstream targets. For deuteron targets, we used four films of self-supporting deuterated polyethylene (C^2H_2, denoted in the following as CD_2) [45] with thicknesses of 100–220 mg/cm^2. In addition to deuteron targets, we used polyethylene (CH_2) films with thicknesses of 90–190 mg/cm^2 as proton targets for the np measurements. Graphite targets were also employed for the purpose of carbon background subtraction.

The trajectory of the outgoing particles were measured with six wire planes ($XX'UU'$VV$'$) in the target box and by the FEC. Both MWDC boxes are rotated around the LAS pivot according to the setting angle of LAS. Thus, the various target areas presented to the neutron beam depended upon the LAS setting.

A gas mixture of argon (50%) and ethane (50%) was used for the counter gas. For the np measurements, hydrogen in the chamber gas could be a source of background. However, the hydrogen content of the gas was less than 1% of that in the polyethylene targets, so the uncertainty in the data caused by hydrogen contamination is smaller than the systematic uncertainty of the target thickness.

C. Measurements

The recoil deuterons or protons were momentum analyzed by LAS [46], which has a large momentum bite of $p_{\rm max} = 1.3 p_{\rm min}$ with an angular acceptance of 20 msr. Such a large acceptance allows us to cover the angular range of $\Delta\theta_{\rm lab} = \pm 3.5°$ in one setting. It also covers an effective target size of $30^W \times 20^H$ mm^2. The intrinsic energy resolution of LAS is better than $\Delta E = 100$ keV for 250 MeV protons.

The focal plane detectors consisted of a pair of vertical drift chambers (VDC) [47] and two planes of ΔE plastic scintillation counters. Each VDC consisted of wire planes with the XU configuration.

D. Data reduction

Data reduction included particle identification, ray tracing, and background subtraction. First of all, the outgoing deuterons (protons) were identified by using the particle TOF

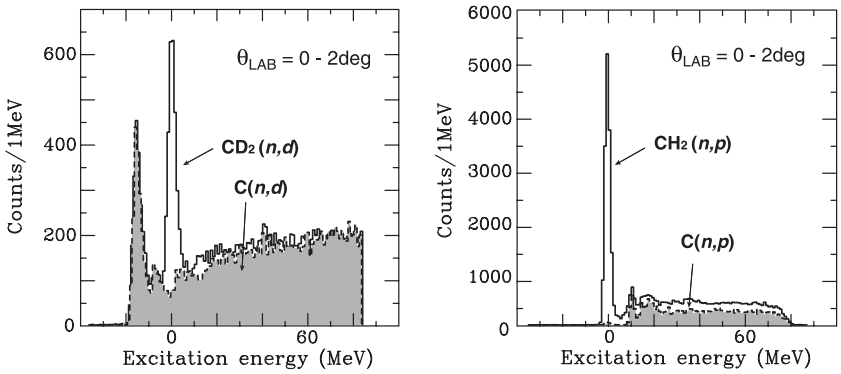

FIG. 2. Solid lines in left and right panels show the spectra of $CD_2(n, d)$ and $CH_2(n, p)$, respectively. Shaded spectra were obtained from measurements with graphite targets. By subtracting the spectra of graphite targets from those of CD_2 and CH_2, we obtained the spectra of *nd* and *np* elastic scattering.

through the spectrometer and the charge information in the plastic scintillation counters at the focal plane. The protons and deuterons were clearly distinguished from each other. The energy of the recoiled particle was obtained by using the ion optical matrix of the LAS. The information from MWDCs of the target system was used to correct for the energy loss in targets and deduce the reaction angle. Figure 2 shows the spectra obtained with CD_2 (left side) and CH_2 (right side) targets. In the figure, the spectra obtained with graphite targets are also shown by shaded area. Normalization factors were determined from target thicknesses and beam charges without additional parameters. By subtracting the normalized spectrum of the graphite target from that of the CD_2 or CH_2 target, we obtained the yields of the *nd* and *np* elastic scatterings, respectively.

III. EXPERIMENTAL PROCEDURE FOR FORWARD SCATTERING

The measurements for the forward angle region ($\theta_{\text{c.m.}} \leqslant 60^\circ$) were carried out at the RCNP neutron time-of-flight (NTOF) facility [48]. The neutron beam, produced by the ^{7}Li$(p, n)^7$Be reaction, bombarded a deuteron target. Energies of the scattered neutrons were determined via TOF, with neutron detectors located at a 70 m flight path. A deuterated liquid scintillator target (LST) was used as the deuteron target and coincidence measurements of neutrons and deuterons were performed.

A. Polarized neutron beam

The polarized proton beam was accelerated to 250 MeV by the Ring cyclotron and transported to the N0 experimental hall. The beam pulsing device, which is installed in the injection line between the AVF and the Ring cyclotrons, was used to reduce the wraparound of slow neutrons from preceding beam pulses. In the present study, one of every three beam pulses was used, resulting in a beam pulse interval of 207 ns.

The beam polarization was monitored by a beamline polarimeter (BLP) placed in the beamline between the Ring cyclotron and the N0 experimental hall. The polarimetry of the BLP is the same as that described in Sec. II A.

Figure 3 shows a schematic view of the NTOF facility. The primary proton beam was transported to the ^{7}Li target within a vacuum chamber and then swept into the beam dump in the wall by the swinger magnet. The energy of the neutrons thus produced was 248 MeV with a spread of 2 MeV FWHM. The vacuum chamber has an exit window of polyethylene with a thickness of 1 mm. The produced neutrons passed through the window and bombarded the deuteron target. The active deuteron target was located 2 m downstream from the ^{7}Li target at an angle of 0° with respect to the incident proton beam. The scattering angle of the ^{2}H(n, n) reaction was varied between $\theta_{\text{lab}} = 0^\circ$–$38^\circ$ ($\theta_{\text{c.m.}} = 0^\circ$–$60^\circ$) by moving the positions of the ^{7}Li target along the proton beam trajectory and adjusting the positions of the deuteron target accordingly. The neutron detector position was fixed in the TOF tunnel at a distance of 70 m from the ^{7}Li target for all scattering angles.

B. Targets

A deuterated liquid scintillator BC537 was used as an active deuteron target. Coincidence measurements of neutrons and protons were performed to reduce background events. The liquid target was contained in a 1 mm thick aluminum cylinder with a diameter of 9 cm and length of 6 cm. This container had a window of hard glass (Pyrex) to which a photomultiplier tube (PMT) was attached through a light guide. A booster circuit was installed in the base of the PMT to compensate for the reduction in gain during high counting rates. The inside of the container was coated with MgO_2 reflecting paint. A reservoir tube was connected to the container to absorb the expanded volume of the liquid scintillator.

A veto counter of a $70^W \times 90^H \times 0.1^t$ cm^3 plastic scintillator was positioned 10 c.m. upstream of the active target. Signals from this counter were used to reject events due to charged particles.

To remove background events originating from γ rays, we introduced neutron-gamma ($n\gamma$) discrimination, which is based upon the difference between the pulse shapes for the different type of radiations. To distinguish the different pulse shapes, the integrated charge from two analog-to-digital converter (ADC) gates with different integration times were obtained for each event. One gate covered the peak region of the light pulse and had a width of 100 ns (peak ADC), and the other corresponded to the tail component and had a width of 350 ns (tail ADC).

The *np* elastic scattering using an NE213 liquid scintillator as the proton target was measured for the purpose of normalization.

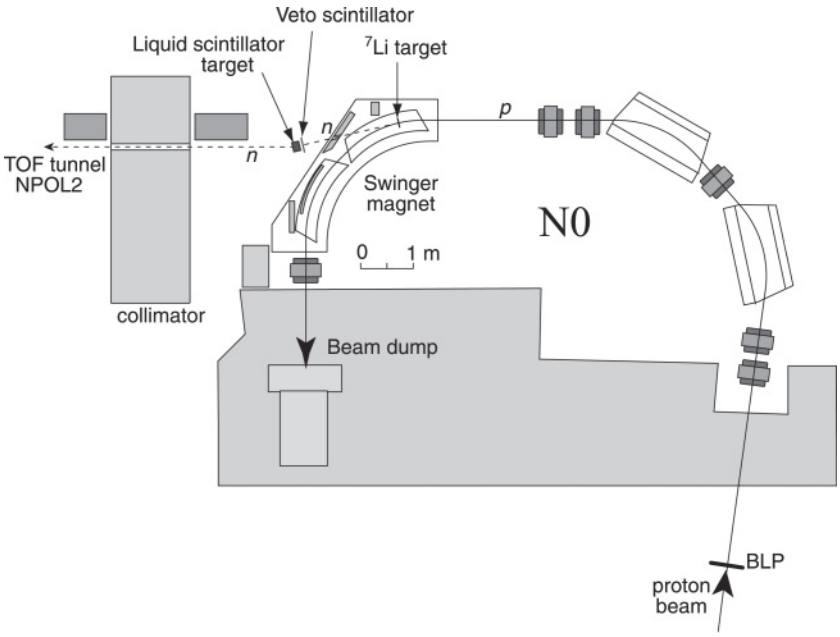

FIG. 3. Schematic layout of neutron time-of-flight (NTOF) facility at RCNP. This facility mainly consists of a swinger magnet, thick collimator wall, 100 m TOF tunnel, and neutron detector NPOL II. Scattered neutrons and the recoiled deuterons are detected by the NPOL II and the active deuteron target, respectively.

C. Measurements

The scattered neutrons traversed the 70 m flight path in the TOF tunnel and were subsequently detected by the neutron detector NPOL II [49]. It consists of six planes of two-dimensionally position-sensitive neutron detectors. The upstream four planes are BC519 liquid scintillator counters with dimensions of $1^H \times 1^W \times 0.1^t$ m^3, and the other two planes are BC408 plastic scintillator counters with the same dimensions. A PMT was attached to each corner (left-up, left-down, right-up, right-down). Three sets (left, middle, right) of thin plastic scintillators with a size of $102^H \times 35^W \times 0.5^t$ cm^3, placed in front of each neutron detector, distinguished neutrons from charged particles. Pairs of PMTs and light guides were attached to the tops and bottoms of these plastic counters. The neutron detection efficiency was determined from the measurement for the ^{7}Li$(p, n)^7$Be(g.s.+0.43 MeV) reaction, which is known to have an almost constant center-of-mass cross section of $\sigma_{\text{c.m.}}(0^\circ) = 27.0 \pm 0.8$ mb/sr over a wide energy range [42]. The total efficiency for the six planes of neutron detectors was measured to be $25.0 \pm 0.8\%$ when the threshold level of the light output was set to 5 MeV$_{ee}$. The energy of the detected neutron was determined by its TOF, defined as the calibrated time difference between the neutron trigger and RF signal.

D. Data reduction

Data reduction included determination of the neutron TOF, particle identification in the active targets, and background subtractions.

Scattered neutrons were identified at the NPOL II, the energies of which were determined from their calibrated TOF. In addition, events originating from the neutron beam were selected by applying the $n\gamma$ discrimination method to the active targets. To discriminate neutron events from γ events, we calculated the ratio of peak-ADC to tail-ADC as

$$\text{ADC}_{\text{ratio}} = (\text{ADC}_{\text{tail}} - \alpha)/\text{ADC}_{\text{peak}}, \quad (1)$$

where the constant α was determined empirically. The correlation between peak-ADC and the ADC ratio as well as the gate applied for selection of valid neutron events is illustrated in the left panel of Fig. 4. Most γ rays and background neutrons were rejected. In that case, the events of neutron elastic or inelastic scattering at low excitation energy from the carbons in the active target did not contribute to the true coincidence events, because the energies of recoiled carbons were smaller enough than that of recoiled deuterons. Remaining background events and the contribution from carbons were removed by subtracting the accidental coincident events. The timing information of the liquid scintillator target was used in this process. The middle and right panels of Fig. 4 show the energy spectra of nd and np elastic scattering, respectively, including the accidental backgrounds (white histogram) and that of the accidental backgrounds only (gray histogram). By subtracting the spectrum of accidental events, yields of the elastic scattering peak were obtained.

IV. THEORETICAL FORMALISM

The energy of this work is just above the pion production threshold at 215 MeV. Realistic NN potentials have been obtained by analyzing the NN database up to 350 MeV, corresponding to the same center-of-mass energy as 259 MeV in the nd system. All formalisms dealt with in this section do not include pion production, the use of which with the NN potentials is still acceptable at 250 MeV.

A. Formulation with 3NFs

The breakup operator T of the $3N$ system, in which nucleons interact through the NN potential V and the $3N$ force V_4, obeys the equation [50,51]

$$T = tP + (1 + tG_0)V_4^{(1)}(1 + P) + tPG_0T + (1 + tG_0)V_4^{(1)}(1 + P)G_0T\,. \quad (2)$$

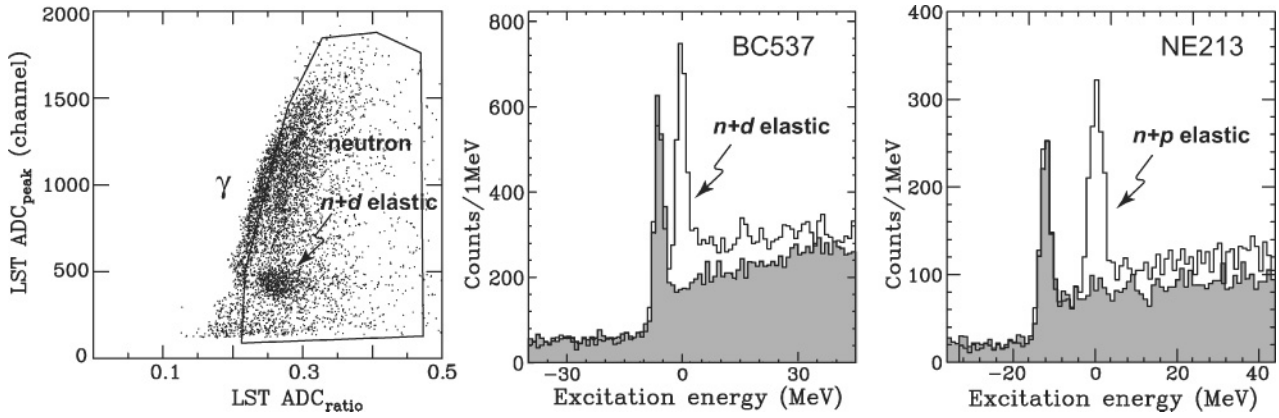

FIG. 4. Left panel shows the discrimination of neutron beam events from γ beam events; cluster of nd elastic events can be seen. Middle and right panels show the spectra at $\theta_{\rm lab} = 13^\circ$ obtained with the BC537 and NE213 scintillators. White and gray histograms represent the energy excitation spectra corresponding to true coincidences and accidental coincidences, respectively.

Here t is the two-body t-matrix resulting from V through the Lippmann-Schwinger equation. The potential $V_4^{(1)}$ is symmetric under exchange of nucleons 2 and 3. Together with $V_4^{(2)}$ and $V_4^{(3)}$ they sum up to V_4. The quantity G_0 is the free $3N$ propagator and the permutation operator $P = P_{12}P_{23}+P_{13}P_{23}$, where P_{ij} interchanges nucleons i and j. By use of T, the elastic scattering cross section is obtained from the elastic scattering transition matrix element $\langle\phi'|U|\phi\rangle$

$$\langle\phi'|U|\phi\rangle = \langle\phi'|PG_0^{-1} + V_4^{(1)}(1+P) + PT + V_4^{(1)}(1+P)G_0T|\phi\rangle\,. \quad (3)$$

The initial state $|\phi\rangle = |\vec{q}_0\rangle|\phi_d\rangle$ is composed of a deuteron wave function $|\phi_d\rangle$ and a momentum eigenstate of the nucleon-deuteron motion with relative momentum $\vec{q}_0$. In the outgoing state $|\phi'\rangle$, the direction of this momentum is changed.

Currently Eq. (2) is solved numerically using a momentum space partial-wave basis. In order to achieve convergence at 250 MeV, all partial-wave states with total angular momenta in the $2N$ subsystem up to $j = 5$ were used, and all total angular momenta in the $3N$ system up to $J = 25/2$ were taken into account. For a shorter range 3NF, inclusion of up to $J = 13/2$ was sufficient. The details of the formalism and the numerical performance are given in Refs. [50–53]. We use the modern $2N$ potentials AV18, CD Bonn, and Nijmegen I and II, and combine them with the TM99 3NF [54] taking the cutoff values $\Lambda = 4.764$, 4.469, 4.690, and 4.704 in units of m_π, respectively. These Λ values were determined for each NN potential so as to reproduce the ^{3}H binding energy under combination with the TM99 3NF. The TM99 is a recent version of the TM force which is more consistent with chiral symmetry [55,56]. We also combine the AV18 potential with the Urbana IX 3NF.

B. Formulation with explicit Δ-isobar excitation

An alternative theoretical description is given in the framework employed in Ref. [57]. The dynamics is based on the charge-dependent CD Bonn potential [58] and its coupled-channel extension allowing for the single excitation of a nucleon to a Δ isobar [59]. That extension, called CD Bonn + Δ, provides a high-quality fit to the two-nucleon data as is the case for the CD Bonn potential. The Δ isobar mediates an effective 3NF in the three-nucleon system besides other Δ-isobar effects. Prominent contributions are of the Fujita-Miyazawa type [10] and of the Illinois ring type [7]. The contributions are based on all meson exchanges, i.e., π, ρ, σ, and ω exchanges, contained in the coupled-channel potential. Thus, the arising effective 3NF is much richer with respect to Δ excitation and also has shorter range components than standard irreducible 2π-exchange 3NFs. However, an irreducible 3NF covering other physics mechanisms is not used.

The elastic scattering transition matrix U is obtained from the symmetrized Alt-Grassberger-Sandhas equation [60]

$$U = PG_0^{-1} + Pt\,G_0U, \quad (4)$$

which, when irreducible 3NFs are neglected, is equivalent to Eqs. (2) and (3). Equation (4) is solved in momentum space using a partial-wave expansion. The two-baryon interaction up to total angular momentum of $j = 8$ is taken into account, and three-particle partial waves up to total angular momentum $J = 35/2$ are included. In the case of pd scattering, the above technique is extended as described in Refs. [35,61] to include the Coulomb interaction between the charged baryons.

C. Relativistic formalism

In view of the relatively large incident energy of the present nd system, we have also studied the effects of relativity on the elastic scattering cross section and vector analyzing power. This is done assuming that only $2N$ forces are acting. We follow the formalism of Ref. [62] to treat the relativistic three-body Faddeev equations with a boosted two-nucleon potential V expressed in terms of the relativistic potential v given in the $2N$ c.m. system as

$$V(\vec{p}) \equiv \sqrt{[\omega(\vec{k}) + v]^2 + \vec{p}^{\,2}} - \sqrt{\omega(\vec{k})^2 + \vec{p}^{\,2}}\,. \quad (5)$$

The momentum $\vec{p}$ is the total momentum of the two-nucleon system, $\vec{k}$ and $-\vec{k}$ are the individual momenta of the nucleons in their $2N$ c.m. system, and $\omega(\vec{k}) \equiv 2\sqrt{\vec{k}^2 + m^2}$ is the $2N$ free mass operator. We do not treat the boosted potential matrix element in all its complexity [63] but restrict it only to the leading order in p/ω expansion

$$V(\vec{k}, \vec{k}'; \vec{p}) = v(\vec{k}, \vec{k}') \left[1 - \frac{p^2}{8\sqrt{\vec{k}^2 + m^2}\sqrt{\vec{k}'^2 + m^2}} \right]. \quad (6)$$

A relativistic potential v is generated from the nonrelativistic CD Bonn NN force by performing the scale transformation of Ref. [64]. This scale transformation provides phase equivalent, nonrelativistic and relativistic potentials which generate t matrices obeying Lippmann-Schwinger type equations with nonrelativistic and relativistic propagators, respectively.

To describe the configuration of three nucleons we use, instead of standard Jacobi momenta [50], the relative momentum $\vec{k}$ of nucleons 2–3 in their $2N$ c.m. subsystem and momentum $\vec{q}$ of the spectator nucleon 1 in the $3N$ c.m. system. In this system, the sum of the momenta of the individual nucleons is zero, and thus $\vec{p} = -\vec{q}$ is the total momentum of the two-body subsystem responsible for the boost of this subsystem. In the nonrelativistic limit,the momentum $\vec{k}$ reduces to the standard Jacobi momentum.

In the relativistic calculations including the approximate potential of Eq. (6), it is important to check the applicability of such approximations. We checked this by calculating the deuteron wave function $\phi_d(\vec{k})$ when the deuteron is moving with momentum $\vec{p}$. In Ref. [65], we calculated the binding energy E_d and D-state probability of the deuteron in motion as a function of laboratory energy of the incoming neutron. The results are obtained using the approximation of Eq. (6) and two additional approximations [65]. In one of them, the boost effects are neglected completely such that

$$V(k, k'; p) = v(k, k'), \quad (7)$$

and in the other, only the leading term of p/m is kept in the expansion of $V(k, k'; p)$ as

$$V(k, k'; p) = v(k, k') \left[1 - \frac{p^2}{8m^2} \right]. \quad (8)$$

When boost effects are properly taken into account, the results must provide the deuteron binding energy and D-state probability approximately equal to the values for the deuteron at rest. The approximation in Eq. (6) approaches very closely the exact result even at large boosts. The complete neglect of boost [Eq. (7)] or restriction to only the p/m leading term [Eq. (8)] yield poor approximations.

Presently we solve Lippmann-Schwinger type equations numerically with partial-wave decomposition. When effects of the boost on spins are included, a construction of the partial-wave states is performed with the total spin s of the $2N$ subsystem defined in its c.m. system. This leads to Wigner spin rotations [65,66]. The solution of $3N$ relativistic Faddeev equations with Wigner spin rotations taken into account is very time consuming. We found in $j < 2$ calculations that the changes of the cross section due to Wigner spin rotations are smaller than 1%. For the analyzing power, these changes are slightly larger, but they do not exceed 3%, with the exception of zero crossing angle regions. Thus when performing the fully converged calculation ($j < 6$, $J \leqslant 25/2$), we neglected Wigner spin rotations completely.

V. RESULTS AND DISCUSSION

In this section, the experimental results for the differential cross sections and vector analyzing powers are compared with their respective theoretical predictions. They were extracted from the yields of the nd and np elastic scattering obtained and discussed in Secs. II and III.

A. Differential cross section

The absolute values of the nd elastic scattering cross sections were deduced by normalizing the data to the np scattering cross sections as given by the NN phase shift analysis program SAID [67].

For the backward angle region, the differential cross sections measured at the (n, p) facility were deduced as

$$\frac{d\sigma}{d\Omega}_{nd:\text{c.m.}} = \frac{d\sigma}{d\Omega}_{np:\text{c.m.}} \frac{Y_{nd}}{Y_{np}} \frac{J_{nd}}{J_{np}} \times \left(\frac{N^{\text{eff}}_{\text{target}:nd}\, \epsilon_{\text{MWDC}:nd} \epsilon_{\text{VDC}:nd}\, I_{nd}}{N^{\text{eff}}_{\text{target}:np}\, \epsilon_{\text{MWDC}:np} \epsilon_{\text{VDC}:np}\, I_{np}} \right)^{-1}, \quad (9)$$

where $d\sigma/d\Omega_{np}$ are np differential cross sections obtained from the SP03 phase-shift solution of Arndt [67], Y is the number of events, J is the Jacobian, $N^{\text{eff}}_{\text{target}}$ is the effective target thickness, I is the total number of incident neutrons, and ϵ is the efficiency of the detectors. The np differential cross section $d\sigma/d\Omega_{np}$ changes slightly depending on which of the NN models is used in the phase shift analysis. This results in a systematic error of up to $\pm 3\%$.

We assumed that the detector solid angle in the laboratory system $\Delta\Omega(\theta)_{\text{lab}}$ is the same for the nd and np experiments and does not appear in Eq. (9) due to cancellation. This assumption causes a systematic uncertainty of up to $\pm 5\%$. The yields Y_{nd}, Y_{np} and the target thicknesses have systematic errors of $\pm 8\%$, $\pm 6\%$, and $\pm 2\%$, respectively. The total systematic uncertainty of the cross sections is estimated to be about $\pm 11\%$.

Cross sections are plotted in Fig. 5 as solid circles, and their numerical values together with statistical errors are given in Table I. These statistical errors range from 3% to 8%. Some data points obtained at identical angles in the different runs are consistent within statistical errors.

For the forward angle region, the nd differential cross sections measured at the NTOF facility were deduced as

$$\frac{d\sigma}{d\Omega}_{nd:\text{c.m.}} = \frac{d\sigma}{d\Omega}_{np:\text{c.m.}} \frac{Y_{nd}}{Y_{np}} \frac{J_{nd}}{J_{np}} \left(\frac{N^{\text{eff}}_{\text{target}:nd}\, I_{nd}}{N^{\text{eff}}_{\text{target}:np}\, I_{np}} \right)^{-1}. \quad (10)$$

TABLE I. Cross section for *nd* elastic scattering at 248 MeV obtained at the (n, p) facility in 2003 (upper rows) and 2000 (lower rows). Only statistical errors are given.

$\theta_{\text{c.m.}}$(deg)	$(d\sigma/d\Omega)$(mb/sr)	$\Delta(d\sigma/d\Omega)$(mb/sr)
63.5	0.310	0.014
66.5	0.287	0.013
67.0	0.251	0.016
70.5	0.209	0.008
74.5	0.157	0.008
75.5	0.135	0.008
79.5	0.115	0.006
83.5	0.115	0.008
84.5	0.112	0.008
88.5	0.091	0.006
92.5	0.076	0.006
169.5	0.249	0.007
174.0	0.272	0.010
84.5	0.097	0.005
88.5	0.094	0.004
92.5	0.079	0.005
94.5	0.076	0.006
98.5	0.072	0.004
104.5	0.073	0.005
118.5	0.072	0.003
122.5	0.080	0.004
135.0	0.102	0.005
139.0	0.119	0.005
145.0	0.133	0.005
149.0	0.154	0.005
155.5	0.184	0.007
159.5	0.199	0.007
163.5	0.223	0.011
169.5	0.256	0.009
174.0	0.276	0.014
178.0	0.289	0.013

They are plotted in Fig. 5 as solid squares, and their numerical values are given in Table II. The statistical errors range from 5% to 9% except for the data of $\theta_{\text{c.m.}} = 60^\circ$ which have an error of ±25%. The systematic errors of Y_{nd}, Y_{np}, $\frac{d\sigma}{d\Omega}_{np:\text{c.m.}}$, and $N_{\text{target}}^{\text{eff}}$ are ±8%, ±6%, ±6%, and ±8%, respectively. From these values, the total systematic uncertainty of the present data is estimated to be ±15%.

TABLE II. Cross section for *nd* elastic scattering at 248 MeV obtained at the NTOF facility. Only statistical errors are given.

$\theta_{\text{c.m.}}$(deg)	$(d\sigma/d\Omega)$(mb/sr)	$\Delta(d\sigma/d\Omega)$(mb/sr)
11.1	11.15	0.78
20.6	6.18	0.33
29.9	2.68	0.16
39.2	1.64	0.14
58.6	0.81	0.20

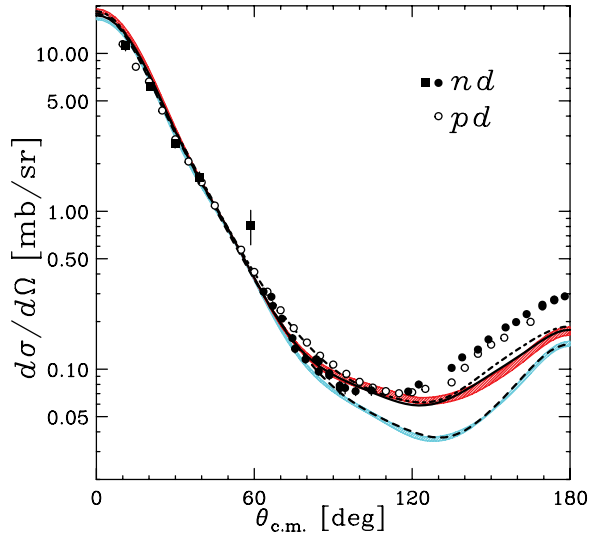

FIG. 5. (Color online) Differential cross section for *Nd* elastic scattering at 250 MeV. Solid circles and solid squares represent *nd* elastic scattering cross sections at 248 MeV obtained with the (n, p) and the NTOF facility, respectively. Error bars represent only statistical errors. Open circles are data for *pd* elastic scattering [27]. Light shaded (blue) band contains predictions of realistic *NN* potentials: AV18, CD Bonn, Nijmegen I and II. Dark shaded (red) band shows results of combining these potentials with the TM99 3NF. Solid line is a prediction obtained with the AV18 + Urbana IX combination. Dot-dashed and dashed lines are predictions based on CD Bonn + Δ and CD Bonn potentials as described in Sec. IV B, respectively.

The *nd* cross sections are compared in Fig. 5 with different theoretical predictions and with the elastic *pd* scattering cross sections of Ref. [27]. The predictions with various *NN* forces are very close to each other, as shown with a narrow light shaded band. This reflects a weak dependence of the cross section on the set of *NN* potentials used in these calculations. The predictions with *NN* forces clearly underestimate the data for c.m. angles $\theta_{\text{c.m.}} > 90^\circ$. Especially large differences up to about 70% exist in the region of the cross section minimum around $\theta_{\text{c.m.}} = 130^\circ$. The dark shaded band shows the predictions for various combinations of *NN* force with the TM99 3NF, and the solid line shows the AV18 prediction when combined with the Urbana IX 3NF. The inclusion of the TM99 or Urbana IX 3NFs leads to a better description of the data. However, even when they are included, the theory significantly underestimates the data for $\theta_{\text{c.m.}} > 120^\circ$. This is in contrast to the 135 MeV/*A* results [18], where predictions of the realistic *NN* interactions combined with the TM99 or Urbana IX 3NF described the data well over the whole angular region with the exception of forward angles $\theta_{\text{c.m.}} < 40^\circ$.

It is possible that one of the origins of the remaining discrepancy between data and theory can be the lack of contributions of other than the 2π exchange components of 3NFs to the potential energy of three nucleons. The 3NFs caused by heavy meson exchanges are considered to have a shorter range than the 2π-exchange 3NFs. In general, contributions of short-range interactions become larger at

higher energy. As a consequence, inclusion of π-ρ or ρ-ρ exchange type 3NFs is a plausible possibility for removal of the discrepancy between the data and the theory containing only 2π-exchange 3NFs. An effective 3NF due to π-ρ and ρ-ρ exchange with intermediate Δ-isobar excitation is taken into account in the calculations based on the CD Bonn + Δ potential as discussed in Sec. IV B. The results are shown in Fig. 5 as dot-dashed (NN + 3NF) and as dashed (NN only) lines. It is seen that the prediction with Δ-isobar excitation is similar to the results obtained with the TM99 or Urbana IX 3NF. Thus, the coupled-channel approach is also unable to improve the agreement between the theoretical predictions and the data. The effect of an explicit inclusion of the π-ρ exchange TM 3NF [68] has yet to be checked.

Recently, calculations inclusive of relativistic effects have been done to see if they could account for the discrepancies at higher energies. We will discuss them in Sec. V C.

In Fig. 5, the open circles show the results of the pd elastic scattering at 250 MeV measured at RCNP [27]. We can see some differences between the nd and pd data which will be discussed in Sec. V D.

B. Vector analyzing power

The experimental results for analyzing powers are shown in Fig. 6 by solid squares and solid circles. The numerical values are given in Tables III and IV. The systematic uncertainty of the analyzing powers is estimated to be about $\pm 18\%$, mainly due to the systematic uncertainty of the polarization transfer coefficient D_{NN} in the neutron production reaction. Because statistical errors in the analyzing powers are large in magnitude, it is difficult to draw any definite conclusions about the effects of 3NFs by comparing present data to the theoretical predictions. In the figure, pd elastic scattering data [27] are represented by open circles. The data for nd and pd scattering

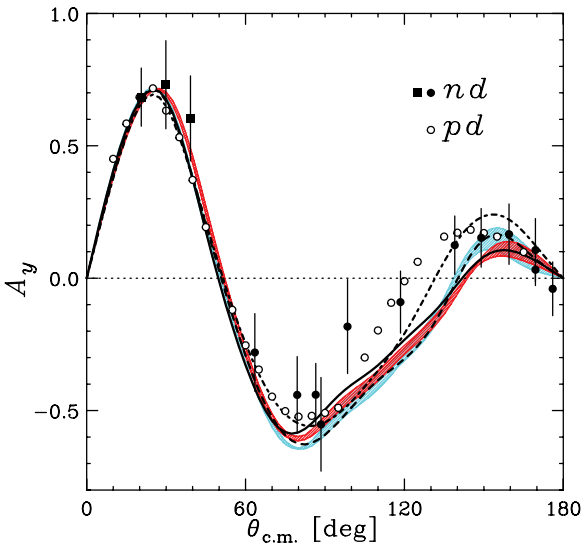

FIG. 6. (Color online) Nucleon vector analyzing powers in Nd elastic scattering at 250 MeV. For the description of data and theoretical curves, see Fig. 5. Error bars represent statistical errors only.

TABLE III. Nucleon vector analyzing power of nd elastic scattering at 248 MeV obtained at the (n, p) facility in 2003 (upper rows) and 2000 (lower rows). Only statistical errors are given.

$\theta_{\rm c.m.}$(deg)	A_y	ΔA_y
63.5	−0.28	0.15
79.5	−0.44	0.14
88.5	−0.55	0.18
169.5	0.032	0.060
86.5	−0.44	0.12
98.5	−0.18	0.18
118.5	−0.090	0.12
139.0	0.12	0.11
149.0	0.15	0.11
159.5	0.17	0.11
169.5	0.11	0.12
176.0	−0.040	0.10

are consistent with each other within statistical errors. We can see that the calculations fail to reproduce the data in the angular region $\theta_{\rm c.m.} = 110°$–$140°$. The experimental data change sign at about 120°, while in the calculation this happens at around 140°. Our results show that the inclusion of 3NFs in the calculations does not improve the description of the data, as was the case for the proton analyzing powers measured at 200 MeV at Indiana University Cyclotron Facility (IUCF) [24].

C. Relativistic effects

Since inclusion of current 3NFs fails to explain the discrepancy between pure $2N$ force predictions and cross section data, it might be instructive to estimate the magnitude of relativistic effects at this energy. In Figs. 7 and 8, we show the theoretical predictions including the relativistic corrections as described in Sec. IV C. The dashed, dotted, and dash-dotted lines represent the results corresponding to the approximation given by Eqs. (6), (8), and (7), respectively. In the differential cross section, only the result with poor approximation (dash-dotted line) shows a significant deviation from the nonrelativistic result. The relatively large (10–27%) effect introduced by inclusion of relativistic potentials is restricted to the backward angle region ($\theta_{\rm c.m.} \geqslant 160°$). In the region of the cross section minimum around $\theta_{\rm c.m.} = 130°$, relativistic effects increase

TABLE IV. Vector analyzing power of nd elastic scattering at 248 MeV obtained at the NTOF facility. Only statistical errors are given.

$\theta_{\rm c.m.}$(deg)	A_y	ΔA_y
20.6	0.68	−0.11
29.9	0.73	−0.17
39.2	0.60	−0.16

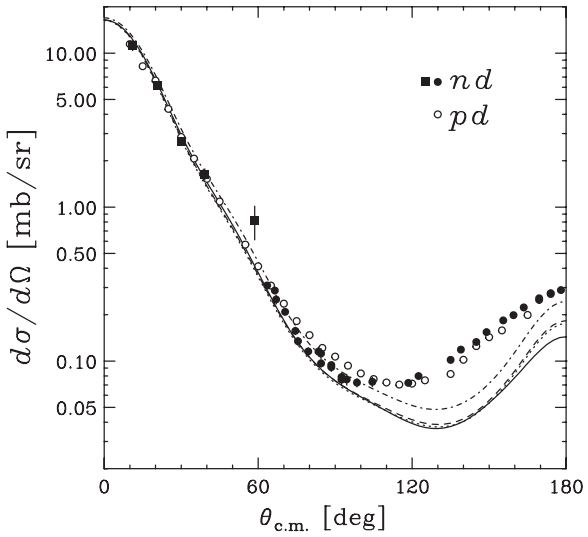

FIG. 7. Differential cross sections for *Nd* elastic scattering at 250 MeV. Solid line is the result of nonrelativistic Faddeev calculation with CD Bonn potential. Relativistic predictions which include the approximations of Eqs. (6), (8), and (7) are shown by the dashed, dotted, and dash-dotted lines, respectively. For explanation of data points, see Fig.5.

the cross section by no more than 7%. The relativistic effects would be unable to improve drastically the agreement between the data and the calculations including 3NFs.

In Ref. [30], the corrections to the *nd* total cross section resulting from relativistic kinematics were found to increase with energy and were comparable in size to 3NF effects. In a similar way, at 250 MeV the relativistic phase-space factor for the elastic scattering is estimated to be 18% larger than the nonrelativistic one. The magnitude of relativistic effects in the cross section are relatively small, because the relativistic

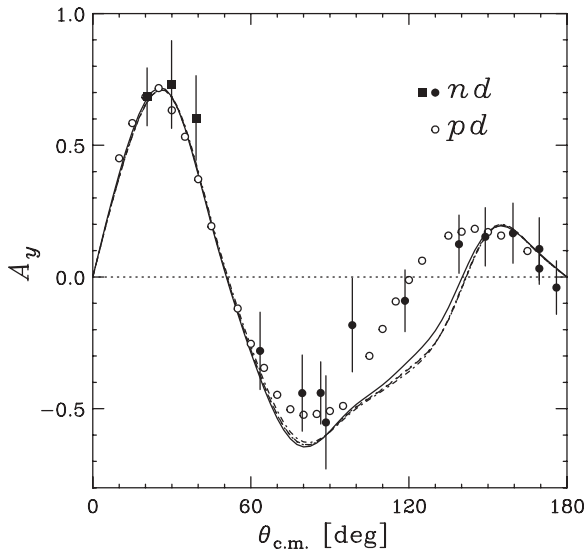

FIG. 8. Nucleon vector analyzing powers A_y for *Nd* elastic scattering at 250 MeV. For the description of data and curves, see Fig. 7.

phase-space factor increases while dynamical effects work in opposite directions. As can be seen in Fig. 7, the boost effects in the potential matrix element work in opposition to the kinematical effects, restricting relativistic effects to the backward angle region only.

Contributions from the relativistic effects upon the analyzing power are restricted to the angular range $\theta_{\rm c.m.} = 100^\circ$–$150^\circ$, and they shift the relativistic theory away from the data as shown in Fig. 8.

D. Comparison of *pd* and *nd* cross sections

Although very important, the question of the magnitude of the charge asymmetry effects in the $3N$ continuum is, up to now, only partly resolved. The most important contribution to the charge asymmetry is from the *pp* Coulomb interaction. From a theoretical standpoint, accurate calculations using various configuration-space techniques [31–33,69] have been performed to include the Coulomb force for the $3N$ bound state and for the elastic *pd* scattering below and above [34] the deuteron breakup threshold. However, only recently were the calculations of *pd* scattering at intermediate energies including Coulomb forces performed via the screening and renormalization approach in the momentum-space framework [35]. The results of theoretical calculations with CD Bonn + Δ potential reproduced very well the differential cross section data for the dp elastic scattering at 135 MeV/A. At this energy, the Coulomb effect is shown to be confined to the forward angles, $\theta_{\rm c.m.} \leqslant 30^\circ$.

Experimentally, the only way to find out the importance of the *pp* Coulomb force is by directly comparing *pd* and *nd* data. In Ref. [27], the measurement of accurate cross section data, which have systematic errors of 4% and statistical errors less than 1.4%, is reported for *pd* elastic scattering at 250 MeV over a wide angular region. This allows us to directly compare the *nd* and *pd* cross section data. To deduce the experimental *pd* values at the angles corresponding the *nd* data points, we use the cubic spline interpolation method. The ratio of the measured *pd* to *nd* cross sections is shown in Fig. 9 (solid circles). The experimental results include systematic errors which, as shown in the lower panel of Fig. 9, depend upon the scattering angle. At some backward angles, the data show significant deviations from unity.

The curves in Fig. 9 are the theoretical predictions for the pd/nd ratio at 250 MeV obtained with the CD Bonn and CD Bonn + Δ potentials. In the upper panel, three curves represent the predictions obtained when the Coulomb force is included in an approximate way using the approach of Ref. [70]. The solid and dotted lines show the predictions calculated by the Lisbon-Hannover group with and without Δ-isobar excitation, respectively. The dot-dashed curve shows the CD Bonn prediction calculated by Kamada [71]. Here, the amplitude for the *pd* elastic scattering was taken as a sum of the Rutherford amplitude and the Coulomb distorted nuclear amplitude $T_{pd}^{\rm CN}$, obtained from the pure nuclear *nd* scattering amplitude T_{nd} with the following Coulomb modification

$$\langle l|T_{pd}^{\rm CN}|l'\rangle \approx e^{i\sigma_l}\langle l|T_{nd}|l'\rangle e^{i\sigma_{l'}}, \tag{11}$$

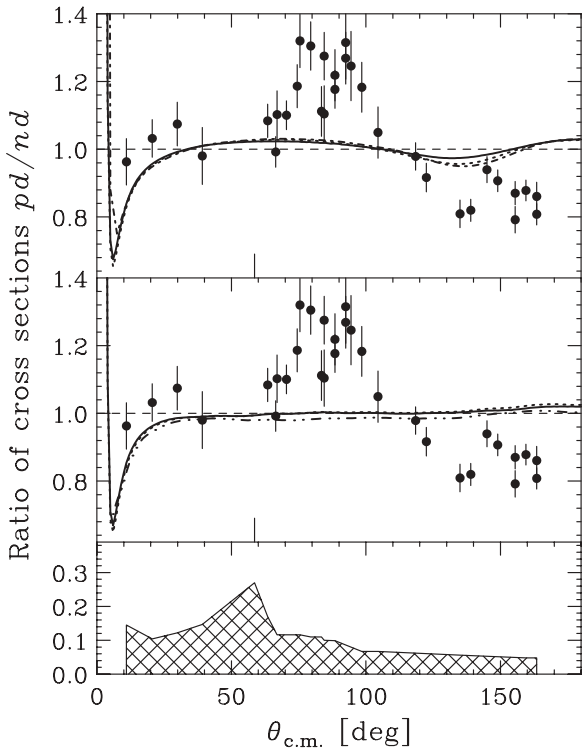

FIG. 9. Angular dependence of ratio between the *pd* and *nd* elastic scattering cross sections. Circles show the results deduced from the *nd* and *pd* data of Ref. [27] with statistical errors only. Hatched area in the lower panel shows systematic errors. Curves show theoretical predictions obtained by including the Coulomb effects in *pd* calculations. Predictions in the upper panel include the Coulomb effect by the Doleschall approximation. Those in the middle panel include the Coulomb effect by the screening and renormalization approach. Solid and dotted lines represent the predictions based on the CD Bonn + Δ and CD Bonn potentials, respectively [35]. Dot-dashed line represents the prediction based on the CD Bonn potential [71]. Dot-dot-dashed line represents the prediction taking into account the 2 MeV energy difference between *pd* and *nd*.

where σ_l and $\sigma_{l'}$ are the Coulomb phases, and l and l' are the angular momenta of the *p*-*d* two-body system in the final and initial state, respectively. The dotted and dot-dashed lines, which include CD Bonn and are calculated by different groups, are almost identical.

As can be seen in the upper panel of Fig. 9, an oscillating structure is present in the predictions. The angle where the experimental value crosses unity is around $\theta_{\text{c.m.}} = 110^\circ$, which is reproduced by the predictions that correspond to an approximate treatment of Coulomb effects.

The middle panel displays the cross section ratio, including the Coulomb interaction calculated by the screening and renormalization approach [35]. These calculations do not exhibit the oscillating structure shown by the calculations in the top panel. The deviations from unity for the theoretical ratio do not exceed 5% for the region of $\theta_{\text{c.m.}} \geqslant 30^\circ$. Regarding the Δ-isobar excitation effect, we can see that the difference between the solid and dotted lines in this panel becomes smaller than that in the upper panel. The prediction for the ratio of the *pd* differential cross section at 250 MeV to the *nd* differential cross section at 248 MeV, based upon the CD Bonn potential [35] is shown as the dot-dot-dashed line in the middle panel. Compared to the dotted line, the dot-dot-dashed line is shifted down by about 2%. Except at the angles around 130°, calculations based upon these potentials predict the data within the sum of statistic and systematic errors. More precise data are soon to be measured in order to directly study Coulomb effects.

VI. CONCLUSIONS AND SUMMARY

We performed measurements of the cross section and neutron analyzing power for the $d(\vec{n}, n)d$ reaction using a 248 MeV polarized neutron beam. To cover a wide angular range, $\theta_{\text{c.m.}} = 10^\circ$–$180^\circ$, we carried out two kinds of experiments at RCNP. The measurements for the backward angle region of $\theta_{\text{c.m.}} = 60^\circ$–$180^\circ$ were performed at the (n, p) facility where the recoil deuterons were detected by using the magnetic spectrometer LAS. The measurements for the forward angle region of $\theta_{\text{c.m.}} = 10^\circ$–$60^\circ$ were performed at the NTOF facility where the energy spectra of the scattered neutrons were obtained by the time-of-flight method.

Comparison of measured *nd* cross sections with theories based on various *NN* potentials revealed a clear difference between pure 2*N* force predictions and the results obtained with inclusion of 3NFs. However, the large discrepancy between *nd* cross sections and *NN* force predictions for $\theta_{\text{c.m.}} \geqslant 90^\circ$ can only be partially removed by including the TM99 or Urbana IX 3NFs or an effective 3NF due to explicit Δ-isobar excitation. Theoretical predictions including 3NFs still underestimate the data by up to 40%. Present-day relativistic Faddeev calculations show that relativistic effects are significant only in the region of backward angles where they increase the cross section by up to 27%. They are relatively small in the region of the differential cross section minimum around $\theta_{\text{c.m.}} = 130^\circ$ where the discrepancies between 2*N* force predictions and data are largest. This implies that the remaining discrepancy between cross section data and calculations is likely due to inadequate modeling of the 2*N* or 3*N* forces used in the present calculations. This discrepancy might be resolved by inclusion of shorter range 3NFs not mediated by Δ isobar, which in the traditional meson-exchange picture might result from π-ρ exchanges between three nucleons [68].

We compare the *nd* and *pd* data directly over a wide angular region. The *nd* cross sections roughly agree with the *pd* data with a reduced χ^2 of 9.7. However, a detailed comparison of *pd* and *nd* data shows a characteristic oscillating angular dependence for the *pd* to *nd* ratio. Recent calculations including the Coulomb effects underestimate the magnitude of the observed oscillation at some angles. Discrepancies between the data and the predictions may imply an isospin dependence of *NN* or 3NF potentials.

The measurements of the elastic *nd* scattering at 95 MeV at TSL Uppsala [72–74] also provide a direct comparison between the *nd* and *pd* data in the intermediate energy region. The *nd* and *pd* data agree with each other with a reduced χ^2

of 2.6, but the *pd* data have large uncertainties. The energy dependence of Coulomb force effects may be studied by making use of the recently obtained data from the RCNP *pd* measurement at 100 MeV [75].

ACKNOWLEDGMENTS

We acknowledge the outstanding work of the RCNP Accelerator group for delivering an excellent proton beam. We also thank Y. Hagihara, D. Hirooka, K. Itoh, T. Ikeda, M. Kato, Y. Kitamura, T. Kudoh, Y. Nagasue, S. Sakoda, Y. Satou, N. Uchigashima for their precious collaboration. Y. M. acknowledges the support of the research grants of the Japan Society for the Promotion of Science (JSPS) for Young Scientists. H.K. thanks Y. Koike for fruitful discussion about the Coulomb effects. H.W. thanks the University of Tokyo and RCNP for hospitality and support during his stay in both institutes. Some of the numerical calculations were performed on the IBM Regatta p690+ of the NIC in Jülich, Germany. A D. is supported by the Portuguese Fundação para a Ciência e a Tecnologia (FCT) grant SFRH/BPD/14801/2003, A.C.F. in part by the FCT grant POCTI/ISFL/2/275, and P.U.S. in part by the Deutsche Forschungsgemeinschaft grant Sa 247/25. This work was supported financially in part by the Grants-in-Aid for Scientific Research Nos. 04402004 and 10304018 of the Ministry of Education, Culture, Sports, Science, and Technology of Japan, and by the Polish Committee for Scientific Research under Grant No. 2P03B00825.

[1] R. B. Wiringa, V. G. J. Stoks, and R. Schiavilla, Phys. Rev. C **51**, 38 (1995).
[2] R. Machleidt, F. Sammarruca, and Y. Song, Phys. Rev. C **53**, R1483 (1996).
[3] V. G. J. Stoks, R. A. M. Klomp, C. P. F. Terheggen, and J. J. de Swart, Phys. Rev. C **49**, 2950 (1994).
[4] A. Nogga, H. Kamada, and W. Glöckle, Phys. Rev. Lett. **85**, 944 (2000).
[5] A. Nogga, H. Kamada, W. Glöckle, and B. R. Barrett, Phys. Rev. C **65**, 054003 (2002).
[6] J. Carlson and R. Schiavilla, Rev. Mod. Phys. **70**, 743 (1998).
[7] R. B. Wiringa, S. C. Pieper, J. Carlson, and V. R. Pandharipande, Phys. Rev. C **62**, 014001 (2000).
[8] S. Coon, M. Scadron, P. McNamee, B. R. Barrett, D. Blatt, and B. McKellar, Nucl. Phys. **A317**, 242 (1979).
[9] B. S. Pudliner, V. R. Pandharipande, J. Carlson, S. C. Pieper, and R. B. Wiringa, Phys. Rev. C **56**, 1720 (1997).
[10] J. Fujita and H. Miyazawa, Prog. Theor. Phys. **17**, 360 (1957).
[11] E. Epelbaum, W. Glöckle, and U.-G. Meißner, Nucl. Phys. **A637**, 107 (1998).
[12] E. Epelbaum, W. Glöckle, and U.-G. Meißner, Nucl. Phys. **A671**, 295 (2000).
[13] E. Epelbaum, Prog. Part. Nucl. Phys. **57**, 654 (2006).
[14] H. Shimizu *et al.*, Nucl. Phys. **A382**, 242 (1982).
[15] H. Rühl *et al.*, Nucl. Phys. **A524**, 377 (1991).
[16] H. Sakai *et al.*, Phys. Rev. Lett. **84**, 5288 (2000).
[17] N. Sakamoto *et al.*, Phys. Lett. **B367**, 60 (1996).
[18] K. Sekiguchi *et al.*, Phys. Rev. C **65**, 034003 (2001).
[19] K. Sekiguchi *et al.*, Phys. Rev. Lett. **95**, 162301 (2005).
[20] K. Ermisch *et al.*, Phys. Rev. Lett. **86**, 5862 (2001).
[21] R. Bieber *et al.*, Phys. Rev. Lett. **84**, 606 (2000).
[22] H. Witała *et al.*, Few-Body Syst. **15**, 67 (1993).
[23] J. Arvieux *et al.*, Phys. Rev. Lett. **50**, 19 (1983).
[24] E. J. Stephenson, H. Witała, W. Glöckle, H. Kamada, and A. Nogga, Phys. Rev. C **60**, 061001(R) (1999).
[25] R. V. Cadman *et al.*, Phys. Rev. Lett. **86**, 967 (2001).
[26] K. Sekiguchi *et al.*, Phys. Rev. C **70**, 014001 (2004).
[27] K. Hatanaka *et al.*, Phys. Rev. C **66**, 044002 (2002).
[28] H. Witała, W. Glöckle, D. Hüber, J. Golak, and H. Kamada, Phys. Rev. Lett. **81**, 1183 (1998).
[29] W. P. Abfalterer *et al.*, Phys. Rev. Lett. **81**, 57 (1998).
[30] H. Witała, H. Kamada, A. Nogga, W. Glöckle, C. Elster, and D. Hüber, Phys. Rev. C **59**, 03035 (1999).
[31] A. Kievsky, M. Viviani, and S. Rosati, Phys. Rev. C **52**, R15 (1995).
[32] A. Kievsky, Nucl. Phys. **A607**, 402 (1996).
[33] A. Kievsky, Phys. Rev. C **60**, 034001 (1999).
[34] A. Kievsky, M. Viviani, and S. Rosati, Phys. Rev. C **64**, 024002 (2001).
[35] A. Deltuva, A. C. Fonseca, and P. U. Sauer, Phys. Rev. C **71**, 054005 (2005).
[36] A. Deltuva, A. C. Fonseca, A. Kievsky, S. Rosati, P. U. Sauer, and M. Viviani, Phys. Rev. C **71**, 064003 (2005).
[37] K. Yako *et al.*, Nucl. Phys. **A684**, 563c (2001).
[38] K. Hatanaka *et al.*, Nucl. Instrum. Methods A **384**, 575 (1997).
[39] T. Wakasa *et al.*, Nucl. Instrum. Methods A **482**, 79 (2002).
[40] R. A. Arndt, L. D. Roper, R. A. Bryan, R. B. Clark, B. J. VerWest, and P. Signell, Phys. Rev. D **28**, 97 (1983).
[41] J. Kamiya *et al.*, RCNP Annual Report 1998, p. 113.
[42] T. Taddeucci *et al.*, Phys. Rev. C **41**, 2548 (1990).
[43] T. Wakasa *et al.*, Phys. Rev. C **51**, R2871 (1995).
[44] R. Henderson *et al.*, Nucl. Instrum. Methods A **257**, 97 (1987).
[45] Y. Maeda *et al.*, Nucl. Instrum. Methods A **490**, 518 (2002).
[46] N. Matsuoka *et al.*, RCNP Annual Report 1987, p. 176.
[47] N. Matsuoka *et al.*, RCNP Annual Report 1991, p. 190.
[48] H. Sakai *et al.*, Nucl. Instrum. Methods A **369**, 120 (1996).
[49] T. Wakasa *et al.*, Nucl. Instrum. Methods A **404**, 355 (1998).
[50] W. Glöckle, H. Witała, D. Hüber, H. Kamada, and J. Golak, Phys. Rep. **274**, 107 (1996).
[51] D. Hüber, H. Kamada, H. Witała, and W. Glöckle, Acta Phys. Pol. B **28**, 1677 (1997).
[52] H. Witała, T. Cornelius, and W. Glöckle, Few-Body Syst. **3**, 123 (1988).
[53] D. Hüber, H. Witała, and W. Glöckle, Few-Body Syst. **14**, 171 (1993).
[54] S. A. Coon and H. K. Han, Few-Body Syst. **30**, 131 (2001).
[55] J. L. Friar, D. Hüber, and U. van Kolck, Phys. Rev. C **59**, 53 (1999).
[56] D. Hüber, J. Friar, A. Nogga, H. Witała, and U. van Kolck, Few-Body Syst. **30**, 95 (2001).
[57] A. Deltuva, K. Chmielewski, and P. U. Sauer, Phys. Rev. C **67**, 034001 (2003).
[58] R. Machleidt, Phys. Rev. C **63**, 024001 (2001).

[59] A. Deltuva, R. Machleidt, and P. U. Sauer, Phys. Rev. C **68**, 024005 (2003).
[60] E. O. Alt, P. Grassberger, and W. Sandhas, Nucl. Phys. **B2**, 167 (1967).
[61] A. Deltuva, A. C. Fonseca, and P. U. Sauer, Phys. Rev. C **72**, 054004 (2005).
[62] W. Glöckle, T.-S. H. Lee, and F. Coester, Phys. Rev. C **33**, 709 (1986).
[63] H. Kamada, W. Glöckle, J. Golak, and C. Elster, Phys. Rev. C **66**, 044010 (2002).
[64] H. Kamada and W. Glöckle, Phys. Rev. Lett. **80**, 2547 (1998).
[65] H. Witała, J. Golak, W. Glöckle, and H. Kamada, Phys. Rev. C **71**, 054001 (2005).
[66] B. D. Keister and W. N. Polyzou, Adv. Nucl. Phys. **20**, 225 (1991).
[67] R. A. Arndt and L. D. Roper, Scattering Analysis Program (SAID), Virginia Polytechnic Institute and State University (unpublished), see also Phys. Rev. C **56**, 3005 (1997), and references therein.
[68] S. A. Coon and M. T. Peña, Phys. Rev. C **48**, 2559 (1993).
[69] S. Ishikawa, M. Tanifuji, and Y. Iseri, Phys. Rev. C **67**, 061001(R) (2003).
[70] P. Doleschall, W. Gruebler, V. Koenig, P. Schmelzbach, F. Sperisen, and B. Jenny, Nucl. Phys. **A380**, 72 (1982).
[71] H. Kamada and Y. Koike in private communication. The prediction is based on the code from Ref. [52].
[72] P. Mermod *et al*., Phys. Lett. **B597**, 243 (2004).
[73] P. Mermod *et al*., Phys. Rev. C **72**, 061002(R) (2005).
[74] P. Mermod *et al*., Phys. Rev. C **74**, 054002 (2006).
[75] Y. Tameshige *et al*. in private communication.

Nuclear Instruments and Methods in Physics Research A 578 (2007) 385–398

www.elsevier.com/locate/nima

A detector system for studying nuclear reactions relevant to Single Event Effects

Yu. Murin[a,*], Yu. Babain[a], M. Chubarov[a], Yu. Tuboltsev[a], V. Pljuschev[a], M. Zubkov[a], P. Nomokonov[b], A. Voronin[c], M. Merkin[c], V. Kondratiev[d], N. Olsson[e], J. Blomgren[e], L. Westerberg[f], C. Ekström[g], A. Kolozhvari[g], H. Jäderström[h], B. Jakobsson[i], P. Golubev[i], Chr. Bargholz[j], L. Gerén[j], P.-E. Tegnér[j], I. Zartova[j], A. Budzanowski[k], B. Czech[k], I. Skwirczynska[k], H.H.K. Tang[l]

[a] *V.G. Khlopin Radium Institute, 2nd Murinski 28, 194021 St. Petersburg, Russia*
[b] *High Energy Laboratory, Joint Institute for Nuclear Research, 141980 Moscow Region, Russia*
[c] *Moscow State University, 119992 Moscow, Russia*
[d] *St. Petersburg State University, 198504 St. Petersburg, Russia*
[e] *Department of Neutron Research, Uppsala University, Box 525, SE 751 20 Uppsala, Sweden*
[f] *Department of Physics, Uppsala University, Box 530, SE 751 21 Uppsala, Sweden*
[g] *The Svedberg Laboratory, Uppsala University, Box 533, SE 751 21 Uppsala, Sweden*
[h] *Department of Nuclear and Particle Physics, Uppsala University, Box 531, SE 751 21 Uppsala, Sweden*
[i] *Department of Physics, Lund University, Box 118, SE 221 00 Lund, Sweden*
[j] *Department of Physics, Stockholm University, AlbaNova, SE 10691 Stockholm, Sweden*
[k] *H. Niewodniczanski Institute of Nuclear Physics, PL 31 342 Cracow, Poland*
[l] *IBM, T.J. Watson Research Center, Yorktown Heights, NY 10598, USA*

Received 28 February 2007; received in revised form 12 May 2007; accepted 14 May 2007
Available online 3 June 2007

Abstract

We describe a device to study reactions relevant for the Single Event Effect (SEE) in microelectronics by means of 200 A and 300 A MeV, inverse kinematics, Si + H and Si + D reactions. The work is focused on the possibility to measure $Z = 2-14$ projectile fragments as efficiently as possible. During commissioning and first experiments the fourth quadrant of the CELSIUS storage ring acted as a spectrometer to register fragments in two planes of Si strip detectors in the angular region $0^\circ-0.6^\circ$. A combination of ring-structured and sector-structured Si strip detector planes operated at angles $0.6^\circ-1.1^\circ$. For specific event tagging a Si+ phoswich scintillator wall operated in the range $3.9^\circ-11.7^\circ$ and Si $\Delta E-E$ telescopes of CHICSi type operated at large angles.
© 2007 Elsevier B.V. All rights reserved.

PACS: 29.30.Aj; 29.40.Wk; 29.40.Mc; 29.40.Gx

Keywords: Single event effects; Fragmentation detectors; Inverse kinematics

1. Introduction

Recent advances in microelectronics are very much based on reducing the size and decreasing the power consumption of the elements in the chips. This increases, however, the probability for functional upsets due to the so named Single Event Effect (SEE) caused by cosmic radiation even at sea level [1,2]. This effect has recently caught considerable interest also from nuclear reaction physicists [1,3] since it appears to be related to the fragmentation process in nucleon–nucleus collisions. To understand the phenomena, comprehensive data on fragment and recoil production in $p(d)$—nucleus reactions at medium energy are needed, since

*Corresponding author. Tel.: +7 49621 48489.
E-mail address: murin@jinr.ru (Yu. Murin).

0168-9002/$ - see front matter © 2007 Elsevier B.V. All rights reserved.
doi:10.1016/j.nima.2007.05.318

it is believed that such products with large Linear Energy Transfer (LET) cause the observed upsets in the sensitive nodes of the device. Especially, heavy recoils, which are produced in most of the inelastic collisions, cause a large LET. However, their ranges are much shorter than most lighter fragments, like H and He ions, and they are therefore difficult to detect in conventional reaction experiments. Consequently, only few experiments of this kind have been carried out, the one discussed in Ref. [4], on 180 MeV p+Al reactions, being an exception.

The basic idea of the present work is to study fragmentation of silicon nuclei induced by medium energy protons and deuterons in inverse-kinematics Si + H, D reactions at the synchrotron and storage ring CELSIUS of The Svedberg Laboratory (TSL), Uppsala, Sweden. Few facilities in the world provide possibilities for experiments of this kind to be carried out. Ref. [5] reports on the exceptional first study of this kind on 80 A MeV Si fragmentation in a H target at the MSU superconducting cyclotron. The basic motivation for the present work is to generate new spallation data in the intermediate energy domain, from a few tens to a few hundred of MeV, use these data to test and tune fragmentation models and then use them to generate necessary tables of fragmentation cross sections for the SEE studies. At present no single reaction model is able to handle this within the precision needed but since long time IBM researchers have been developing simulation programs for similar engineering applications [6]. Several other models for hadron–nucleus and nucleus–nucleus collisions do exist [7–9] and they are often based on a combination of dynamical and statistical processes. Often, they are, however, limited to a certain energy region or a certain type of reactions. In a forthcoming paper we intend to compare the new data from CELSIUS to Dubna Cascade Model (DCM) [7] and JAERI Quantum Molecular Dynamics (JQMD) [8] in order to create a useful concept for predicting any topological cross section of importance for the SEE problem.

In this paper we describe the detectors developed for mounting both inside and outside the ultra-high vacuum system of the CELSIUS ring and present their performance during commissioning and SEE experiments.

2. Experimental setup

2.1. Components

The layout of the specific experimental setup at CELSIUS is shown in Fig. 1. It consists of four detector systems to register reaction products from collisions of 100 A–470 A MeV Si ions with atoms of the internal cryogenic cluster-jet target. The basic elements in the SEE experiments are:

- The synchrotron and storage ring CELSIUS, storing up to 10^9 silicon ions with good timing and focusing properties and a better energy resolution than can be achieved at conventional accelerators.
- Supersonic internal H and D cluster-jet targets providing beam-target luminosity of $\sim 5 \times 10^{27}\,\mathrm{cm^{-2}\,s^{-1}}$ for experiments with Si ions.
- The 24-element Forward Wall Detector (FWD), operating in phoswich mode to detect fragments in the angular range of $3.9^\circ < \theta < 11.7^\circ$.
- The Small-Angle silicon strip Detector (SAD) to detect fragments within $0.6^\circ < \theta < 1.1^\circ$.
- One quadrant of the CELSIUS ring equipped with the Zero Angle Detector (ZAD) and used as magnetic spectrometer to determine the momentum of recoils emitted at $0^\circ < \theta < 0.6^\circ$.
- The silicon $\Delta E - E$ Spectator Tagging Detector (STD) to register spectator protons at $60^\circ < \theta < 120^\circ$.

The secondary particles are detected event-by-event in ZAD, SAD, FWD and STD. The FWD and STD systems and the spectrometer-use of CELSIUS have been utilized in earlier experiments and their operation is described in detail elsewhere [10–15] while the SAD and ZAD systems are described extensively below.

SAD detects essentially fragments and recoils from the Si projectile. The unique properties of the cooled CELSIUS beam are here fully exploited. During the injection and acceleration phase of the operating cycle the cross section of the beam is large and only after electron cooling it shrinks to 2 mm in diameter. To avoid radiation damage of the SAD detectors working very close the beam, they are moved out during injection and returned to their working position only after cooling. The FWD [10] is essentially used for detection of light fragments. In the SEE experiment 24 of the FWD elements were introduced in four angular positions. Each element has a 750 μm Si detector followed by a 10 mm fast-plastic scintillator glued onto an 80 mm long CsI(Tl) crystal. The main task for the FWD is to register light ($A < 10$) fragments emitted at large angles ($3.9^\circ - 11.7^\circ$) in coincidence with the small-angle fragments registered by SAD. $\Delta E - E$ telescopes of Si+Si type from the CHICSi detector [11–13] were mounted inside the target chamber and thus in ultra-high vacuum on a serial, so named, GrandMotherBoard [13]. The main mission for this STD system is to register spectator-like protons in coincidence with the fragments registered by SAD. Such tagging of events is particularly interesting when comparing Si+H data with Si+D data. Comparing inclusive Si+H fragmentation data with corresponding data for Si+D reactions tagged with spectator-like protons could help to single out the information about Si fragmentation on the quasi-free neutron in the deuteron. This process is very interesting since it serves as the closest emulation of recoil measurements of the n+Si reaction—the main source of SEEs in the atmosphere—which has been achieved so far. ZAD is a telescope that comprises two SSD and a plastic scintillator positioned at the focal plane of the magnetic spectrometer, formed by the bending

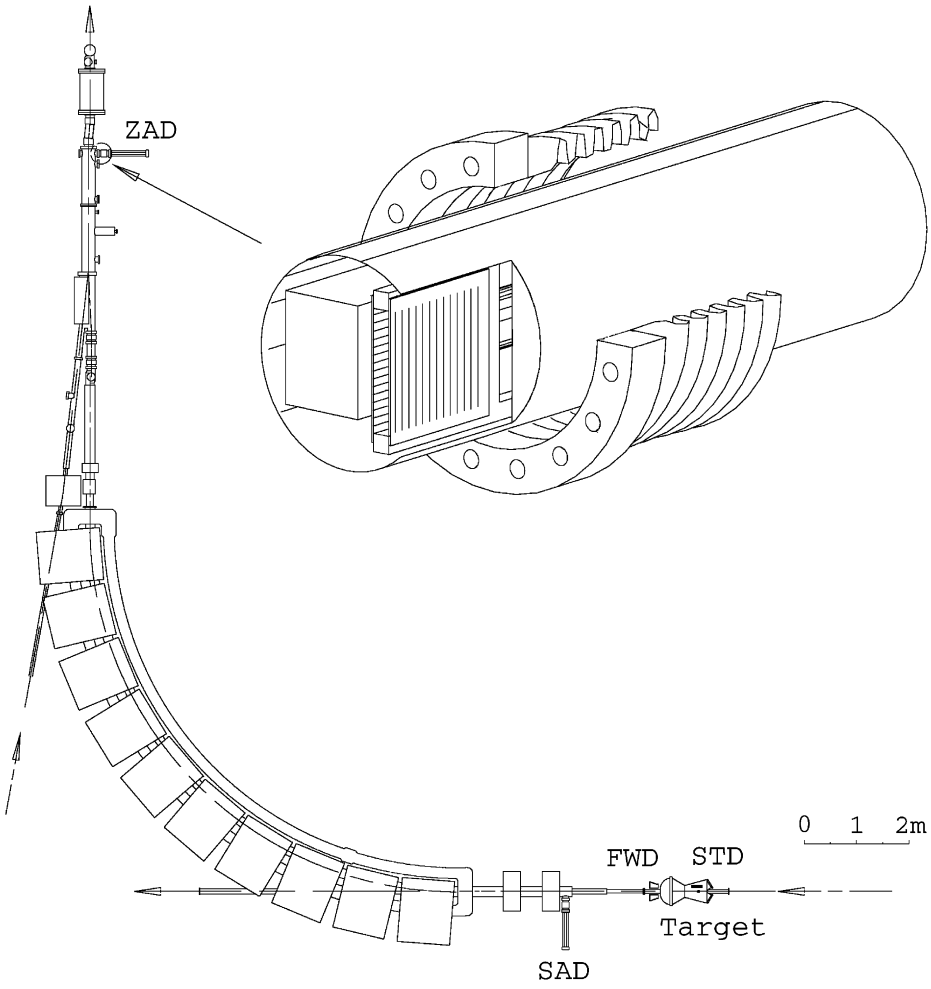

Fig. 1. Top-view of the setup for the SEE experiment at the CELSIUS storage ring.

and focusing elements of the storage ring itself [14,15]. Contrary to SAD, the strips of ZAD make up a 32×32 rectangular net. ZAD is used to detect very small-angle projectile fragments (recoils), identify their charge and determine the position of the hit point with respect to the nominal beam position (see Section 3).

2.2. The SAD telescope

SAD is a telescope comprising two 300 μm SSDs followed by an 8 mm thick plastic scintillator. The first SSD has circular and the second radial strips (Fig. 2, left) in total 32 of each type. A pair of SSDs mounted on a common board that covers an azimuthal angle of π radians makes up a sensor with a triangular cutoff to pass the primary beam (Fig. 2, right). Two such sensors are mounted one after the other and followed by plastic scintillators. The plastic scintillators are used for timing and for triggering the readout cycle. The position of the particles detected by two consecutive SSDs simultaneously is derived from the circular and radial strip numbers. The charge of the fragment is determined by the amplitudes of the signals from the two matching SSDs and the plastic detector.

The SSDs of SAD are designed to operate at a distance of only 10–12 mm from the center of the beam. The detectors were removed during injection and acceleration periods of the beam-cycle. No radiation damage has been observed. This shows that even the halo of the beam was reduced to a diameter $\ll$20 mm. The Si detectors were manufactured by ELMA in Zelenograd, Russia, from 300 μm Wacker silicon wafers with a resistivity of 5000 Ω cm. A photograph of a radial detector is shown in Fig. 2 (left) which also exhibits an additional sector-like sensor located at the closest distance from the beam. This sensor turned out to be quite useful for the direct on-line monitoring of the beam-halo. Two of the circular SAD elements are visible in Fig. 2 (right). Telescopes are triggered by two plastic scintillators, each covering half of the telescope area and placed behind the two SSD planes. These 8 mm thick scintillators provide fast timing for initiation of the read-out cycle of the SSDs. They are coupled to Hamamatsu R7400 photomultipliers through plexiglas lightguides and initially tested with 1 MeV conversion electrons from a ^{207}Bi source. Because of their

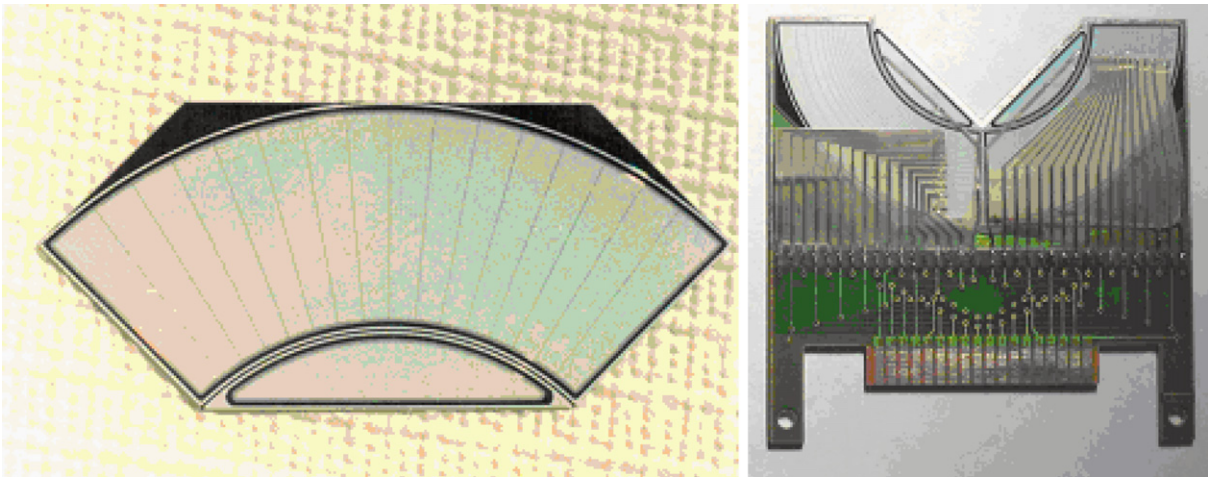

Fig. 2. SSD with radial topology (left) and two circular topology SSDs (right) assembled on-board with connectors for front-end electronics. The board side has a length of 90 mm.

complex geometry and the large area, their energy resolution is quite poor, 35%, which makes them suited for Z identification only after corrections for fragment hit coordinates are applied.

2.3. The ZAD telescope

The CELSIUS ring offered the possibility to use the focusing and bending elements of the quadrant after the target as a magnetic spectrometer (Fig. 1). This device detects fragments emitted from the interaction point only at very small angles ($\theta < 0.6^\circ$) and thus mainly inelastically scattered nuclei with low momentum transfer. These fragments are bent out from the beam by the dipole magnets. The magnetic field in the quadrant can be tuned in such a way that all charged particles with the same magnetic rigidity will be focused to one point, $P(X_f, X_f)$, in the horizontal plane at a certain distance, L, downstream from the target. There, they are registered by the ZAD detector, placed at sufficiently small distance from the beam. ZAD comprises two $60 \times 60\,\mathrm{mm}^2$ SSDs with vertical and horizontal 1.8 mm wide strips, followed by an 8 mm thick plastic scintillator. The 32 strips of each silicon detector determine the Y- and Z-coordinates while the amplitudes of the signals from the silicon and the corresponding scintillator detectors determine the charge of the fragments. Fig. 3 shows the position of ZAD in the coordinate system with origin at the center of the circular beam trajectory. In this coordinate system,

$$L \approx |Y_t| + \pi R/2 + |X_f| \tag{1}$$

where X_f, Y_f are the coordinates of ZAD, X_t, Y_t are the coordinates of the target and R is the radius of the nominal beam trajectory. The rigidity is,

$$r = \alpha \frac{p}{Z} = \alpha \frac{\sqrt{T(T+2M)}}{Z} \tag{2}$$

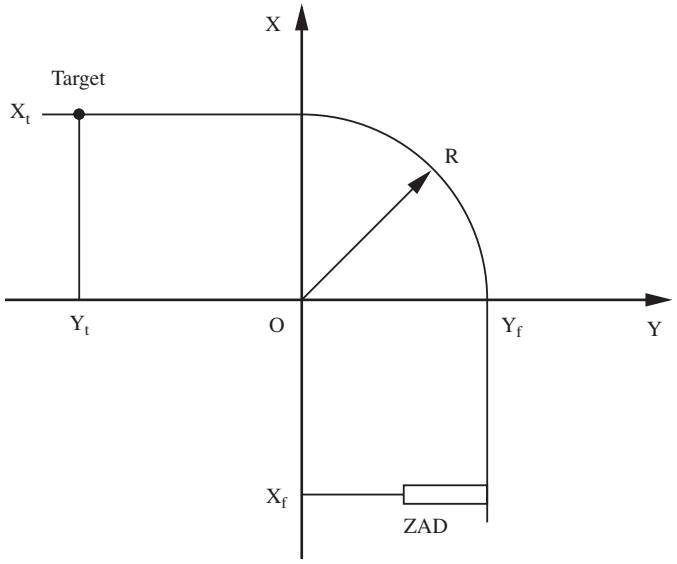

Fig. 3. The position of the ZAD detector with respect to the beam-line in the fourth quadrant of CELSIUS.

where p, T, M, Z are the total momentum, the kinetic energy, the mass and the charge of the fragment, and α is a constant.

For the circulating Si ions ($A = 28$), $T = E \cdot A$, $M = M_{\mathrm{Si}} \cdot A/28$ and $Z = A/2$. Therefore,

$$r_{\mathrm{Si}} = \alpha \frac{p_{\mathrm{Si}}}{Z_{\mathrm{Si}}} \approx \alpha \sqrt{E(E+2)} \tag{3}$$

independent of A. Ions with $A = 2Z$ and the same energy per nucleon, E, will be focused to the same point P, while those with different E will reach the focal plane at a horizontal distance, B, from the point P. The relative rigidity, ρ, is now,

$$\rho = \frac{r}{r_{\mathrm{Si}}} = 1 + c_1 B \tag{4}$$

where the constant c_1 is determined by ray-tracing (below). Thus, a position sensitive detector which is placed in the focal plane and which is capable of identifying the charge of the fragment provides the opportunity to determine the yield and momentum distributions of fragments with $A = 2Z$ by measuring the yield distribution in B. ZAD was placed in the focal plane of the magnetic spectrometer at a distance of $L = 22\,757$ mm from the target and at the closest possible distance of 33.8 mm from the nominal beam line, except during injection and acceleration when the detector was moved out of the beam pipe. This position kept the Si detectors out of the beam halo and ZAD detected the $A = 2Z$ fragments with B-values ranging from 33.8 to 91.3 mm.

2.4. Trigger electronics

Fig. 4 shows the block-diagram of the trigger electronics and the data acquisition system (DAQ) in the experiment which integrates three subsystems connected to the SAD, ZAD, and FWD detectors. It is built up mainly from standard CAMAC, NIM, and VME modules. The only application-designed modules are front-end electronic stations (FES) and ADCs used in SAD and ZAD. The system can be combined logically with separate external detectors such as the STD (CHICSi).

The electronics performed standard tasks for this type of experiment. They were as follows:

- To initialize the data readout cycle by sending the INTERRUPT signal to the DAQ system on different types of triggers i.e. from inclusive SAD, ZAD, FWD events, and coincidence events SAD & FWD, SAD & CHICSi or FWD & CHICSi.
- To initialize measurements of amplitudes of the sensor signals and time intervals between some of them.
- To equalize rates of triggering signals from subsystems with essentially different load of events.
- To synchronize the operation of the subsystems between each other and allow estimation of the dead time of the whole system.

2.5. Front-end electronics for SAD and ZAD

The FES for the SAD and ZAD detectors consists of two Boards (FEBs). The FEBs were designed and manufactured dedicated to the experiment. Their design, however, essentially exploited the technical solution previously found for the similar devices developed for the cosmic ray studies [16]. Each FEB performs amplification, shaping and storage of signals (amplitudes) for 32 strips of SAD SSDs with subsequent transmission to the ADC9225 unit. A schematic diagram is shown in Fig. 5. The basic elements are 16-channel Application Specified Integrated Circuits (ASIC), named CR-1 [16]. Each channel of CR-1, connected to one single strip of the Si detector, comprises a charge-sensitive amplifier, a shaping amplifier and a sample-and-hold circuit. Sixteen channels are multiplexed onto a common output buffer.

The FEB contains a current limiter to protect the Si detectors, bias resistors, HV filters, sources of reference voltage for CR-1 and analogue output offset and multiplexer for two CR-1 chips. The programmable logic chip (PLD) determines the timing of control signals and data reception. A special circuit permits the use of an external, high-precision pulse generator for FEB calibration. Initiated by the FLT signal, FEB holds peak values of detector pulses and transmits these data in a serial code to the ADC unit. Depending on the mode of operation, the transmission starts either automatically or by an external Second Level Trigger (SLT) signal. Fig. 6 shows the timing diagram of the DAQ system for the case of SAD & FWD coincidence and illustrates FLT generation and operation of FES.

It should finally be mentioned that the complete FES units are installed in roman pots of CELSIUS as parts of the SAD and ZAD detector units.

The DAQ system of the SEE experiments was a combination of the SVEDAQ system [17] used as standard acquisition system at TSL and the specific data collection modules of the STD (CHICSi) subsystem [13]. The readout control and the event building are performed by a Motorola 68 040 CPU VME board running under the VxWorks operating system. The SAD, ZAD and FWD subsystems are read out by VME and CAMAC modules while the STD subsystem is read out via VME SBS-414 fiber optics communication modules.

Recording of data by SVEDAQ was carried out differently from the standard version [17] in which data were transmitted from the event builder to the PC via a separate Ethernet network and then stored on a 200 GB hard-disk. The PC with Intel processor was running a code implementing the SVEDAQ data communication protocol. This system provided a reliable performance close to the limit of 100 kb/s imposed by the speed of the Motorola 68 040 CPU of the event builder.

A dedicated data sorting program package for the analysis of SEE data has been developed within the ROOT framework [18]. This allows for a modern and advanced object-oriented sorting, analysis and visualization of large data samples. The package solves three major tasks of the analysis—particle track identification, filtering theoretical data sets through the constraints of the experiment, and confrontation of the experimental results with the theoretical prescriptions. The first step in the analysis process allows unpacking and preliminary data sorting. The output files are then reformatted to ROOT trees and histograms. The ROOT tree structure allows a fast interactive analysis, which is very useful for the adjustment of particle identification algorithms with iterative procedures. The second step filters data provided by reaction models. The models play here the role of event generators producing theoretical data sets in form of ASCII files with

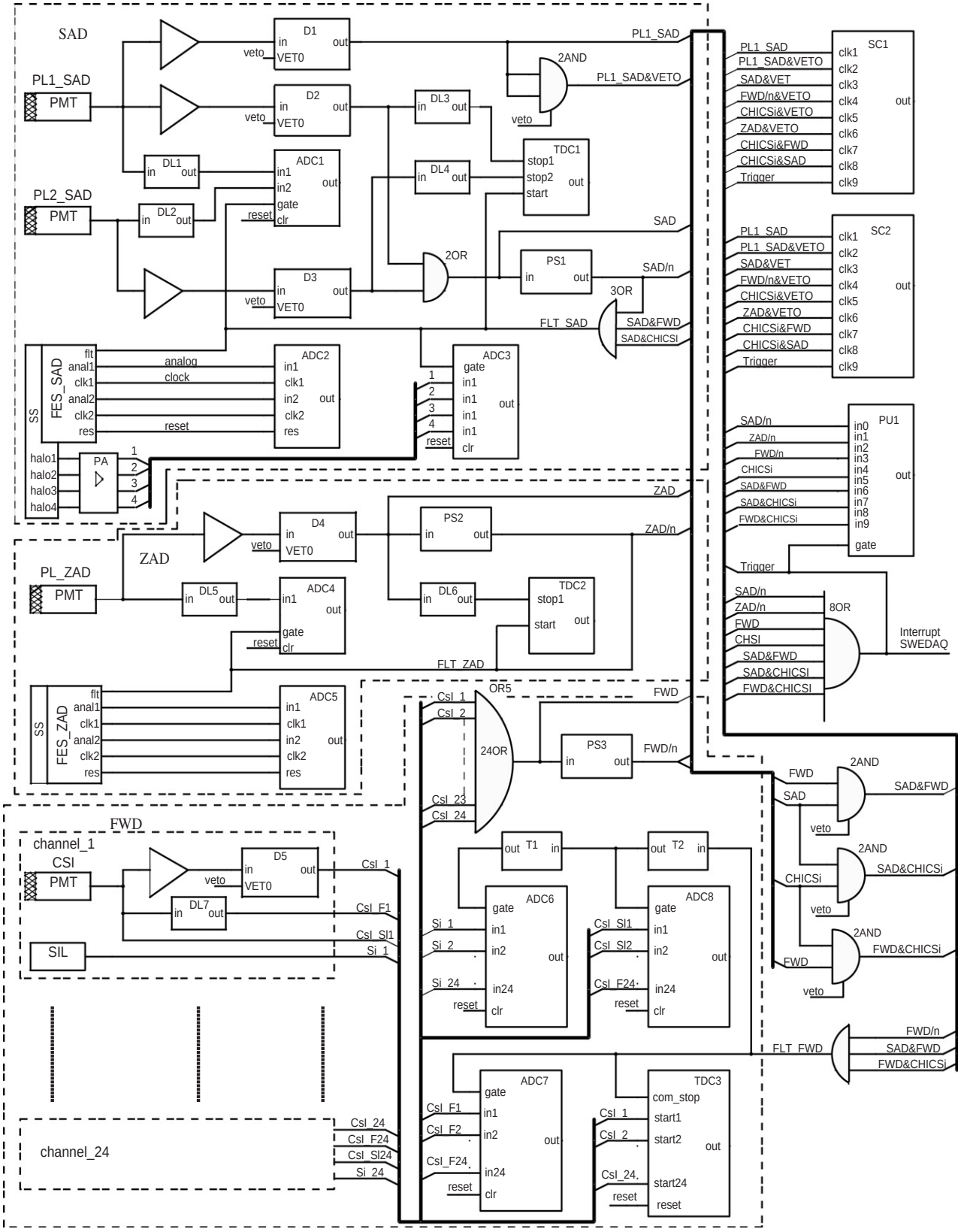

Fig. 4. Block scheme of the trigger electronics setup with different triggers. A—amplifiers, D—discriminators, PS—prescalers, DL—delays, ADC—analog-to-digital converters, TDC—time-to-digital converters, SC—scalers, T—shapers, OR and AND—logical units, PU—pattern unit.

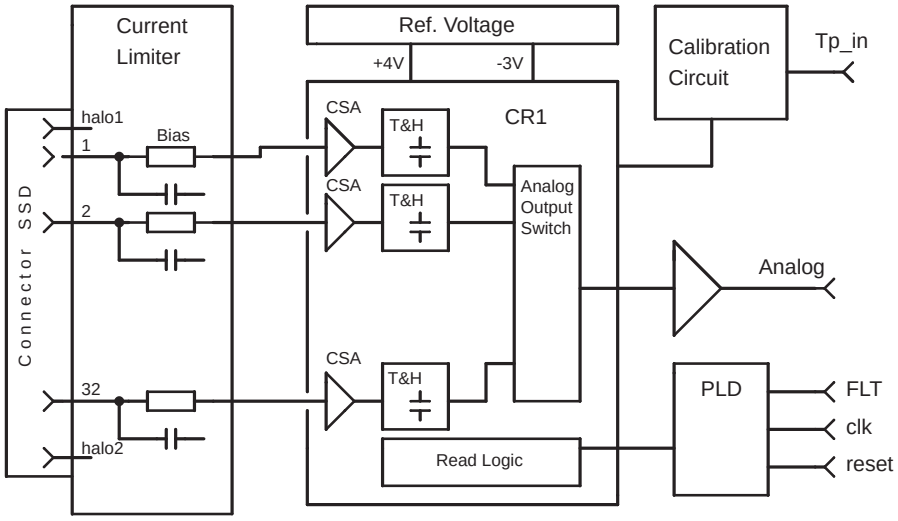

Fig. 5. Block scheme for the SAD front-end electronics (FEB).

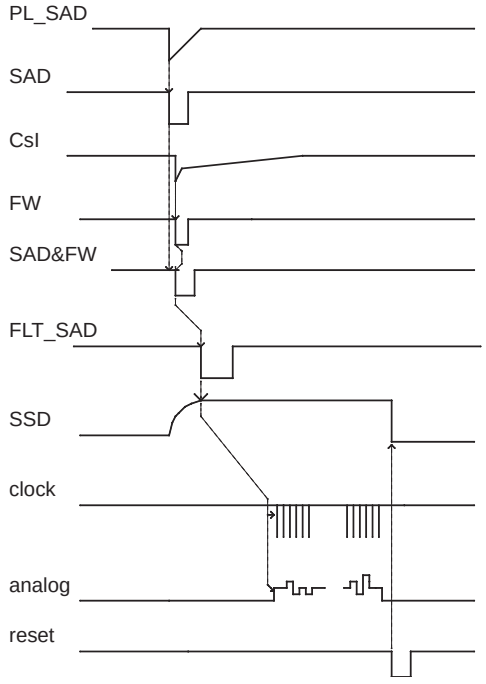

Fig. 6. FLT generation and FES timing diagram for the case of SAD & FWD triggers.

event-by-event sequences of tracks. The filter utilizes geometrical classes of ROOT to formulate the setup constraints. It delivers a collection of filtered events with tracks of particles hitting at least one of the detectors of the setup. The format of the output file is similar to the one used for experimental data storing. The third step in the analysis takes data from theoretical and experimental ROOT trees and presents all desired histograms in such a way that they can be displayed for the final physical analysis with the help of ROOT scripts provided by the program package.

3. Results from the commissioning of the setup

3.1. Charge identification in SAD

After a feasibility study with beams of Si and Ne, data were collected in actual experiments with Si beams, injected, accelerated and stored in the CELSIUS ring at TSL in April 2004 and in April 2005. Si+H and Si+D reactions at 200 A and 300 A MeV were studied. Charge resolution of all fragments registered in ZAD, SAD and FWD is easily achieved since these fragments are fast and move with a speed close to that of the beam nuclei. To illustrate this, Fig. 7 presents a typical pulse amplitude spectrum for fragments from the 300 A MeV Si+D reaction registered in a single strip of the sector-like SSD of SAD.

To reduce the number of parameters for the determination of the charge, we normalized the spectra of the Si fragments (rightmost peak) for each strip. In this way different offsets in the pedestals and gain differences in the individual channels were eliminated. This was done both for the Si strips and for the plastic scintillator corrected for the non-uniform light collection. After that the spectra were fitted with Gaussians and transformation of amplitude spectra to charge spectra was performed. The signal from the plastic scintillator and the Si strips was summed the following way, $\sqrt{\frac{1}{2}(Z_{\mathrm{pl}}^2 + Z_{\mathrm{Si}}^2)}$, where Z_{pl} and Z_{Si} are the transformed signal from the plastic and Si detectors, respectively. The result of such a transformation, from 300 A MeV Si+D data, is shown in Fig. 8. The background was approximated to be linear for the individual peaks, and a Gaussian fit of the peak resulted in a peak to background ratio of ~6.4 for $Z = 12$ for the 300 A MeV Si+D reaction. The statistical uncertainty from the charge identification is less than 1% for all charges $Z > 5$ for all reactions except for the 200 A Si+D reaction where it is between 3% ($Z = 6$) and 1% ($Z = 12$) due to less statistics.

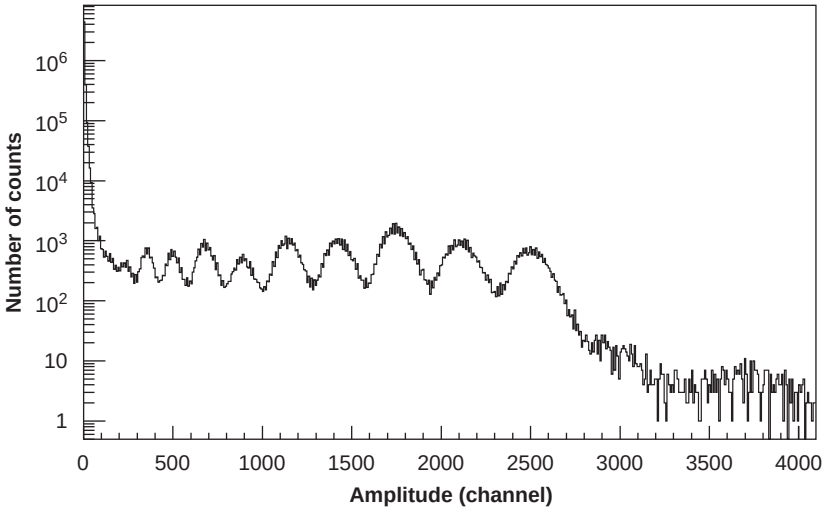

Fig. 7. The energy signal in a single strip of the sector-like SSD of SAD.

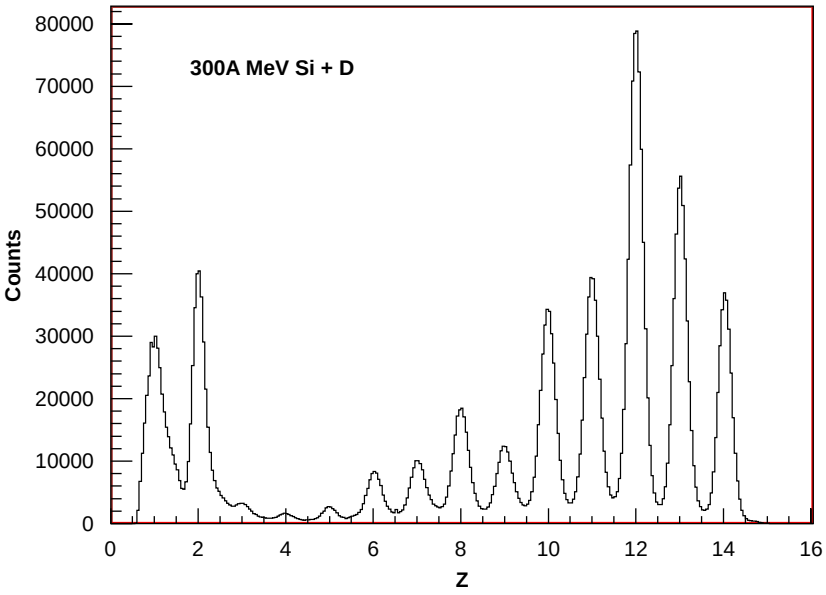

Fig. 8. Charge spectrum of projectile fragments from 300 A MeV Si+D reactions registered by SAD and obtained by means of the algorithm described in the text.

The $\Delta E-E$ (Si–CsI) signal correlations from FWD telescopes (Fig. 9) were treated in a similar way.

Graphical masks are applied to these scatter plots to identify the charge of the fragments. At least H, He, Li and Be fragments are separated by the FWD. Fig. 10 shows the charge spectra of the products of the 300 A MeV Si+D reaction registered with SAD inclusively and in coincidence with the FWD (left), or in coincidence with any of the silicon telescopes from the CHICSi setup (right). The ratios of the semi-inclusive to inclusive spectrum, shown in the lower panels of the figure, demonstrate clearly different charge distributions in FWD and STD triggered events. In SAD & FWD events the charge spectrum measured by SAD is governed very much by charge conservation and therefore the yields of the heaviest recoiling fragments are suppressed. On the contrary, the spectrum triggered by relatively low energy fragments (mostly protons) from the CHICSi telescopes are to large extent governed by the probability for quasi-elastic fragment-p scattering. The preference is then given to peripheral collisions, which also dominate the inclusive event yield. Consequently the charge distributions do not differ very much except for some enhancement of events with the loss of a few charge units in the projectile-like fragment.

3.2. Charge identification in ZAD

Charge identification in ZAD of the most forward peaked fragments, dominated by projectile-like recoils, was performed much in the same way as in SAD. Fig. 11

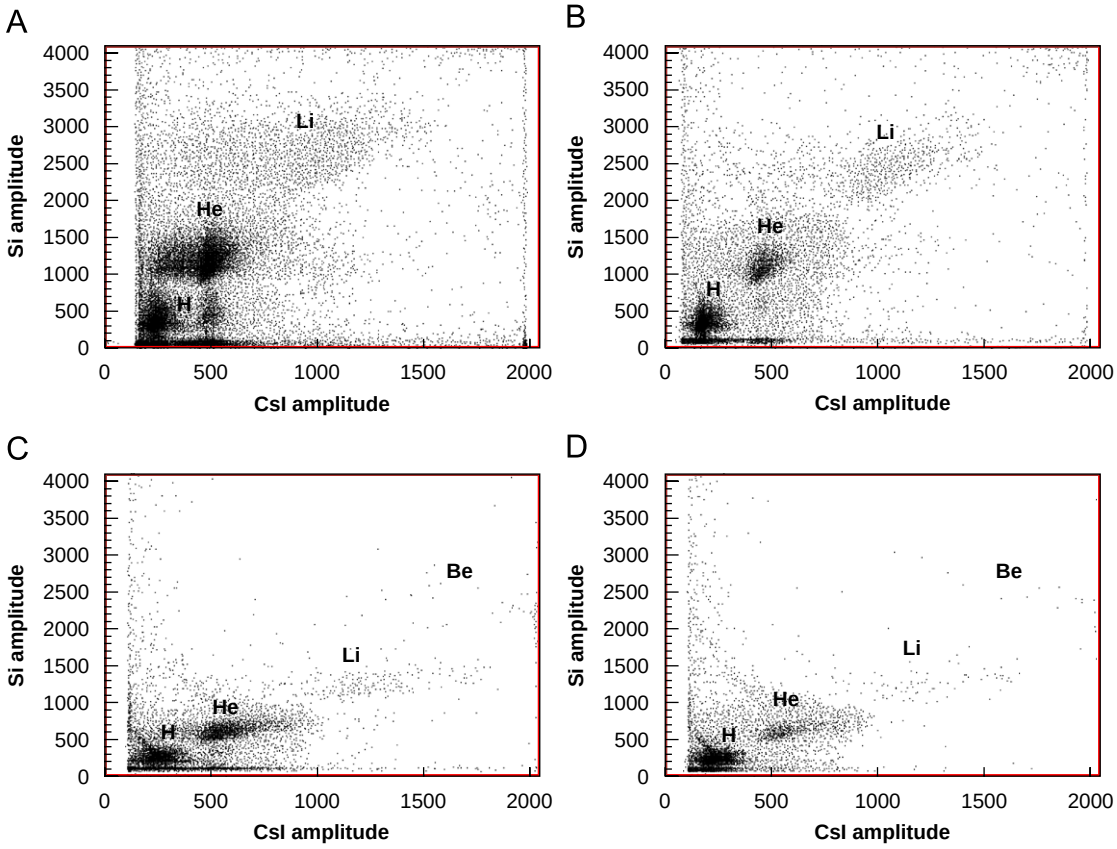

Fig. 9. Typical $\Delta E-E$ scatter plots from FWD telescopes situated in the first (A), the second (B), the third (C) and the fourth (D) azimuthal rings. Results are obtained from the 300 A MeV Si+D reaction.

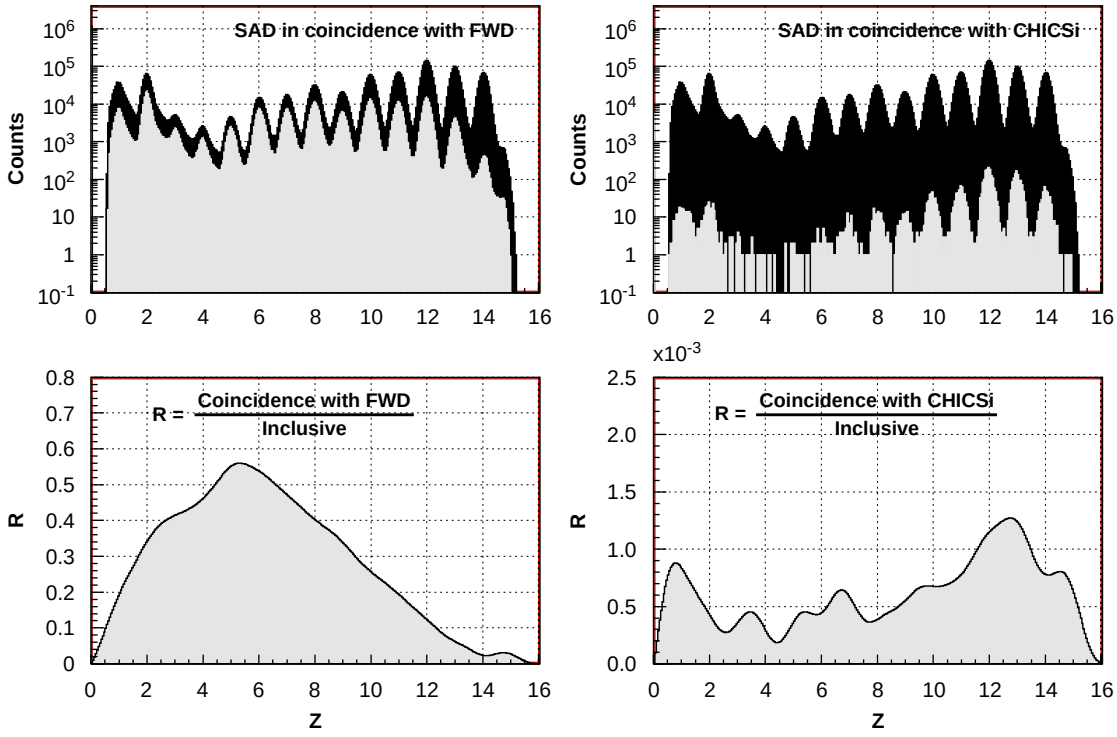

Fig. 10. Charge distributions of fragments registered by SAD from 300 A MeV Si+D reaction. Inclusive events (black) and events in coincidence with FWD (white, left) or with an STD particle (white, right) are presented. The lower panels exhibit the ratio (R) between the number of fragments registered by SAD in coincidence and inclusive events.

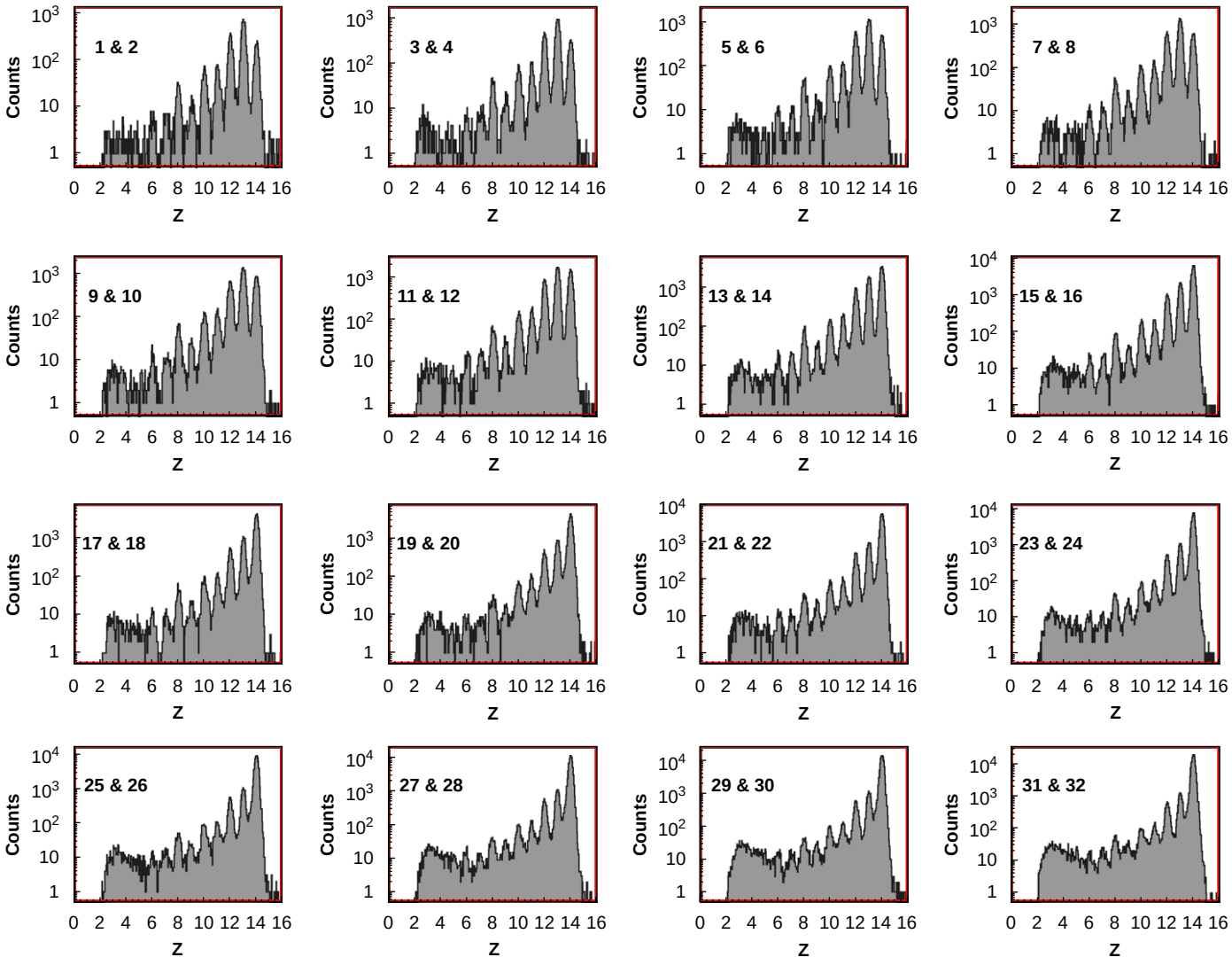

Fig. 11. Charge resolution of ZAD for fragments in different pairs of vertical Si strips obtained for fragments from the 300 A MeV Si+D reaction.

demonstrates the quality of the charge resolution, obtained for fragments registered by different pairs of vertical Si strips.

Fragments emitted at an angle $\theta > \theta_{max} (\approx 0.60^\circ)$ hit the walls of the vacuum chamber of CELSIUS and are thus lost. The data from ZAD obviously comprise the charge identity of the $Z = 6-14$ fragments registered by all individual pixels of the 32×32 strip array of the SSDs. To compare experimental and theoretical charge and momentum distributions, the fragments from a theoretical event generator must be followed from the target to the focal plane (ZAD) and filtered by the experimental conditions. Such simulations were performed for particle transportation in the magnetic field of the ten dipole magnets of the CELSIUS bending quadrant. The coordinate system used in these calculations is shown in Fig. 3 where the Y-axis is parallel to the beam axis in the target straight section and the Z-axis is normal to the plane of the figure. Origin of the system is here in the center of the circular beam trajectory in the bending quadrant and the cluster-jet target position is then (X_t, Y_t). The radius of the nominal beam trajectory within the bending section is $R = 6997$ mm, and the position of the focus as determined by Eq. (1) and Fig. 3 is now (X_f, Y_f).

The Z- and Y-distributions of the fragments in the focal plane were studied to check the quality of the focusing of the spectrometer. Both the experimental and theoretical distributions reveal good (6–8 mm) focusing along the Z-axis for all fragments. This was later confirmed in the experimental measurements.

To check the quality of the selection of $A = 2Z$ nuclei, the rigidity distributions of the fragments were simulated by the theoretical event generator. For the cumulative rigidity distributions of the fragments that reach the focal plane within the ZAD acceptance it was found that only fragments with relative rigidity $\rho \sim 1$ ($Z = N$) reach ZAD, while practically all fragments with $Z = N - 1$ and $Z = N + 1$ are lost in the walls of the vacuum chamber. The

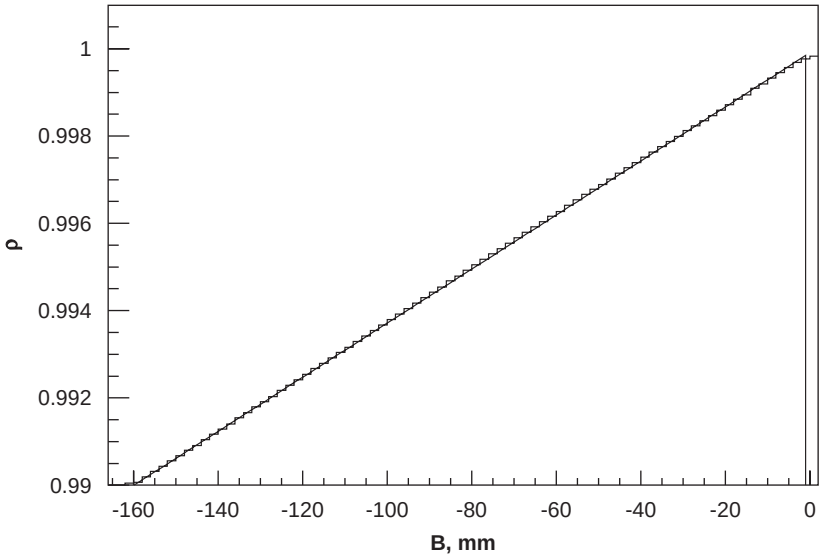

Fig. 12. Relative rigidity of fragments registered by ZAD vs their distance B from the nominal beam position.

simulations provide $B-\rho$ scatter plots for events with fragments that reach ZAD. The $B-\rho$ relation is linear as assumed in Eq. (4). An example of a linear fit to such a $B(\rho)$ distribution is shown in Fig. 12 for simulated trajectories of fragments from the 200 A MeV Si+H reaction registered by ZAD. The parameters from such fits are then used to transform the measured B-distributions to momentum distributions of the fragments registered by ZAD.

The main source of errors in momentum measurements with ZAD appear during the procedure in estimating the nominal position of the beam. During this procedure ZAD has been used as a scraper of the beam and nominal beam position was found at the instant of its disappearance in CELSIUS. We believe that our accuracy in estimating the critical Y values (Fig. 3) at which we observe disappearance of the stored beam is around 2–3 mm. Computer simulations indicate that resulting momentum resolution of ZAD is $\Delta p/p \leqslant 2\%$.

4. Specific problems for internal beam experiments

Two main problems for storage-ring experiments are the difficulties in determining absolute luminosity and coordinates of the interaction points. The luminosity question was only solved in an indirect way by normalizing to the best known topological cross-sections while the determination of the interaction point required a special procedure.

To get the absolute values of the cross sections, we have normalized the experimental data on He production obtained with the FWD to the corresponding predictions of the DCM [7]. Our choice was justified mainly for two reasons. First, He registered with FWD in conventional stationary target layout of the experiment are within the angular range between 40° and 150° and with energies between 5 and 40 MeV. Theory is in fairly good agreement with the experimental data for these channels of reactions [6,7]. On the other hand, the alpha particle yields are high in both the experimental data and the models to make the statistical error negligibly small. We estimate the accuracy of the absolute normalization of the experimental data to be of the order of 15–20%.

The main reason for the poor knowledge of the beam-target intersection point was that the beam monitoring sensors were located far away, ~2 m from the cluster-jet target both upstream and downstream. Consequently, the trajectory of the circulating beam nuclei passing through the 7 mm wide hydrogen-jet was not well known. The precision of the SAD positioning during data taking cycles was ~1 mm and thus of less importance.

An axial asymmetry was in fact found in the yields of the radial SSD strips for all fragments from all reactions. No details in the fragment production mechanism can cause asymmetry, and in absence of any background, which was confirmed experimentally, the observed axial asymmetry must be an artefact of a beam displacement. The displacement can be estimated by comparing the experimental yields of the radial SSD strips of SAD with DCM model simulations with different beam displacements. The asymmetry and the effect of the beam displacement for DCM can be seen in Fig. 13 demonstrating together experimental and simulated SAD sector distributions with and without beam displacement. Fig. 14 shows the χ^2/number of degrees of freedom (n.d.f.) from the comparison for different beam displacements for fragments with $Z = 10-12$ observed in a study of the 300 A MeV Si+D reaction taken as an example. A minimum could be found for all studied reactions indicating a horizontal displacement of the beam of 3 mm to the inside of the accelerator ring and 2 mm above the center of SAD symmetry for the 300 A MeV Si beam. Fragments with $Z = 10-12$ were chosen for the analysis for several reasons. Firstly, it was found that the

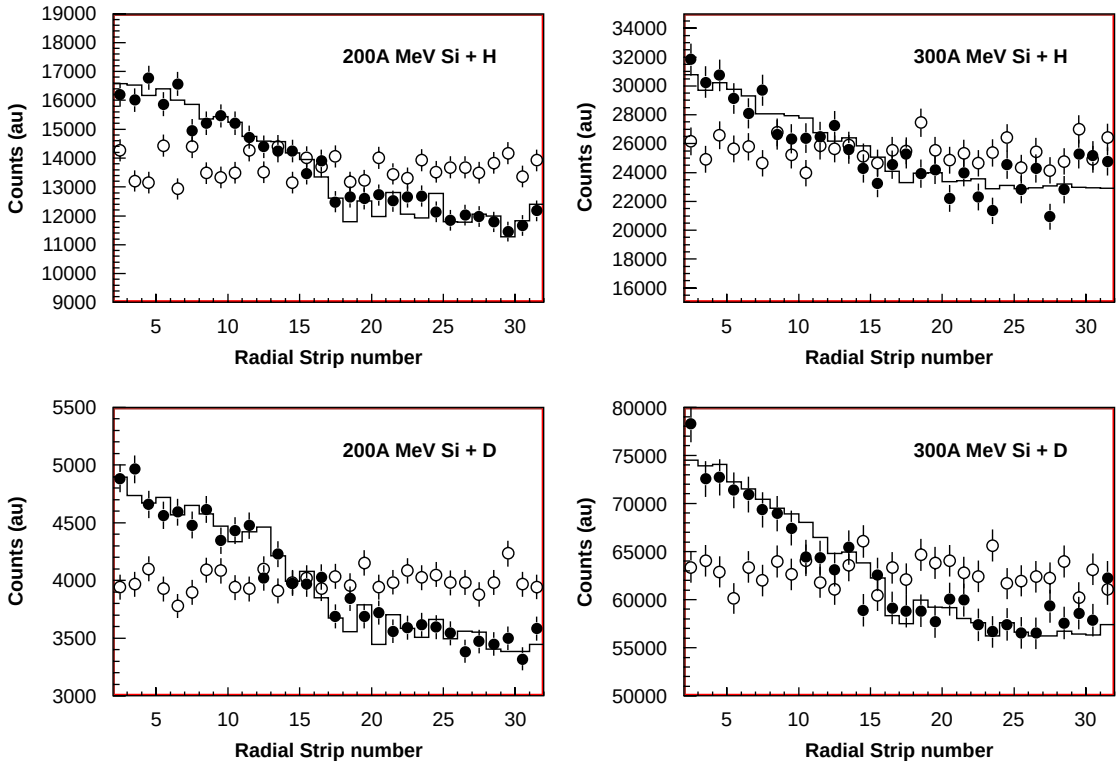

Fig. 13. Experimental yields of the radial SSD strips (histogram) for all measured reactions where the asymmetry can be clearly seen. Shown are the radial strip yields from computer simulations fed by the DCM event generator with (filled circles) and without (open circles) the beam displacement discussed in the text.

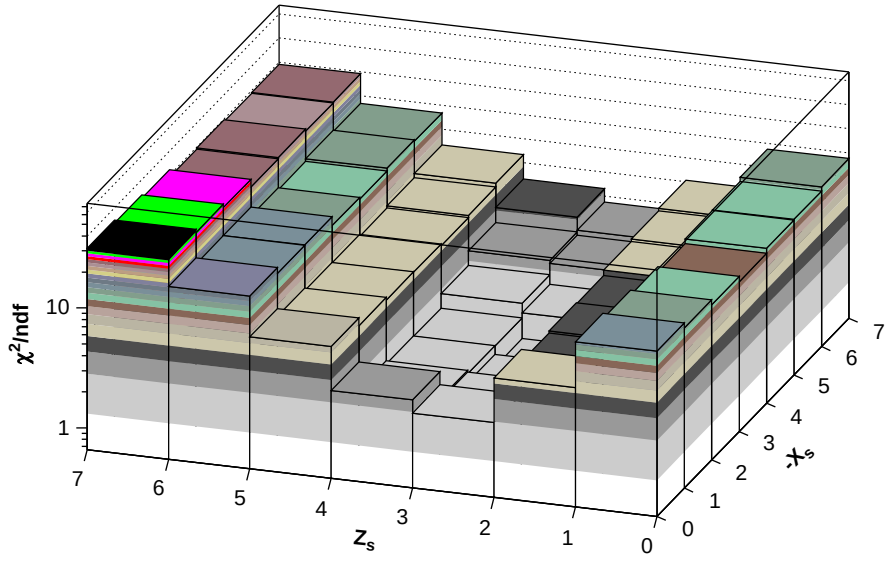

Fig. 14. χ^2/n.d.f for different beam displacement for the 300 A MeV Si+D reaction. A minimum can be found at a displacement of 3 mm in the X (horizontal) and 2 mm in the Z (vertical) directions.

agreement of theoretical and experimental angular distributions for these reaction products was rather good. Secondly, SAD acceptance covers the maximum in $d\sigma/d\theta$, and, finally, cumulative yield of these fragments provided good statistical assurance of the χ^2 analysis used by us for the beam offset estimation.

Once the beam displacement is found, the corrections to θ and ϕ angles for each pixel in SAD can be implemented and final angular distributions of the recoils obtained.

The uncertainty for the beam displacement determination procedure is difficult to estimate directly but, as a first realistic guess, one can use a typical size of the beam

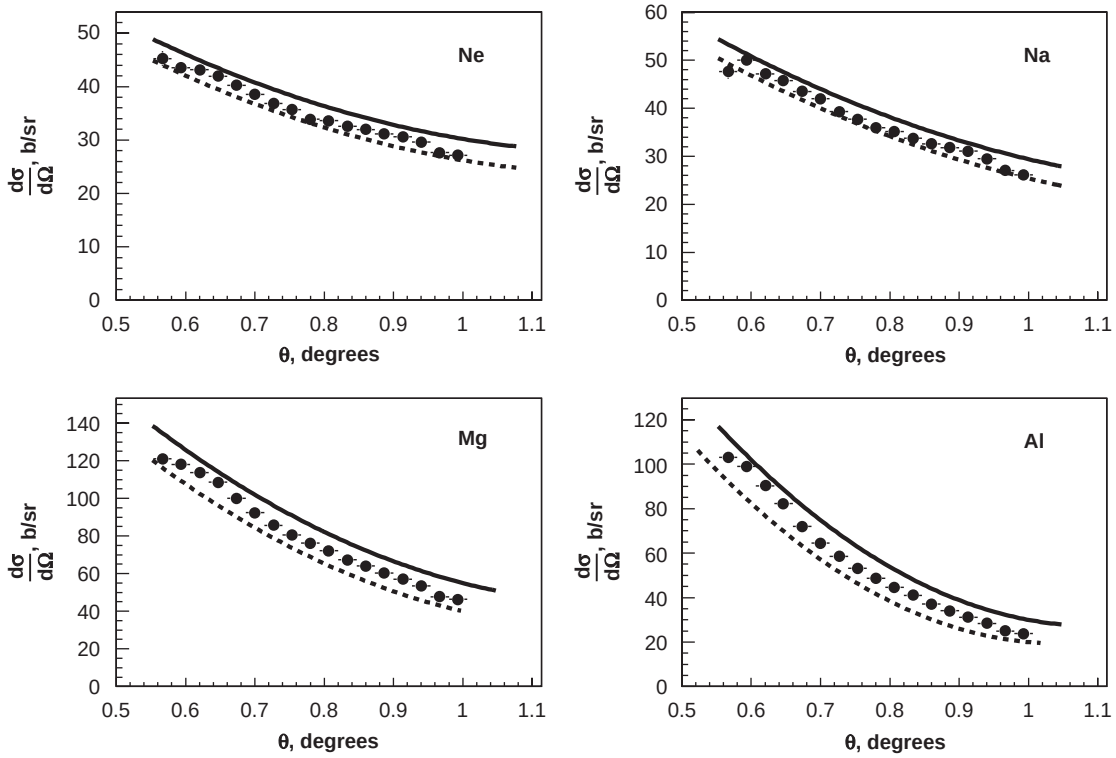

Fig. 15. The differential cross sections for the production of recoils in 300 A MeV+D reactions obtained after the corrections for the beam displacement described in the text (black dots). Lines show the uncertainty caused by the typical displacement of the order of 2 mm from the beam size giving rise to systematic uncertainties in θ of about $\pm 0.05^{\circ}$.

± 2 mm in both horizontal and vertical directions for getting the idea of the consequences of the beam displacement on the measured fragment angular distributions. Thus, a 2 mm uncertainty of the beam displacement results in an uncertainty in the true scattering angle of the fragment registered by SAD. It has been analyzed by plotting the θ distribution for the obtained beam displacement X_s, Y_s together with the same distributions obtained for beam displacements of $X_s \pm 2$ mm, $Y_s \pm 2$ mm. Fig. 15 shows the result of such simulations. Again, the results of a study of 300 A MeV Si+D reaction are depicted, taken as an example. The figure shows the effect of the 2 mm uncertainty in the beam displacement for the θ distributions, and from this plot the uncertainty in theta was estimated to be $\pm 0.05^{\circ}$ for the heavier fragments and it plays almost no role for the lighter fragments.

The effect of the interaction point displacement on the quality of the ZAD data was analyzed only through computer simulations. These simulations indicate that variations in the Z-coordinate of the interaction point do not change the X- or Y-coordinate in ZAD and vice versa. Thus, the observed vertical displacements should not cause any change in any horizontal yield distribution registered with ZAD. The value of the Y distribution is important for fragment momentum determination. A displacement of the interaction point in the target by a few mm in radial direction (X direction in Fig. 3) causes a corresponding displacement of the fragment coordinate in the opposite radial direction (Y direction in Fig. 3) at ZAD location. This displacement is to a large extent canceled since the measured values are actually not the hit coordinate in ZAD but the *difference* between the nominal position of the beam and the hit of the fragment, which also is displaced at ZAD, and the hit of the fragment. In other words, since we were measuring the rigidity of the fragment relative to the rigidity of the beam of a known momentum, the observed displacement of the interaction point did not cause problems in momentum estimation of the fragment registered by ZAD.

5. Conclusion and outlook

A detector system designed for SEE relevant experiments on Si+H(D) reactions at the CELSIUS storage ring by means of inverse kinematics has been assembled and tested. This comprises two systems that operate at very close distance to the cooled beam of Si ions and two additional systems acting as triggers for events that emit light particles or fragments at larger angles. The small-angle systems have telescopes made up of SSDs triggered by plastic scintillators placed behind them. The ability to register all beam-like fragments has been proven in actual experiments at 200 A and 300 A MeV. A method for indirect determination of coordinates of the beam-target intersection point relative to the center of the small-angle detector systems is proposed. The introduction of the large projectile

fragmentation angle phoswich detector wall and the large-angle Si–Si telescope system for quasi-elastically scattered light particles makes it possible to tag on events with different impact parameters.

This project has been funded by the US Party of the International Science and Technology Center for which we are deeply grateful. Thanks are also due to the FOI, Sweden for providing funds to support stays of the international team at TSL and to the Knut and Alice Wallenberg Foundation that funded the STD system within the CHICSi project. We are finally greatly indebted for all efforts to provide beams of good quality made by the TSL accelerator team headed by Dag Reistad.

References

[1] H.H.K. Tang, J. Res. Dev. 40 (1996) 91.
[2] H.H.K. Tang, N. Olsson (Eds.), MRS Bull. 28(2) (2003) (special issue on single event upsets in microelectronics).
[3] H.H.K. Tang, K.P. Rodbell, MRS Bull. 28 (2003) 111.
[4] K. Kwiatkowski, et al., Phys. Rev. Lett. 50 (1983) 1648.
[5] H.H.K. Tang, J.L. Romero, AIP Conf. Proc. 392 (1997) 324.
[6] H.H.K. Tang, et al., Phys. Rev. C 42 (1990) 1598.
[7] K.K. Gudima, S.G. Mashnik, V.D. Toneev, Nucl. Phys. A 401 (1983) 329.
[8] K. Niita, S. Chiba, et al., Phys. Rev. C 42 (1996) 2620; K. Niita, S. Chiba, et al., JAERI-Data/Code 99-042 (1999).
[9] J.P. Bondorf, et al., Phys. Rep. 257 (1995) 133.
[10] A. Budzanowski, et al., Nucl. Instr. and Meth. A 482 (2002) 528.
[11] L. Westerberg, Nucl. Instr. and Meth. A 500 (2003) 84.
[12] P. Golubev, et al., Nucl. Instr. and Meth. A 500 (2003) 96.
[13] L. Carlén, et al., Nucl. Instr. and Meth. A 516 (2004) 327.
[14] Chr. Bargholtz, et al., Nucl. Instr. and Meth. A 390 (1997) 160.
[15] A. Ringbom, et al., Nucl. Instr. and Meth. A 373 (1996) 57.
[16] J.H. Adams, et al., Paper OG 4.1.18, in: Proceedings of the 26th International Cosmic Ray Conference, Salt Lake City, Utah, USA, 1999.
[17] S. Abu-Rameh, et al., in: A. Ingemarsson (Ed.), TSL Progress Report 2000–2001, p. 14 (2002).
[18] R. Brun, F. Rademakers, Nucl. Instr. and Meth. A 389 (1997) 81.

Biomedical aspects of high-energy neutrons

J. Blomgren[1)]

1) Department of Neutron Research, Uppsala University, Box 525, S – 751 20 Uppsala, Sweden. Jan.Blomgren@tsl.uu.se

Abstract: Presently, many new applications of fast neutrons are emerging or under development, like dose effects due to cosmic-ray neutrons for airplane crew, fast-neutron cancer therapy, studies of electronics failures induced by cosmic-ray neutrons, and accelerator-driven incineration of nuclear waste and energy production technologies. All these areas would benefit from improved neutron dosimetry. In this paper, the presently rapid progress on measurements of double-differential neutron-induced nuclear reaction data is described. With such data at hand, the full response of in principle any system, including human tissue, can be calculated in detail. This could potentially revolutionize our understanding of biological effects in tissue due to fast neutrons.

Introduction

Recently, a large number of biomedical applications involving high-energy (>20 MeV) neutrons have become important. It has been established during the last years that airflight personnel receive among the largest radiation doses in civil work, due to cosmic-ray neutrons [1]. Cancer treatment with fast neutrons is performed routinely at several facilities around the world, and today it represents one of the largest therapy modalities besides the conventional treatments with photons and electrons [2].

When a body is irradiated with charged particles, like electrons, the dose, i.e., the energy released per volume, is deposited directly. When uncharged particles are used, like photons or neutrons, an additional step is needed, i.e., the conversion of kinetic energy of the incident uncharged particle to charged particles within the volume. It is well known that the effect of a certain dose, i.e., a given deposited energy, can be very different for different particles in a biologic system. As an example, the cell survival rate for 1 Gy of 5 MeV electrons or 1 Gy of 5 MeV alpha particles differs by an order of magnitude. Thereby, the same dose given in, e.g., electron and neutron therapy can result in rather different biologic effects.

When comparing various therapy modalities, there are some striking features. Charged particles all deposit dose directly, but with different biologic results. Uncharged particles, i.e., photons and neutrons, first have to interact with tissue, resulting in charged particles being released. After having been released, these secondary charged particles deposit energy resulting in tissue damage.

When comparing photons and neutrons as primary particles, there is one striking difference. Photon interactions result almost exclusively in release of electrons, while neutrons induce emission of many different charged particles. This means that a fundamental understanding of the effects in tissue due to neutrons require knowledge of two stages. First, the probability for neutrons to create charged particles must be known, and this information has to be detailed, i.e., the particle type, its energy and direction has to be known. Second, the biologic effect of this secondary particle at its energy must be known.

Today, the biologic effects of the various charged particles released after neutron interaction in the most common atomic nuclei in tissue are relatively well known. Thus, the second stage above is under reasonable control. What is not equally well known is the first stage, i.e., the microscopic cross sections for creation of those charged particles.

In this paper, the presently rapid progress on measurements of double-differential neutron-induced nuclear reaction data is described. With such data at hand, the full response of in principle any system, including human tissue, can be calculated in detail. This could allow a fully reductionistic approach to the entire problem of understanding the biologic effects due to neutron radiation, as being outlined below.

Because cross sections for neutron-induced reactions are in general poorly known, the existing dosimetry methods and treatment techniques are to a large extent based on experience, rather than on knowledge of fundamental physics. Due to the recent development

of neutron beams with good intensity and energy resolution, it is today possible to study all the fundamental processes involved in detail, and thus dramatically improve both the dose determination in neutron fields and the radiation quality planning in connection with tumour therapy.

In the relevant energy range (up to about 70 MeV for therapy and even higher for aviation doses), it is unfortunately difficult to describe nuclear processes theoretically in a simple way. Compound nuclear processes, direct processes and intermediate or pre-compound processes are all important and nuclear reaction models must take into account all these processes and, where appropriate, the competition between them. As a result, predictions based on theory are sometimes uncertain to 30 % or more. Such uncertainties are far larger than acceptable in, e.g., a treatment situation.

This situation is different in photon and electron interaction with tissue, which is governed by the well-known electromagnetic interaction, in which theory predictions of cross sections can be made with an accuracy of far better than 1 %, i.e., other uncertainties dominate. If cross sections cannot be computed, they have to be measured, but the data base for neutrons is meagre in this energy region.

High-energy neutron data are also of primary importance in other applications, like single-event effects in electronics [3] and accelerator-driven systems for incineration of nuclear waste [4]. All the areas above are of interest from dosimetry point of view. For the applications involving tissue, it is evident that techniques for dose determinations are of great importance. Concerning electronics effects onboard aircraft, there is a need for light and inexpensive neutron intensity monitors, similar to the dosemeters used for estimation of health effects.

Links between fundamental physics and tissue effects

Like X-rays and gamma-rays, neutrons exert their biological effect through secondary charged particles, but whereas photons interact with atomic electrons, neutrons interact with nuclei and the secondary particles are nuclear particles such as protons, deuterons, alpha-particles and heavier nuclear recoils. Evidently, a neutron transfers its energy to tissue in two stages. The first stage involves the interaction of a neutron with a nucleus, which can result in a wide range of secondary charged particles. The second stage involves the transfer of energy from secondary charged particles to tissue through excitation and ionization. The quantity kerma, an acronym for Kinetic Energy Released in MAtter, is used to describe the initial interaction, i.e., the first stage. It corresponds to the kinetic energy released by the primary neutrons per unit mass in the form of secondary charged particles [5].

Absorbed dose is defined as energy absorbed per unit mass from the secondary charged particles, i.e., the second stage. Thus, the concepts of kerma and absorbed dose are not identical, because the secondary particles have a certain range and deposit their energy predominantly downstream their point of origin. The secondary charged particles are preferentially emitted in the forward direction, which means that the absorbed dose is low at the surface and rises with depth towards the range of the charged particles. Kerma, on the other hand, does not rise but falls slowly with depth as the incident beam is attenuated [6]. In photon dosimetry, kerma is a more directly useful quantity than for neutrons [7], since the difference between kerma and dose is smaller in this case.

It is important to emphasize that in neutron dosimetry, the kerma coefficient is only a measure of how much energy per unit fluence is given to light charged particles and residual nuclei in a certain volume, regardless of the nature of and energy spectrum of the secondary particles. Since the biological response varies dramatically with ionization capability, i.e., the particle type and energy, the same kerma or dose does not necessarily correspond to the same damage (see below).

There are two ways kerma coefficients are determined; from direct calorimetric measurement of kerma, and from calculation of kerma coefficients from basic nuclear cross sections. Direct measurement of kerma coefficients can be difficult and values are available only for a few elements and neutron energies. Moreover, such measurements require total particle equilibrium in the studied volume. This is not always the case in practice, which necessitates significant corrections. Calculation of kerma from basic nuclear data requires information on all significant reaction channels, including angular and/or energy distributions of secondary reaction particles, which have to be explicitly represented. Such information is

taken from nuclear data libraries, which normally are obtained by evaluation of experimental microscopic cross sections and nuclear model predictions.

Radiation quality

Different types of ionizing radiation cause different tissue damage, in spite of the same energy being deposited. This is primarily due to the fact that the cell damage proceeds via two mechanisms, namely creation of free radicals and DNA strand breaks.

In the first mechanism, molecules in the cell are being ionized and become chemically much more reactive, which affects the cell chemistry and metabolism. This requires very little energy transfer, of the order of a few eV, and whether the creation of these reactive chemical elements is well localized or more diffuse does not make a very large difference. Instead, the total number of created reactive elements is most important, and thus the total deposited energy per unit mass gives a reasonable estimation of the cell damage. Thus, which type of particle causes the ionization is not very crucial.

In the second mechanism, the ionizing radiation breaks the DNA molecule and thereby disturbs the cell reproduction. This damage is much more efficient if both strands are struck close to each other. If just one strand is broken, the remaining one can often be used in the repair process. Thus, this mechanism is more efficient for radiation with large ionization per unit length, i.e., well localized radiation. This argument points towards relatively heavy ions, like alpha particles, which have a much larger ionization per unit length than, e.g., electrons.

Ionization per unit length is often expressed in terms of Linear Energy Transfer (LET). The "biological effectiveness" is related to LET, but not linearly. The lowest LET radiation is due to photons and electrons. The biological effect increases with increasing LET, until a maximum is reached at about 200 keV/μm. Going to even higher LET makes the effectiveness go down again, simply because a cell cannot be killed more than once, no matter how much localized dose is given.

Since high-energy neutrons produce a multitude of secondary particles, from high-energy protons, with relatively low LET, to low-energy alpha particles and heavier recoils, which have very high LET, the damage caused by neutrons is a complicated function of the delivered energy, or kerma.

Beyond KERMA

As mentioned above, the kerma coefficient is the average energy transferred from neutrons to charged particles (including recoils) per unit mass of material per unit neutron fluence. It is widely used for dosimetry in neutron therapy and radiation protection. Where applicable, mostly in the low-energy region, kerma coefficients can be directly measured. This is the reason why the kerma concept is being used; it allows a determination of the dose even if microscopic cross sections are unavailable. Alternatively, one can calculate kerma coefficients from microscopic nuclear data. A comparison of the calculated and the measured kerma coefficients provide a valuable integral test of the microscopic cross section data.

However, what is of more interest, especially in treatment planning, is the absorbed dose in the treatment volume, including all aspects playing a role, like, e.g., ionization density and oxygen abundance. Although kerma coefficients could be used for a rough estimate of the biologic effect, there is no simple relation between kerma and cell damage. In addition, such a calculation is not performed from first principles. The whole kerma concept could actually be omitted by calculating the biologic effect in a specific volume directly by a Monte Carlo radiation transport code.

It should be pointed out that double-differential cross sections contain much more information than kerma. Kerma can be obtained by integrating double-differential cross sections over all ejectile energies and angles, but in this process, valuable information is lost. For instance, it is possible that two reactions give the same kerma, but significantly different tissue damage, because the different particles are released, or energy or angular distributions can be different. On the other hand, knowledge of kerma does not allow double-differential cross sections to be determined. With the rapid development of computing power and numeric methods, full Monte Carlo modelling of radiation effects can be expected to become the standard tool within a relatively short future, and estimations based on kerma might gradually become less important.

Which data are important?

About half the dose in human tissue due to neutrons of several tens of MeV comes from proton recoils in neutron-proton (*np*) scattering, 10-15 % from nuclear recoils due to elastic neutron scattering and the remaining 35-40 % from neutron-induced emission of light ions, i.e., protons, deuterons, tritons, ^{3}He- and α-particles. With double-differential cross sections for all these reactions in tissue-relevant nuclei, i.e., carbon, nitrogen, oxygen and calcium at hand, the dose distribution could be calculated in detail.

If it is clear which data are of most importance when determining the dose in human tissue, it is less obvious which cross sections to determine for improving dosimetry. Many different nuclear reactions are employed in dosemeters. This also involves reactions not taking place in tissue. An example is fission in bismuth, which has some nice features for dosimetry of high-energy neutrons. The cross section is very small all the way up to about 50 MeV, so it is very useful for dosimetry of high-energy neutrons in a low-energy neutron background. Fission is a good nuclear reaction for simple and portable equipment, because it releases extremely large energy per reaction, making the detection of it relatively unambiguous. With the presently rapidly increasing interest in dose effects in human tissue due to high-energy neutrons, a coordinated research programme spanning over the border between dosimetry and nuclear physics is well motivated, to establish a priority list concerning which nuclear cross sections to measure for development of fast-neutron dosimetry.

The nuclear data situation above 20 MeV

As was mentioned above, the relevant nuclear data for assessing the dose due to fast neutrons are *np* scattering, elastic scattering from nuclei, and light-ion production reactions. An extensive list of references to all experimental data obtained before 2003 is found in ref. [8], and only more recent data are explicitly refereed below.

Of these, the *np* scattering data are of the highest quality. The global data base comprises several thousand data points from thermal energies and up to about 1 GeV, and typically the experimental uncertainties are in the 5 % range. Recently, there has been an intense debate about the *np* scattering cross section at backward angles, where different data sets deviate by 10 % or even more (see ref. [9] for a review). These discrepancies, however, affect only a rather limited angular range, and for the present applications, this is of little importance, because the solid angle subtended is small, which results in very small contributions to the total uncertainty in dose determinations.

The data situation on elastic scattering from nuclei is rather satisfactory up to about 30 MeV. Above this energy, there are published measurements from UC Davis on a few nuclei, including carbon, at 65 MeV. A project on elastic scattering at 100 MeV is in progress at TSL in Uppsala. Up to now, data on hydrogen, deuterium, carbon, oxygen and lead have been published [10,11], and data on nitrogen, silicon, calcium, iron and yttrium are under analysis. The most important finding from a biomedical point of view is that the present nuclear models generally underestimate the cross sections for inelastic scattering on carbon and oxygen in the most important angular range, resulting in a kerma about 30 % too low.

Studies of light-ion production above 20 MeV have been undertaken at UC Davis, UCL Louvain-la-Neuve and Tohoku University. The UC Davis setup was used to measure all light ions emitted from carbon, nitrogen and oxygen at 27, 40 and 61 MeV. In the case of carbon, data are extensive in the forward direction, but more scarce at backward angles, whilst the nitrogen and oxygen data extend only out to 65°. At UCL Louvain-la-Neuve, measurements of the same light ions have been performed between 25 and 75 MeV for carbon and oxygen. The UC Davis and UCL Louvain-la-Neuve data display considerable discrepancies, especially for oxygen in the low-energy domain. Proton and deuteron data from Tohoku have been published for carbon at 65 and 75 MeV. These data, however, have a very high low-energy limit because the experiment was carried out in air.

Recently, similar data have been measured at 96 MeV at TSL Uppsala, covering the entire 20-160° range for all light ions. Full data on oxygen [12] and silicon [13] have been published, and data on carbon are under analysis [14]. It is found that the proton spectra on both carbon and oxygen have a higher cross section in the mid- to high-energy range at forward angles compared to recent state-of-the-art evaluations (see figure 1).

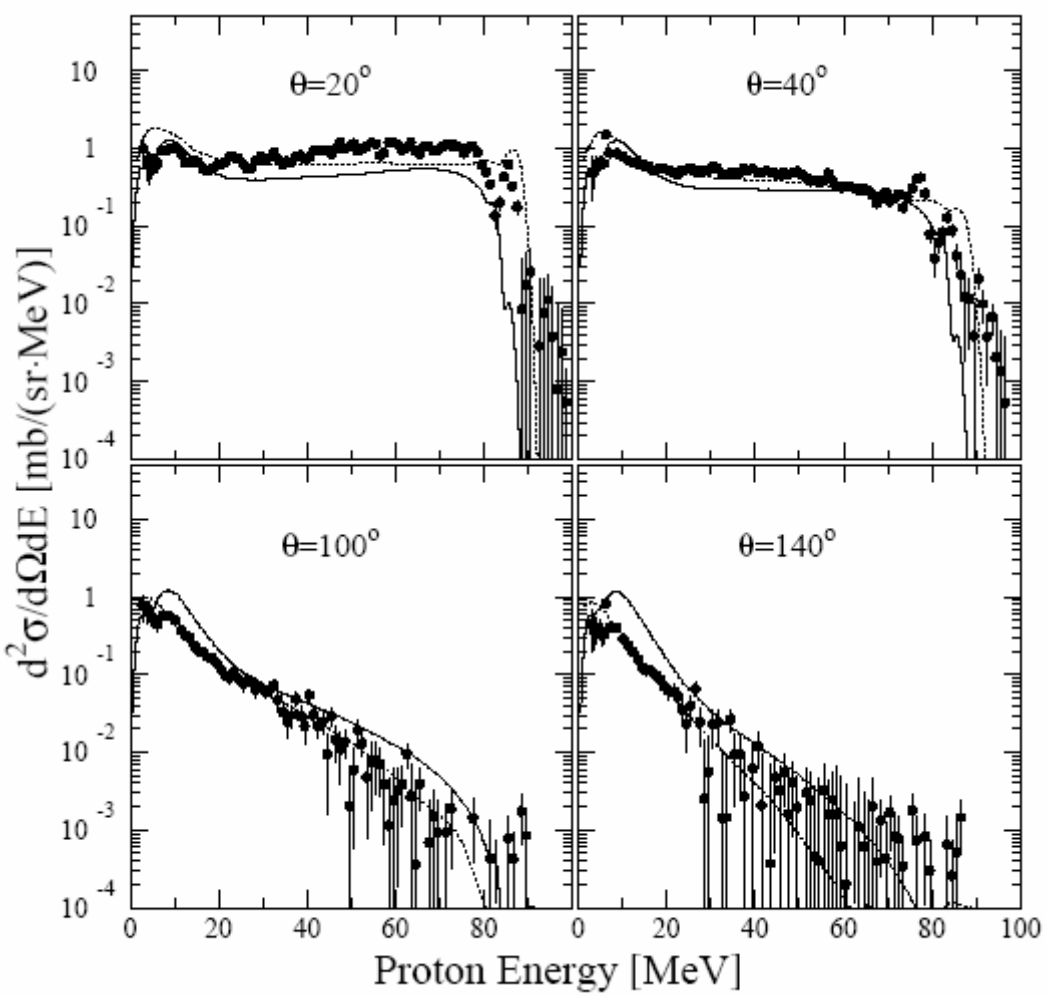

Figure 1: Neutron-induced production of protons on oxygen at 96 MeV [12]. The curves refer to recent theory predictions. See the paper for details.

This feature is probably caused by a stronger component of direct reaction mechanisms, e.g., quasi-elastic scattering, and leads, because of the energy weighting, to a partial kerma coefficient that is 35 % higher. Since protons give a large contribution to the total kerma, the obtained value for carbon is about 25 % higher than that given in the evaluations. It is notable that the new data at 96 MeV support a trend observed for similar data up to 73 MeV, both concerning cross sections and kerma coefficients. It is also striking that the kerma coefficients based on microscopic cross sections seem to be systematically higher than those determined using other techniques.

New data at an even higher energy is of high priority to better understand the evolution of various reaction mechanisms with neutron energy, and ultimately to resolve the problems of increasing discrepancy between data and theory with increasing energy. Such a measurement program at 180 MeV is in progress at TSL.

Proton, deuteron and triton production on carbon has been measured in the 300-580 MeV range at angles from 51° to 165° using the white neutron source at PSI. At these high energies, the cross sections can be reasonably well described by relatively simple scaling relations. This is an interesting observation, and it makes sense from basic nuclear physics arguments. At energies above 200 MeV or so, the reaction mechanisms are relatively simple, because only a few nucleons are involved. This means that information from free scattering can be used for reasonably precise predictions, while at lower energies, the effects of the nuclear medium are large, making the theory much more complicated.

Although these energies are higher than common treatment energies, they are of interest for dose delivery due to cosmic-ray neutrons. In addition, they can be of use to guide theory,

also for lower energies. Effects clearly visible at 300 MeV might have their onset at much lower energy without being apparent.

To summarize, it seems as the biologic effects of high-energy neutrons have been underestimated. Recently, a re-evaluation of the effects of the Hiroshima and Nagasaki nuclear weapons have indicated that the biologic effect of neutrons might have been underestimated also at low energies (0-5 MeV) [15]. If this result is corroborated, it might affect future recommendations for radiation protection concerning neutrons.

Summary and conclusions

Many new applications of fast neutrons require improved understanding of the fundamental processes involved for their further development. With the presently rapid progress in high-quality measurements of neutron-induced nuclear cross sections, as well as in numeric computation and modelling, it is possible that Monte Carlo methods might become a standard tool within a foreseeable future for detailed calculations of the full response of in principle any system, including human tissue or detector media.

This could allow a fully microscopic approach to assessment of biologic effects in tissue due to neutrons, and this could potentially revolutionize our understanding of these effects. A prerequisite for this development is, however, a continuing rapid growth of the experimental data base on double-differential cross sections for light-ion production in relevant nuclei.

Acknowledgements
This work was supported by the European Union Council, the Swedish Natural Science Research Council, the Swedish Nuclear Fuel and Waste Management Company, the Swedish Nuclear Power Inspectorate, Ringhals AB, the Swedish Defence Research Agency, the Swedish International Development Authority, the Thai Ministry of University Affairs and the International Program in the Physical Sciences at Uppsala University.

References

[1] Bartlett, D.T. et al. , Radiat. Res. Congress Proceedings **2**, 719-723 (2000). See also the Proceedings of the International Conference on Cosmic Radiation and Aircrew Exposure, Radiat. Prot. Dosim. **86(4)** (1999).
[2] Tubiana, M., Dutreix, J. and Wambersie, A., *Introduction to Radiobiology*, Taylor & Francis (1990).
[3] J. Blomgren, EU enlargement workshop on Neutron Measurements and Evaluations for Applications, Budapest, Hungary, November 5-8, 2003. EUR Report 21100 EN, Luxembourg, ISBN 92-894-6041-5, European Communities, 2004, p. 130.
[4] J. Blomgren, EU enlargement workshop on Neutron Measurements, Evaluations and Applications, Bucharest, Romania, October 20-23, 2004. EUR Report 22136 EN, Luxembourg, ISBN 92-894-8618-X, European Communities, 2006, p. 1.
[5] A definition can be found in ICRU Reports **60** (1998) and **63** (1999).
[6] Bewley, D. K., *The Physics and Radiobiology of Fast Neutron Beams (Medical Science Series)*, Adam Hilger Ltd., Bristol and New York, p. 18 (1989).
[7] Elford, J. H. and Cunningham, J. R. *The Physics of Radiology (American Lectures series; Publication no 1054)*, 4th edition, Charles C. Thomas Publisher, Illinois, p. 218 (1983).
[8] J. Blomgren and N. Olsson, Radiat. Prot. Dosim. **103(4)** (2003) 293.
[9] *Critical Issues in the Determination of the Pion-Nucleon Coupling Constant*, ed. J. Blomgren, Phys. Scr. **T87 (**2000).
[10] J. Klug et al., Phys. Rev. **C 68** (2003) 064605.
[11] P. Mermod et al., 95 MeV neutron scattering on hydrogen, deuterium, carbon and oxygen, submitted to Phys. Rev. C.
[12] U. Tippawan et al., Phys. Rev. **C 73** (2006) 034611.
[13] U. Tippawan et al., Phys. Rev. **C 69** (2004) 064609.
[14] U. Tippawan et al., *Light charged-particle production in 96 MeV neutron-induced reactions on carbon and oxygen*, in Proceedings of Tenth International Symposium on Neutron Dosimetry (NEUDOS10), Uppsala, Sweden, June 12-16, 2006, eds. J. Blomgren and L. Lindborg, to appear in Radiat. Prot. Dosim.
[15] W. Rühm, *The role of neutrons in Hiroshima and Nagasaki on cancer risk estimates from the a-bomb survivors*, in Proceedings of Tenth International Symposium on Neutron Dosimetry (NEUDOS10), Uppsala, Sweden, June 12-16, 2006, eds. J. Blomgren and L. Lindborg, to appear in Radiat. Prot. Dosim.

Tenth International Symposium on Neutron Dosimetry

The Tenth International Symposium on Neutron Dosimetry (NEUDOS 10) took place in Uppsala, Sweden, June 12-16, 2006. The conference had the theme “Progress in dosimetry of neutrons and light nuclei“, reflecting the widening of the scope of the conference to include not only neutron dosimetry, but all hadronic particles. This is also a recognition of the fact that the dose due to neutrons is delivered not by the neutron itself, but via secondary particles created in neutron-induced nuclear reactions, i.e., protons, deuterons, alpha particles and various other ions released in tissue. Thereby, the dosimetry of neutrons has a large scientific overlap with dosimetry in proton and heavy ion therapy.

Historic development

This series of conferences started in 1972 and a historical view of these symposia provides testimony of the development of the field. In the first three meetings (1972-77) the program was to about 90 % composed of topics on dosimetry for radiotherapy ("beam dosimetry") and only about 10% on radiation protection dosimetry. The conferences were primarily motivated by the research needs for therapy with fast neutrons, and participants primarily came from EU and the US. At these meetings, nuclear and atomic data, microdosimetry, and facilities for fast neutron therapy were prevalent issues that later have decreased in importance.

In the 1980’s, the programme had shifted to about equal fractions of beam dosimetry and radiation protection dosimetry. Radiation protection issues had at that time gained importance, influenced by new ICRU quantities. Increased attention was thus given to calibration aspects and calibration facilities, as well as microdosimetric principles for radiation protection. Also, the first papers using transport calculations appeared.

In the 1990’s, the balance had moved even further, to 20 % beam dosimetry and 80 % radiation protection dosimetry, reflecting a decline of fast neutron therapy. New topics were BNCT and proton therapy, electronic dosemeters for neutrons, and cosmic radiation and aircraft crew dosimetry.

There was an eight-year period without a conference of this series, but in 2003 the series was revived with NEUDOS9. Still the agenda comprised similar weights of beam dosimetry and radiation protection dosimetry, and this was the case also at NEUDOS10. At both symposia, many contributions have concerned aircraft crew dosimetry. Criticality and retrospective dosimetry have grown in importance. The attendance has increased and the age profile has changed dramatically; there were relatively many young participants, and participants new to the field. Europe provided the largest number of attendants with Japanese attendance now being larger than that of the USA. In total, 177 participants, whereof 20 % women, from 26 countries participated in Uppsala.

Conference programme

The conference dealt with five sessions:

A. Basic Aspects

B. Instrumentation and Techniques
C. Radiation Quality
D. Radiation Protection
E. Radiotherapy

These sessions were rather unequal in size with B and D being slightly larger than A, and C and E being together about as large as A.

The number of oral presentations was rather limited, since no parallel sessions were organized. Therefore, a vast majority of the papers were presented in poster sessions. These poster sessions were opened with an overview report. The authors of poster contributions provided summaries of their papers in a one-page slide before the conference, and selected reporters gave an introduction to all papers of the entire poster session before the audience left the plenary hall and went out to the posters.

Invited talks

Lars-Erik Holm, director of the Swedish Radiation Protection Authority, but invited in the role as chairman of the International Commission on Radiation Protection (ICRP), presented the new ICRP recommendations that had been issued in preliminary form shortly before the conference.

Arjan Koning, expert scientist at the Nuclear Research and consultancy Group (NRG), the Netherlands, reported on recent development in nuclear theory of biomedical relevance. He and his group have developed user-friendly codes and nuclear data libraries that allow high-quality nuclear data handling without requiring wide expertise of the users.

Grady Hughes of the MCNP team at Los Alamos National Laboratory, USA, gave a talk, by himself depicted as anecdotal, on uncertainties in Monte Carlo calculations beyond statistics. This talk was motivated by the fact that numerical methods have now become a standard tool in the field, and it is important that reliability issues become identified. One particular example presented was that the exact composition of concrete can be of large importance in shielding of neutrons. Unfortunately, the composition is often poorly documented, and sometimes even impossible to know with sufficient precision, because the final porosity and water content can be beyond control in the casting process.

Werner Rühm of GSF, Germany, presented a recent re-evaluation of the biological information that can be extracted by judging the effects of the Hiroshima and Nagasaki nuclear bombs. Their conclusion is that it might be possible that the relative biologic effect of neutrons have been underestimated. Since the combined effect of neutrons and gamma rays is better known than the contribution from each type of radiation, this might simultaneously imply that gamma rays might be somewhat less severe than previously thought. If these results gain acceptance, they might influence recommendations for radiation protection. It should be pointed out, however, that the uncertainties in this type of research are large.

Takashi Nakamura of Tohoku University and National Institute of Radiological Sciences, Japan, presented recent progress in development of phoswich detectors for fast neutron detection. John Gueulette of Louvain-la-Neuve, Belgium, gave an overview of the present knowledge of biologic effects of high-LET radiation. Rick Tanner of the Health and Radiation Protection Authority, United Kingdom, presented lessons learned from EVIDOS, an EC sponsored project which investigated the dosimetry of mixed neutron-photon fields in workplaces of nuclear industry..

Bengt Glimelius of the Academic Hospital, Uppsala, informed about the plans for a national facility for particle therapy to be built in Uppsala with first treatments planned for 2011. The decision to build the new center was taken only a few days before the conference, so this invited talk was no doubt of the largest news value.

Highlights

Selecting highlights from a conference is always a sensitive matter, because it can be interpreted as a grading of research quality. Instead of giving our subjective view, we here report the highlights from a media perspective. The re-evaluation of Hiroshima and Nagasaki attracted the most wide-spread attention from media, and was reported in newspapers and national scientific radio. The contributed presentations by Frank Cucinotta, Hooshang Nikjoo et al. on expected doses to future astronauts on Mars missions were also reported in national radio. Newspaper articles on the neutron beam facility at The Svedberg Laboratory in Uppsala and the research carried out there were also prevalent, being of local importance.

Proceedings

Proceedings of the conference will be published in Radiation Protection Dosimetry in a dedicated issue, planned for late spring 2007. Jan Blomgren and Lennart Lindborg, the latter affiliated with the Swedish Radiation Protection Authority, are joint guest editors for this volume. They are assisted by five co-editors, one for each session: Helmut Schuhmacher, Natalia Golnik (Institute of Atomic Energy, Otwock-Swierk, Poland), Bo Stenerlöw (Uppsala University, Sweden), Frantisek Spurny (Academy of Sciences of the Czech Republic, Prag, Czech Republic) and Dan Jones (iThemba LABS, Cape Town, South Africa).

Social program

A number of social events took place during the conference. The scientific and educational history of Uppsala provided theme for an afternoon, in which the participants visited the vacation home of Carl Linnaeus, the inventor in the 18th century of the biologic systematic system still used, followed by a visit to the Uppsala cathedral including a choir concert. A conference dinner was held at the historic settings of the Uppsala castle, built around the year 1500. In this dinner, a musical program with lyrics by Dag Hammarskjöld, the UN secretary general 1953-61, was presented. His father was governor of Uppsala, and therefore Dag lived at the castle during his adolescence years.

The local The Svedberg Laboratory, equipped with facilities for proton therapy and neutron physics and dosimetry research, was the subject of a combined scientific and social event, in which sandwiches and beverages were served as part of the visit.

Acknowledgments

We would like to thank all persons involved in the organization, as well as all participants for having created a nice atmosphere during the conference. The NEUDOS10 conference was

financially supported by the Swedish Research Council, the Swedish Foundation for Strategic Research, the Technical University Delft (organizers of NEUDOS9), the Swedish Cancer Society, the Swedish Radiation Protection Authority, the Swedish Nuclear Power Inspectorate, the Swedish Nuclear Technology Centre, the Forsmark Nuclear Power company, the Ringhals Nuclear Power company, Synodys Instruments, and the council of Uppsala city.

Next conference

The NEUDOS symposia are organized under the auspices of the European Radiation Dosimetry Group, EURADOS, which stimulates collaboration between European laboratories in the field of dosimetry of ionising radiation. Conferences with similar scope are not regularly organized outside Europe, and therefore the NEUDOS conferences have become of global importance, although with a European dominance. Recognizing this feature, NEUDOS11, will be the first symposium in the series to be organized outside Europe. You are welcome to Cape Town, South Africa, in October 2009!

Jan Blomgren
Department of Neutron Research
Uppsala University, Sweden
NEUDOS10 chairman

Helmut Schuhmacher
Physikalisch-Techniche Bundesanstalt
Braunschweig, Germany
EURADOS chairman

Elastic scattering of 96 MeV neutrons from iron, yttrium and lead

A. Öhrn, J. Blomgren,* P. Andersson, A. Ataç, C. Gustavsson,
J. Klug, P. Mermod, S. Pomp, P. Wolniewicz, and M. Österlund
Department of Neutron Research, Uppsala University, Box 525, S-75120 Uppsala, Sweden

L. Nilsson
Department of Neutron Research, Uppsala University, Sweden and
The Svedberg Laboratory, Uppsala University, Sweden

B. Bergenwall
Department of Neutron Research, Uppsala University, Sweden and
Department of Radiation Sciences, Uppsala University, Sweden

K. Elmgren and N. Olsson
Department of Neutron Research, Uppsala University, Sweden and
Swedish Defence Research Agency (FOI), Stockholm, Sweden

U. Tippawan
Department of Neutron Research, Uppsala University, Sweden and
Fast Neutron Research Facility, Chiang Mai University, Thailand

S. Dangtip and P. Phansuke
Fast Neutron Research Facility, Chiang Mai University, Thailand

P. Nadel-Turonski
Department of Radiation Sciences, Uppsala University, Sweden and
George Washington University, Washington, D.C., USA

O. Jonsson, A. Prokofiev, and P.-U. Renberg
The Svedberg Laboratory, Uppsala University, Sweden

V. Blideanu, C. Le Brun, J.F. Lecolley, F.R. Lecolley, M. Louvel, N. Marie-Noury, and C. Schweitzer
LPC, ISMRA et Université de Caen, CNRS/IN2P3, France

Ph. Eudes, F. Haddad, and C. Lebrun
SUBATECH, Université de Nantes, CNRS/IN2P3, France

E. Bauge, J.P. Delaroche, M. Girod, and X. Ledoux
DPTA/SPN CEA, Bruyères-le-Châtel, France

K. Amos
School of Physics, University of Melbourne, Victoria 3010, Australia

S. Karataglidis
Departments of Physics and Electronics, Rhodes University, Grahamstown, 6140, South Africa

R. Crespo
Departamento de Fisica, Instituto Superior Técnico, Lisboa, Portugal

W. Haider
Department of Physics, AMU, Aligarh, India

Data on elastic scattering of 96 MeV neutrons from ^{56}Fe, ^{89}Y and ^{208}Pb in the angular interval 10-70° are reported. The previously published data on ^{208}Pb have been extended, as a new method has been developed to obtain more information from data, namely to increase the number of angular bins at the most forward angles. A study of the deviation of the zero-degree cross section from Wick's limit has been performed. It was shown that the data on ^{208}Pb are in agreement with Wick's limit

while those on the lighter nuclei overshoot the limit significantly. The results are compared with modern optical model predictions, based on phenomenology and microscopic nuclear theory. The data on ^{56}Fe, ^{89}Y and ^{208}Pb are in general in good agreement with the model predictions.

PACS numbers: 24.10.Ht, 25.40.Dn, 28.20.Cz

I. INTRODUCTION

The study of a system consisting of an incident nucleon interacting with a target nucleus requires the solution of a many-body equation. The system can, however, be approximated by considering two bodies interacting via a complex mean-field potential. This so called optical model potential (OMP) is an important ingredient in calculations of cross sections, e.g., elastic and inelastic scattering, (p,n) and (n,p) reactions. In other words, a good global optical model is a powerful tool for predicting observables for energies and nuclides for which no measurements exist.

The optical models of today predict data successfully, but there are still needs of data for further developments. One commonly repeated request is neutron elastic scattering data at high energies [1]. The reason for this is that above 20 MeV very little high-quality neutron data exist. There are high-quality neutron total cross section data on a series of nuclei up to about 600 MeV [2]. In addition, (n,p) data in the forward angular range at modest excitation energies are available up to about 300 MeV for a rather large number of nuclei [3, 4].

Apart from the extensive measurements of the *np* scattering cross section [5], there are very few measurements on neutron elastic scattering from nuclei heavier than $A = 6$. Above 30 MeV neutron energy, only three experiments have produced data with an energy resolution adequate for resolving individual nuclear states; an experiment at MSU at 30 and 40 MeV [6, 7], one at UC Davis at 65 MeV [8, 9] and one at LAMPF from 65 to 255 MeV [10]. Experiments at 55, 65 and 75 MeV have been performed at TIARA, Japan Atomic Energy Research Institute, and were published in Ref. [11, 12], having energy resolutions in the $10 - 20$ MeV range. Also available are a few measurements in the $0-30^\circ$ range, between 80 and 350 MeV, all with energy resolutions of 15 MeV or more [13–17]. At small angles, this poor energy resolution is not a drawback, as elastic scattering dominates heavily. At larger angles, however, such a resolution makes data very difficult to interpret. An overview of the neutron elastic scattering experiments is given in Table I, where studied nuclei, neutron energies, energy resolutions and angular ranges are shown.

In the present paper, new data on elastic neutron scattering at 96 MeV from ^{56}Fe and ^{89}Y are published. They conclude a series of measurements to which the previously published data on ^{12}C, ^{16}O and ^{208}Pb belong [18, 19]. The analysis of the data on ^{208}Pb has been extended as part of this work and the results will be published here. A new method has been developed to extract more information from data, i.e., to increase the number of angular bins for the most forward angles. The re-analysis has not been performed for ^{12}C and ^{16}O as the angular distributions show little structure at small angles. The new data on ^{208}Pb supersedes those previously published.

Elastic neutron scattering at high energies is not only of academic interest, but has several applications in industry and medicine. One major application, which has attracted considerable interest lately, is the handling of nuclear waste by incineration in subcritical reactors fed by fast neutrons produced in spallation targets. New nuclear data are requested for feasibility assessments of these techniques. Four elements have attracted special interest; lead as spallation/cooling material, iron for shielding and construction, uranium as fuel and zirconium as fuel cladding. Our measurements cover three of these four requests. The deformed shape of the ^{238}U nucleus makes measurement of elastic neutron scattering difficult, mainly because of problems of resolving the ground state. In our experiments, we have used ^{89}Y instead of ^{90}Zr simply because the desired amount of ^{90}Zr was not possible to obtain. Instead of using natural zirconium, a monoisotopic target was preferred.

An interesting feature of the optical model is that it establishes a lower limit of the differential cross section at 0° if the total cross section is known, referred to as Wick's limit [20, 21]. For a large range of energies and target masses, the zero-degree cross section falls very close to the limit. Therefore it has been suggested that this apparent equality could be used for normalization in lack of other methods [22]. The analysis of the previous data on ^{12}C [18] and an investigation of data from a previous experiment at 65 MeV [9] indicate, however, that the 0° cross sections can exceed Wick's limit significantly. After the publication of these two data sets, a theoretical study of this effect has been performed, see Ref. [23]. This has motivated a systematic study versus target mass, which is presented in Section IV C.

This paper is organized in the following way: A presentation of the neutron facility and the detector setup is given in Section II. The procedure of data reduction and discussion of the results are given in Sections III and IV. Finally, a summary and conclusions are given in Section V.

*Corresponding author. Tel. +46 18 471 3788. E-mail address: jan.blomgren@tsl.uu.se

II. EXPERIMENTAL ARRANGEMENT

A. Neutron beam and detector setup

The present experiments were performed at the The Svedberg Laboratory, Uppsala, Sweden. A detailed description of the neutron beam facility has been published in Ref. [24] and therefore only a brief summary will be given here.

An overview of the facility is presented in Fig 1. Neutrons of 96 MeV were produced by protons impinging on a neutron production target, consisting of lithium enriched to 99.98 % in ^{7}Li, using the ^{7}Li(p,n) reaction. After the lithium target, the proton beam was bent into a well-shielded beam dump. The resulting neutron spectrum consisted of a peak at 96 ± 0.5 MeV (1.2 MeV FWHM) and a low-energy neutron tail, which was suppressed by time-of-flight techniques. The neutron beam was defined by a system of three collimators. At the scattering target, the beam diameter was 9 cm with a typical neutron yield of $2.5{\cdot}10^6$ s^{-1} over the whole beam area. The neutron beam was dumped in a tunnel about 10 m downstreams of the experimental position. Neutron monitoring was performed by a fission counter (TFBC) and the integrated proton beam current from the proton beam dump.

The experimental setup SCANDAL (SCAttered Nucleon Detection AssembLy) was used to detect the scattered neutrons (see Fig. 2). The detection of neutrons is based on conversion to protons and detection of the recoil protons. The setup consists of two identical arms placed on each side of the beam, covering the angular ranges 10–50° and 30–70°. Each arm has a 2 mm thick veto scintillator for fast charged-particle rejection, a 10 mm thick neutron-proton converter scintillator, a 2 mm thick ΔE plastic scintillator for triggering, two drift chambers for proton tracking, another 2 mm thick ΔE plastic scintillator which is also part of the trigger, and an array of CsI detectors (12 on each arm) for energy determination of the recoil protons produced in the converter by *np* scattering. The trigger, when detecting neutrons, is defined by a coincidence of the two trigger scintillators, with the front detector acting as a veto. It is also possible to run SCANDAL in proton mode, by changing the veto detector to accept charged particles. The total energy resolution of the individual CsI crystals is different, and on average 3.7 MeV (FWHM), see Ref. [24].

B. Experimental procedure

The experiments were carried out in different runs of about one week each. Data on lead have previously been published in Ref. [18] where details about that particular experiment are given. Each experimental week begun with a calibration measurement in which a CH_2 target was placed in the neutron beam and recoil protons from *np* scattering were detected.

After calibration, the SCANDAL setup was changed to neutron detection mode in which the veto scintillator signals are used for charged-particle rejection. The lower limit of the angular range, 10°, represents an arm position where the scintillator detectors barely avoid being hit by the neutron beam. The largest angle, 70°, is the upper limit where it is possible to achieve reliable statistics in one week of data taking time. The overlapping angular range 30-50°, allows studies of the consistency between the two arms. Four scattering targets were used, a natural iron cylinder (91.8 % ^{56}Fe, 5.8 % ^{54}Fe, 2.1 %^{57}Fe and 0.3 % ^{58}Fe), 5 cm high and 5 cm in diameter, with a mass of 777 g, an yttrium cylinder, 5.2 cm high and 5 cm in diameter, with a mass of 456 g, a radiogenic lead cylinder (88 % ^{208}Pb, 11 % ^{206}Pb and 1 % ^{207}Pb), 6.3 cm high and 2.9 cm in diameter, with a mass of 444 g, and a carbon cylinder, 5 cm high, 5 cm in diameter and with a mass of 178 g, which was used to provide data for normalization. Background data were recorded by removing the scattering cylinder from the setup.

The dead time in the data acquisition system varied with the different experiments. For iron, yttrium and lead, it was around 14 %, 6 % and 4 %, respectively, and for the background measurements about 2 %.

III. DATA ANALYSIS

A. Calibration

The data were analyzed offline event-by-event using the ROOT package [25].

In a first stage, the time information from the drift chambers was converted to positions. The angular information and detector hit positions of the particle trajectories were calculated, based on the obtained drift chamber coordinates. It was required that the the calculated coordinates of the detected particle corresponded to a position within the volume between the trigger scintillators. The coordinates were also used to trace the trajectories of the protons, which in turn were used to establish the hit positions for the CsI detectors and the conversion points in the converter scintillator.

Each CsI detector was calibrated individually with *np* data from the calibration runs.

Two calibration peaks in each CsI detector were identified; the pedestal channel corresponding to zero-energy deposition in the detector, and the *np* scattering peak. A linear relationship was assumed between pulse height (PH) and deposited energy. The energy of the *np* peak was obtained by calculating the energy loss of the proton through the detector setup from the target to the CsI in question. The centroid channel was determined by fitting a gaussian to the *np* peak.

Each plastic scintillator has two PM tubes attached to one of the longer horizontal sides. They were calibrated by choosing a narrow, central section of the scintillator, i.e., where the distance is approximately the same to both

PM tubes and where it can be assumed that these detect half the light each of the deposited energy. Also for the plastic scintillators, the pedestal channel and the proton peak were used as calibration points. The total deposited energy of the plastic scintillators (ΔE) was obtained by adding the contribution from the two PM tubes. The shape of the plastic scintillators give rise to a geometric effect, i.e., protons with the same energy yield slightly different ΔE signals depending on where they hit the detector. The deviation from the expected ΔE value was mapped over the detectors as a function of the location in the scintillator, both horizontally and vertically, and could subsequently be compensated for.

To obtain the correct energy loss throughout the whole detector setup, the energy losses in materials where the proton is not detected, such as detector wrapping, drift chamber foils, drift chamber gas and air, were calculated.

Finally, the total energy of the charged particle was calculated as the sum of the different contributions from the detectors and other materials. This resulted in excitation-energy spectra for the different angles in the laboratory system related to the position of the CsI crystal in which the proton was stopped.

B. Data reduction

Protons were separated from other charged particles, mostly deuterons originating from the converter scintillator, by a $\Delta E - E$ technique. A two-dimensional cut was applied to a scatter plot where the sum of the detected energy losses in the two trigger scintillators was plotted versus the energies in the CsI detectors. Since the Q-value for ^{12}C(n,d) is -13.7 MeV, there is no physical background of deuterons in the energy range of elastic scattering and this cut is not crucial for the extraction of elastic scattering events.

To reject events from the low-energy tail of the neutron spectrum, a time-of-flight (TOF) cut was used. The TOF was defined as the time difference between the first trigger detector and a signal from the cyclotron radiofrequency system. This information is, however, not important for the present experiment as a low-energy neutron in the beam cannot induce emission of a full-energy neutron from the scattering target.

In previous experiments using the SCANDAL setup, (see Refs. [19, 24, 26]), each CsI crystal defined an angular bin. For the present experiments, however, the CsI area for the crystals at the most forward angles, where the statistics allow such a procedure, has been divided into two areas to obtain more data points. This resulted in 36 angular bins for ^{56}Fe, 32 bins for ^{89}Y and 30 for ^{208}Pb. The statistics were better for the iron experiment and therefore allowed more CsI detector hit areas to be split up.

To distinguish which events belonged to which bin, a scatter plot with the horizontal and vertical hit positions was constructed. In these scatter plots, two-dimensional cuts were applied in order to select the accepted hit area. Since the energy determination for events where a proton passes through more than one CsI detector is very poor, due to large straggling effects in CsI wrapping materials, it was important that the position cuts were set in such a way that the protons were completely stopped in a single detector.

Since the converter scintillator contains both carbon and hydrogen, neutrons can be converted to protons by the ^{12}C(n,p) reaction instead of the desired *np* scattering, i.e., H(n,p). The Q-value for the ^{12}C(n,p) reaction is -12.6 MeV meaning that at forward angles, an energy cut is sufficient to distinguish between the two reactions. At conversion angles larger than about 20°, the proton energies from the two processes overlap and it cannot be decided from which reaction the proton originates. Therefore, an opening angle criterion was set, demanding that the conversion angle be less than 10°. The procedure described above was also applied to the background data.

Up to this point, the data reduction was performed event-by-event. Subsequently, the data were stored in excitation-energy histograms, one for each angular bin. Background data were subtracted from the signal spectra after normalization to the same neutron fluence and taking dead time into consideration. The corresponding operations were also performed to produce variance histograms, to be used later for estimation of the statistical errors.

C. Extraction of elastic scattering events

To obtain the number of elastic scattering events at each angle, gaussians were fitted to the ground state peak and the lowest excited states, and subsequently, the area of the gaussians were calculated. An example of this is given in Fig. 3. The heights, positions and widths of the ground state gaussians were treated as free parameters. The same width was used for the gaussians describing low-lying excited states, but the heights were allowed to vary independently. The centroids of the inelastic states were fixed relative to the ground state peak by the energy calibration. At excitation energies of about 10 MeV and up, protons from the ^{12}C(n,p) reaction in the converter formed a rather structureless distribution, approximated by a gaussian. The width and the height of the corresponding gaussian were treated as free parameters. Simultaneously, a spectrum function was constructed to describe the entire spectrum to 14 MeV above the ground state peak. The choice of which inelastic states to include was a rather pragmatic decision, based on visual inspection of the excitation spectra and by studying proton inelastic scattering at nearby energies, as well as neutron inelastic scattering at lower energies. For ^{56}Fe, a gaussian was fitted to the excited state at 4.5 MeV [27], and for ^{89}Y, gaussians were fitted to states at 5.0, 7.0 and 9.0 MeV [28].

The variance of the number of elastic scattering events

was extracted by applying this method also to the variance histograms. At large angles, the fitting procedure described above could not be used due to poor statistics. For those angles, the ground state yield was extracted by integration, with limits determined by visual inspection.

D. Cross section calculation and normalization

The number of neutrons in the beam was given by either the fission counter (TFBC) or the integrated proton beam current. The number of target nuclei was calculated from the weight and volume of the scattering target. The solid angles for protons detected in the CsI crystals are individual for each crystal depending on the distance to the target and the size of the accepted detection area. A computer code was developed to calculate this, see Ref. [18]. The code also takes into account the neutron energy (which varies with neutron angle) as it will affect the conversion probability, due to the energy dependent *np* cross section. The result is individual effective solid angles for each CsI, containing the geometric solid angle and the probability that a converted proton hits the crystal.

The same code was used to calculate the average neutron scattering angle for each bin. Since the energy resolution is different for individual CsI crystals, the low-energy continuum originating from the ^{7}Li(p,n) reaction will contribute differently to the full-energy *np* peaks at different angles and hence to the ground state peaks in the excitation-energy spectra. This contribution, which is a function of the peak width [29] has been determined using experimental neutron spectra for the ^{7}Li(p,n) reaction measured by Byrd and Sailor [30]. Correction factors for this effect were used when calculating the cross section. The effect is typically around 3 % and always less than 6 %.

The proton detection efficiency has contributions from the efficiencies of each drift chamber plane, the efficiency of selecting the correct drift chamber wire in multiple-hit events and the CsI efficiency. The total drift chamber efficiency has been measured to 0.75 ± 0.10 (an average of 0.93 per plane). The efficiency of selecting the correct wire has been measured to 0.93 (0.98 per plane) and the CsI efficiency, i.e., the probability that a proton slowing down in the CsI crystal does not undergo a nuclear reaction before coming to rest, to 0.92 ± 0.01. This makes a total proton detection efficiency of 0.64 ± 0.10.

The absolute scale of the cross sections was given by the number of neutrons in the beam. The TFBC, however, has an uncertainty of more than 10 % and therefore further normalization was required. The data on iron and yttrium were measured relative to carbon. In Ref. [18] a new normalization procedure was introduced, using the known data on the total cross section and the reaction cross section, to calculate the total elastic cross section to which the elastic differential cross section was normalized. For carbon, the normalization uncertainty was estimated to 3 %. Measuring relative to carbon has been adopted by us as a secondary standard for normalization of our data. We estimate the normalization procedure to have an uncertainty of about 5 %.

Since extended targets have been used for the present experiments, corrections for neutron attenuation and multiple scattering were necessary. These corrections have been performed using a Monte Carlo code [31]. As input to the code, an angular distribution in the laboratory system was given, in this case the experimental data obtained with SCANDAL. After conversion to the c.m. system and calculation of the attenuation, the code simulated the experiment. The aim of the program was to find a distribution that, when used as input for the simulation, resulted in an output reproducing the measured angular distribution. For the new dataset on ^{208}Pb this turned out not to be a good method as the angular distribution showed so prominent structure that the code could not succesfully describe it. Instead a simulation of the experiment was carried out by an MCNPX [32] calculation, using the cross section predicted by the ENDF-VI/B library [33]. First, the code simulated elastic neutron scattering using a point target of ^{208}Pb. The second step was to simulate the reaction using a lead cylinder of the actual size of the experiment. The two angular distributions obtained were compared and correction factors could be calculated from the ratio of the two simulations. Finally, the data on ^{208}Pb were corrected for the content of ^{206}Pb.

E. Estimation of experimental uncertainties

A thorough investigation of the experimental uncertainties is described in Ref. [18] and therefore only an overview will be given here.

Since the purpose of the present experiment has been to obtain a set of relative differential cross section data, which is finally normalized using previously known information, only uncertainties that affect the shape of the angular distribution are of importance.

The random error is due to counting statistics and includes contributions from the background subtraction. It varies significantly with scattering angle, due to the steepness of the cross sections.

The Monte Carlo simulation for correction of multiple scattering, adds a statistical error to the point-to-point uncertainty. The total statistical errors, including both these contributions, are calculated in the program and given as output together with the corrected angular distribution. The results are listed in Tables II, III and IV. In addition to the total errors, the relative statistical errors in the measurements, i.e., before corrections, are shown.

The correction (< 6 %) for the contribution from the low-energy continuum of the ^{7}Li(p,n) spectrum to the *np* scattering peak introduces a systematic uncertainty that varies with peak width and is therefore different for

each CsI crystal due to their individual energy resolutions. Assuming a relative uncertainty of 10 % in the correction, an error in the data of at most 0.6 % arises.

For nuclei like ^{208}Pb which have a pronounced angular dependence for the elastic scattering differential cross section, small uncertainties in the angular information can produce significant uncertainties in the result. The effect is present also for iron and yttrium but is not as strong. The angular uncertainties in the present experiment are dominated by the incomplete knowledge of the positions of the target and the drift chambers. Both these are known to slightly better than 1 mm, resulting in an angular uncertainty of about 1°. This uncertainty results in an equal shift of all data points produced by the same SCANDAL arm. The drift chambers contain, however, many drift cells, which work as physically independent detectors, each with its own TDC for time recording. Imperfect calibration can produce conversion position errors up to about 0.5 mm, which corresponds to about 0.5° shift of the presumed angle. This uncertainty is randomly distributed among the data points. The uncertainties are given in Tab. II-IV.

IV. RESULTS AND DISCUSSION

A. Model predictions

Angular distributions of elastic neutron scattering from ^{56}Fe, ^{89}Y and ^{208}Pb are presented in Fig. 4, where they are compared with phenomenological (left panel) and microscopic (right panel) optical model predictions. The theoretical curves have been folded with the experimental angular resolution to facilitate comparisons with data.

It is important to realize that the phenomenological and microscopic formed optical potentials are critically different, not only in their formulation but also in their intent. The phenomenological approach is a data driven formulation. Data is required in advance to define the parameter values of the potential. On the other hand, microscopically formed optical potentials are predetermined, and their success or not in reproducing measured data reflects on whatever inadequacies there may be in the underlying facets of their formulation.

Predictions by a phenomenological global optical model potential (OMP) of Koning-Delaroche [1] are given by the solid curves in the left panel of Fig. 4. This global OMP is valid for incident nucleon energies between 1 keV and 200 MeV and masses from 24 to 209. It is based on a smooth functional form for the energy dependence of the potential depths, and on physically constrained geometry parameters. An extensive collection of experimental data sets for different types of observables was used to determine the parameters of this OMP.

The dotted line in the left panel of Fig. 4 shows the result of a scattering calculation performed in 1990 by Kozack and Madland [34], using their global nucleon-nucleus intermediate-energy potential based on Dirac phenomenology for ^{208}Pb [35]. The potential contains scalar and vector terms, based upon the Walecka model [36], and includes isospin dependence through a relativistic generalization of the Lane model [37]. The isospin dependence was determined by simultaneous least-squares adjustment with respect to measured proton elastic scattering and neutron total cross section observables. Symmetrized Saxon-Wood form factors are used, and the potential contains a total of 20 parameters to describe nucleon scattering from ^{208}Pb in the energy range 95–300 MeV.

An OMP calculation by Romain and Delaroche [38], based on a dispersive OMP approach treating nonlocality in a manner similar to that of Buck and Perey [39] for energy dependencies, is presented as the dash-dotted line in the left panel of Fig. 4.

Comparisons were also made with the cross sections given by the evaluated nuclear data files in the ENDF/B-VI library, Release 6 (ENDF-6) [33] and are presented with dashed curves in the left panel.

Amos *et al.* have developed a microscopic (g-folding) prescription for the optical potentials [40]. Therein an effective, medium dependent and complex NN interaction has been determined in coordinate space and mapped from g-matrices that are solutions of Brueckner-Bethe-Goldstone equations built upon the free Bonn-B NN interaction. This effective interaction is subsequently folded with microscopic model wave functions of the target to define a complex, fully non-local optical potential; the non-locality arising from the nucleon exchange amplitudes due to the effects of the Pauli principle. The full non-local form of the Schrödinger equations are solved. While simple shell models have been used to define the ground state structures for ^{56}Fe and ^{89}Y, in the case of ^{208}Pb a Skyrme-Hartree-Fock model has been used in the folding process. This structure model, obtained with a constraint on the neutron equation of state giving a neutron skin $S = 0.16 \pm 0.02$ fm for ^{208}Pb, lead to g-folding predictions of 65 and 200 MeV proton and neutron scattering cross sections in excellent agreement with data [41]. The predictions are presented as the solid line in the right panel of Fig. 4.

Bauge, Delaroche and Girod have developed a Lane-consistent, semi-microscopic OMP [43], which is built by folding radial matter densities from a Hartree-Fock-Bogoliubov calculation (using the Gogny D1S effective interaction) with an OMP in nuclear matter based on an extension of that of Jeukenne, Lejeune and Mahaux (JLM) [46]. The result is presented as the dashed line in the right panel of Fig. 4. This extended OMP features strong re-normalizations of its isovector components, and has been tested extensively against (p,p) and (n,n) data, as well as (p,n) IAS data [43].

Haider and Saliem have developed a local microscopic optical potential [44], where the Bethe-Goldstone integral equation is solved using the soft-core Urbana v-14 inter-nucleon potential [45] to obtain the self-consistent

nuclear matter optical potential as described in Ref. [46]. The radially dependent numerical g-matrices in different isospin states of the two-nucleon system are obtained as described in Refs. [44, 47, 48] and from this, the direct and exchange g-matrices for incident protons and neutrons are obtained. This was followed by folding the g-matrices over the point proton and neutron densities in the target to obtain the neutron-nucleus optical potential. In the present work [44], point proton and neutron densities obtained in the relativistic mean field approach have been used. The prediction is presented as a dotted line in the right panel in Fig 4.

Finally, Crespo and Moro have made a prediction [49], illustrated by the dash-dotted line in the right panel, where the elastic observable was generated by a multiple scattering expansion of the optical potential in terms of the free *NN* transition amplitude, calculated in the single scattering, 'tρ', approximation [49]. In the description of the target nucleus, there is no distinction between protons and neutrons. For ^{56}Fe and ^{89}Y , the matter density distribution is given by a Fermi density distribution with parameters taken from Ref. [50]. In the case of ^{208}Pb, a two-parameter Fermi matter density distribution with half-density radius $c = 6.624$ fm and diffuseness $a = 0.549$ fm has been used.

B. Comparison with experimental data

The three data sets were compared with the results of the model predictions described above. The reduced χ^2 (from now on called χ^2) was calculated to investigate the agreement between theory and data. As a normalization error could produce a major χ^2 contribution, it was also tested to re-normalize all theory models to produce a minimum χ^2. It should be noted that none of the predictions contain parameters adjusted to the present experiment.

Visual inspection of the ^{56}Fe data and theory predictions shows that all models except Crespo-Moro describe the shape of the experimental angular distribution reasonably well. χ^2 values were calculated and the results were 9 for Haider-Saliem, 20 for Koning-Delaroche, 36 for Amos *et al.* 46 for Bauge *et al.* and 57 for ENDF-6. For the re-normalization test, the four data points at the angles 21.0°, 22.6°, 24.8° and 25.3° were removed. The reason for this is that these data points are in the first minimum, where the formal errors are small, but there are unknown systematic errors due to the multiple scattering correction which we believe are large. If not removed for the re-normalization test, they will dominate the calculation. With re-normalization, all χ^2 values were lowered significantly. Haider-Saliem required least re-normalization (0.95) resulting in a slightly improved χ^2, but still around 9. Koning-Delaroche required a re-normalization of 1.20 resulting in a χ^2 value of 4. The lowest χ^2 was obtained for Amos *et al.* (3.5) with a fairly large re-normalization (1.30). The other models require about 25–40 % re-normalization with optimum χ^2 values between 5 and 10. All models, except Haider-Saliem predict a deep first minimum in the angular distribution.

The theory predictions describe the shape of the measured angular distribution of ^{89}Y well. The lowest χ^2 value (1.5) is obtained for the Koning-Delaroche model and for the other models a χ^2 around 5 is obtained. Re-normalization produces χ^2 values that are slightly lower. The Koning-Delaroche prediction has a χ^2 value of 1.1 for 1.08 re-normalization, while the other models produce χ^2 values around 3. Amos *et al.* and Bauge *et al.* require for optimum χ^2 0.80 re-normalization , while Crespo-Moro and Haider-Saliem require re-normalization of 0.98 and 0.82, respectively.

Comparison of the ^{208}Pb data with the model predictions, shows that the models are in reasonably good agreement with the experimental data. Calculations of χ^2 give resulting values around 3 for Bauge *et al.* , ENDF-6, Koning-Delaroche and Romain *et al.* around 7 for Amos *et al.* and Crespo-Moro, and around 12 and 16 for Madland-Kozack and Haider-Saliem, respectively. For the re-normalization test, three data points at 13.0°, 14.4° and 17.2° were removed. These data points represent the first minimum of the angular distribution. The formal errors are small in this region, but there are unknown systematical errors due to the multiple scattering correction, which we believe are large. Re-normalization reduces the χ^2 value for all models, with none exceeding 5. Bauge *et al.* and Koning-Delaroche required 0.97 re-normalization, ENDF-6 and Romain *et al.* 0.93 and the other models $0.75 - 0.85$.

C. Wick's limit

A basic feature of the optical model is that it establishes a lower limit on the differential elastic scattering cross section at 0° if the total cross section is known. This is often referred to as Wick's limit [20, 21],

$$\frac{d\sigma(0^\circ)}{d\Omega} \geq (\frac{\sigma_T}{4\pi\lambda\!\!\!^{-}})^2.$$

For most neutron scattering experiments below 30 MeV, it has been found that the zero-degree cross section is very close to the limit [51, 52] and in the abscence of a good experimental normalization this has lead to the suggestion that Wick's limit should be treated as an equality [22]. There is, however, no *a priori* reason why the 0° cross section cannot exceed the limit significantly, which has also been studied in Ref. [23]. Optical model calculations using the model of Koning-Delaroche have been performed for various nuclei and energies. From those data, the deviation from Wick's limit has been calculated. It was found that over a wide range of incident energies and target masses, the deviations of the zero-degree differential cross section from Wick's limit are small, at most a few percent. For ^{208}Pb this range is 4−80 MeV while the

corresponding range for ^{89}Y is 10−60 MeV. The range becomes more narrow, the lighter the nucleus. There is, however, for all nuclei a wide energy range over which the deviation from Wick's limit does not exceed a few percent, while below and above this range the deviations are significant.

In our previous measurement [18], the data on ^{208}Pb was in good agreement with Wick's limit while the ^{12}C data overshoot the limit with about 70 %. Investigations of the zero-degree cross section for ^{16}O [19], ^{56}Fe and ^{89}Y show that the data exceed Wick's limit with 54 %, 14 % and 9 %, respectively (see Table V). Since our measurements do not reach 0°, extrapolations using the various models described above (except for the Crespo-Moro model), have been used to determine the cross section at 0°. The theory models have been normalized to our data set, so that their predicted cross section at the lowest measured angles coincide with our measured values. The average value at 0° of all model extrapolations has been adopted for the Wick's limit comparison. The estimated error has been determined to about 10 %, with contributions from the normalization procedure with a 3 % uncertainty (see Ref. [18]), and the standard deviation of the calculated average value.

Deviations from equality have also been observed in the neutron scattering experiments at 65 MeV [9] and at 65 − 225 MeV [10], although not explicitly pointed out by the authors. Based on the information in the publication from the 65 MeV experiment [9], we conclude that the C data lie about 30 % above the limit, the data on Si, Ca about 10 % above whereas Sn and Pb agree with the limit. From the experiment at 65-225 MeV [10], we conclude that the data on Ca are about 10 % above the limit at 65 MeV and the deviation grows larger with increasing energy to reach about 100 % deviation from the limit at 225 MeV. The Pb data are in agreement with the limit up to about 130 MeV. At the higher energies, the extrapolated data at 0° are about 10 % above the limit. Comparison with Ref. [23] corroborates these results. The extrapolated cross sections at 0° for the C measurements [10] are, however, below our result and the result we obtained when studying Ref. [9].

V. SUMMARY, CONCLUSIONS AND OUTLOOK

We report differential cross sections of elastic scattering of 96 MeV neutrons from ^{56}Fe, ^{89}Y and ^{208}Pb. The ^{208}Pb data, previously published in Ref. [18], have been re-analyzed, resulting in additional angular bins at forward angles, where the cross section is very steep. The new data set supersedes the old one. The overall agreement for ^{56}Fe, ^{89}Y and ^{208}Pb with predictions from theoretical models, both phenomenological and microscopic, is reasonably good. These measurements provide important input to the development of optical models, not the least because of the scarcity of elastic neutron scattering data above 20 MeV.

A study of the deviation from Wick's limit has been performed. The extrapolated 0° cross section for ^{208}Pb is in agreement with the limit, but large deviations have been found for the lighter nuclei we have studied. These results show the same trend as the previous neutron scattering experiments at 65 MeV [9] and 65-225 MeV [10], and are in agreement with predictions in a recently published paper [23].

The SCANDAL setup is being upgraded with thicker CsI crystals, which will allow for measurements at higher energies, i.e., up to 175 MeV which is the maximum energy that can be delivered at the neutron beam facility at the The Svedberg Laboratory (TSL). Data at this energy will certainly be beneficial for the future development of optical models [1].

The isovector term in optical models can be determined from neutron and proton elastic scattering data if the data are obtained at the same energy and if they range over a series of nuclei. Data on elastic proton scattering exist already in literature and together with the present data set on elastic neutron scattering, a determination of the isovector term should be possible. Such an investigation is underway.

Acknowledgments

We wish to thank the technical staff of the The Svedberg Laboratory for enthusiastic and skillful assistance. This work was supported by Barsebäck Power AB, Forsmark AB, Ringhals AB, the Swedish Nuclear Power Inspectorate, the Swedish Nuclear Fuel and Waste Management, the Swedish Defense Research Agency, the European Council and the Swedish Research Council.

[1] A.J. Koning, J.P. Delaroche, Nucl. Phys. **A713**, 231 (2003).
[2] R.W. Finlay, W.P. Abfalterer, G. Fink, E. Montei, T. Adami, P.W. Lisowski, G.L. Morgan, R.C. Haight, Phys. Rev. C **47**, 237 (1993).
[3] J. Rapaport, E. Sugarbaker, Ann. Rev. Nucl. Part. Sci. **44**, 109 (1994).
[4] W.P. Alford, B.M. Spicer, Adv. Nucl. Phys. **24**, 1 (1998).
[5] V.G.J. Stoks, R.A.M. Klomp, M.C.M. Rentmeester, J.J. de Swart, Phys. Rev. C **48**, 792 (1993).
[6] R.P. DeVito, S.M. Austin, W. Sterrenburg, U.E.P. Berg, Phys. Rev. Lett. **47**, 628 (1981).
[7] R.P. DeVito, S.M. Austin, U.E.P. Berg, R. De Leo, W. A. Sterrenburg, Phys. Rev. C **28**, 2530 (1983).
[8] F.P. Brady, T.D. Ford, G.A. Needham, J.L. Romero, C.M. Castaneda, M.L. Webb, Nucl. Instr. Meth. **A 228**, 89 (1984).
[9] E.L. Hjort, F.P. Brady, J.L. Romero, J.R. Drummond, D.S. Sorenson, J.H. Osborne, B. McEachern, L.F. Hansen, Phys. Rev. C **50**, 275 (1994).
[10] J.H. Osborne, F.P. Brady, J.L. Romero, J.L. Ullman, D.S. Sorensson, N.S.P. King, R.C. Haight, J. Rapaport, R.W. Finlay, A. Ling, E. Bauge, J.P. Delaroche, A.J. Koning, Phys. Rev. C.**70**, 054613 (2004).
[11] M. Ibaraki, M. Baba, T. Miura, Y. Nauchi, Y. Hirasawa, N. Hirakawa, H. Nakashima, S. Meigo, O. Iwamoto, S. Tanaka, J. Nucl. Sci. Technol., Suppl. **1**, 683 (2000).
[12] M. Baba, M. Ibaraki, T. Miura, T. Aoki, Y. Hirasawa, H. Nakashima, S. Meigo, S. Tanaka, J. Nucl. Sci. Technol., Suppl. **2**, 204 (2002).
[13] A. Bratenahl, S. Fernbach, R.H. Hildebrand, C.E. Leith, B.J. Moyer, Phys. Rev. **77**, 597 (1950).
[14] G.L. Salmon, Nucl. Phys. **21**, 15 (1960).
[15] C.P. van Zyl, R.G.P. Voss, R. Wilson, Phil. Mag. **1**, 1003 (1956).
[16] R.S. Harding, Phys. Rev. **111**, 1164 (1958).
[17] A. Ashmore, D.S. Mather, S.K. Sen, Proc. Phys. Soc. A **71**, 552 (1958).
[18] J. Klug, J. Blomgren, A. Ataç, B. Bergenwall, A. Hildebrand, C. Johansson, P. Mermod, L. Nilsson, S. Pomp, U. Tippawan, K. Elmgren, N. Olsson, O. Jonsson, A.V. Prokofiev, P.-U. Renberg, P. Nadel-Turonski, S. Dangtip, P. Phansuke, M. Österlund, C. Le Brun, J.F. Lecolley, F.R. Lecolley, M. Louvel, N. Marie-Noury, C. Schweitzer, Ph. Eudes, F. Haddad, C. Lebrun, A.J. Koning, E. Bauge, J.P. Delaroche, M. Girod, X. Ledoux, P. Romain, D.G. Madland, K. Amos, P.K. Deb, S. Karataglidis, R. Crespo, A.M. Moro, Phys. Rev. C **68**, 064605 (2003).
[19] P. Mermod, J. Blomgren, B. Bergenwall, C. Johansson, J. Klug, L. Nilsson, N. Olsson, A. Öhrn, M. Österlund, S. Pomp, U. Tippawan, P. Nadel-Turonski, O. Jonsson, A. Prokofiev, P.-U. Renberg, Y Maeda, H. Sakai, A. Tamii, K. Amos, R. Crespo, A. Moro, Phys. Rev. C **74**, 054002 (2006).
[20] G.C. Wick, Atti. R. Accad. Naz. Lincei, Mem. Cl. Sci. Fis. Mat. Nat. **13**, 1203 (1943).
[21] G.C. Wick, Phys. Rev. **75**, 1459 (1949).
[22] P.E. Hodgson, The Optical Model of Elastic Scattering (Oxford University Press, 1963), p. 34.
[23] F.S. Dietrich, J.D. Anderson, R.W. Bauer, S.M. Grimes, Phys. Rev. C **68**, 064608 (2003).
[24] J. Klug, J. Blomgren, A. Ataç, B. Bergenwall, S. Dangtip, K. Elmgren, C. Johansson, N. Olsson, S. Pomp, A.V. Prokofiev, J. Rahm, U. Tippawan, O. Jonsson, L. Nilsson, P.-U. Renberg, P. Nadel-Turonski, A. Ringbom, A. Oberstedt, F. Tovesson, V. Blideanu, C. Le Brun, J.F. Lecolley, F.R. Lecolley, M. Louvel, N. Marie, C. Schweitzer, C. Varignon, Ph. Eudes, F. Haddad, M. Kerveno, T. Kirchner, C. Lebrun, L. Stuttgé, I. Slypen, A. Smirnov, R. Michel, S. Neumann, U. Herpers, Nucl. Instr. Meth. A **489**, 282 (2002).
[25] http://root.cern.ch
[26] C. Johansson, J. Blomgren, A. Ataç, B. Bergenwall, S. Dangtip, K. Elmgren, A. Hildebrand, O. Jonsson, J. Klug, P. Mermod, P. Nadel-Turonski, L. Nilsson, N. Olsson, S. Pomp, A.V. Prokofiev, P.-U. Renberg, U. Tippawan, M. Österlund, Phys. Rev. C **71**, 024002 (2005).
[27] N. Olsson, E. Ramström, B. Trostell, Nucl. Physics. A**513**, 205 (1990).
[28] N. Marty, M. Morlet, A. Willis, V. Comparat, R. Frascaria, Nucl. Phys A**238**, 93 (1975).
[29] J. Rahm, J. Blomgren, H. Condé, S. Dangtip, K. Elmgren, N. Olsson, T. Rönnqvist, R. Zorro, A. Ringbom, G. Tibell, O. Jonsson, L. Nilsson, P.-U. Renberg, T.E.O. Ericson, B. Loiseau, Phys. Rev. C **57**, 1077 (1998).
[30] R.C. Byrd and W.C. Sailor, Nucl. Instr. Meth. A **264**, 494 (1989).
[31] B. Holmqvist, B. Gustavsson, T. Wiedling, Ark. Fys. **34**, 481 (1967). Later updates: N. Olsson.
[32] http://mcnp-green.lanl.gov/index.html L.S. Waters, MCNPX Users' Manual - Version 2.1.5, Los Alamos National Laboratory, November 14, (1999).
[33] P.F. Rose, C.L. Dunford, ENDF-102: Data Formats and Procedures for the Evaluated Nuclear Data File ENDF-6, Technical Report BNL-NCS-44945 (Brookhaven National Laboratory, National Nuclear Data Center, Upton, NY, 1991), and V. McLane, ENDF201: ENDF/B-VI Summary Documentation, Technical Report BNL-NCS-17541, Ed. 4, **Suppl. 1** (Brookhaven National Laboratory, National Nuclear Data Center, Upton, NY, 1996). For Internet access, see www.nndc.bnl.gov.
[34] R. Kozack, D.G. Madland, Nucl. Phys. A **509**, 664 (1990).
[35] R. Kozack, D.G. Madland, Phys. Rev. C **39**, 1461 (1989).
[36] B.D. Serot, J.D. Walecka, Adv. Nucl. Phys. **16**, 1 (1986).
[37] A.M. Lane, Nucl. Phys. **35**, 676 (1962).
[38] P. Romain, J.P. Delaroche, Proceedings of a Specialists Meeting, (OECD, Paris, 1997), (http://db.nea.fr/html/science/om200/), p. 167.
[39] F. Perey, B. Buck, Nucl. Phys. **32**, 353 (1962).
[40] K. Amos, P.J. Dortmans, H.V. von Geramb, S. Karataglidis, J. Raynal, Adv. Nucl. Phys. **25**, 275 (2000).
[41] S. Karatiglidis, K. Amos, B.A. Brown, P.K. Deb, Phys. Rev. C **65**, 044306 (2002).
[42] R. Machleidt, Adv. Nucl. Phys. **19**, 189 (1989).
[43] E. Bauge, J.P. Delaroche, M. Girod, Phys. Rev. C **63**, 024607 (2001).
[44] S.M. Saliem, W. Haider, J. Phys. G **28**, 1313, (2002).
[45] I.E. Lagaris, V.R. Pandharipande, Nucl. Phys. A **359**, 331 (1981).
[46] J.P. Jeukenne, A. Lejeune, C. Mahaux, Phys. Rev. C **16**, 80 (1977).

[47] B.A. Brieva, J.R. Rook, Nucl. Phys. A **291**, 299 (1977), Nucl. Phys. A **291**, 317 (1977), Nucl. Phys. A **297**, 206 (1978), Nucl. Phys. A **307**, 493 (1978).
[48] N. Yamaguchi, S. Nagata, J. Matsuda, Prog. Theor. Phys. **70**, 459 (1983), Prog. Theor. Phys. **76**, 1289 (1986).
[49] R. Crespo, R.C. Johnson, J.A. Tostevin, Phys. Rev. C **46**, 279 (1992).
[50] R.C. Barret, D.F. Jackson, Nuclear Sizes and Structure, Clarendon Press, ISBN 0198512724 (1979).
[51] N. Olsson, B. Trostell, E. Ramström, B. Holmqvist and F.S. Dietrich, Nucl. Phys. A**472**, 237 (1987).
[52] J.H. Coon, R.W. Davis, H.E. Felthauser, D.B. Nicodemus, Phys. Rev. **111**, 250 (1958).
[53] F. S. Dietrich, private communication (2007).

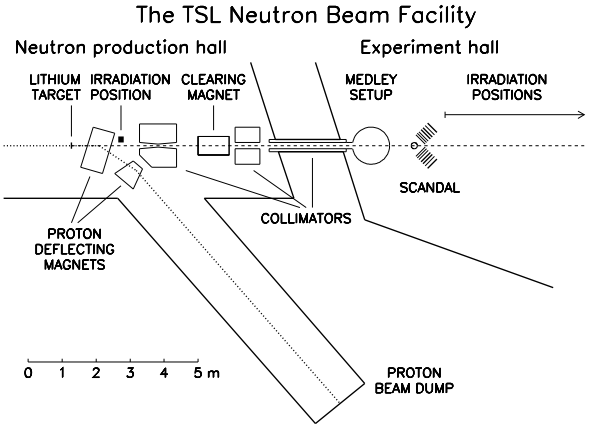

FIG. 1: Overview of the Uppsala neutron beam facility.

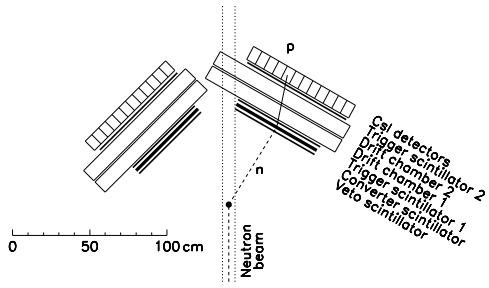

FIG. 2: Schematic layout of the SCANDAL setup. A typical event is indicated.

TABLE I: Neutron elastic scattering experiments with neutron energies $E_n \geq 30$ MeV.

Reference	Target	Energy (MeV)	Resolution (MeV at FWHM)	Angular range (°)
[6, 7]	Ca, Si	30, 40	0.15	15–140
[11, 12]	C, Si, Fe, Zr, Pb	55, 65, 75	10–20	2–57
[9]	C, Si, Ca, Fe, Sn, Pb	65	2.7	6–50
[13]	Al, Cu, Pb	84	30	2–25
[10]	C, Ca, Pb	65–225	4.5	7–23
[14]	Li, Be, C, Al, Cu, Cd, Pb, U	96	24	1–29
[15]	Li, Be, C, N, O, Al, Cu, Cd, Pb	136	27	0–20
[16]	C, Al, Cu, Cd, Pb	155	60	3–30
[17]	C, Al, Cu, Sn, Pb	350	15	1–20
[18, 19]	C, O	96	3.7	10–70
Present experiment	Fe, Y, Pb	96	3.7	10–70

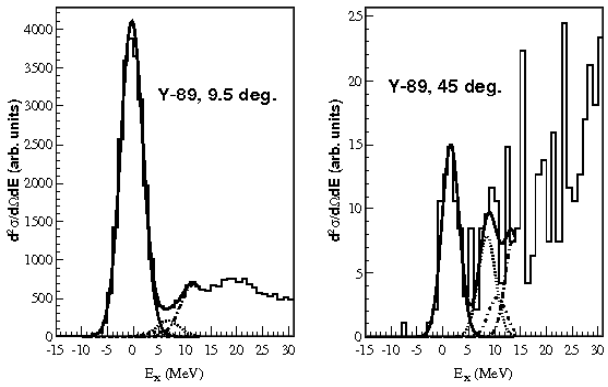

FIG. 3: Example of spectrum functions used to extract the number of elastic scattering events. The gaussian fitted to the ground state peak is solid. The gaussian at 7 MeV is dotted. The distribution of protons from ^{12}C(n,p) reactions in the converter is dash-dotted and the barely visible state at 5 MeV is dashed. The inelastic state at 9 MeV (only visible in the right panel) is described with a dash-dotted line. The sum of the contributions form the spectrum function drawn as a thick solid line. See the text for details.

TABLE II: Differential cross sections for elastic neutron scattering from ^{56}Fe at 96 MeV. The total statistical errors in the column "$\Delta d\sigma/d\Omega$" include random errors constituted by counting statistics and contributions from the multiple scattering corrections, while the column "Δrel." shows the relative statistical errors in the experiment, before these corrections are made. The columns "Δang." refer to cross section uncertainty due to the angle uncertainty in the measurement, as described in the text.

$\theta_{c.m.}$ (Deg.)	$d\sigma/d\Omega$ (mb/sr)	$\Delta d\sigma/d\Omega$ (mb/sr)	Δrel. (%)	Δang. (mb/sr)
9.5	4734	16	0.4	522
11.1	3461	16	0.5	436
12.9	2207	11	0.5	304
14.7	1167	8.7	0.7	208
17.1	420.4	4.3	0.8	89
18.5	275.9	4.8	1.2	42
21.0	130.8	3.1	1.2	5.0
22.6	121.3	3.3	1.4	2.0
24.8	112.8	3.3	1.8	0.5
25.3	143.6	3.2	1.5	1.0
25.9	105.3	2.8	1.9	1.5
26.7	108.0	2.6	1.8	2.5
28.4	110.5	2.6	1.9	9.0
29.2	80.9	1.7	1.8	5.5
29.6	84.2	2.1	2.1	5.5
30.8	68.1	1.9	2.3	2.5
32.2	47.9	1.7	2.8	4.5
33.6	40.2	1.6	2.9	3.0
33.6	36.9	1.5	3.0	3.0
35.2	21.0	1.1	3.6	5.0
37.3	15.7	0.8	2.7	1.0
37.6	13.4	1.0	3.9	0.8
39.2	14.1	1.0	4.2	0.8
41.5	10.3	0.6	3.7	0.1
42.3	7.8	0.7	6.2	0.3
43.5	6.4	0.6	7.1	0.3
46.0	10.7	0.5	4.3	0.3
47.0	4.9	0.4	7.5	0.4
50.2	4.9	0.4	6.4	0.3
51.0	3.7	0.4	7.2	0.2
54.4	1.3	0.3	8.6	0.1
54.6	2.3	0.4	8.1	0.1
58.6	1.0	0.3	16	0.04
62.6	0.65	0.22	31	0.05
66.6	1.0	0.2	16	0.04
70.6	0.48	0.13	21	0.01

TABLE III: Differential cross sections for elastic neutron scattering from ^{89}Y at 96 MeV. See Table II for details.

$\theta_{c.m.}$ (Deg.)	dσ/dΩ (mb/sr)	Δdσ/dΩ (mb/sr)	Δrel. (%)	Δang. (mb/sr)
9.5	5632	65	0.7	960
10.8	3478	45	0.8	750
13.0	1663	33	1.2	393
14.4	539.2	16	1.8	204
17.1	208.2	8.9	2.7	34
18.5	227.5	11.4	3.1	5.5
21.0	238.6	10.5	2.8	8.0
22.6	272.3	12.9	3.0	5.0
24.8	200.3	12.5	3.9	23
25.3	174.1	9.8	3.5	50
26.1	149.4	9.7	4.1	17
26.7	118.4	8.0	4.2	17
28.4	91.0	7.7	5.3	17.5
29.2	54.0	5.0	5.7	9.0
29.8	50.6	5.7	7.1	4.0
30.8	48.8	5.0	6.4	2.0
33.0	26.9	2.7	6.3	0.8
34.5	29.6	2.7	5.7	0.1
37.2	24.3	2.8	7.1	1.0
38.4	22.0	2.3	6.6	1.0
41.5	12.0	8.9	1.7	1.3
42.8	5.9	1.2	12.6	1.0
46.0	6.9	1.2	10.7	0.3
47.1	5.5	1.2	13.4	0.3
50.2	4.7	1.3	16.5	0.2
51.0	6.0	1.4	14.6	0.2
54.4	4.2	1.1	15.7	0.2
54.6	3.8	1.2	19.6	0.2
58.6	1.5	0.6	25	0.1
62.6	1.3	0.5	0.3	0.02
66.6	1.4	0.7	31.5	0.03
70.6	0.7	0.4	36.3	0.04

TABLE IV: Differential cross sections for elastic neutron scattering from ^{208}Pb at 96 MeV. See Table II for details.

$\theta_{c.m.}$ (Deg.)	dσ/dΩ (mb/sr)	Δdσ/dΩ (mb/sr)	Δrel. (%)	Δang. (mb/sr)
9.8	4396	47	1.0	1783
10.8	1792	28	1.3	869
13.0	961	28	1.9	89
14.4	623	18	2.1	88
17.2	640	15	2.1	34
18.5	787	16	2.0	89
21.0	287	10	3.1	82
22.5	282	13	3.7	39
24.8	171	12	5.0	4.0
25.3	119	8.3	5.3	9.8
25.9	132	12	5.0	7.3
26.7	103	7.1	5.8	4.5
29.5	128.6	5.3	3.6	11.4
30.0	109.6	4.1	3.5	12.6
33.4	52.1	3.4	5.3	10.7
34.4	34.4	2.7	6.0	4.7
37.6	29.6	2.4	6.8	1.0
38.7	26.3	2.2	7.4	0.2
41.9	18.7	2.0	9.3	3.1
43.2	18.3	1.9	8.9	2.8
46.3	7.6	1.3	12	0.2
47.2	8.6	1.3	12	0.1
50.3	5.9	1.0	15	0.4
51.0	8.8	1.3	13	0.6
54.6	3.4	0.9	22	0.5
54.9	3.5	0.7	18	0.6
59.3	2.0	0.7	26	0.1
63.6	1.0	0.5	43	0.2
67.2	0.5	0.4	66	0.1
71.2	0.7	0.5	52	0.1

TABLE V: Wick's limit, $(\sigma_T/4\pi\lambda\!\!\!^{-})^2$, with an error of at most 1 % coming from the determination of the total cross section, and the differential cross sections at 0°. The error for the extrapolated cross section at 0° contains contributions from the normalization procedure and the standard deviation of the calculated average value of the extrapolated cross section at 0°. Predictions from Ref. [23, 53] are also tabulated.

Nucleus	Wick's limit	$d\sigma(0^\circ)/d\Omega$	Ratio (present data/Wick's limit)	Pred. by [23, 53]
^{12}C	0.77	1.3 ± 0.13	1.70 ± 0.17	-
^{16}O	1.30	2.0 ± 0.2	1.54 ± 0.15	-
^{56}Fe	10.4	12.0 ± 1.3	1.14 ± 0.12	1.22
^{89}Y	20.9	22.7 ± 2.2	1.09 ± 0.10	1.13
^{208}Pb	63.7	60 ± 14	0.95 ± 0.22	1.03

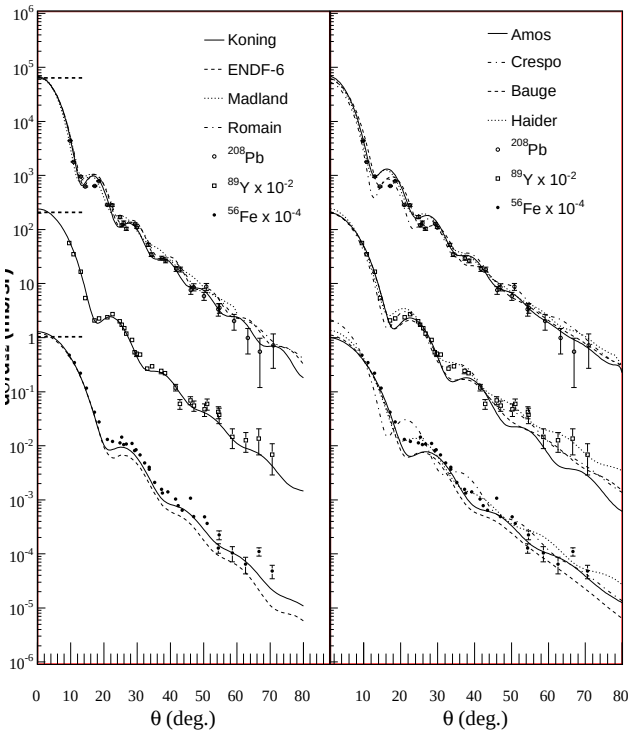

FIG. 4: Angular distributions of elastic neutron scattering from ^{56}Fe (closed circles), ^{89}Y (squares) and ^{208}Pb (open circles) at 96 MeV incident energy. Only statistical uncertanties are shown. The ^{56}Fe and ^{89}Y data have been multiplied with 10^{-4} and 10^{-2}, respectively. Left panel: predictions by phenomenological optical model potentials (OMP) The thick dotted horizontal lines show Wick's limit for the three nuclei. Right panel: predictions by microscopic OMP. The curves are identified in the text.

Three-body forces in nuclei

J. Blomgren[1)]
1) Department of Neutron Research, Uppsala University, Box 525, 751 20 Uppsala, Sweden
Jan.Blomgren@tsl.uu.se

Abstract: In systems of three nucleons, there are forces present that cannot be derived from summation of two-nucleon interactions. For obvious reasons, these forces are called three-nucleon forces, or more generally, three-body forces. In principle such three-body forces can be found in many physical systems, but it turns out that few-nucleon systems display particularly strong effects. In this article, an introduction to three-nucleon forces is presented. Recent experimental work corroborating the existence and nature of these forces are shown, with emphasis on neutron-deuteron scattering.

What are three-body forces?

From the days of Galilei until today, physics has been remarkably successful in describing complex phenomena of many-particle systems by summing two-body interactions. It is known on fundamental grounds, however, that in some cases there must exist special force effects when many particles are present, effects which are not there in two-body systems.
Before dealing with the nature of three-body forces, it might be useful to tell what three-body forces are *not*. Once I heard a distinguish colleague who dismissed the entire concept of three-body forces by stating that it is just a theory trick introduced to remedy deficiencies in two-body forces. He claimed that if we had a better description of two-body forces, three-body forces should not be required in the description of three-body systems. This statement is, however, wrong.
Force effects that can be attributed to combinations of genuine two-body interactions are normally not referred to as being three-body forces. Maybe the easiest way to distinguish three-body forces is to define three-body forces as *an interaction with an interaction*.

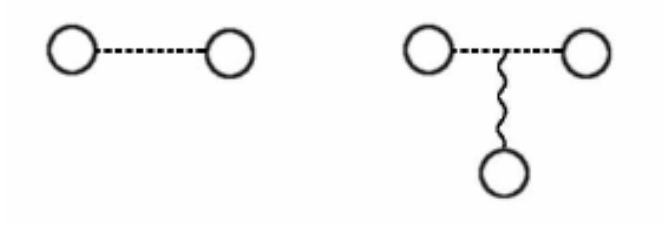

Figure 1.*Two- and three-body forces. The dashed line represents a two-body interaction, while the wavy line represents a three-nucleon force.*

This is illustrated in Fig. 1. The dashed line represents a two-body interaction, while the wavy line represents a three-nucleon force. In this case, the third nucleon interacts not directly with either one of the two other nucleons, but with the exchange quantum of the two-body force between the first two nucleons. Such an interaction would not occur if the two-body force between the first two nucleons would not be present.
We can make a human analogy to three-body forces: jealousy (see Fig. 2). Let us presume we have a man, his wife and his best (male) friend. All these have two-body interactions. If an erotic interaction between the wife and the friend takes place, jealousy will occur. This new interaction is the visible result not of the two-body forces between him and his wife or between him and his friend, but of the interaction between him and the force between his wife and his friend. Thus, this effect cannot be reduced to a summation of independent two-body forces.

Figure 2. *Jealousy, an example of a human three-body force.*

With the definition above, we can realize that there are several types of three-body forces, as displayed in Fig. 3. This example is taken from nuclear physics, i.e., the strong interaction in the nuclear sector. This is not the only place where three-body forces should be present, but for reasons explained later, few-nucleon physics is the domain in which these effects are the strongest.

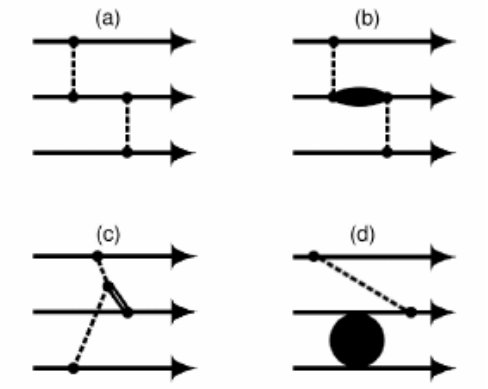

Figure 3. *Different types of three-nucleon forces. The interaction in panel (a) is not a genuine three-nucleon force, because it can be reduced to two consecutive two-nucleon interactions. In (b), however, the first interaction modifies the second nucleon, and therefore the interaction between the second and third nucleon is not reducible to two consecutive two-nucleon interactions. This is an example of a typical two-pion-exchange 3N interaction. In (c), one nucleon exchanges a scalar meson or a vector meson (double line) with a pion. In (d), there is a correlation between two of the nucleons while the pion is "in flight".*

Where should we look for three-body forces?

As stated above, nuclear physics is not the only place where three-body forces should be present, but few-nucleon physics is the theatre in which these effects are the strongest. This can be understood from some rather general physics arguments.

It is reasonable that two-body effects in general are much stronger than three-body forces, just because of time. A three-body interaction can take place only during the time when an exchange quantum is traveling from one body to the other, and a third object is within reach. Two-body forces, on the other hand, can always take place. A second pre-requisite is that the interaction between the third body and the exchange particle between the first two objects needs to be fairly strong.

These two arguments provides some guidance on where to look for three-body forces. In the case of gravitation and electromagnetic interaction, the interaction has infinite range. Thereby, it is possible for any object to interact with very many objects more or less simultaneously. Therefore, disentangling three-body forces from the sum of all two-body interactions taking place can be expected to be very difficult. Moreover, for both gravitation and the electromagnetic interaction, the coupling between the exchange quantum and another

incoming force carrier is weak. In the case of electromagnetism, the coupling constant α is 1/136, which ultimately makes three-body force effects at most of the order of less than one per cent. This is not primarily an experimental problem, because measurements of electromagnetic properties can often be performed with very high accuracy, but a problem in the interpretation of the data.

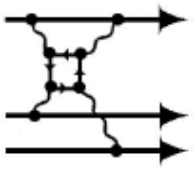

Figure 4. *A possible three-body interaction between electrons.*

Another problem in electromagnetism is that three-body forces become complicated – and correspondingly weaker – because the exchange particle, the photon, cannot couple to other photons. This makes the most simple interaction diagrams forbidden, and only higher-order interactions can take place. An example of a possible three-body interaction between electrons is presented in Fig. 4. Since photons cannot couple to photons, a loop of virtual fermions is needed to propagate the three-body force. This process does, however, contain eight vertices, making the absolute strength negligible.

One could, naively, think that a photon emitted by one electron could fluctuate into a fermion-antifermion pair, and that another photon could couple to either one of these (anti)fermions. This process, where two photons go into one photon is, however, forbidden since the electromagnetic interaction conserves charge conjugation (C-symmetry), and photons are C-odd.

The strong interaction is of particular interest because there the coupling is strong (well, you can hear that already on the name!), and since the exchange particles can interact with other exchange particles, the suppression mechanisms in electromagnetism should not be present. Before continuing the search for a favourable case, we need to make a distinction because the strong interaction has a Janus face, resulting in apparently different mechanisms in nuclei and free elementary particles.

At a more fundamental scale, strong interactions take place between quarks and gluons. Due to the fact that gluons, the mediator of the strong interaction, carry colour charge, they can interact directly with each other. A gluon emitted by one quark can couple to another quark, or to a gluon emitted by another quark. In the latter case, three-body forces can occur, as illustrated in Fig. 5.

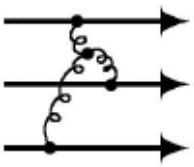

Figure 5. *A possible three-body interaction between quarks.*

In principle, contributions of the type in Fig. 5 should affect properties of baryons, but it turns out to be very difficult to identify them. The reason is that the strong interaction does not generally allow perturbation theory to be used. Perturbation theory is valid if all vertices are hard (i.e., large momentum transfer), but at this order (four vertices), many other diagrams must be taken into account, thus complicating the calculations. In a realistic case, however, the vertices are more likely to be soft (small momentum transfer) and then perturbation theory cannot be used, not even for two-body interactions. It is difficult to imagine any kind of perturbative (and thereby calculable) process where three-quark forces would play a non-neglible role. Moreover, it is hard to think of any measurement that might be sensitive to such a contribution.

This leaves us with the strong interaction in the nuclear sector as the most promising candidate for a hunting ground for three-body forces. In nuclei, the strong interaction is not carried by the fundamental exchange particle (gluons), but by composed objects (mesons). Mesons can couple to other mesons, and thereby three-body forces are possible in reaction mechanisms with a fairly small number of vertices, which should make them relatively strong. Moreover, the coupling in each vertex is rather strong, and thereby the three-body forces do not have to be dramatically weaker than the two-body interaction. Thus, few-nucleon physics should be a good place when searching for three-body forces.

Three-body forces in nuclear physics

The obvious place to look for three-body forces is in three-nucleon (*3N*) systems. The most well-known indication of the existence of *3N* forces is the binding energies of the two bound *3N* systems, ^{3}H and ^{3}He. Of these, the binding energy of ^{3}H provides the most stringent theory test, because present-day *3N* models cannot take Coulomb interaction into account. Thus, a *3N* system without Coulomb repulsion is a better test case than one containing two protons.

No present-day *NN* interaction theory can reproduce the binding energy of ^{3}H (nor of ^{3}He), if computing the binding as the sum of *2N* interactions. Typically, all theory underpredicts the binding by about 700 keV or so. Given that the binding energy is about 8 MeV, this is a serious discrepancy. Inclusion of *3N* models solves that problem. Since the binding energy is very well known experimentally, it is actually used to calibrate *3N* theory. What is done then is to compute the binding energy with a combination of *2N* and *3N* forces, tuning parameters of the *3N* force to match the experimental binding energy.

Not only the binding energy, but also other bound-state properties, are affected by *3N* forces. For instance, the description of ^{3}H and ^{3}He form factors is also improved when including *3N* forces.

Although bound-state information is a good starting point, scattering data are needed to get more guidance on the *3N* interactions. At the low-energy limit, the *nd* (and *pd*) scattering lengths are sensitive to *3N* forces. For instance, the *nd* doublet scattering length can be used to fix two important theory parameters. Recently, the coherent *nd* scattering length, which is almost equivalent to the doublet *nd* scattering length, has been measured at very low neutron energy (about 10 meV, i.e., below thermal energy) [1]. This experiment showed that *3N* forces are necessary to get reasonably close to the experimental value, but it also showed that none of the combinations of *2N* and *3N* forces on the market could perfectly describe the data. Thus, there is certainly room for improvement in the theoretical description.

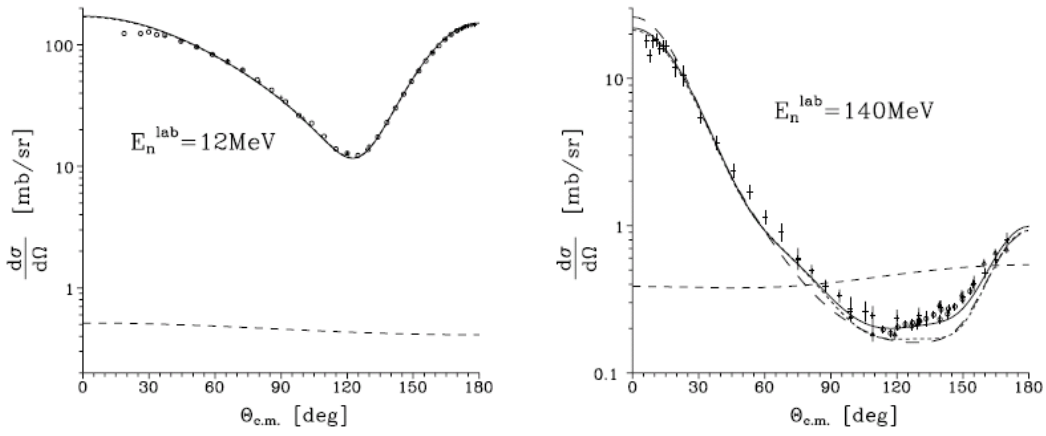

Figure 6. *Nucleon-deuteron scattering cross sections at 12 and 140 MeV. The solid lines refer to calculations combining 2N and 3N forces, whilst the long-dashed and dotted lines refer to calculations based on 2N interactions only. The rather flat dashed lines in both panels refer to cross section calculations based on 3N theory only.*

The region where there is most activity at present is in intermediate energy nuclear physics, i.e., at energies in the 100-300 MeV range [2]. There are good reasons for this. In general, it can be said that if *2N* forces are strong, detection of signatures for *3N* effects will be experimentally difficult. At energies lower than about 50 MeV, the cross sections for *pp* and *np* scattering are large, reflecting that *2N* interactions are strong. Not surprisingly, no significant signatures of *3N* forces have been found in scattering experiments below 50 MeV, with the exception of the extreme low-energy experiment above. The reason that extreme low energy is useful is that at such low energy, very precise data (± 0.1 %) can be obtained with interferometry techniques, while at higher energies standard detection methods typically result in about 5 % uncertainty.
In general, the signatures for *3N* forces get gradually more visible the higher incident energy is used. This is illustrated in Fig. 6. With a slight oversimplification, it can be said that the *3N* force contributions to the *pd* and *nd* scattering cross sections are rather flat with angle, whilst the *2N* contributions are preferentially peaked at 0 and 180 degrees.
The latter can be understood from the dominating mechanism of *2N* interaction, one-pion exchange. In *np* scattering, the exchange quantum is a pion that can either be uncharged (π^0) or charged ($\pi^{\pm}$), as illustrated in Fig. 7 [3].

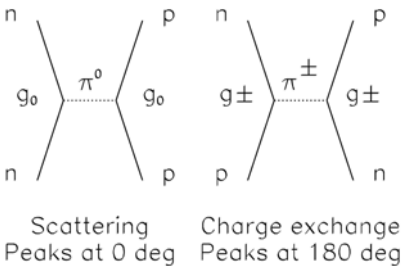

Figure 7. *Simplified diagrams of the one-pion contributions to the np scattering cross section.*

In π^0 exchange, the cross section is forward peaked, whilst in $\pi^{\pm}$ exchange, the neutron changes into a proton and the proton into a neutron. Thus, the neutron and proton exchanges identity with each other, which results in a peak at backward angles for the outgoing neutron (i.e., the proton that formerly was a neutron is emitted in the forward direction) relative to the incident neutron direction. This makes two peaks in the *np* scattering cross section, as illustrated in Fig. 8.

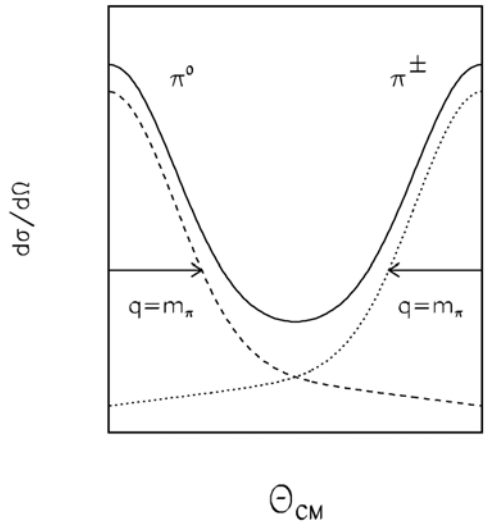

Figure 8. *Schematic illustration of the np scattering cross section if one-pion exchange were the only contributing mechanisms.*

In *nn* scattering, charged pions cannot be exchanged and therefore the cross section only contains the forward peak[1]. Thus, in *nd* scattering, which if no *3N* forces were present could be described as the sum of *nn* and *np* scattering, one would expect the cross section to be peaked at 0 and 180 degrees, with the 0 degree peak being larger. Admittedly, this description is an oversimplification, because one-pion exchange is not the only mechanism involved, but it gives a rough idea why the spectrum looks the way it does.
Returning to the *nd* scattering cross sections displayed in Fig. 6, it can be seen that the cross section actually peaks at 0 and 180 degrees, as expected from the simple model described above. Three-body force contributions are generally small, and display relatively flat angular distributions. At 12 MeV, the *2N* interactions are so strong that they overwhelm the *3N* contributions at all angles, and it is not possible to identify *3N* effects in cross section measurements. At these energies, other observables, like spin degrees of freedom have to be employed in the search for *3N* force effects. At 140 MeV, the *2N* interactions are much weaker, making it possible to identify *3N* force effects in the cross section minimum at around 120-150 degrees [2].

Recent experimental work on three-nucleon forces

Until recently, essentially all experimental information came from *pd* scattering. That *pd* data are much more abundant than *nd* data is no surprise. It is just a consequence of that neutron beams are so difficult to produce. The primary reason for running *nd* scattering is that present-day *3N* theory models cannot treat Coulomb repulsion in an exact way. Therefore, all theory models used for comparisons with *pd* data are actually calculations of the *nd* cross section (sometimes with a rather phenomenological Coulomb correction), and it is implicitly assumed that Coulomb effects are small. Testing this assumption is of vital importance to the further development of the field. If it can be conclusively shown that Coulomb effects are indeed negligible, *pd* data can be used with much better confidence to benchmark various *3N* theories.
Studies of *nd* scattering has also other beneficial properties. One problem in all experiments of this type is the absolute normalization of cross sections. In *pd* scattering, it has happened that the proton beam heats the target, leading to evaporation of deuterium, which can lead to an error in the cross section determination. In the case of neutron beams, no such heating takes place. Problems with uncertainties due to uneven target thickness also are less important with neutron beams. Another advantage of neutron-induced reactions is that several targets can be used simultaneously. Thereby *np* and *nd* scattering can be studied at the same time with the same detector, which in turn means that the ratio of *np* (*2N*) to *nd* (*3N*) scattering can be measured much more accurately than each of the cross sections separately. This is important because it allows an accurate identification of *3N* effects.
An important deficiency of present *3N* theory is that all models are non-relativistic. This indicates that the most stringent tests should be performed at relatively low energy to minimize the relativistic effects. This is, however, not the whole story. If you want to get a full understanding of *3N* forces, it is not sufficient to study scattering at one energy only. Slightly oversimplified, it can be said that different momentum transfers in the reaction correspond to different interaction distances. Therefore, to map out how *3N* forces vary with distance, different momentum transfers have to be studied, and this means that a range of incident energies have to be used.
Recently, results from two high-quality *nd* scattering experiments have been published, one at 95 MeV [4-6] and one at 250 MeV [7]. These two measurements complement each other in a very nice way, because of the arguments presented above. Three-nucleon effects are hard to see at all below 65 MeV, while they give contributions of about 30 % in the cross section minimum at 95 MeV incident energy. With typical experimental uncertainties of about 5 %, *3N* effects should be clearly visible. Thereby, 95 MeV should be about the lowest useful energy. It should be expected that relativistic effects are modest at this energy, while they could be significant at 250 MeV. On the other hand, Coulomb effects typically gets smaller at high energy, so the Coulomb contributions should be larger at 95 MeV than at 250 MeV.

[1] To be correct, the resulting cross section nevertheless displays a backward peak, because the two outgoing neutrons cannot be distinguished.

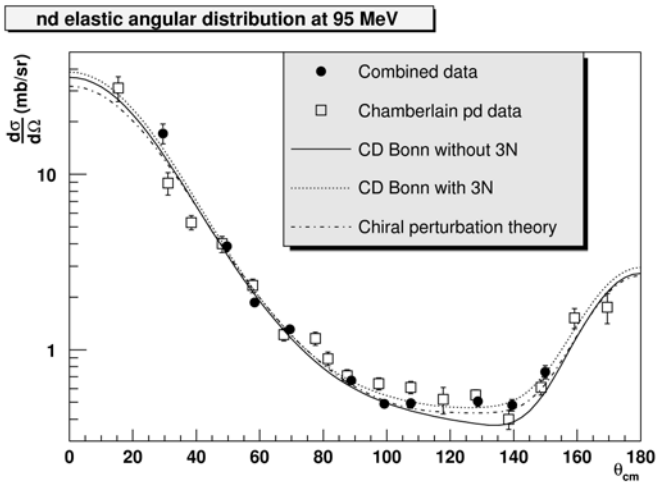

Figure 9. *The neutron-deuteron scattering cross section at 95 MeV [4]. The solid dots are nd data, whilst the open symbols are (very old) pd data. The solid line is a cross-section prediction based on 2N forces only, while the dashed line is a prediction taking 3N contributions into account. The dot-dashed line is a calculation based on chiral perturbation theory, in which 2N and 3N contributions are treated simultaneously.*

The results at 95 MeV are presented in Fig. 9. As can be seen, theories involving *3N* forces do better account for the data. The most interesting region is blown-up in Fig. 10. The dual error bars represent statistical errors only (inner bar) and total errors including systematical errors (outer bar). When comparing the data with various theory models, typical values of χ^2 is around 20 for predictions not taking *3N* forces into account, while they are about 2-3 for models including *3N* effects.

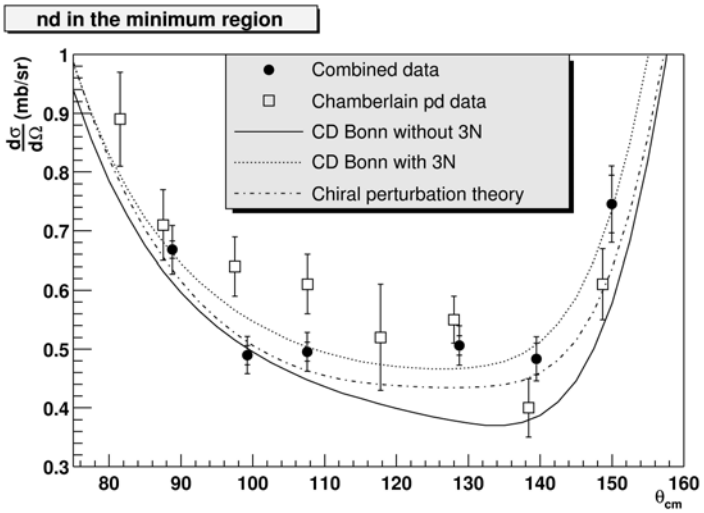

Figure 10. *The neutron-deuteron scattering cross section at 95 MeV, i.e., the same as Fig. 9, but a blown-up view of the cross section minimum.*

A fairly large contribution to the χ^2 in the analyses above is due to the normalization of data. For a given theory model, by renormalizing data with up to 4 %, which is the quoted normalization uncertainty, χ^2 could be reduced from above 2 down to about 1. One way of making the data independent of the normalization is to analyze the ratio of *np* to *nd* scattering obtained simultaneously with the same setup. This is presented in Fig. 11. In this case, χ^2 values around 1 are found for two different theory models, and the others studied reside in the χ^2 = 2-3 range.

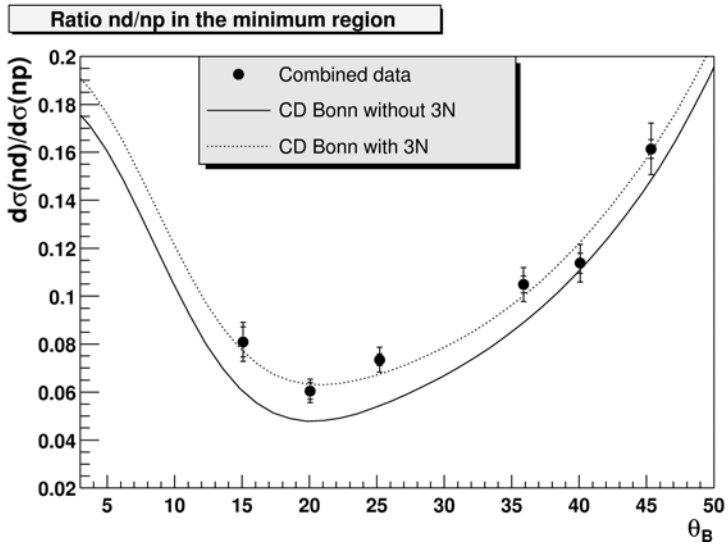

Figure 11. *The ratio of nd and np scattering cross sections in the minimum region. The raw data are the same as in Figs. 9 and 10, but with this presentation, the normalization errors cancel.*

Thus, it can be concluded that *3N* theory gives a very good description of data at 95 MeV. The situation is different when going to 250 MeV, as illustrated in Fig. 12. Also here, the inclusion of *3N* forces improves the description of data, but not all the way. Models including *3N* forces still underpredict the data in the critical angular range, but they do a better job than pure *2N* theory.
What causes these discrepancies is at presently not known, but it is a common presumption that they are primarily due to relativistic effects. It has, however, been attempted to include relativistic effects approximately, and this makes some improvement, but not at all to the extent needed.

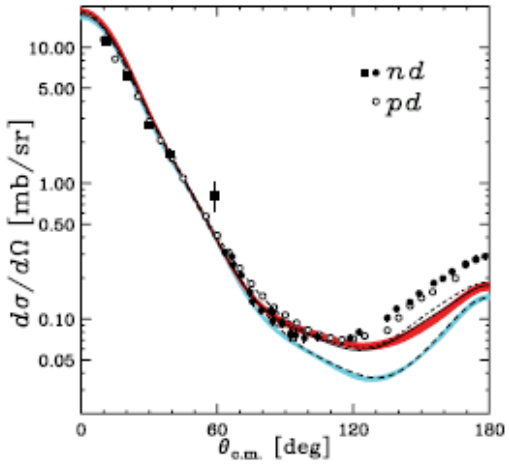

Figure 12. *The nd scattering cross section at 250 MeV [7].The light blue band (dashed lines) contains predictions of 2N models, while the red band (close to the solid line) represents models taking 3N effects into account.*

Next issue is Coulomb effects. At 250 MeV, precise *pd* data have been published, allowing a detailed analysis of Coulomb effects when confronted with *nd* data, as illustrated in Fig. 13.

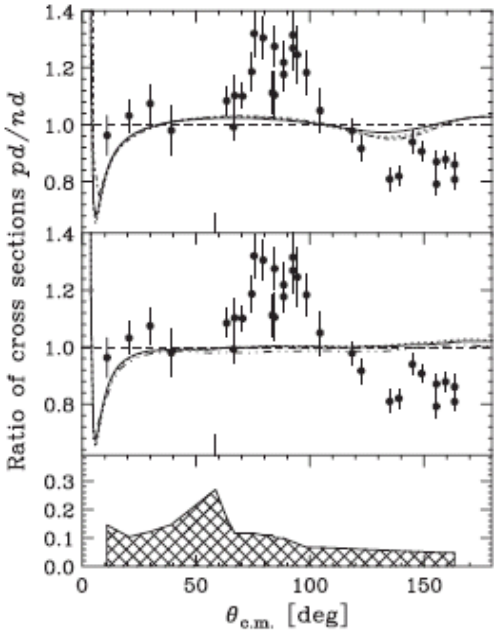

Figure 13. *The ratio of pd and nd scattering cross sections at 250 MeV [7].The upper and middle panels show theory predictions of this ratio, while the lower panel shows the systematic uncertainties in the ratio data.*

As can be seen in Fig. 13, the data deviate significantly from the theory predictions. Overall, the ratio is close to unity, but there is an oscillatory behaviour. If this is not due to experimental artifacts, one possible explanation could be isospin dependence in the *2N* or *3N* models, or both.

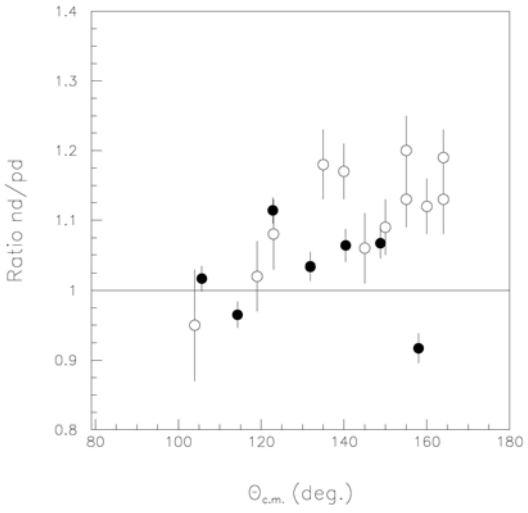

Figure 14. *The ratio of nd and pd scattering cross sections at 95 MeV (filled symbols).The error bars display the full uncertainty, statistical and systematical, with respect to the nd data. An additional 5 % uncertainty should be attributed to the pd data. The pd data have been measured at 90 MeV, and have been scaled down by 8 % to take the energy dependence of the pd cross section into account. The data at 250 MeV [7] is shown as unfilled symbols.*

In Fig. 14, the ratio *nd/pd* data at 95 MeV is displayed. There is no high-quality *pd* experiment at 95 MeV, but recently data at 90 MeV have been published [8], and an experiment at 100 MeV is under analysis [9]. In the figure, the 90 MeV data have been used, scaled to 95 MeV (8 % reduction in cross section, derived from the energy dependence of predictions based on

the AV18 *2N* force [10] in combination with the U-IX *3N* force [11,12]). No theory prediction of the Coulomb correction is presently available at this energy. It can be noted that like at 250 MeV, the *nd* data are above the *pd* data at 95 MeV in the 100-160 degree range, although slightly less so. It should be noted, however, that, if the *pd* data are renormalized further down by 5 %, which is their reported systematic uncertainty, the effect is compatible with the situation at 250 MeV.

Although scattering data are the most sensitive to *3N* effects, it has also been found that inclusion of *3N* forces improves the description of the *nd* total cross section [13]. The total cross section is not as sensitive as such, but on the other hand the total cross section can be measured with an uncertainty of about 1 %, i.e., an order of magnitude more precisely than elastic scattering data.

Although the present paper is focused on *nd* scattering, it is impossible not to even briefly mention the main conclusions drawn from *pd* scattering experiments. Due to the favourable conditions compared to neutron-induced experiments, there are much more data on *pd* scattering than *nd* scattering. Such measurements can be performed in relatively small increments in beam energy, allowing the energy evolution of *3N* forces to be mapped out in some detail. Another important aspect is that spin degrees of freedom are easier to study. Proton beams can be polarized to a high degree, whilst highly polarized neutron beams are very difficult to obtain.

If briefly summarizing the results from the wealth of *pd* experiments, a few main findings can be mentioned. First, in most (or even close to all) cases the inclusion of *3N* forces moves the prediction in the right direction, compared to predictions based on *2N* forces only. This does not mean, however, that the description always get better. Sometimes the inclusion changes the prediction by such a large amount that the deviation is even larger than before, but on the other side of the data.

Personally, I am not too worried about such shortcomings. If the *3N* forces move the predictions in the right direction, the fact that the magnitude is wrong is in most cases possible to remedy by adjustment of various theory parameters. If the effects go the wrong way, it is most often a sign that the underlying physics processes assumed are incorrect, which is a much harder problem.

Another important *pd* result is the description of spin observables. In general, I think it is fair to say that inclusion of *3N* forces do not improve the description of spin degrees of freedom to the extent they do for cross sections.

Are there four-body forces?

With the modern *3N* forces at hand, it is possible to calculate the binding energies of heavier systems, i.e., four nucleons or more. The α particle binding energy is very well described with *2N* and *3N* forces, suggesting the role of *4N* forces to be negligible [14]. If *4N* forces are insignificant, it is reasonable to presume that *5N* forces and to even higher order are also not of significance.

Recently, binding energies of light nuclei up to carbon (A=12) have been performed with good agreement if *2N* and *3N* forces are combined [15,16]. The inclusion of *3N* forces generally improve the description by increasing the binding energies, but also by rearranging the level order and improving the level spacing of low-lying states.

Outlook

With the recent experiments, it seems today as the main challenges are theoretical. The uncertainties in the experimental data are far smaller than the theory uncertainties. The most important theory challenges are to make the calculations relativistically correct, and to get Coulomb repulsion under good control. On the experimental side, one major challenge is to perform studies of spin observables with neutron beams. Another area of possible experimental development is break-up experiments. Such experiments have been performed in the *pd* system [17]. High-quality data on *nd* breakup would present a major experimental challenge, but possibly worth the effort since some predictions indicate that very strong *3N* effects should be present in some kinematics configurations of the outgoing particles [18]. Attempts to study these effects experimentally are underway [19].

Acknowledgements
The input in general, and the drawings in particular, by Philippe Mermod are gratefully acknowledged. This work was financially supported by the Swedish Nuclear Fuel and Waste Management Company, the Swedish Nuclear Power Inspectorate, Ringhals AB, Barsebäck Power AB, Forsmark Power AB, the Swedish Defense Research Agency, the Swedish Research Council, the Swedish Nuclear Safety and Training Centre, and the European Union.

References

[1] T.C. Black, P.R. Huffman, D.L. Jacobson, W.M. Snow, K. Schoen, M. Arif, H. Kaiser, S.K. Lamoreaux, S.A. Werner, Phys. Rev. Lett. **90** (2003) 192502.
[2] H. Witała, W. Glöckle, D. Hüber, J. Golak, H. Kamada, Phys. Rev. Lett. **81** (1998) 1183.
[3] J. Blomgren, N. Olsson, J. Rahm, Phys. Scr. **T87** (2000) 33.
[4] P. Mermod, J. Blomgren, B. Bergenwall, A. Hildebrand, C. Johansson, J. Klug, L. Nilsson, N. Olsson, M. Österlund, S. Pomp, U. Tippawan, O. Jonsson, A.V. Prokofiev, P.-U. Renberg, P. Nadel-Turonski, Y. Maeda, H. Sakai, A. Tamii, Phys. Lett. **B 597** (2004) 243..
[5] P. Mermod, J. Blomgren, B. Bergenwall, A. Hildebrand, C. Johansson, J. Klug, L. Nilsson, N. Olsson, M. Österlund, S. Pomp, U. Tippawan, O. Jonsson, A.V. Prokofiev, P.-U. Renberg, P. Nadel-Turonski, Y. Maeda, H. Sakai, A. Tamii, Phys. Rev. C **72** (2005) 061002(R).
[6] P. Mermod, J. Blomgren, C. Johansson, A. Öhrn, M. Österlund, S. Pomp, B. Bergenwall, J. Klug, L. Nilsson, N. Olsson, U. Tippawan, P. Nadel-Turonski, O. Jonsson, A.V. Prokofiev, P.-U. Renberg, Y. Maeda, H. Sakai, A. Tamii, K. Amos, R. Crespo, A. Moro, Phys. Rev. C **74** (2006) 054002.
[7] Y. Maeda, T. Kawabata, K. Suda, H. Sakai, K. Fujita, K. Hatanaka, H. Okamura, Y. Sakemi, Y. Shimizu, Y. Tameshige, A. Tamii, M.B. Greenfield, M. Hatano, H.Kuboki, T. Saito, M. Sasano, K. Yako, J. Kamiya, J. Rapaport, K. Sekiguchi, T. Wakasa, J. Blomgren, P. Mermod, A. Öhrn, M. Österlund, H. Witała, J.Golak, R. Skibinski, A. Deltuva, A.C. Fonseca, P.U. Sauer, W. Glöckle, H. Kamada, A. Nogga, Phys. Rev. C **76** (2007) 014004.
[8] H.R. Amir-Ahmadi, R. Castelijns, A. Deltuva, M. Eslami-Kalantari, E.D. van Garderen, M.N. Harakeh, N. Kalantar-Nayestanaki, M. Kis, H. Löhner, M. Mahjour-Shafiei, H. Mardanpour, J.G. Messchendorp, B. Mukherjee, D. Savran, K. Sekiguchi, S.V. Shende, H.Witała, and H.J. Wörtche, Phys. Rev. C **75** (2007) 041001(R).
[9] K. Hatanaka, private communication (2007).
[10] R.B. Wiringa, V.G.J.Stoks, R. Schiavilla, Phys. Rev. C **51** (1995) 38.
[11] S.C. Pieper, V.R. Pandharipande, R.B. Wiringa, J. Carlson, Phys. Rev. C **64** (2001) 014001.
[12] B.S. Pudliner, V.R. Pandharipande, J. Carlson, S.C. Pieper, R.B. Wiringa, Phys. Rev. C **56** (1997) 1720.
[13] W.P. Abfalterer, F.B. Bateman, F.S. Dietrich, Ch. Elster, R.W. Finlay, W. Glöckle, J. Golak, R.C. Haight, D. Hüber, G.L. Morgan, H. Witała, Phys. Rev. Lett. **81** (1998) 57.
[14] A. Nogga, H. Kamada, W. Glöckle, B.R. Barrett, Phys. Rev. C **65** (2002) 054003.
[15] P. Navrátil, W.E. Ormand, Phys. Rev. C **68** (2003) 034305.
[16] B.R. Barrett, P. Navrátil, A. Nogga,W.E. Ormand, J.P. Vary, Nucl. Phys. **A746** (2004) 579.
[17] St. Kistryn, E. Stephan, A. Biegun, K. Bodek, A. Deltuva, E. Epelbaum, K. Ermisch, W. Glöckle, J. Golak, N. Kalantar-Nayestanaki, H. Kamada, M. Kiš, B. Kłos, A. Kozela, J. Kuros-Zołnierczuk, M. Mahjour-Shafiei, U.-G. Meissner, A. Micherdzinska, A. Nogga, P.U. Sauer, R. Skibi´nski, R. Sworst, H. Witała, J. Zejma, W. Zipper, Phys. Rev. C **72** (2005) 044006.
[18] J. Kuros-Zołnierczuk, H. Witała, J. Golak, H. Kamada, A. Nogga, R. Skibinski, W. Glöckle, Phys. Rev. C **66** (2002) 024003.
[19] J. Mattews, private communication (2007). To appear in proceedings of MENU2007.

THREE-BODY FORCE EFFECTS IN NEUTRON-DEUTERON SCATTERING AT 95 MeV

J. Blomgren, P. Mermod, C. Johansson, J. Klug, L. Nilsson, N. Olsson[1], *S. Pomp, U. Tippawan*[2], *A. Öhrn, M. Österlund*
Department of Neutron Research
Uppsala University
Uppsala, Sweden

B. Bergenwall, P. Nadel-Turonski[3]
Department of Radiation Sciences
Uppsala University
Uppsala, Sweden

O. Jonsson, A. Prokofiev, P.-U. Renberg
The Svedberg Laboratory
Uppsala University
Uppsala, Sweden

Y. Maeda, H. Sakai, A. Tamii
Department of Physics
Tokyo University
Tokyo, Japan

Abstract

Three-body force effects have been studied in neutron-deuteron scattering at 95 MeV. Three different experiments, performed with different experimental setups, have been used to provide data covering the full angular distribution with unprecedented precision in the region of the cross section minimum, where three-nucleon forces are expected to be significant. The use of different

[1]Also at Swedish Defence Research Agency, Stockholm, Sweden
[2]Also at Fast Neutron Research Facility, Chiang Mai University, Chiang Mai, Thailand
[3]Presently at George Washington University, Washington, D.C., USA

setups allow detailed studies of systematic effects in the experimental data. Measurements of the ratio between neutron-proton and neutron-deuteron scattering have been performed to provide data free from systematic uncertainties related to cross-section normalization. The data display significant deviations from predictions based on two-nucleon interactions only, while they are perfectly described by theories including three-nucleon forces.

1 Introduction

The nucleon-nucleon (NN) interaction can be used as a basic tool to describe the properties and interactions of nuclei. For this purpose, NN potentials, which are based on meson-exchange theories, have been developed: the most widely used ones are the Paris potential [1], the Argonne AV18 potential [2], the CD-Bonn potential [3, 4] and the Nijmegen potentials [5]. After proper adjustment of the free parameters, these models are able to describe very well a restricted *pp* and *np* data base below 350 MeV [6].

The next step to demonstrate the success of this approach is to test the NN potentials in three-nucleon ($3N$) systems. Quantitative descriptions of $3N$ systems can be provided rigorously by using NN potentials in the Faddeev equations [7]. However, theoretical considerations indicate that the description of systems made of more than two nucleons is not complete if three-body forces are not taken into account (and, in principle, also four-body forces, five-body forces, etc.). Formally, $3N$ forces can be represented by introducing a $3N$ potential in the Faddeev equations. The most widely used $3N$ potentials are the Tucson-Melbourne [8,9] and Urbana [10,11] forces. As a first experimental evidence, the ^{3}H and ^{3}He binding energies can be reproduced model-independently taking $3N$ forces into account [12], while calculations using only NN interactions underestimate them by typically half an MeV [3]. Interestingly, the ^{4}He binding energy can also be described correctly with combined NN and $3N$ forces [13], indicating that the role of four-nucleon forces is not significant.

The ultimate goal of nuclear physics would be to have a single consistent theory that could describe both nucleon and nuclear properties and dynamics. As pointed out in, e.g., Refs. [6] and [14], an appropriately tailored effective field theory, rooted in the symmetries of QCD, might be a tool powerful enough to succeed in such an ambitious program, at least for few-nucleon systems. In particular, chiral symmetry breaking can be analyzed in terms of an effective field theory, called chiral perturbation theory (CHPT). This model can be applied to describe consistently the interaction between pions and nucleons, as well as the pion-pion interaction. Calculations made within

the CHPT framework at next-to-next-to-leading order implicitly include $3N$ forces [15, 16]. Calculations at the next higher order were made recently [17, 18], allowing for instance an excellent description of NN phase shifts.

Experimental investigations of three-nucleon systems are essential for determining the properties of $3N$ forces. Besides the ^{3}H and ^{3}He binding energies, a number of observables that may reveal the effects of $3N$ forces have been identified. We will concentrate our discussion to nucleon-deuteron scattering in the energy range 65−250 MeV. At these energies, significant $3N$-force contributions can potentially be seen in the elastic scattering angular distribution [19, 20] as well as for various spin-transfer observables in elastic scattering [7]. In addition, observables in the break-up process in various kinematical configurations are also expected to provide signatures of $3N$ forces [21, 22]. Existing proton-deuteron elastic scattering data between 65 and 250 MeV can be found in Refs. [23–35], and proton-deuteron break-up data in Refs. [36–40]. Except for Refs. [23, 26], these data were obtained with polarized beams, and polarization observables could be extracted. Comparison of experimental analysing powers with theoretical predictions show a puzzling picture where data and predictions agree only partially with each other. Many of these results call for a better understanding of the spin structure of the three-nucleon forces: possible solutions could be a refinement of the $3N$ force terms in CHPT [15] or the introduction of new types of diagrams in the $3N$ potentials [41]. While polarization observables are extremely valuable especially for studying the details of the $3N$ interactions, in order to validate the whole approach of introducing $3N$ forces at all, an observable that would give a clear and unambiguous signal is desirable. As pointed out in, e.g., Ref. [19], the differential cross section of nucleon-deuteron elastic scattering is expected to reveal substantial effects of $3N$ forces in the minimum region of the angular distribution. This can be understood in the following way: the contributions from NN interactions are strongly forward and backward peaked, while the contributions from $3N$ interactions should be roughly isotropic. Thus, the $3N$-force contribution to the cross section would be particularly significant relative to NN interactions in the angular range of the cross-section minimum. Around 100 MeV, the effect of $3N$ forces is expected to increase the cross section by about 30% in the minimum, as predicted [19] by Faddeev calculations including the Tucson-Melbourne $3N$ force [8] with parameters adjusted to the triton binding energy.

Thus, both neutron-deuteron (nd) and proton-deuteron (pd) elastic scattering differential cross sections should provide robust investigations of $3N$ forces. The existing pd elastic scattering data [23–29, 32–34] tend to show the expected effects in the cross-section minimum: the descriptions are generally improved when taking $3N$ forces into account. The contribution from the

Coulomb interaction in *pd* scattering is not known with certainty to be negligible in the minimum region, thus complicating the interpretation of these results. Recent calculations suggest that Coulomb interactions should not result in significant effects in the minimum of the *pd* elastic scattering angular distribution above 65 MeV [42,43]. The question of Coulomb effects−and thus also the question of $3N$ force effects−can be definitively settled by *nd* scattering experiments. There are *nd* data at 67 MeV [44] consisting essentially of an analyzing power measurement. Three *nd* experiments at 95 MeV, previously reported in Refs. [45–47], agree well with the predictions including $3N$ forces. Existing data at 152 MeV [48] give the same picture. Recent data at 250 MeV [49], together with *pd* data at the same energy [33], reveal an effect in the cross-section minimum which is too large to be accounted for by any theory. At such large energies, part of the explanation for this failure could be the lack of a full relativistic treatment in the calculations. Pioneering studies [50, 51] show that relativistic effects are expected to increase the cross section in the region of backward angles at large energies. At 95 MeV, the energy of the present work, such effects are not expected to contribute significantly.

In the present work, data from three *nd* scattering experiments are presented. By detecting either the scattered neutron or the recoil deuteron, we were able to cover the angular range from 15 to 160 degrees in the c.m. system. By using two different detector setups in various configurations, we could keep the systematic uncertainties under control. Additionally, by measuring the neutron-proton (*np*) scattering differential cross section and, in the case where scattered neutrons were detected, also elastic scattering in carbon (i.e., the ^{12}C(n,n) reaction), the systematic error due to uncertainties in the normalization factors was minimized.

The present *np* data give supplementary information about the *np* angular distribution at 95 MeV (for previous data, see, e.g., Refs. [52, 53]). In many experiments, neutron cross sections are measured relative to the *np* cross section [53], i.e., it is used as a cross-section standard. Neutron-proton scattering plays an important role in nuclear physics, since it can be used to validate *NN* potentials and to derive a value of the absolute strength of the strong interaction. The extensive database of *np* differential cross sections is not always consistent and, not unrelated, there are still problems with the determination of a precise value of the πNN coupling constant [6, 54, 55].

In the *nd* experiment where the scattered neutrons were detected, we could also obtain elastic scattering angular distributions for carbon and oxygen at 95 MeV, which are not discussed further here. Besides their interest in fundamental nuclear theory, these data are relevant for medical treatment of tumors with fast neutrons as well as in dosimetry, since the human body

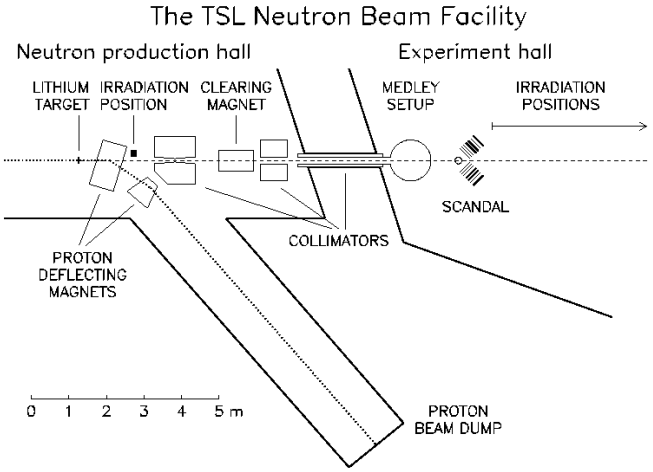

Figure 1: Schematic view of the Uppsala neutron beam facility before its upgrade in 2004.

contains significant amounts of carbon and oxygen. Recoil nuclei from elastic and inelastic scattering are expected to account for more than 10% of the cell damage, the rest being mainly due to *np* scattering and neutron-induced emission of light ions [57, 58]. The oxygen data may also be relevant for future incineration of nuclear waste in subcritical reactors fed by a proton accelerator, where the nuclear fuel might be in oxide form. These data were obtained as by-products of the target handling, e.g., due to the use of heavy water as deuterium target.

2 Experimental procedure

2.1 Neutron beam and detector setups

A full account of the experimental details and analysis procedures have been published in Ref. [47], and only an introduction is presented here. The present experiments were performed with the two experimental setups MEDLEY [59] and SCANDAL [60] at the neutron beam facility (before upgrade, see Fig. 1) at The Svedberg Laboratory in Uppsala, Sweden. This facility has been described in detail in Ref. [60], and therefore only a brief outline will be given here. The neutrons were produced with the ^{7}Li(p,n)^{7}Be reaction, using a 98

MeV proton beam of about 5 μA hitting an 8 mm thick neutron production target consisting of lithium enriched to 99.98% in ^{7}Li. The resulting neutron spectrum consisted of a high-energy peak at 94.8±0.5 MeV with an energy spread of 2.7 MeV (FWHM) and a low-energy tail which was suppressed by time-of-flight techniques. After the production target, the proton beam was bent into a well-shielded beam dump where the beam current was integrated in a Faraday cup for relative beam monitoring consistency checks. At the MEDLEY target position 9.15 m after the neutron production target, the neutron beam was about 8 cm in diameter and had an intensity of about 5×10^4 s^{-1}cm^{-2}. At the SCANDAL target position 10.70 m after the lithium target, the beam was about 9 cm in diameter and had an intensity of about 4×10^4 s^{-1}cm^{-2}. The neutron beam was transported in a vacuum system which was terminated with a 0.1 mm thick stainless steel foil at the exit of the MEDLEY chamber. Immediately after the foil, two fission detectors were mounted for relative monitoring of the neutron fluence: one monitor was based on thin-film breakdown counters (TFBC) [61] and the other one, which was more stable and had much better statistics, on an ionization chamber (ICM). The MEDLEY target, the vacuum chamber exit foil, and the neutron monitors were thin enough to consider the neutron beam as negligibly affected.

The MEDLEY vacuum chamber is a cylinder of 80 cm inner diameter. Targets were mounted onto frames attached to the center of the ceiling, with a remote control allowing to switch between up to three different frames without opening the vacuum chamber. Eight telescopes were placed on rails emerging radially at 20° separation from each other on a rotatable table. Two silicon detectors and one CsI detector could be mounted inside each telescope. Thin (50 or 60 μm thickness) and thick (400 or 500 μm thickness) silicon detectors were available. The CsI crystals were thick enough to detect protons with energies up to 110 MeV. This combination of silicon detectors and CsI crystals allowed light ion detection, identification and energy measurement in the energy range 3−110 MeV. In order to define precisely the active detection area (and solid angle), either active plastic scintillators or passive aluminum rings were used as collimators. A full description of the MEDLEY setup is given in Ref. [59].

The SCANDAL (SCAttered Nucleon Detection AssembLy) setup, previously described in Ref. [60], consists of two identical arms that can be positioned on either side of the beam and rotated around the target position. Each SCANDAL arm was equipped with a 2 mm thick veto scintillator for charged-particle rejection, two converter scintillators of 20 mm and 10 mm thickness for neutron-proton conversion, a 2 mm thick ΔE plastic scintillator for triggering, two drift chambers (DCH) giving two horizontal and

two vertical coordinates for proton tracking, another 2 mm thick ΔE plastic scintillator for triggering, and an array of twelve CsI detectors that defined twelve angular bins. The CsI detectors as well as the plastic scintillators were read out by photomultiplier (PM) tubes. The CsIs had one PM tube each, and the scintillators two each, mounted adjacent to each other on one of the longer, horizontal sides. The proton energy resolution was on average 3.7 MeV (FWHM) [60], varying between the individual CsI crystals due to internal properties of the detectors. The setup could be used for direct detection of protons or deuterons coming from the target by simply removing the veto and converter scintillators. This option allowed to measure *np* and *nd* elastic scattering at backward angles. In proton/deuteron detection mode, a multitarget (MTGT) box permitted to use up to seven targets at the same time, sandwiched between multiwire proportional counters (MWPCs). In this way it was possible to determine in which target the reaction took place and to veto charged particles in the beam.

3 Results and discussion

The final results for *np* and *nd* scattering, recently reported in Refs. [45–47], are shown in Fig. 2. The *nd* differential cross section is shown in the middle panel. For the data in proton/deuteron detection mode, the ratio of *nd* to *np*− a quantity which is independent of the absolute normalization−is plotted in the bottom panel as a function of the proton/deuteron angle in the laboratory.

The *np* data are valuable in the sense that they increase the database in the intermediate energy region, where the systematic uncertainties are not always under satisfying control. Many applications involve measurements relative to the *np* cross section, and new data are therefore most welcome. The *np* data from the three present experiments are in good overall agreement with each other and with predictions based on modern *NN* interactions. This allows us to validate the quality of the *nd* data since the *np* and *nd* differential cross sections were measured under essentially the same conditions.

The *nd* data agree well with each other in the regions where they overlap. We can compare them with Faddeev calculations using various *NN* potentials, and see if the description is improved when including $3N$ potentials. The curves obtained with the CD-Bonn *NN* potential [4] including (dashed line) and not including (solid line) the Tucson-Melbourne $3N$ potential TM99 [9] are shown in Fig. 2. Predictions obtained with the Argonne AV18 *NN* potential [2] and the Nijmegen potentials Nijm1 and Nijm2 [5], which can also be combined with the TM99 $3N$ potential, are not shown in

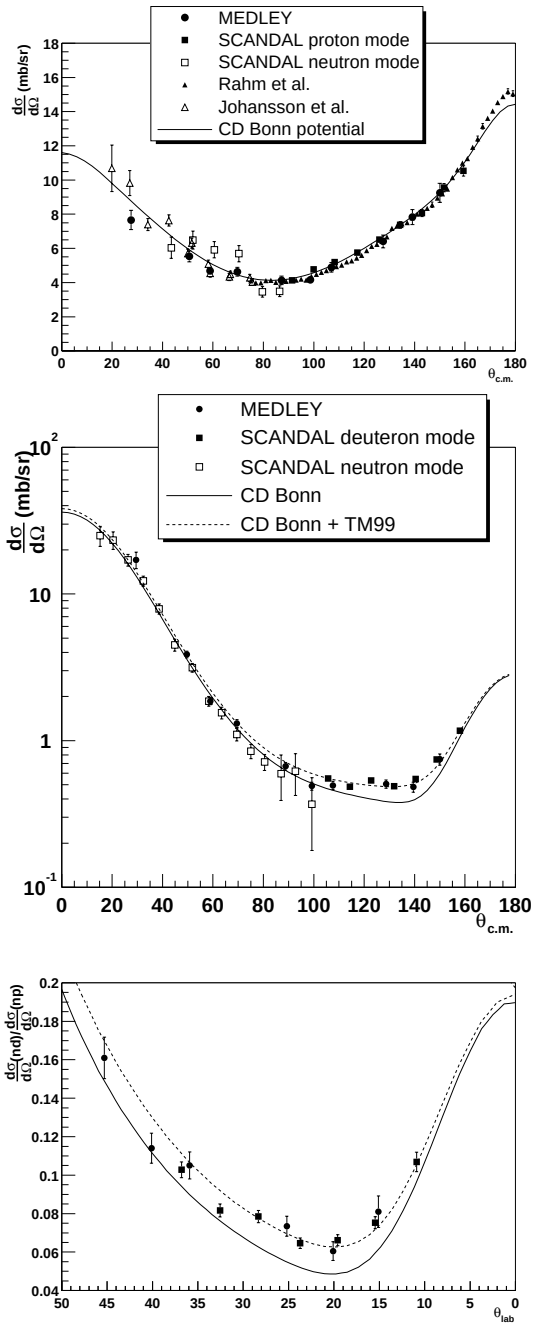

Figure 2: Combined data of the three present experiments, for the *np* (top panel), *nd* (middle panel) and the ratio between *nd* and *np* (bottom panel) elastic scattering differential cross sections at 95 MeV. The theoretical curves for *nd* scattering were obtained with Faddeev calculations [19] with the CD-Bonn (2001) potential [4] without $3N$ forces (solid line) and with the TM99 $3N$ potential [9] (dashed line).

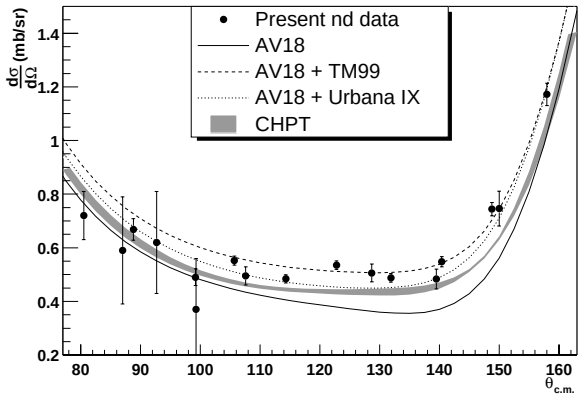

Figure 3: The present *nd* data (filled dots) in the angular range 80°< $\theta_{c.m.}$ <160°. The solid, dashed, and dotted curves were obtained from Faddeev calculations with the Argonne AV18 potential [2] without $3N$ forces, with the Tucson-Melbourne (TM99) $3N$ potential [9], and with the Urbana IX $3N$ potential [11], respectively. The gray band was obtained from chiral perturbation theory at next-to-next-to-leading order [15].

this figure since they give very similar predictions. In the minimum region, our data are well described by the Faddeev calculations including the TM99 $3N$ potential, while they are incompatible with the same calculations without $3N$ forces. This behavior is also observed when considering the ratio of the *nd* to the *np* cross sections (bottom panel of Fig. 2), which is free from normalization uncertainties. The AV18 potential can also be combined with the Urbana IX $3N$ potential [11]. The curve obtained with this choice for the $3N$ force (shown as a dotted line in Fig. 3) gives a different description than the curve obtained with the TM99 $3N$ potential (dashed line). The theoretical prediction obtained from CHPT at next-to-next-to-leading order [15] is shown as a gray band in Fig. 3.

It is quantitatively illustrative to compute the reduced χ^2 between our data and the calculations for the *nd* differential cross section in the minimum, i.e., in the angular range 80°< $\theta_{c.m.}$ <160° (the 17 data points shown in Fig. 3). The reduced χ^2 for different choices of the potentials used in the Faddeev calculations are listed in Table 1. When no $3N$ forces are included, the χ^2 are unreasonably large, in minimum 18. The best description is given by the CD-Bonn potential (version 1996) with the TM99 $3N$ force, with a χ^2 of 2.1. With the AV18 potential, the *nd* differential cross section is slightly better described with the TM99 $3N$ potential ($\chi^2 = 2.3$) than with

Table 1: Reduced χ^2 between the present measured *nd* differential cross section in the minimum ($80°< \theta_{c.m.} <160°$, or all points shown in Fig. 3) and the Faddeev calculations with different models for the potentials, either without $3N$ forces or combined with a $3N$ potential.

NN potential	Without $3N$	TM99 [9]	Urbana IX [11]
AV18 [2]	25	2.3	3.5
CD Bonn (1996) [3]	21	2.1	–
CD Bonn (2001) [4]	18	2.2	–
Nijm1 [5]	21	3.2	–
Nijm2 [5]	25	2.4	–

Table 2: Reduced χ^2 for the ratio of the *nd* to the *np* differential cross sections in the minimum ($10°< \theta_{lab} <46°$, or all points shown in the bottom panel of Fig. 2). The present data are compared with calculations with different models for the potentials (for *nd* scattering, either without $3N$ forces or combined with a $3N$ potential).

NN potential	Without $3N$	TM99 [9]	Urbana IX [11]
AV18 [2]	17	2.7	1.2
CD Bonn (1996) [3]	13	0.6	–
CD Bonn (2001) [4]	12	1.7	–
Nijm1 [5]	15	3.8	–
Nijm2 [5]	18	2.8	–

the Urbana IX potential ($\chi^2 = 3.5$). The CHPT prediction at next-to-next-to-leading order gives a χ^2 of 6.5 (not given in the table). Note that the deviations from unity may be partly due to the normalization uncertainties in the data [46]. For this reason, the ratio of the *nd* differential cross section to the *np* differential cross section– in this ratio, many sources of uncertainties (including the uncertainty in the absolute normalization) are cancelled out–is a more practical observable for testing the models. The reduced χ^2 between our data (for the 13 data points shown in the bottom panel of Fig. 2) and calculations using different *NN* and $3N$ potentials for *nd* scattering are listed in Table 2. When the ratio is considered, the AV18 potential combined with Urbana IX gives a near-perfect description ($\chi^2 = 1.2$), and the best description is still given by CD-Bonn (1996) + TM99 ($\chi^2 = 0.6$).

The present *nd* data can be compared with *pd* data at the same energy to examine the effects of the Coulomb force in *pd* scattering (see Fig. 4).

At 250 MeV, precise *nd* and *pd* data have been published, allowing a detailed analysis of Coulomb effects [62]. The data deviate significantly from

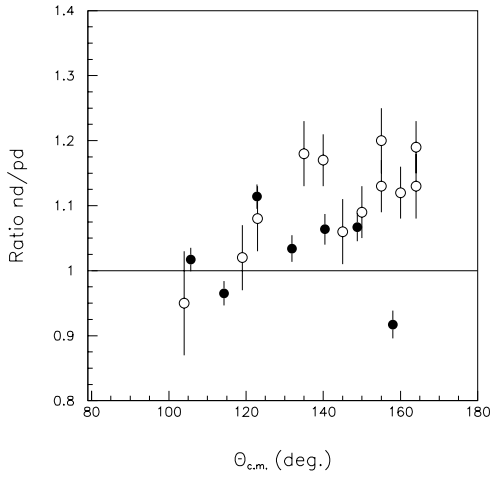

Figure 4: The ratio of *nd* and *pd* scattering cross sections at 95 MeV (filled symbols).The error bars display the full uncertainty, statistical and systematical, with respect to the *nd* data. An additional 5 % uncertainty should be attributed to the *pd* data. The *pd* data have been measured at 90 MeV, and have been scaled down by 8 % to take the energy dependence of the *pd* cross section into account. The unfilled symbols show the same ratio at 250 MeV [62].

the theory predictions. Overall, the ratio is close to unity, but there is an oscillatory behaviour, with *nd* cross sections about 20 % lower than *pd* around 90 degrees, and 20 % higher than *pd* around 120–160 degrees. If this is not due to experimental artifacts, one possible explanation could be isospin dependence in the $2N$ or $3N$ models, or both.

In Fig. 4, the ratio *nd*/*pd* data at 95 MeV is displayed. There is no high-quality *pd* experiment at 95 MeV, but recently data at 90 MeV have been published [63], and an experiment at 100 MeV is under analysis [64]. In the figure, the 90 MeV data have been used, scaled to 95 MeV (8 % reduction in cross section, derived from the energy dependence of predictions based on the AV18 2N force [2] in combination with the U-IX 3N force [11]). No theory prediction of the Coulomb correction is presently available at this energy.

It can be noted that like at 250 MeV, the *nd* data are above the *pd* data

at 95 MeV in the 100-160 degree range, although slightly less so. It should be noted, however, that, if the *pd* data are renormalized further down by 5 %, which is their reported systematic uncertainty, the effect is compatible with the situation at 250 MeV.

4 Conclusions

We have measured the full *nd* angular distribution at 95 MeV in three independent experiments, using the MEDLEY setup and the SCANDAL setup either in deuteron or neutron detection mode. The absolute normalization was obtained relative to either the *np* cross section or the total ^{12}C(n,n) elastic scattering cross section, with an accuracy of $\pm 4\%$. We obtained excellent precision in the angular range of the *nd* cross-section minimum. The data are in good agreement with Faddeev calculations using modern *NN* potentials and including $3N$ forces from a 2π-exchange model, while the calculations without $3N$ forces fail to describe the data. CHPT calculations at next-to-next-to-leading order represent an improvement compared to calculations with *NN* forces only, but still underestimate the data in the minimum region.

The present experimental work provides valuable pieces of information with the purpose of being able to describe nuclear interaction from the basic interactions between nucleons. The *np* and *nd* data help to refine the *NN* and $3N$ potentials as well as effective field theories, which can be applied in systems of more than three nucleons. Thanks to the ongoing advances in computational resources, microscopic calculations directly producing nuclear shell structure from two- and three-nucleon potentials have become feasible and have been attempted for nuclear masses up to A=13 [11, 65]. The inclusion of a $3N$ potential in these calculations has generally a positive effect on the nuclear binding energy and on the level ordering and level spacing of the low-lying excitation spectra. The success of this method depends on the quality of the $3N$ potentials, which can be effectively tested versus experimental data in three-nucleon systems.

Acknowledgments

We wish to thank the technical staff of the The Svedberg Laboratory for enthusiastic and skillful assistance. We are very grateful to E. Epelbaum, W. Glöckle, H. Kamada and H. Witała for contributions concerning the theoretical part. We have appreciated the precious collaboration of K. Hatanaka and N. Kalantar-Nayestanaki. This work was supported by the Swedish Nuclear

Fuel and Waste Management Company, the Swedish Nuclear Power Inspectorate, Ringhals AB, the Swedish Defence Research Agency and the Swedish Research Council.

5 References

References

[1] M. Lacombe, B. Loiseau, J.M. Richard, R. Vinh Mau, J. Côté, P. Pirès, and R. de Tourreil, Phys. Rev. C **21**, 861 (1980).

[2] R.B. Wiringa, V.G.J. Stoks, and R. Schiavilla, Phys. Rev. C **51**, 38 (1995).

[3] R. Machleidt, F. Sammarruca, and Y. Song, Phys. Rev. C **53**, R1483 (1996).

[4] R. Machleidt, Phys. Rev. C **63**, 024001 (2001).

[5] V.G.J. Stoks, R.A.M. Klomp, C.P.F. Terheggen, and J.J. de Swart, Phys. Rev. C **49**, 2950 (1994).

[6] R. Machleidt and I. Slaus, J. Phys. G **27**, R69 (2001).

[7] W. Glöckle, H. Witała, D. Hüber, H. Kamada, and J. Golak, Phys. Rep. **274**, 107 (1996).

[8] S.A. Coon, M.D. Scadron, P.C. McNamee, B.R. Barrett, D.W.E. Blatt, and B.H.J. McKellar, Nucl. Phys. **A317**, 242 (1979); S.A. Coon and W. Glöckle, Phys. Rev. C **23**, 1790 (1981).

[9] J.L. Friar, D. Hüber and U. van Kolck, Phys. Rev. C **59**, 53 (1999); S.A. Coon and H.K. Han, Few-Body Syst. **30**, 131 (2001).

[10] J. Carlson, V.R. Pandharipande, and R.B. Wiringa, Nucl. Phys. **A401**, 59 (1983).

[11] B.S. Pudliner, V.R. Pandharipande, J. Carlson, Steven C. Pieper, and R.B. Wiringa, Phys. Rev. C **56**, 1720 (1997).

[12] A. Nogga, A. Kievsky, H. Kamada, W. Glöckle, L.E. Marcucci, S. Rosati, and M. Viviani, Phys. Rev. C **67**, 034004 (2003).

[13] A. Nogga, H. Kamada, W. Glöckle, and B.R. Barrett, Phys. Rev. C **65**, 054003 (2002).

[14] Ulf-G. Meissner, Nucl. Phys. **A737**, 110 (2004).

[15] E. Epelbaum, A. Nogga, W. Glöckle, H. Kamada, Ulf-G. Meissner, and H. Witała, Phys. Rev. C **66**, 064001 (2002).

[16] P.F. Bedaque and U. van Kolck, Annu. Rev. of Nucl. Part. Sci. **52**, 339 (2002).

[17] D.R. Entem and R. Machleidt, Phys. Rev. C **68**, 041001(R) (2003).

[18] E. Epelbaum, W. Glöckle, and Ulf-G. Meissner, Nucl Phys. **A747**, 362 (2005).

[19] H. Witała, W. Glöckle, D. Hüber, J. Golak, and H. Kamada, Phys. Rev. Lett. **81**, 1183 (1998).

[20] S. Nemoto, K. Chmielewski, S. Oryu, and P.U. Sauer, Phys. Rev. C **58**, 2599 (1998).

[21] L.D. Knutson, Phys. Rev. Lett. **73**, 3062 (1994).

[22] J. Kuroś-Żołnierczuk, H. Witała, J. Golak, H. Kamada, A. Nogga, R. Skibiński, and W. Glöckle, Phys. Rev. C **66**, 024003 (2002).

[23] O. Chamberlain and M.O. Stern, Phys. Rev. **94**, 666 (1954).

[24] H. Postma and R. Wilson, Phys. Rev. **121**, 1229 (1961).

[25] K. Kuroda, A. Michalowicz, and M. Poulet, Nucl. Phys. **88**, 33 (1966).

[26] G. Igo, J.C. Fong, S.L. Verbeck, M. Goitein, D.L. Hendrie, J.C. Carroll, B. McDonald, A. Stetz, and M.C. Makino, Nucl. Phys. **A195**, 33 (1972).

[27] R.E. Adelberger and C.N. Brown, Phys. Rev. D **5**, 2139 (1972).

[28] H. Shimizu, K. Imai, N. Tamura, K. Nisimura, K. Hatanaka, T. Saito, Y. Koike and Y. Taniguchi, Nucl. Phys. **A382**, 242 (1982).

[29] H. Sakai *et al.*, Phys. Rev. Lett. **84**, 5288 (2000).

[30] R.V. Cadman *et al.*, Phys. Rev. Lett. **86**, 967 (2001).

[31] K. Ermisch *et al.*, Phys. Rev. Lett. **86**, 5862 (2001).

[32] K. Sekiguchi *et al.*, Phys. Rev. C **65**, 034003 (2002).

[33] K. Hatanaka *et al.*, Phys. Rev. C **66**, 044002 (2002).

[34] K. Ermisch *et al.*, Phys. Rev. C **68**, 051001(R) (2003).

[35] K. Sekiguchi *et al.*, Phys. Rev. C **70**, 014001 (2004).

[36] M. Allet *et al.*, Phys. Rev. C **50**, 602 (1994).

[37] M. Allet *et al.*, Phys. Lett. B **376**, 255 (1996).

[38] J. Zejma *et al.*, Phys. Rev. C **55**, 42 (1997).

[39] K. Bodek *et al.*, Few Body Syst. **30**, 65 (2001).

[40] St. Kistryn *et al.*, Phys. Rev. C **68**, 054004 (2003);
St. Kistryn *et al.*, Phys. Rev. C **72**, 044006 (2005).

[41] L. Canton and W. Schadow, Phys. Rev. C **62**, 044005 (2000); L. Canton and W. Schadow, Phys. Rev. C **64**, 031001(R) (2001).

[42] A. Kievsky, M. Viviani, and L.E. Marcucci, Phys. Rev. C **69**, 014002 (2004).

[43] A. Deltuva, A.C. Fonseca, and P.U. Sauer, Phys. Rev. C **71**, 054005 (2005).

[44] H. Rühl *et al.*, Nucl. Phys. **A524**, 377 (1991).

[45] P. Mermod *et al.*, Phys. Lett. B **597**, 243 (2004).

[46] P. Mermod *et al.*, Phys. Rev. C **72**, 061002(R) (2005).

[47] P. Mermod *et al.*, Phys. Rev. C **74**, 054002 (2006).

[48] J.N. Palmieri, Nucl. Phys. **A188**, 72 (1972).

[49] Y. Maeda, Ph.D. thesis, University of Tokyo (2004), unpublished.

[50] H. Witała, J. Golak, W. Glöckle, and H. Kamada, Phys. Rev. C **71**, 054001 (2005).

[51] K. Sekiguchi *et al.*, Phys. Rev. Lett. **95**, 162301 (2005).

[52] J. Rahm *et al.*, Phys. Rev. C **63**, 044001 (2001).

[53] C. Johansson *et al.*, Phys. Rev. C **71**, 024002 (2005).

[54] J. Blomgren, N. Olsson, and J. Rahm, Phys. Scr. **T87**, 33 (2000).

[55] M. Sarsour *et al.*, Phys. Rev. Lett. **94**, 082303 (2005).

[56] J. Klug *et al.*, Phys. Rev. C **68**, 064605 (2003).

[57] M.B. Chadwick, P.M. DeLuca Jr., and R.C. Haight, Radiat. Prot. Dosim. **70**, 1 (1997).

[58] J. Blomgren and N. Olsson, Radiat. Prot. Dosim. **103**, 293 (2003).

[59] S. Dangtip *et al.*, Nucl. Instr. Meth. **A 452**, 484 (2000).

[60] J. Klug *et al.*, Nucl. Instr. Meth. **A 489**, 282 (2002).

[61] A.N. Smirnov, V.P. Eismont, and A.V. Prokofiev, Rad. Meas. **25**, 151 (1995).

[62] Y. Maeda, *et al.*, Phys. Rev. C **76**, 014004 (2007).

[63] H.R. Amir-Ahmadi *et al.*, Phys. Rev. C **75**, 041001(R) (2007).

[64] K. Hatanaka, private communication.

[65] P. Navrátil and W.E. Ormand, Phys. Rev. C **68**, 034305 (2003).

Author Index

Subject Index

International Conference on Nuclear Data for Science and Technology 2007
DOI:

CANDIDE - Coordination Action on Nuclear Data for Industrial Development in Europe

J. Blomgren[1,a], E. Bauge[2], D. Cano Ott[9], S. Csifrus[5], K. Dahlbacka[6], I. Gonçalves[13], E. Gonzalez[9], H. Henriksson[15], R. Jacqmin[2], A. Koning[4], D. Lecarpentier[12], E. Malambu[8], A. Mengoni[14], R. Mills[11], A. Plompen[3], G. Rimpault[2], V. Starý[7], C. Trakas[10], P. Vaz[13], and C. Zimmerman[11]

[1] Uppsala University, Dept of Neutron Research, Box 525, SE-75120 Uppsala, Sweden
[2] Commissariat à l'Energie Atomique, France
[3] Joint Research Centre – Institute for Reference Materials and Measurements, EU
[4] Nuclear Research and consultancy Group, the Netherlands
[5] Budapest University of Technology and Economics, Hungary
[6] Teollisuuden Voima Oy, Finland
[7] Nuclear Research Institute Řež, Czech Republic
[8] Studiecentrum voor Kernenergie · Centre d'étude de l'Energie Nucléaire, Belgium
[9] Centro de Investigaciones Energéticas, Medioambientales y Tecnológicas, Spain
[10] AREVA, France
[11] Nexia Solutions, United Kingdom
[12] Electricité de France, France
[13] Instituto Tecnológico e Nuclear, Portugal
[14] International Atomic Energy Agency, UN
[15] Nuclear Energy Agency, OECD

Abstract. A Co-ordinated Action has been launched with the ambition to establish a durable network on nuclear data efforts that are important in the context of minimising the high-level waste stream of nuclear energy. This implies optimal incineration of all actinides that nowadays constitute spent nuclear fuel, in critical and sub-critical reactors. As a consequence, the scope of the CA encompasses transmutation in fast critical reactors as well as sub-critical systems (ADS). The purpose is to identify the needs for improved nuclear data, assess the present status of knowledge, and to estimate what accuracy can be reached with state-of-the-art techniques.

1 Introduction

The EC-supported Coordination Action (CA) CANDIDE, Co-ordination Action on Nuclear Data for Industry Development in Europe, addresses the following two objectives:

- Establishment of better links between academia, research centres and industry end users of nuclear data. This is reflected in the project name.
- Assessment of nuclear data needs for advanced nuclear reactors. The emphasis is on the radioactive waste issue, i.e., either waste transmutation in critical or sub-critical devices or minimizing the production of nuclear waste in future nuclear reactors, as envisaged in some fast critical systems.

For a long time activities concerning all aspects of nuclear data for commercial nuclear power reactors, i.e., nuclear data production, theory, evaluation, validation and industrial use, have been part of a well-organized international community, monitored by large international organizations, like OECD. Recently, a new nuclear data community has been formed around the production of nuclear data for accelerator-driven systems, while the other ingredients of traditional nuclear data work (e.g. evaluation and validation) have to a large degree been missing up to now. The present project aims at establishing links for this new community to the existing structure of coordinated nuclear data activities in general, and to provide links to industry in particular.

Another recent development in Europe has been the enlargement of the EU, which opens new possibilities in the realm of nuclear data. Integration - both of different research communities and between new and previous member states - is an important objective of the CANDIDE project. Moreover, improved training and integration are essential parts of the CA, exemplified by the development of a European course on nuclear data to be part of the project.

In the public literature, the concept of transmutation is quite often used in a restricted sense, synonymous to accelerator-driven systems for incineration of spent nuclear fuel. CANDIDE has been designed with the intention to consider transmutation in a broader, more general sense, i.e., incineration of spent nuclear fuel by changing the nature of the elements through nuclear reactions. As a consequence, the scope of the proposed CA will encompass transmutation in fast critical reactors as well as sub-critical systems (ADS). The purpose of CANDIDE is not to produce new experimental data or evaluations, but to review the current modes of nuclear data production, assess the present status of our knowledge, estimate what accuracy can be reached with state-of-the-art numerical simulation techniques, identify the needs for

[a] Presenting author, e-mail: jan.blomgren@tsl.uu.se

improved nuclear data, and suggest appropriate actions to be taken to meet those needs. A large fraction of the existing data were obtained far back in time, and it might be beneficial to identify cases where new experiments on already measured reactions could exploit technology improvements. Key input is expected from industrial partners, since they are closely involved in application of nuclear data libraries and their performance.

The final result of the CA will be a report describing the state-of-the-art and giving recommendations to EC outlining how nuclear data research should be organized in FP7 and beyond. Moreover, the organisation of workshops and a training course will lead to broader European involvement in the subject.

2 Nuclear data for transmutation of spent nuclear fuel

In the public debate of today, the concept of *transmutation* has often become synonymous with accelerator-driven systems (ADS) for incineration of nuclear waste. This is not surprising, because ADS represents a very innovative option, while the use of critical reactors represent a more conventional alternative. In CANDIDE, however, we will consider transmutation in a very broad sense, not restricted to a particular system or scenario. Presently, nuclear waste transmutation options are investigated as part of reactor and fuel cycle studies for existing reactor types (PWR, BWR, CANDU), i.e., GEN-III, for evolutionary designs of existing reactors, GEN-III+ (EPR, AP600, etc), for GEN-IV reactors (SFR, GFR, LFR, MSR, SCWR, VHTR) or for dedicated transmuters (such as ADS). All these activities generate a significant amount of nuclear data needs either for the feasibility phase of these studies or for the performance phase.

Up to now, there has been a very large research volume spent on data on neutron-induced nuclear reactions up to 20 MeV. This was carried out from around 1950 until today, and was motivated by the needs in the development of civil nuclear power, as well as weapons applications and fusion technology. During the last decade, nuclear data at higher energies have been in the limelight due to the discussions about ADS.

The approaches in these two disciplines differ significantly. This is neither a surprise nor a bad choice, because the underlying physics differs significantly, resulting in different research strategies. Below 20 MeV, a single cross section can be of paramount importance to the entire application. An example is the neutron capture resonance at 6.7 eV in ^{238}U that provides the Doppler effect so important for the stability of critical reactors. Moreover, some cross sections are fundamentally inaccessible to theory, in particular in the resonance region. As a result, at low energies more or less complete data coverage for major elements is required. Above 20 MeV, the situation is fundamentally different. The cross sections are slowly varying in energy, and the behaviour of the system is always dictated by the sum of a large number of reactions, none of which strongly dominates the performance. Therefore, getting a grip on the overall picture has been a more natural ambition in an initial stage, rather than providing precision data on a single reaction.

Thanks to the nuclear data campaigns for ADS in FP5 and FP6, we have now reached a stage where such an overall picture, although fairly rough in many respects, is appearing. As a consequence, the uncertainty in modelling of various ADS concepts due to nuclear data uncertainties have decreased significantly during the last few years. There is, however, still plenty of room for improvement of ADS-relevant nuclear data, only part of which will be fulfilled by IP-EUROTRANS [1].

Up to now, nuclear data at the energies of critical reactors (less than 10 MeV) and accelerator-driven systems (up to 1 GeV) have not been systematically treated on an equal basis. The importance of this aspect was recently highlighted at the International Workshop on Nuclear Data Needs for Generation IV Nuclear Energy Systems [2], after which a WPEC subgroup was established to investigate the nuclear data needs for advanced reactor systems [3]. We find it important for the further development of nuclear data activities for transmutation, and even for the entire research on transmutation, that the nuclear data from these very different regimes can be compared and used in a consistent manner. This is a major underlying theme of CANDIDE.

In general, the safe, economical, and reliable operation of a nuclear reactor depends on the use of nuclear data to predict several important characteristics of plant operation. In the case of transmutation in general, the major benefit of accurate nuclear data relates specifically to avoiding unnecessary conservatism in design and operation such as shielding requirements, power coefficients for a core loaded with minor actinides, and the related power requirements of the proton accelerator for ADS systems.

Another important difference between a dedicated transmutation system - critical or sub-critical - and a conventional critical power reactor is that for the latter, deficiencies in detailed nuclear data can partly be overcome through normalizing calculations to existing reactor measurements or experience from the operation of prototypes and test rigs. The desire to pursue new designs (Gen-IV as well as ADS concepts) without performing extensive reactor experiments dictates using nuclear data that will support reactor calculations that give dependable results even without experimental re-normalization.

On a (very) broad level, the nuclear data requirements for transmutation of waste fall into two classes: (1) resonance and fast neutron reactions for materials that are specific to transmutation: unconventional structural materials, coolants and (in the case of ADS) targets, and minor actinides, whose abundance in the core is much larger than in a conventional reactor, (2) energy regimes that extend beyond the fast neutron region (up to hundreds of MeV) for the above materials and conventional materials. The first class applies to any transmutation method, i.e., including critical reactors, whereas the second class exclusively applies to ADS. In this project, we will consider both classes. Although the motivation for the present project arises from waste minimization using novel reactor types, conventional power reactors can still benefit from the outcome of the CA. Indeed, nuclear data needs that apply to a critical power system, in general also apply to transmutation systems, critical as well as sub-critical. For example, the important interplay between ^{238}U fission, capture and inelastic scattering, is crucial for a precise determination

of criticality. Minimizing the uncertainties in these data is also important for transmutation systems. One interest of the CA is to identify needs that are common to various applications.

3 Training and networking

CANDIDE is not limited to involvement of existing activities, but will also promote growth for the future. Therefore, an important part of the project is the development of a dedicated training course on nuclear data for young professionals, the European course on EXperiment, Theory and Evaluation of Nuclear Data (EXTEND) to be held in Budapest. The target group of this course are young professionals, primarily recently employed staff in industry and at research centres, as well as PhD students in the field.

Summer schools in nuclear engineering (e.g., the Eugene Wigner School on Reactor Physics [4] within the ENEN [5] association or the Frederic Joliot - Otto Hahn summer school [6]) are regularly organized, and there are relatively frequent summer schools on fundamental nuclear physics. Up to now, however, there have been few initiatives to bridge these two communities. EXTEND has been designed to fill this gap.

Besides the development of EXTEND, other activities on training and mobility of young industry professionals and researches, as well as European integration are also foreseen. The most visible example is the planned extension of NEMEA workshops [7], organized by IRMM, which are included in the CA. The previous NEMEA workshops have been targeting nuclear data research in Eastern Europe, but will now be enlarged to be open to all Europe. Our intention is to make these workshops meeting places for all European scientists in the field, including the nuclear industry, which has previously not been the case. The outcomes of two previous such workshops have been beneficial for the present proposal, in so far that they have promoted valuable links between old and new member states in general, and scientists from these in particular.

4 Project strategy

As has been described above, we have identified possibilities to enlarge the nuclear data activities in Europe by integrating the new research communities (ADS research, new member and candidate states) into the already existing structures for nuclear data work, and CANDIDE will address these issues by organizing open workshops intended for bridging gaps between these communities. Moreover, the project itself has been designed to make industry a more visible player in the research-related activities via the top-down approach of CANDIDE. Last but not least, the development of a new course for young professionals is in line with these goals, but it is also intended to foster closer links between nuclear physics and reactor physics.

The project involves a wide range of industry partners. Three reactor construction or manufacturing organizations are represented. AREVA (France) is a leading manufacturer of nuclear reactors in Western Europe, having received widespread attention recently with the two EPRs under construction in Finland and France. The BNFL group (UK) has a wide range of reactors on its repertoire, gas-cooled reactors in the UK as well as light-water reactors (LWR) manufactured by Westinghouse. The Skoda corporation in the Czech Republic is constructing heavy structural parts to nuclear reactors, like reactor vessels, and are represented in the present CA via their technical support organization, NRI Řež.

Two power utilities, TVO (Finland) and EdF (France), participate in the project, representing light water reactor technology. Fuel manufacturing is represented by Nexia/BNFL and AREVA, while reprocessing is represented by Nexia/BNFL. Design of future ADS-related facilities is represented by SCK·CEN (Belgium) and CIEMAT (Spain).

The validation (CEA Cadarache, NRG Petten) and evaluation (CEA Cadarache, CEA Bruyères-le-Châtel, NRG Petten) teams of the proposed CA represent leading European competence in the field. ITN (Portugal) contributes expertise in nuclear data related to spallation targets. The current-day computer power enables sophisticated nuclear reaction modelling and validation against integral experiments with both deterministic and Monte Carlo software.

On the experimental side, IRMM Geel is the dedicated EU lab for reactor-relevant nuclear data (0-20 MeV), while TSL Uppsala is the primary European facility for neutrons above 20 MeV (up to 200 MeV), which will cover important input for ADS neutronics.

With these partners, we cover the entire chain from industry to experiments, with a top-down approach. The industry partners define the needs from the end-users perspective, and their participation guarantees that the work is application-oriented. The role of the non-industry partners is to assess the possibilities to provide data of sufficient quality to meet the application needs. As a consequence, the issue of which data is required or need to be improved is primarily an industry concern, while the question of how to reach those goals is mostly dealt with by the non-industry partners. Efficient dissemination is guaranteed by the involvement of the IAEA and OECD/NEA Data Banks.

Improved training, as well as integration of new member states, are important issues for the CA. Improvement of training on nuclear data is undertaken in close collaboration with European Nuclear Education Network (ENEN) [5], and it brings educational resources in old and new member states together. Additional integration is provided by the strong involvement of industry throughout Europe. Close contacts with the EFNUDAT [8] integrated infrastructure initiative have been established.

5 Project scientific content

As outlined above, the project concerns the integration of nuclear data efforts for all types of transmutation-relevant nuclear systems, i.e., critical thermal and fast reactors, as well as accelerator-driven systems. Up to now, various nuclear-data projects have concentrated on different sub-sets of the global issue. In the present CA, we attempt to unify important aspects of these activities, with the ambition to provide a consistent basis for comparisons of various waste transmutation options.

A general approach to nuclear data for waste management would imply a very large project. To keep the task limited

to a reasonable size, but still with the potential to provide results of relevance to the assessment of various transmutation strategies, the work has to be concentrated to a few issues that are of key importance to both fast critical reactors and ADS.

Up to now, the nuclear data research at classical reactor energies, up to 20 MeV, and the ADS-motivated research above 20 MeV have been conducted with very different approaches. This has made sense, because the pre-conditions have been very different. With the recent development in nuclear data for ADS, resulting from FP5 and FP6 projects, we believe it is now possible to conduct research on what is common to critical reactors and ADS. A major unifying aspect is the role of neutrons. In both concepts, the major incineration is due to neutron-induced fission. Moreover, other neutron-induced reactions, like capture and scattering, play significant roles in all these techniques. Another common aspect is that the core will contain large amounts of minor actinides, although the composition differs among various systems. Furthermore, the design studies around GEN-IV type systems encompass not only the core but also the full fuel cycle. One important GEN-IV criterion is the reduction of radioactive waste that is competing against other criteria such as sustainability (full use of Uranium or Thorium ores), economics, safety and reliability, proliferation resistance and physical protection.

As a natural consequence of this, a study that could cover only the transmutation aspect of a core would not be complete. We therefore envisage the project to cover all nuclear data that have some relation to the reactors and their associated fuel cycles, whether they are dedicated specifically to transmutation (just like ADS) or if transmutation is only one of their key features.

In the present CA, we intend to assess the data situation for all neutron energies, from thermal and up to the highest available (200 MeV), both experimentally and theoretically. In the first instance, the focus of the CA should be on cores of fast reactors and ADS. Nuclear data are of great relevance also for irradiation effects on materials, radiation protection and a number of other issues. A possible list of data to be studied is given below:

- General purpose files that include (1) cross-sections induced by neutrons, protons and gammas, (2) secondary particle energy distributions, and (3) fission spectra and energy release.
- Gamma production induced by different reaction types.
- Fuel cycle data (fission yields, spallation yields, decay heat).
- Activation files.

Participants from nuclear industry should give guidance on the proper parameters to be investigated and optimised. These needs should be translated into data evaluation and measurement requests, to be carried out in FP7 and beyond. Part of the effort in this CA consists of a critical assessment of major and minor actinide data in the latest nuclear data libraries and an assessment of the corresponding uncertainties. This should in a natural way lead to well-focused measurement requests.

As has been emphasized, the industrial needs will drive the assessment within the CA. It is worthwhile to point at the close connection of the present collaboration with the OECD-NEA High Priority Request List for nuclear data, where such well-defined requests are collected and reviewed to mobilise the community for their resolution. CANDIDE will serve to identify and propagate the EU interests in this domain and to provide the focus for future EU research on nuclear data. Also in the area of follow up on the formulated requests, CANDIDE is well connected to running EC projects, especially the JEFF project, as mentioned previously.

This work was financially supported by the European Union, contract 036397.

References

1. EUROTRANS - European Research Programme for the Transmutation of High-Level Nuclear Waste in an Accelerator-Driven System. http://nuklear-server.ka.fzk.de/eurotrans/.
2. Proceedings of the International Workshop on Nuclear Data Needs for Generation IV Nuclear Energy Systems, ed. P. Rullhusen (Antwerpen, Belgium, 5-7 April 2005). http://www.jrc.cec.eu.int/gen4-workshop/main.html.
3. M. Salvatores et al., in these proceedings.
4. The Eugene Wigner School on Reactor Physics. http://www.reak.bme.hu.
5. The European Nuclear Education Network. http://www.sckcen.be/ENEN.
6. The Frédéric Joliot & Otto Hahn Summer School on Nuclear Reactors. http://www-cadarache.cea.fr/fr/cadarache/ecoles/fjohss2007.htm
7. The most recent event in this series was NEMEA-3, 3rd Workshop on Neutron Measurements, Evaluations and Applications, October 25-28, 2006, Borovets, Bulgaria. http://www.irmm.jrc.be/html/events/events/nemea-3.htm
8. G. Barreau on behalf of the EFNUDAT consortium, in these proceedings. www.efnudat.eu.

A proposal for an integral neutron data experiment in the 100-200 MeV region

J. Blomgren[1)], *K. Chtioui*[1,2)]

1) Department of Neutron Research, Uppsala University, Box 525, S-751 20 Uppsala, Sweden
Jan.Blomgren@tsl.uu.se
2) Université de Caen, France

Abstract: Cross section data for neutron-induced nuclear reactions at higher energies than for traditional applications of nuclear physics is required for the further development of sub-critical accelerator-driven systems (ADS) for transmutation of spent nuclear fuel. During the last decade, the situation on microscopic cross sections has improved significantly, to the extent that for the most important reactions, cross section data with uncertainties of about 10 % or less are available for a few key elements at some selected energies. Based on these data, nuclear data libraries up to about 200 MeV have been developed.
It is now motivated to make assessments of the predictive power of these libraries through integral experiments. In this paper, we present a pre-study of such a possible integral experiment on neutron data at two energies, 96 and 175 MeV. The reason for these two energies is the existence the high-intensity quasi-monoenergetic neutron source at The Svedberg Laboratory, Uppsala, Sweden. The envisaged experiment is on transmission and scattering of neutrons when passing blocks of iron or lead, with thicknesses ranging from 10 to 100 cm. Simulations of the proposed experiment have been performed with MCNP with two nuclear data libraries, JEFF-3.1 and ENDF/B-VI. The present project is part of the CANDIDE (Coordination Action on Nuclear Data for Industrial Development in Europe) project.

Introduction

As outlined in many places elsewhere in these proceedings, integral experiments are an indispensable activity in the evaluation and validation of nuclear data. Procedures for such validation are since long well established in the classical neutron energy range up to 20 MeV, i.e., the neutron energy range of relevance to critical fission reactors (thermal and fast), as well as fusion applications.
With the advent of accelerator-driven systems (ADS), the energy range in which information on neutron-induced nuclear reactions are required for design activities has been significantly increased. In a spallation-driven system, neutrons of energies all the way up to the incident proton energy, i.e., up to GeV energies, are present. Although relatively few neutrons reside at these high energies, their large capability to induce, e.g., materials damage necessitates the nuclear data libraries to be improved significantly above 20 MeV.
The ADS research activities funded by the EU have so far (FP 4, 5 and 6) been dominated by measurements of microscopic cross sections, a fact which has been motivated by the state of knowledge at the time these projects were launched. In particular the HINDAS project [1] in FP5 has resulted in fairly complete data bases on neutron elastic scattering and neutron-induced production of light ions up to about 100 MeV. In addition, fission total cross sections up to 200 MeV on a series of nuclei are now available, to a large extent thanks to ISTC projects. Total cross section data from LANL up to about 600 MeV on a series of nuclei complement the picture [2]. Thus, the most important microscopic cross sections are now available up to at least 100 MeV.
The recent achievements of these projects now motivate an increased attention to integral experiments, especially at ADS-relevant energies, i.e., above 20 MeV, where such experiments are almost absent. Thus, a few existing high-quality integral experiments should be identified. Above 20 MeV some shielding experiments exist, notably the 43 and 68 MeV TIARA transmission measurements for concrete and iron, which is mainly important for structural material studies [3].

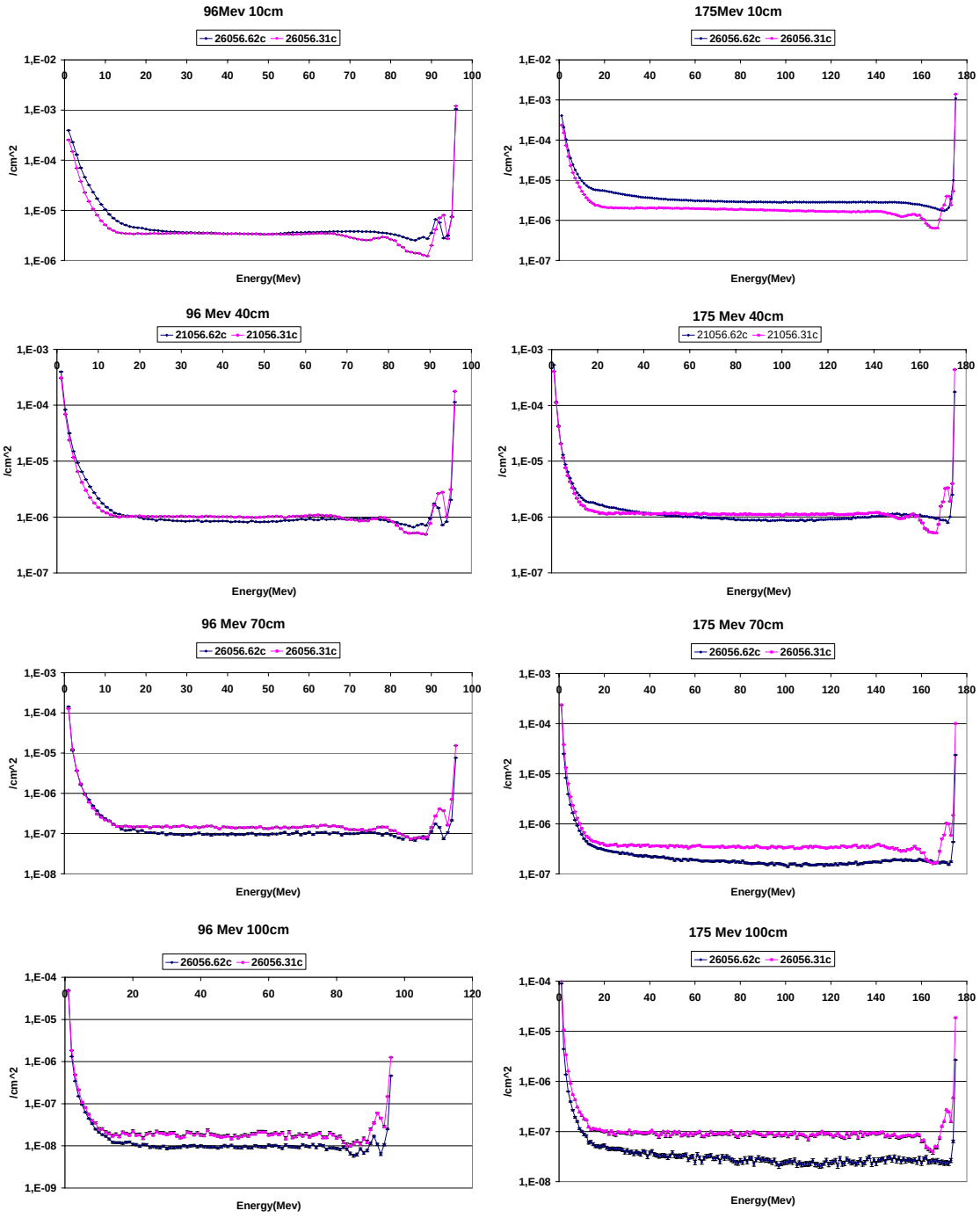

Figure 1: Neutron transmission spectra for iron at 96 MeV (left column) and 175 MeV (right). From top to bottom, the spectra show transmission through 10, 40, 70 and 100 cm material thickness. The blue (dark) lines and the violet (light) lines show predictions by ENDF/B-VI and JEFF-3.1, respectively.

What is missing is a clean experiment on core material that allows analysis of the impact of high-energy neutrons. An integral experiment of neutrons on a block of uranium would enable a thorough test of evaluated neutron data files above 20 MeV.
More complex systems, such as MEGAPIE [4], serve to test ADS calculations as a whole. The complex design of such target systems makes it, however, difficult to draw conclusions on the quality of the underlying nuclear data based on the performance of the full system.

The necessity and feasibility of integral experiments above the present maximum energy of 68 MeV will be investigated in the CANDIDE project [5]. In the present work, a first step towards this goal is presented. We have simulated the transmission of 96 and 175 MeV neutrons through slabs of iron and lead. The selections of materials have been dictated by the needs of ADS development. Iron is a representative construction material and lead is a candidate for coolant. Investigations of uranium constitute future work.

Simulation procedure

The transmission of neutrons through slabs of various thicknesses has been simulated using the MCNPX code [6]. We have used realistic dimensions of the neutron beam facility [7] at The Svedberg Laboratory (TSL), Uppsala, Sweden in all simulations. Neutrons are in reality produced by the ^{7}Li(p,n) reaction, which produces a quasi-monoenergy neutron spectrum, in which about half the neutrons have energies slightly below the energy of the incident proton beam, with a width of typically 1-2 MeV, and the remaining neutrons are spread out about equally on all energies from maximum down to zero energy. In our simulations, we have used strictly mono-energetic neutrons for simplicity and to accentuate the effects at high energies, where the nuclear data are the least well known. For proper detailed design of a realistic experiment, the neutron spectrum of the ^{7}Li(p,n) reaction should be used.
The neutron production is by all practical measures point-like. The neutrons are collimated to a narrow cone. At a distance of 401 cm from the production, the neutron beam impinges on a transmission target. At this position, the beam diameter is 10.9 cm. The transmission target is composed of slabs of target material, in our case iron or lead. We have simulated total thickness of 10, 40, 70 and 100 cm targets at two energies, 96 and 175 MeV. The choice of energies has been dictated by the maximum energies of the two operational modes of the TSL neutron beam facility.
In this exploratory study, we have used two nuclear data libraries, ENDF/B-VI [8] and JEFF-3.1 [9]. It is implicitly assumed that the differences in results between these two high-quality libraries reflect the underlying uncertainty in the knowledge of the true value of the cross section data.

Results

Results of transmission simulations on iron and lead are shown in Figs. 1 and 2, respectively. In both figures, results at 96 and 175 MeV are shown in the left and right panels, respectively. In general, all simulations show a similar pattern. There is a large peak at full energy, corresponding to neutrons transmitted without undergoing nuclear reactions. The compound peak at low energies is due to statistical decay, and the flat region in between is due to various types of pre-equilibrium reactions.
It was anticipated beforehand from basics physics considerations that the main differences should arise close to the full-energy peak, where the spectrum is sensitive to direct nuclear reactions. The reason for this is that calculations of cross sections for direct reactions are sensitive to nuclear physics details in the input. Thus, in the cases experimental data are absent, the evaluated data files have to rely on nuclear theory with fairly large uncertainties. In the other end of the spectrum, the compound peak at low energies should not display large deviations between the libraries, because it is governed by the well-known statistical emission. In between, some deviations can be found, manifesting differences in pre-equilibrium treatment.
These features are present in the results. It can be seen that there is indeed no significant differences between the libraries in the compound peak region. In both iron and lead, there are significant differences in the giant resonance region, i.e., at excitation energies of 5-20 MeV. One notable feature is that there are no visible giant resonance structures in lead at 175 MeV for any library, but there are such structures clearly predicted by ENDF/B-VI at 96 MeV, and to a lesser extent also by JEFF-3.1. It is difficult to identify a reason why such structures should not be present at 175 MeV, when they are clearly there at 96 MeV. Thus, this feature in the simulations is itself a reason for an experimental investigation. The libraries agree in general fairly well in the preequilibrium part of the spectrum, with the notable exception of iron at 175 MeV.

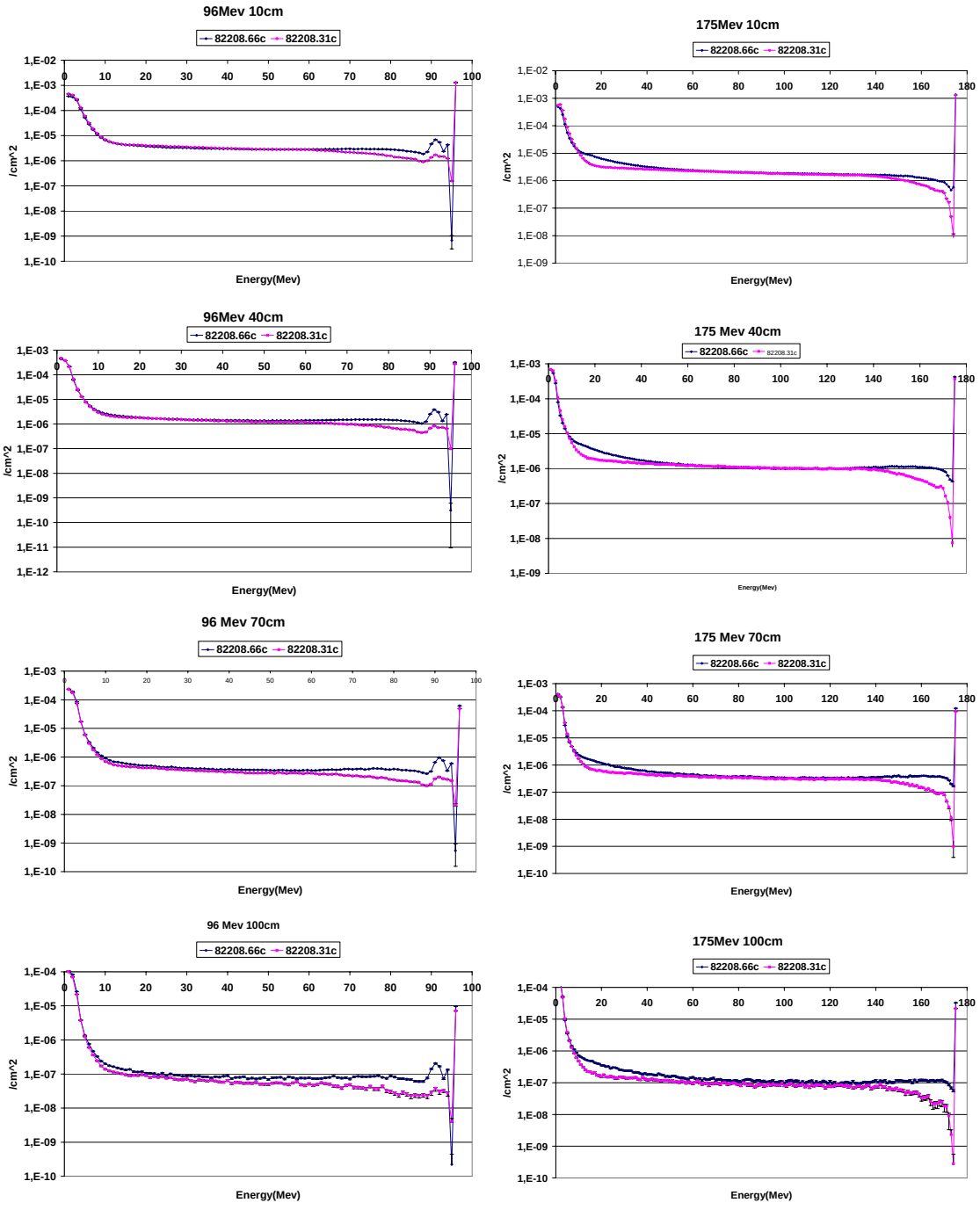

Figure 2: Neutron transmission spectra for lead at 96 MeV (left column) and 175 MeV (right). From top to bottom, the spectra show transmission through 10, 40, 70 and 100 cm material thickness. The blue (dark) lines and the violet (light) lines show predictions by ENDF/B-VI and JEFF-3.1, respectively.

Another important feature that might no be very obvious from the figures is the high-energy peak. It is especially notable in Figure 1 that the content in the high-energy peak for iron differs by a factor two at 96 MeV and almost a factor ten at 175 MeV for 100 cm target thickness. Measurement of this high-energy peak is a rather straight-forward procedure, with potential to yield valuable information.

In the case of lead, the differences in the high-energy peak are small. This does not necessarily reflect that the true value is well known. It could be the result of that these two evaluations use the same input. Thus, verifying the data on lead still has high priority.

It should be pointed out that in the case of lead, there are sharp dips in the spectra just below the high-energy peak. This is an artefact in the simulations. It just happens that there is no physical state in that particular bin. In reality, the experiment will be conducted with a resolution of, say, 5 MeV and then this dip will not appear.

Design of an integral experiment

The findings above are used as guidelines for a future integral experiment. Obviously, the expected differences are moderate or small at low neutron energies, whilst the most important discrepancies are found at fairly high energies, i.e., in the upper half of the energy range. This makes the detection easier in a gedanken experiment at TSL. The SCANDAL [7] neutron detector system at TSL is capable of detecting neutrons above 30-40 MeV with a resolution of typically 4 MeV. SCANDAL was originally designed for neutrons up to 130 MeV, but is presently being upgraded to work up to 180 MeV. Thus, SCANDAL can cover the maximum energy peak, the giant resonance region and most of the pre-equilibrium spectrum.
It would be valuable to cover also lower energies, preferably all the way down to zero energy. For these lower energies, other detectors have to be used. At present, a liquid scintillator for proton recoil detection and spectrum unfolding is being developed. This could possibly be used for these experiments. Another possibility is to use time-of-flight methods, but this is hampered by the relatively poor time structure of the beam. Moreover, wrap-around effects make part of the data ambiguous. Various detection schemes based on fission are also under consideration.

Outlook

What remains to be done is first to repeat these simulations also for uranium. Secondly, it would be interesting to test the sensitivity to individual cross sections in the libraries. Thus, it is planned to change one particular cross section and study in which way the transmission spectrum is changed.
These studies should be followed by detailed computations of experiment parameters. One crucial aspect is beam time. Already now, it is clear that with the differences displayed between the leading libraries in the present work, a well-designed experiment requires less than one week of beam time (i.e., a very realistic beam time) to reach sufficient accuracies for distinction between various libraries.

Acknowledgements
This work was financially supported by the European Union, contract 036397, Barsebäck Power AB, Forsmark AB, Ringhals AB, the Swedish Nuclear Power Inspectorate, the Swedish Nuclear Fuel and Waste Management, the Swedish Defense Research Agency and the Swedish Research Council.

References

[1] A. Koning, H. Beijers, J. Benlliure, O. Bersillon, J. Blomgren, J. Cugnon, M. Duijvestijn, Ph. Eudes, D. Filges, F. Haddad, S. Hilaire, C. Lebrun, F.-R. Lecolley, S. Leray, J.-P. Meulders, R. Michel, R.-D. Neef, R. Nolte, N. Olsson, E. Ostendorf, E. Ramström, K.-H. Schmidt, H. Schuhmacher, I. Slypen, H.-A. Synal, R. Weinreich, J. Nucl. Sci. Tech., Suppl. **2** (2002) 1161.
[2] R.W. Finlay, W.P. Abfalterer, G. Fink, E. Montei, T. Adami, P.W. Lisowski, G.L. Morgan, R.C. Haight, Phys. Rev. C **47** 237 (1993) 237.
[3] H. Nakashima, N. Nakao, S. Tanaka, T. Nakamura, K. Shin, S. Tanaka, H. Takada, S. Meigo, Y. Nakane, Y. Sakamoto, M. Baba, J. Nucl. Sci. Eng. **124** (1996) 243.
[4] W. Wagner, Y. Dai, H. Glasbrenner, M. Grosse, E. Lehmann, Nucl. Instr. Meth. **A 562** (2006) 541.
[5] J. Blomgren, E. Bauge, D. Cano Ott, S. Csifrus, K. Dahlbacka, I. Gonçalves, E. Gonzalez, H. Henriksson, R. Jacqmin, A. Koning, D. Lecarpentier, E. Malambu, A. Mengoni, R. Mills,

A. Plompen, G. Rimpault, V. Starý, C. Trakas, P. Vaz, C. Zimmerman, in these proceedings.

[6] L.S. Waters, MCNPX Users' Manual – Version 2.1.5, Los Alamos National Laboratory, November 14, (1999).

[7] J. Klug, J. Blomgren, A. Atac, B. Bergenwall, S. Dangtip, K. Elmgren, C. Johansson, N. Olsson, S. Pomp, A.V. Prokofiev, J. Rahm, U. Tippawan, O. Jonsson, L. Nilsson, P.-U. Renberg, P. Nadel-Turonski, A. Ringbom, A. Oberstedt, F. Tovesson, V. Blideanu, C. Le Brun, J.F. Lecolley, F.R. Lecolley, M. Louvel, N. Marie, C. Schweitzer, C. Varignon, Ph. Eudes, F. Haddad, M. Kerveno, T. Kirchner, C. Lebrun, L. Stuttgé, I. Slypen, A. Smirnov, R. Michel, S. Neumann, U. Herpers, Nucl. Instr. Meth. **A 489** (2002) 282.

[8] ENDF/B-VI, IAEA-NDS-100, Rev. 11 (1994). See also, e.g., www.nea.fr.

[9] JEFF-3.1, www.nea.fr.

NUCLEAR ENERGY AGENCY
NUCLEAR SCIENCE COMMITTEE

SUMMARY RECORD

EIGHTEENTH MEETING OF THE NUCLEAR SCIENCE COMMITTEE

13-15 June 2007
NEA Headquarters, Issy-les-Moulineaux [France]

JT03230221

Document complet disponible sur OLIS dans son format d'origine
Complete document available on OLIS in its original format

/

TABLE OF CONTENT

OPENING 4

ADOPTION OF THE AGENDA 4

INTRODUCTION BY THE DIRECTOR GENERAL 4

APPROVAL OF THE SUMMARY RECORD OF THE 17TH MEETING 5

STATUS OF COMMITTEE PROJECTS 5

Review of progress of the NSC Working Parties 5
Working Party on Nuclear Criticality Safety (WPNCS) 5
Working Party on Scientific Issues of Reactor Systems (WPRS) 6
Working Party on Scientific Issues of the Fuel Cycle (WPFC) 6
Working Party on International Nuclear Data Evaluation Cooperation (WPEC) 7
Short review of NSC expert groups 7
Needs of research and test facilities in nuclear science 7
Workshops, meetings and conferences 8
Follow-up to recent NSC organised workshops 8
NSC organised workshops in 2008 8
Request for NSC sponsorship of future meetings and conferences 9
Other meetings 9

IN-DEPTH DISCUSSIONS 9

Simulation of materials and fuels 9
Simulation and modelling of Generation-III reactors 10

REPORT FROM THE 16TH MEETING OF THE NSC EXECUTIVE GROUP 11

FOLLOW-UP ACTIONS TO THE NSC SELF-EVALUATION 11

INTEREST OF POLAND IN THE WORK OF THE NSC AND ITS WORKING PARTIES 11

REPORTS FROM OTHER NEA DIVISIONS, OTHER INTERNATIONAL ORGANISATIONS AND NEW OBSERVERS 11

The Nuclear Development division 11
The EC 12
The IAEA 12
Russia 12

NEXT NSC MEETING 12

Date of next meeting 12
Topics for in-depth discussion 12

ELECTION OF COMMITTEE OFFICERS 13

ANY OTHER BUSINESS 13

Annex 1 14

List of actions adopted at the meeting 14

Annex 2 15

List of Participants 15

Annex 3 21

Mandate of the Working Party on Scientific Issues of Reactor Systems (WPRS) 21
Mandate of the WPRS Expert Group on Minor Actinide Burning in Thermal Reactors 24
Mandate of the Working Party on Scientific Issues of the Fuel Cycle (WPFC)..... 25
Mandate of the Working Party on Nuclear Criticality Safety (WPNCS) 27

Annex 4 29

Report to the Nuclear Science Committee from the Sixteenth Meeting of the Executive Group..... 29

SUMMARY RECORD OF THE EIGHTEENTH MEETING OF THE NUCLEAR SCIENCE COMMITTEE

13-15 June 2007

OPENING

1. Th. Dujardin opened the meeting by informing the delegates about the absence of the NSC chair, T. Lefvert, due to the very recent passing away of his wife. A letter of condolences, signed by all delegates, was sent to T. Lefvert.

2. The vice-chair, J. Herczeg, agreed to chair the meeting.

3. The new member from Canada, K. Kozier, AECL Chalk River, participated for the first time. The WPNCS chair, J. Gulliford, UK, was invited to present progress in the work of WPNCS, including a proposed new mandate, and D. Nowak, USA, was invited to the in-depth discussion on "simulation of materials and fuels".

4. Apologies for absence had been received from E. Nonbøl, Denmark, T. van der Hagen, the Netherlands, P. Vaz, Portugal, J. Pena, Spain, and J. Coadou, EC. A list of participants is given in Annex 1.

ADOPTION OF THE AGENDA [NEA/SEN/NSC(2007)1]

5. The proposed agenda was adopted with the modification that the meeting would start with point 5.1.3 to accommodate the limited availability of the WPNCS chair, J. Gulliford. The in-depth discussions were as usually scheduled for the morning of the second day.

INTRODUCTION BY THE DIRECTOR GENERAL

6. L. Echavarri, Director General of the NEA, informed the delegates that Russia had become an official observer to the NEA and its committees, following the signing of a Joint Declaration of Co-operation between the Government of the Russian Federation and the NEA in March 2007. The NEA was also investigating the possibility to increase the cooperation with China and an agreement in the area of nuclear safety was under negotiation. In addition, it was envisaged to enlarge this cooperation to cover other areas, such as nuclear science.

7. Poland had approached the NEA expressing its interest to become ad-hoc participant in three different NEA standing technical committees, including the NSC and the NSC working parties WPFC and WPRS. **L. Echavarri asked the delegates to evaluate the mutual benefit of this request from Poland and to make a recommendation to the NEA Steering Committee, well before its meeting in mid October 2007**.

8. The policy debate at the last NEA Steering Committee meeting had been devoted to "nuclear energy research". The main conclusions of the debate were that the role of governments in nuclear research is primarily for addressing regulatory needs, as well as long-term issues that will not likely be addressed by industry; that there is a need to continue research on nuclear safety, nuclear science, nuclear technology development and radioactive waste management for both current and future reactors; that there are different needs in countries with or without nuclear infrastructure; that it is important to establish effective

links for transfer of knowledge between researchers and nuclear operators; and that pooling resources, both nationally and internationally, is more effective. The Steering Committee supported the continued involvement of the NEA in nuclear research, as well as in the associated international initiatives, and supported the idea of the Secretariat preparing a written proposal regarding the role of governments in helping to ensure the availability of qualified human resources. The policy debate at the forthcoming Steering Committee meeting would be devoted to the newly approved ICRP recommendations on radiological protection.

9. The NEA would celebrate its 50th anniversary in 2008 and the secretariat had started to draft a "nuclear energy outlook" publication, which would be issued in time for the anniversary celebrations in October 2008.

10. Finally, L. Echavarri reported that the NEA Deputy Director General, Gail Marcus, had left the organisation and would be replaced by Janice Dunn Lee, from the US NRC. J. Dunn Lee would take up duty in the second half of July 2007.

APPROVAL OF THE SUMMARY RECORD OF THE 17TH MEETING [NEA/SEN/NSC(2006)3]

11. The summary record of the seventeenth meeting of the NSC was approved without modifications.

STATUS OF COMMITTEE PROJECTS [NEA/SEN/NSC(2007)2]

Review of progress of the NSC Working Parties

Working Party on Nuclear Criticality Safety (WPNCS)

12. J. Gulliford, WPNCS chair, presented progress in the areas covered by the Working Party. He highlighted recent publication and described on-going work in the expert groups on burn-up credit, on source convergence analysis and on criticality excursions. He also mentioned the newly established expert group on assay data for spent nuclear fuel, which will compile new assay data into the SFCOMPO database and write a state-of-the-art report on assay data of spent nuclear fuel, establishing "best-practice" to help guide future Post Irradiation Examination (PIE) composition programmes.

13. The September 2007 issue of the international handbook of evaluated criticality safety benchmark experiments (ICSBEP) will contain about 250 new configurations, bringing the total number of configuration to over 4000.

14. The NSC study on "Proposed Integral Criticality Experiments with Low-moderated MOX fuels" had been completed in October 2006 at a meeting in Paris, where the selected experiments, performed at IPPE Obninsk, Russia, and funded by US and France, had been presented. The conclusions and analysed data will be published as a NSC report in early 2008.

15. The International Conference on Nuclear Criticality Safety (ICNC-2007) had been held in St. Petersburg, Russia on 28 May-1 June 2007. The conference had been attended by close to 200 scientists. The next conference in this series will most probably be held in Edinburgh, UK in 2011.

16. The next meeting of the Working Party, which will be held at the end of August 2007, will discuss possible future activities, such as spent fuel reprocessing and repository safety, as well as the possibility to organise a workshop in autumn 2008 on "Needs of Research on Nuclear Criticality Safety for future nuclear system".

17. A new Working Party mandate, covering the period June 2007 to June 2010, was presented. **The NSC approved the proposed mandate with a correction to the list of official observers**. The new mandate can be found in Annex 2.

Working Party on Scientific Issues of Reactor Systems (WPRS)

18. The WPRS chair, K. Hesketh, gave an overview of the WPRS activities, following a first year of work under the new structure, which had been approved at the last NSC meeting in June 2006. The activities had been grouped into three work areas: experiments, reactor and fuel analysis, and radiation transport and dosimetry.

19. In the reactor and fuel cycle work area, it was especially noted that the task force on reactor-based plutonium disposition would be fully incorporated in the WPRS, and K. Hesketh thanked the former chair of the task force, P. D'Hondt, for his excellent work in guiding the group.

20. The importance of uncertainty analysis in modelling was stressed, as it will have an important impact on safety analysis using best estimate methods and enable the determination of confidence bounds for calculated safety parameters. It was noted that the activity is a challenging one and will require investments in method development and validation in member countries.

21. The recently established expert group on minor actinide burning in LWRs will organise a first meeting in autumn 2007. The Canadian delegate, K. Kozier, asked if it was possible to include also heavy water reactors in the study. K. Hesketh responded that it would be possible and that K. Kozier was welcome to make a proposal to the first meeting of the group. The name of the expert group was changed to the Expert Group on Minor Actinide Burning in Thermal Reactors. The mandate of the Expert Group can be found in Annex 2.

22. When discussing the proposed new WPRS mandate and especially the long list of deliverables for the next three years, J. Herczeg asked if it would be possible to receive a more detailed planning of the deliverables. **K. Hesketh agreed to provide a Gantt chart of deliverables for the next NSC meeting.**

23. **The committee approved the proposed mandate of WPRS**. The new mandate can be found in Annex 2.

Working Party on Scientific Issues of the Fuel Cycle (WPFC)

24. In the absence of the chair, K. McCarthy, Y. J. Choi presented the activities of the WPFC. The work was performed by three expert groups, one on Lead-Bismuth Eutectic (LBE) technology, one on chemical partitioning and one on fuel cycle transition scenario studies. The Working Party is also responsible for organising the series of workshops on Utilisation and Reliability of High Power Proton Accelerators (HPPA) and on Actinide and Fission Product Partitioning and Transmutation.

25. The expert group on LBE technology had recently published a very comprehensive handbook on LBE technology, covering alloy and lead properties, materials compatibility, as well as thermal-hydraulics. In addition, the expert group is about to launch a benchmark study of thermal-hydraulic loop models for lead-alloy cooled advanced nuclear systems.

26. The expert group on fuel cycle transition scenario studies is about to publish a status report covering issues associated with transition to future nuclear fuel cycle technologies and structures, country-dependent scenarios and key technologies for implementing advanced fuel cycles. The group is also pursuing two benchmark exercises, one on scenario code performance and one on regional (European)

scenarios. The group will work in close coordination with the recently establish NDC group on fuel cycle transition scenarios.

27. R. Chawla posed a question about the relevance of the WPFC work programme in relation to the preoccupations in member countries. The result of the discussion that followed was that **the WPFC was asked to review the programme of work at their next meeting** and report back in time for the NSC bureau meeting in late autumn 2007.

28. **The committee approved the proposed mandate of WPFC** with a minor correction in the paragraph on liaison with other NEA bodies. However, **the WPFC was asked to review the part of the mandate devoted to "fuels and materials"**, taking into account the results of the in-depth NSC discussion on "Simulation of materials and fuels" (see paragraph X) and, if necessary, submit a revised mandate to the NSC. The approved mandate can be found in Annex 2.

Working Party on International Nuclear Data Evaluation Cooperation (WPEC)

29. The former WPEC chair, A. Koning, gave an overview of recent achievements and the status of on-going activities. Among the recent achievements were mentioned the publications describing the recent release of the nuclear data reactions standards, and the resolution of a nuclear data problem related to the systematic reactivity under-prediction of thermal low-enriched uranium fuelled LWRs. The WPEC had also published a comprehensive study of activation cross sections and an investigation of discrepancies in summation calculations of fission product decay heat.

30. The on-going work comprised in principal three subjects: fission product data, nuclear data needs, and covariance data. The nuclear data needs were covered by two subgroups, the maintenance of the High Priority Request List (HPRL) for nuclear data and a subgroup devoted to data needs for advanced reactor systems. The efforts on uncertainty (covariance) data were mainly dedicated to developing methodologies, rather than producing the data themselves.

31. Two new subgroups had been established at the WPEC meeting in mid April 2007, one on the ^{235}U capture cross section in the keV to MeV energy range and one on the improvement of the quality and accessibility of the EXFOR database of experimental reaction data.

32. The NSC took note of the progress.

Short review of NSC expert groups

Needs of research and test facilities in nuclear science

33. P. D'Hondt presented the status of the work on needs of research and test facilities in nuclear science. The expected output is a report on "Research and Test Facilities Required in Nuclear Science and Technology" and an associated database containing information about more than 750 research and test facilities. The database was almost ready for release, whereas the report would be issued in mid 2008. I. Yamagishi demonstrated the content of the database.

34. A. Koning asked if the delegates would be able to review the report before the publication. Th. Dujardin answered that this possibility was granted by the guidelines for NSC working methods decided by the committee in June 2006 where it is stated that "*The committee members would also be given the possibility to review the output of each NSC activity before publication*".

35. The NSC discussed the database release policy and, following a proposal by **J. Herczeg, it was agreed to release the database in mid July 2007, protected with a generic password. The NSC**

delegates were asked to clarify their domestic position on the possibility to release the public part of the database without password protection. A final decision would be taken at the NSC bureau meeting in late autumn 2007.

Workshops, meetings and conferences

Follow-up to recent NSC organised workshops

9th Information Exchange Meeting on Actinide and Fission Product Partitioning & Transmutation

36. F. Mompean reported on the highlights from the 9th Information Exchange Meeting on Actinide and Fission Product Partitioning & Transmutation, which had been organised in Nîmes, France on 25-29 September 2006. The meeting, which had gathered 170 participants, had been organised in cooperation with the NDC and had been hosted by CEA. The summary session debate covered subjects such as storage or transmutation of Curium, the lack of fast reactors for irradiation experiments, and a number of issues related to nuclear waste management. The proceedings are expected to be published by the end of the summer 2007.

5th International Workshop on the Utilisation and Reliability of High Power Proton Accelerators

37. P. D'Hondt gave an overview of the outcome of the workshop on the Utilisation and Reliability of High Power Proton Accelerators, which had been held in Mol, Belgium on 6-9 May 2007, hosted by SCK-CEN. More than 40 papers had been presented, covering the following six topics: the MEGAPIE programme, accelerator programmes and applications, accelerator reliability, spallation target development and coolant technology, sub-critical system design and ADS simulations, and ADS experiments and test facilities. Eighty (80) scientists participated in the workshop. The proceedings will be published in the autumn 2007.

Workshop on Structural Materials for Innovative Nuclear Systems (SMINS)

38. The outcome of the workshop on Structural Materials for Innovative Nuclear Systems (SMINS), hosted by FzK in Karlsruhe, Germany on 4-6 June 2007, was presented during the in-depth discussion on "Simulation of materials and fuels" (see below).

NSC organised workshops in 2008

Workshop on Advanced Reactors with Innovative Fuels (ARWIF-2008)

39. T. Mori informed the delegates that the next workshop on Advanced Reactors with Innovative Fuels (ARWIF-2008) would be held in Tsuruga, Japan on 20-22 February 2008. The meeting would be hosted by JAEA. The next WPRS meeting would be held in conjunction with the workshop. The first announcement of the workshop would be circulated in July 2007.

Shielding Aspects of Accelerators, Targets and Irradiation Facilities (SATIF-9)

40. E. Sartori notified the committee members about the plans for the next meeting on Shielding Aspects of Accelerators, Targets and Irradiation Facilities (SATIF-9). The meeting would be held on 21-23 April 2008, hosted by the Spallation Neutron Source (SNS) facility at the Oak Ridge National Laboratory, USA.

10th IEM on Actinide and Fission Product Partitioning & Transmutation

41. The preparation work for the 10th information exchange meeting on Actinide and Fission Product Partitioning & Transmutation was presented by Y. J. Choi. The meeting would be held in Mito, Japan on 20-24 October 2008 and would be hosted by JAEA. It had been decided to make a small change to the meeting programme by introducing, at every second meeting in the series, a special session in place of the normal presentation of country reports. The special session at the 10th meeting would be devoted to "Fuel cycle transition scenarios", profiting from the fact that both NSC and NDC have on-going activities in this area.

Nuclear Production of Hydrogen

42. J. Herczeg informed the delegates that France and USA had agreed that the next information exchange meeting on Nuclear Production of Hydrogen would be held in the USA. The meeting would tentatively be held at Argonne National Laboratory in October 2008. The exact date and place would be communicated in the very near future.

Request for NSC sponsorship of future meetings and conferences

Speciation techniques and facilities for radioactive materials at synchrotron light sources (XAS-2008)

43. F. Mompean presented a proposal from France (CEA and CNRS) for NSC to co-sponsor the next meeting on "Speciation techniques and facilities for radioactive materials at synchrotron light sources (XAS-2008)", which would be held at the synchrotron facility SOLEIL, near Saclay, France. The NSC has cosponsored the previous meetings in this series and the NEA has printed the proceedings.

44. Y. Guerin and R. Chawla supported the request and suggested that the action be handled by the NSC activity in the field of material science.

45. **The NSC agreed to cosponsor the XAS-2008 meeting and to publish the proceedings.**

Other meetings

46. R. Chawla informed the committee about the PHYSOR-2008 conference, which will be held at Interlaken, Switzerland on 14-19 September 2008, and invited the delegates to encourage submission of papers to the conference.

IN-DEPTH DISCUSSIONS

Simulation of materials and fuels

47. The in-depth discussion was started with a presentation on "Proposed Activities and Framework of the NSC Expert Group on *ab initio* Modelling and Simulation of Advanced Nuclear Fuel" prepared by J. Tulenko and presented by D. Nowak. The presentation gave an overview of current issues in the simulation of nuclear fuel and proposed that the expert group be one part of a Working Party on "Nuclear Materials Modelling and Simulation" and that its main deliverable would be a state-of-the-art report on the modelling of nuclear fuel.

48. In the discussion that followed, Y. Guerin felt that the proposed programme was somewhat optimistic, considering that it was supposed to cover all from atomistic to the macroscopic scale for both fuels and structural materials. G. van Goethem informed the committee about the EC PERFECT

programme and he also stressed that need for experimental validation and the involvement of end users in the work.

49. C. Fazio presented the outcome of the recently organised workshop on Structural Materials for Innovative Nuclear Systems (SMINS) held in Karlsruhe, Germany. The workshop had been attended by about 100 scientists and, following five keynote speeches, the four technical sessions covered: materials for very high temperature reactors, materials for metal-cooled reactors, material for water-cooled reactors and a session on multi-scale modelling.

50. A "brainstorming session" was organised at the end of the workshop to discuss future activities and possible proposals to the NSC. The following five recommendations were agreed upon:

1. Review of multi-scale modelling and simulation, and related experimental validation
2. Assess the state-of-the art for specific areas to be considered as priority areas of research
3. Agree on experimental protocols and standards, and share available experimental installations.
4. Establish a common experimental database
5. Organise a second SMINS workshop (within about 2 years)

51. C. Ganguly informed the committee of the material science activities within the IAEA and encouraged cooperation between these activities and any future NEA activity in the field. K. Hesketh and J. Blomgren suggested to benefit from lessons learned in other research areas making use of modelling, for example drug development and separation chemistry.

52. F. Mompean introduced the discussion on the future organisation of the NSC activities in materials science. Two scenarios were forwarded for discussion. One scenario was based on a Working Party on Material Science with three expert groups on fuels, on structural materials and on experimental issues and validation. The second scenario was based on the already approved expert group on "*ab initio* and multi-scale modelling and simulation of advanced nuclear fuels", with an extended scope to cover also structural materials and validation exercises. It was noted that a majority of delegates preferred the establishment of a working party, as the subject was considered to merit a longer term effort. It was also noted that at least 13 countries were willing to provide experts to the proposed activity.

53. **The NSC decided to establish a working party on material science**. A proposal to name the new activity the "Working Party on Multi-scale Modelling of Fuels and Structural Materials for Nuclear Systems" was adopted. The NEA secretariat would first circulate a draft mandate for approval by the NSC and then, following the approval of the mandate, ask member countries to nominate suitable experts to the working party. A first meeting of the Working Party would be held in autumn 2007 to suggest a suitable organisation of the activities for endorsement by the NSC.

54. Following the establishment of the working party mentioned above, **the Working Party on scientific issues of the Fuel Cycle (WPFC) was asked to review its mandate**, specifically the part of the mandate concerning fuels and materials.

Simulation and modelling of Generation-III reactors

55. J. Aragones informed the committee that the person foreseen to make the presentation had finally not been able to come. The present status in modelling and simulation of Generation-III reactors had been adequately presented at the joint international topical meeting on Mathematics and Computation (M&C) and Supercomputing in Nuclear Applications (SNA), held in Monterey, CA, USA on 15-19 April 2007. A short summary of the keynote speeches at this meeting was given, as well as a presentation of the European NURESIM effort and its 5 sub-activities.

56. The NSC took note of the presentation and the fact that there were, at present, no specific proposals for new NSC activities.

REPORT FROM THE 16TH MEETING OF THE NSC EXECUTIVE GROUP

57. The chair of the NSC Executive Group, P. D'Hondt, presented the outcome of the meeting, which this time had been prolonged with half a day to discuss ideas about the future work programme of the NEA Data Bank. The report by the chair can be found in Annex 3.

58. **The NSC endorsed the NEA Data Bank programme of work and budget for 2008**.

FOLLOW-UP ACTIONS TO THE NSC SELF-EVALUATION

59. The result of the NSC self-evaluation had been discussed at the last NSC meeting and the question about introducing country reports at the annual meetings had been referred to the NSC bureau, who in turn could not reach a consensus on the question. I. Yamagishi presented the other NEA technical committees' approach to the question of country reports, which showed that three committees out of seven regularly presented some country reports at their meetings.

60. J. Herczeg proposed a scheme where the presentation of country reports rotated between delegates. R. Chawla suggested that at least the countries with a large nuclear programme presented reports. **It was decided that J. Herczeg would give a 15 minute country report from the USA at the next NSC meeting as a trial**.

INTEREST OF POLAND IN THE WORK OF THE NSC AND ITS WORKING PARTIES

61. Th. Dujardin recalled L. Echavarri's introduction about the interest of Poland to participate in some of the NEA work and in particular in the work of the NSC, WPRS and WPFC. The NEA secretariat had contacted a designated person in Poland to collect more information about their interest in and their possible contribution to the work of the NSC, but had not yet received any answer.

62. **The NEA secretariat would provide the NSC delegates with more background information to judge if there would be a mutual benefit of having Polish participation in the NSC, WPRS and WPFC and then collect the views of committee members**.

REPORTS FROM OTHER NEA DIVISIONS, OTHER INTERNATIONAL ORGANISATIONS AND NEW OBSERVERS

The Nuclear Development division

63. S. Gordelier reported on recent publications from the NEA Committee for Technical and Economic Studies on Nuclear Energy Development and the Fuel Cycle (NDC). He also presented results from some recently completed studies and outlined the progress in current activities, with special emphasis on activities of relevance to the NSC programme of work. He specifically highlighted the NSC-NDC cooperation on fuel cycle transition scenarios and also **invited the NSC to participate in the NDC project on "Limits to the Development of Nuclear Energy"**.

The EC

64. G. van Goethem gave an overview of the EURATOM efforts to promote the synergy between nuclear research, innovation and education. He outlined the main challenges for Generation–II, III and IV reactor systems and described the EURATOM holistic view on research and development (R&D) and demonstration and deployment (D&D) including the necessary education and training. He also presented the EC efforts towards a Strategic Energy Technology (SET) plan and the role of nuclear fission in the transition to a low carbon energy mix by 2050, exemplified by the Sustainable Nuclear Fission Technology Platform (SNF-TP) and the Partitioning and Transmutation European Roadmap for Sustainable nuclear energy (PATEROS) initiative.

The IAEA

65. N. Ramamoorthy gave an overview of the IAEA Nuclear Science Programme, which is a cross cutting activity between the division of Physical and Chemical Sciences and the division of Nuclear Fuel Cycle and Waste Technology. He highlighted recent achievements in the different work areas, including the publication of reports and organisation of meetings and workshops.

66. C. Ganguly presented the IAEA nuclear fuel cycle programme (B1 –B4), comprising Uranium resources and production, nuclear power reactor fuel engineering, management of spent fuel from nuclear power plants and topical issues of nuclear fuels and fuel cycles for advanced & innovative reactors. The IAEA is also developing an Integrated Nuclear Fuel Cycle Information System (iNFCIS), which can be accessed by registered users through the Internet.

Russia

67. O. Patarakin, head of the Nuclear Science & Technology division at Rosatom, informed the committee members of the recent nuclear development in the Russian Federation. He specifically mentioned the Russian experience in areas such as materials and fast reactors, pointing to the Dimitrovgrad and Obninsk laboratories. He was also looking forward to a productive and mutual beneficial cooperation with the NSC.

NEXT NSC MEETING

Date of next meeting

68. It was agreed to hold the next meeting in the middle of June 2008 at the NEA Headquarters. The dates would be either 17-20 June or 24-27 June 2008. The secretariat would communicate the final dates before the end of June 2007. **After the meeting, it has been decided to hold the next NSC meeting on 25-27 June 2008**[*].

69. The dates of the NSC bureau meeting would be decided by the bureau and communicated to the committee members as soon as possible. **After the meeting, it has been decided to hold the next NSC bureau meeting on 20 November 2007**.

Topics for in-depth discussion

70. The following proposals for topics for in-depth discussion at the next NSC meeting were suggested:

[*] These dates correspond to one of the two alternatives discussed during the meeting.

- Nuclear data and material properties of minor actinides (T. Mori)
- Information on the development of small nuclear reactors (R. Mach)
- Gen-IV type fast reactors with different coolants (R. Chawla)
- Important output from a NSC Working Party (A. Zaetta)

Delegates were encouraged to communicate additional proposals in time for the final decision by the NSC bureau in late autumn 2007.

ELECTION OF COMMITTEE OFFICERS

71. Th. Dujardin informed the committee that, in consultation with Tomas Lefvert and in line with the OECD policy of rotating chairmanship, it had been agreed that the present chair would step down. Following consultation with many committee members the NEA secretariat proposed J. Herczeg as new chair of the NSC and R. Chawla as new member of the bureau.

72. The proposal was supported by several committee members and, as there were no other proposals, **it was agreed to elect J. Herczeg as chair, re-elect P. D'Hondt, T. Mori and A. Zaetta as vice-chair and elect R. Chawla as vice-chair of the NSC**.

73. The committee expressed its appreciation and gratitude to Tomas Lefvert for his excellent chairman ship during the past six years.

ANY OTHER BUSINESS

74. **C.** Nordborg informed the delegates that all documents and PowerPoint slides presented at the meeting would be available on a dedicated NSC webpage in a few days time. The exact internet address would be communicated later.

75. J. Gado felt that this NSC meeting, including the in-depth discussion on the simulation of materials and fuels, had become too administrative in nature as most of the scientific discussions had been moved to the Working Parties, following the recent restructuring of the NSC activities. **It was agreed to bring up this concern for discussion at the NSC bureau meeting, with a view to having the next NSC meeting more scientifically interesting**.

76. J. Aragones suggested that more efforts be made to present the NSC programme of work at different conferences. Th. Dujardin agreed to the suggestion but preferred that such presentations be made, as far as possible, by NSC members rather than by the NEA secretariat.

Annex 1

List of actions adopted at the meeting

1. K. Hesketh	To provide, before the next NSC meeting, a Gantt chart of WPRS deliverables during the working party mandate period (2007-2010).
2. WPFC chair	To organise a review of the WPFC programme of work at the next working party meeting and to reconsider the mandate for the WPFC expert group on fuels and materials, taking into account the newly established NSC Working Party on "Multi-scale Modelling of Fuels and Structural Materials for Nuclear Systems".
3. All members	To clarify, before November 2007, the domestic positions on the possibility to release the public part of the Research and Test Facilities (RTF) database without password protection.
4. NEA secretariat	To circulate a proposed mandate for the new Working Party on "Multi-scale Modelling of Fuels and Structural Materials for Nuclear Systems" for approval by the NSC.
5. All members	To nominate suitable experts to the new Working Party on "Multi-scale Modelling of Fuels and Structural Materials for Nuclear Systems" following the approval of the mandate.
6. J. Herczeg	To prepare and present a 15 minute "country report" from the USA at the next NSC meeting.
7. All members	Following the distribution of additional information by the NEA secretariat, consider the request from Poland to become ad-hoc participants in NSC, WPRS and WPFC and report back to the NEA secretariat before the end of September 2007.
8. All members	To communicate additional proposals for subjects for in-depth discussion well before the NSC bureau in November 2007.
9. Bureau members	To discuss, at the next NSC bureau meeting, the concern that the annual committee meetings had become too administrative in nature, with a view to having a more scientifically oriented NSC agenda in June 2008.

Annex 2

List of Participants

AUSTRIA

LEEB, Helmut
Atominstitut der Oesterreichischen Univ.
Technische Universitaet Wien
Wiedner Hauptstrasse 8-10
A-1040 WIEN

Tel: +43 (0)1 58801 14258
Fax: +43 (0)1 58801 14299
Eml: leeb@kph.tuwien.ac.at

BELGIUM

D'HONDT, Pierre Joseph
Director Reactor Safety
SCK-CEN
200 Boeretang
B-2400 MOL

Tel: +32 14 33 22 00
Fax: +32 14 32 15 29
Eml: pdhondt@sckcen.be

CANADA

KOZIER, Kenneth
Reactor Physics, Stn. E3
Office of the Chief Engineer
Atomic Energy of Canada Ltd. (AECL)
Chalk River Laboratories
Chalk River, ON K0J 1J0

Tel: +1 613 584 8811+ext 5059
Fax: +1 613 584-8047
Eml: kozierk@aecl.ca

CZECH REPUBLIC

MACH, Rostislav
Nuclear Physics Institute
Academy of Science
CZ-250 68 Rez

Tel: +420 (2) 66172136
Fax: +420 (2) 20941002
Eml: mach@ujf.cas.cz

FINLAND

ANTTILA, Markku
VTT Processes
P.O. Box 1000
FI-02044 VTT

Tel: +358 20 722 5012
Fax: +358 20 722 5000
Eml: Markku.Anttila@vtt.fi

FRANCE

GUERIN, Yannick
CEA
Department of Fuel Studies
Cadarache, Bat. 151
F-13108 St. Paul-lez Durance Cedex

Tel: +33 4 42 25 79 14
Fax: +33 4 42 25 47 47
Eml: yannick.guerin@cea.fr

FRANCE (cont.)

MADIC, Charles
CEA/Saclay
Direction de l'Energie Nucléaire
DEN/DDIN, Bat. 125
F-91191 Gif-sur-Yvette

Tel: +33 1 69 08 82 07
Fax: +33 1 69 08 32 32
Eml: charles.madic@cea.fr

ZAETTA, Alain
CEA-DEN/DER
Cadarache
Bat. 707 – B.P. 1
F-13108 St.-Paul-lez-Durance

Tel: +33 (0) 4 42 25 27 61
Fax: +33 (0) 4 42 25 76 27
Eml: alain.zaetta@cea.fr

GERMANY

FAZIO, Concetta
Programme NUKLEAR
Forschungszentrum Kalsruhe (FZK) Gmbh
Hermann von Helmholtz Platz 1
D-76344 Eggenstein-Leopoldshafen

Tel: +49 7247 82 5517
Fax: +49 7247 82 5508
Eml: concetta.fazio@nuklear.fzk.de

SCHOLTEN, Christoph
Counsellor
Delegation of Germany to the OECD
9, rue Maspéro
F-75116 PARIS

Tel: +33 (0)1 55 74 57 08
Fax: +33 (0)1 55 74 57 40
Eml: christoph.scholten@germany-oecd.org

HUNGARY

GADO, Janos
Director
KFKI Atomic Energy Research Institute
1121 Budapest
Konkoly Thege Miklos u. 29-33
H-1525 Budapest, Pf. 49

Tel: +36 1 395 9159
Fax: +36 1 395 9293
Eml: gado@sunserv.kfki.hu

ITALY

TINTI, Renato
ENEA FIS-NUC
Via Martiri di Monte Sole, 4
I-40129 BOLOGNA

Tel: +39 051 609 8470
Fax: +39 051 609 8785
Eml: renato.tinti@bologna.enea.it

JAPAN

MORI, Takamasa
Research Group for Reactor Physics
Japan Atomic Energy Agency
Shirakta-shirane, Tokai-mura, Naka-gun
Ibaraki-ken, 319-1195

Tel: +81 29 282 5360
Fax: +81 29 282 6122
Eml: mori.takamasa@jaea.go.jp

NETHERLANDS

KONING, Arjan
NRG Nuclear Research and Consultancy Group
Building 34.213
Westerduinweg 3, P.O. Box 25
NL-1755 ZG PETTEN

Tel: +31 (224) 56 40 51
Fax: +31 (224) 56 84 90
Eml: koning@nrg-nl.com

NORWAY

WIESENACK, Wolfgang
Project Manager
OECD Halden Reactor Project
Institutt for Energiteknikk
Os Alle 13 - P.O. Box 173
N-1751 HALDEN

Tel: +47 69 21 2347
Fax: +47 69 21 2201
Eml: wowi@hrp.no

RUSSIAN FEDERATION

PATARAKIN O. O.
Head, Division for Nuclear Science & Technology
Rosatom
Srt. B. Ordyinka, 24/26
119017 Moscow

Tel: +7 495 951 8687
Fax: +7 495 230 2420
Eml: opatarakin@uant.faae.ru

SLOVAK REPUBLIC

BAHNA, Ján
VUJE
Dept. 0190
Okruzna 5
918 64 TRNAVA

Tel: +421 33 599 1197
Fax: +421 33 599 1157
Eml: bahna@vuje.sk

SLOVENIA

TRKOV, Andrej
Institute Jozef Stefan
Jamova 39
1000 Ljubljana

Tel: +386 40 20 37 39
Fax:
Eml: Andrej.Trkov@ijs.si

SPAIN

ARAGONES BELTRAN, Jose Maria
Dpto. Ingenieria Nuclear
ETSI-Industriales
Univ. Politecnica de Madrid
Jose Gutierrez Abascal 2
E-28006 MADRID

Tel: +34 91 336 3108
Fax: +34 91 336 3002
Eml: arago@din.upm.es

SWEDEN

BLOMGREN, Jan
Dept. of Neutron Research
INF, Uppsala University
Box 525
SE-751 20 UPPSALA

Tel: +46 18 471 37 88
Fax: +46 18 471 38 53
Eml: jan.blomgren@tsl.uu.se

SWITZERLAND

CHAWLA, Rakesh
Laboratory for Reactor Physics
and Systems Behaviour
Paul Scherrer Institute
CH-5232 VILLIGEN PSI

Tel: +41 56 310 23 26
Fax: +41 56 310 23 27
Eml: Rakesh.Chawla@psi.ch

UNITED KINGDOM

GULLIFORD, Jim
B168 Curie Av.
Harwell Business Centre
Didcot
Oxfordshire
OX11 0QT

Tel: +44 01925833450
Fax: +44 01925832161
Eml: jim.gulliford@nexiasolutions.com

HESKETH, Kevin
Nexia Solutions
B709 Springfields
Salwick Preston
Lancashire PR4 0XJ

Tel: +44 1772 76 23 47
Fax: +44 1772 76 24 70
Eml: Kevin.W.Hesketh@nexiasolutions.com

UNITED STATES OF AMERICA

BRIGGS, J. Blair
Idaho National Laboratory
P.O. Box 1625, MS-3860
2525 North Fremont
IDAHO FALLS, ID 83415-3860

Tel: +1 208 526 7628
Fax: +1 208 526 2930
Eml: j.briggs@inl.gov

HERCZEG, John W.
U.S. DOE
Office of Nuclear Energy, NE-20
19901 Germantown Rd
Germantown, MD 20874

Tel: +1 301-903-1175
Fax: +1 301-903-5057
Eml: john.herczeg@nuclear.energy.gov

NOWAK, David
Argonne National Laboratory
9700 South Cass Avenue
ARGONNE, IL 60439-4842

Tel: +1 (630) 252-3312
Fax:
Eml: nowak-bb@anl.gov

INTERNATIONAL ORGANISATIONS

International Atomic Energy Agency (IAEA)

GANGULY, C.
Head, Fuel Cycle & Materials Section
Dept. of Nuclear Energy
IAEA
P.O.Box 100
A-1400 WIEN
Tel: +43 1 2600 22766
Fax: +43 1 26007
Eml: c.ganguly@iaea.org

RAMAMOORTHY, N.
Director
Division of Physical and Chemical Science
Dept. of Nuclear Sciences and Application
IAEA
P.O. BOX 100
A-1400 Vienna
Tel: +43 1 2600 21700
Fax: +43 1 26007
Eml: n.ramamoorthy@iaea.org

European Commission (EC)

RULLHUSEN, Peter
EC – JRC - Institute for Reference
Materials and Measurements
Joint Research Center
Retieseweg 111
B-2440 GEEL
Tel: +32 (14) 57 14 76
Fax: +32 (14) 57 18 62
Eml: peter.rullhusen@cec.eu.int

VAN GOETHEM, Georges
European Commission
DG RTD, Unit J.2 Nuclear Fission
and Radiation Protection, CDMA 1/47
rue du Champ de Mars 21
B-1049 Brussels
Tel: +32 02 29 51424
Fax: +32 02 29 54 991
Eml: Georges.Van-Goethem@ec.europa.eu

Nuclear Energy Agency (NEA)

CHOI, Yong-Joon
Data Bank
Tel: +33 145 24 10 91
Eml: yongjoon.choi@oecd.org

DUJARDIN, Thierry
Deputy Director, Science and Development
Tel: +33 145 24 10 06
Eml: thierry.dujardin@oecd.org

GALAN, Juan
Data Bank
Tel: +33 145 24 10 08
Eml: galan@nea.fr

GORDELIER, Stan
Head, Nuclear Development Division
Tel: +33 145 24 10 65
Eml: stan.gordelier@oecd.org

HASEGAWA, Akira
Head, NEA Data Bank
Tel: +33 145 24 10 70
Eml: akira.hasegawa@oecd.org

Nuclear Energy Agency (NEA) (cont.)

HENRIKSSON, Hans
Data Bank
Tel: +33 145 24 10 84
Eml: henriksson@nea.fr

KODELI, Ivo
IAEA representative at the NEA Data Bank
Tel: +33 145 24 10 74
Eml: kodeli@nea.fr

MOMPEAN, Federico
NEA Data Bank
Tel: +33 145 24 10 83
Eml: federico.mompean@oecd.org

NORDBORG, Claes
Head, Nuclear Science Section
Tel: +33 145 24 10 90
Eml: claes.nordborg@oecd.org

RUGAMA, Yolanda
Data Bank
Tel: +33 145 24 10 99
Eml: rugama@nea.fr

SARTORI, Enrico
Data Bank
Tel: +33 145 24 10 72
Eml: sartori@nea.fr

YAMAGISHI, Isao
Nuclear Science Section
Tel: +33 145 24 11 52
Eml:isao.yamagishi@oecd.org

Annex 3

Mandate of the Working Party on Scientific Issues of Reactor Systems (WPRS)

Chair:	Kevin W. Hesketh (UK)
Vice-Chair:	Pierre D'hondt (Belgium)
Members:	All NEA member countries
Participation in the work:	European Commission (*Under the NEA Statute*)
	International Atomic Energy Agency (*By agreement*)
Observer:	The Russian Federation
Date of creation:	June 2004
Duration:	June 2010
Mandate:	Agreed at the 15th meeting of the Nuclear Science Committee (NSC) on 9-11 June 2004 [NEA/SEN/NSC(2004)3], extended at the 18th meeting of the NSC, 13-15 June 2007 [NEA/SEN/NSC(2007)3].

SCOPE

Under the guidance of the Nuclear Science Committee the Working Party will deal with reactor physics, fuel cycle, radiation transport and dosimetry, fuel behaviour, thermal hydraulics and dynamics/safety and uncertainty analysis of present and future nuclear power systems.

OBJECTIVES

To provide the Member Countries with up-to-date information to preserve knowledge on and develop consensus regarding:

- Reactor physics, fuel behaviour, thermal hydraulics and dynamics/safety issues associated with innovative fuels in present and future nuclear power systems.

  Reactor physics aspects considered include:
  - Reactivity characteristics
  - Core power/flux distributions
  - Core kinetics and reactivity control
  - Reactivity coefficients
  - Safety/system dynamics
  - Vessel dosimetry
  - Uncertainty Analysis in Modelling
- Fuel cycle aspects considered will focus on fuel loading and discharge requirements, fission product and minor actinide inventories and radiotoxicity profiles versus time.
- Fuel behaviour, thermal hydraulics and kinetics/safety, coupled core-plant analysis will be considered insofar as they impinge on the reactor performance.
- Radiation transport and dosimetry will cover aspects relevant for reactor vessels and internals, and irradiation facilities

Reactor types considered include, but are not limited to the following:

- Present generation LWRs with advanced and innovative fuels, evolutionary and innovative LWRs and HWRs
- Novel reactor systems (GNEP, Gen IV Systems)
- Accelerator driven (sub-critical) and critical systems for waste transmutation

To liaise closely with other relevant NEA working groups, especially those operating under the guidance of the NDC and CSNI, to ensure the respective work programmes are complementary and to provide advice and support where required and undertake common work where appropriate. Particularly close working relationships will be maintained with the Working Party on the scientific issues in Fuel Cycle (WPFC).

To provide advice to the nuclear community on the developments needed to meet the requirements (data and methods, validation experiments, scenario studies) for different reactor systems.

Deliverables

- UOX depletion benchmark
- MOX depletion benchmark
- Boiling Water Reactor Turbine Trip (BWRTT) Benchmark:
    - Volume IV: Best-Estimate Coupled 3-D Core/Thermal-Hydraulic System Modeling
- VVER-1000 Coolant Transient Benchmarks Phase 1 (V1000CT-1):
    - Volume III: Coupled 3-D Kinetics/Core Thermal-Hydraulic Response Evaluation
    - Volume IV: Best-Estimate Coupled 3-D Core/Thermal-Hydraulic Plant Transient Modeling
- VVER-1000 Coolant Transient Benchmarks Phase 2 (V1000CT-2)
    - Volume I: Specifications of the VVER-1000 Vessel Mixing Problem
    - Volume II: Main Steam-Line Break (MSLB) Problem Specification
    - Volume III: Comparison of Computational Fluid Dynamics and Coarse Mesh Calculations with Measured Data
    - Volume IV: MSLB Coupled 3D Neutronics / Vessel TH Simulation
    - Volume V: MSLB Best Estimate Coupled Simulation
- NUPEC BWR Full Size Bundle Tests (BFBT)
    - Volume II : Uncertainty and Sensitivity Analysis of Void Distribution and Critical Power
    - Volume III : Benchmark Results for Void Distribution
    - Volume IV : Benchmark Results for Critical Power
- PBMR Coupled Neutronics/Thermal Hydraulics Transient Benchmark the PBMR-400 Core Design :
    - Volume I: Benchmark Definition
    - Volume II: Steady State Benchmark
    - Volume III: Transient Benchmark
- State-of-the-art report on Minor Actinide Burning in LWRs
- Proceedings of ARWIF-2008
- DOE WG-MOX Fuel Irradiation Experiment Benchmark
- PRIMO Ramped MOX Fuel Rod BD8 Benchmark
- Venus Recycling Benchmark 07
- Uncertainty Analysis in Modelling:

  - Volume I: Neutronics Phase Specification
  - Volume II: Neutronics Phase Results
- Benchmark on Accuracy of Solution of 3-Dimensional Transport Codes and Methods over a Range in Parameter Space

Mandate of the WPRS Expert Group on Minor Actinide Burning in Thermal Reactors

Members:	All NEA Member countries
Date of creation:	June 2007
Duration:	June 2009

SCOPE

The Expert Group will carry out a technical assessment of minor actinide burning in thermal reactors. Though the main focus will be on Light Water Reactors (LWRs), consideration will also be given to other thermal systems such as Heavy Water Reactors (HWRs). However, high Temperature Reactors (HTRs) are specifically excluded because minor actinide burning in HTRs is already the subject of the European Union 6th Framework project PUMA.

The scope will include assessments of the implications for enrichment, fuel fabrication, in-core fuel management, thermal-hydraulics, fuel behaviour, fuel cycle economics and irradiated fuel and waste management. It is intended that the Expert Group would be a joint activity between the Working Party on the Scientific Issues of Reactor Systems (WPRS) and the Working Party on the Scientific Issues of the Fuel Cycle (WPFC) and would also liaise closely with the Nuclear Development Committee (NDC) on economics.

OBJECTIVES

To produce a state-of-the-art report on minor actinide burning in LWRs and HWRs. The principal objective is to review and summarise previous work and to present a consensus view.

Specifically, the report should cover for LWRs and HWRs:

- The different technical approaches to minor actinide burning, including an assessment of the effectiveness of different approaches in terms of kg of minor actinides destroyed per TWhe electrical output and the irradiation timescales.
- To construct, if feasible, estimates of the net contribution of the various minor actinide nuclides to the overall neutron balance and thereby determine the penalty on initial fissile loading.
- Design and behaviour of fuels containing minor actinides.
- Nuclear design aspects of reactor cores containing minor actinide fuels.
- Thermal-hydraulic design of reactor cores containing minor actinide fuels.
- The implications for fabrication of fuel containing minor actinides.
- The implications for operations of reactor cores containing minor actinides.
- The implications for the fuel cycle, including spent fuel and waste management, minor actinide separation.
- The economics of LWRs and HWRs containing minor actinide fuels.

Deliverables

Completion of a state-of-the-art report within two years of the initial meeting of the Expert Group.

Mandate of the Working Party on Scientific Issues of the Fuel Cycle (WPFC)

Chair:	Ms. Kathryn A. McCarthy (USA)
Members:	All NEA member countries
Participation in the work:	European Commission (*Under the NEA Statute*)
	International Atomic Energy Agency (*By agreement*)
Observers:	The Russian Federation
Date of creation:	June 2004
Duration:	June 2010
Mandate:	Agreed at the 15th meeting of the Nuclear Science Committee (NSC) on 9-11 June 2004 [NEA/SEN/NSC(2004)3], extended at the 18th meeting of the NSC, 13-15 June 2007 [NEA/SEN/NSC(2007)3].

SCOPE

Under the guidance of the Nuclear Science Committee, the Working Party will deal with scientific issues in various existing and advanced nuclear fuel cycles, including fuel cycle physics, associated chemistry and flowsheets, development and performance of fuels and materials, and accelerators and spallation targets.

OBJECTIVES

- To provide the Member Countries with up-to-date information on and develop consensus regarding:
  - Separations science.
    - Develop a scientific basis for optimisation of the use of future nuclear waste repositories.
    - Establish a methodology for evaluating impacts of various existing and advanced fuel cycle scenarios on potential storage and repositories.
    - Provide a means for the development and evaluation of advanced processing concepts, including design bases for future reprocessing plants.
  - Fuel cycle scenarios.
    - Assemble and organise scientific information critical to the understanding of the issues involved in transitioning from current fuel cycles to future fuel cycles.
    - Provide scientific bases for fuel cycle deployment strategies.
  - Chemical partitioning.
    - Keep updated information on separation technologies, including advanced aqueous and pyrochemical processing issues.
    - Perform a detailed scientific study of separations processes for different fuel cycle scenarios.
  - Fuels and materials.
    - Undertake studies needed for development of fuels and materials for implementing advanced nuclear fuel cycles.
    - Deal with performance and behaviour of advanced fuels.
    - Update the handbook on lead and lead-bismuth eutectic (LBE) technology as new information becomes available.
    - Thermal-hydraulic studies of lead-alloy coolants.

  - Accelerators and targets.
    - Deal with accelerator reliability issues.
    - Target performance, including spallation products.
    - Window performance, including thermal stress and radiation damage, windowless targets.

- To liaise closely with other relevant NSC Working Parties and NEA Standing Technical Committees, especially the Committee for Technical and Economic Studies on Nuclear Energy Development and the Fuel Cycle (NDC) and the Radioactive Waste Management Committee (RWMC), to ensure the respective work programmes are complementary and to provide advice and support where required and undertake common work where appropriate. Particularly close working relationships will be maintained with the Working Party on scientific issues of Reactor Systems (WPRS).
- To provide advice to the nuclear community on the developments needed to meet the requirements for implementing advanced long-term sustainable nuclear fuel cycles, including partitioning and transmutation.

Deliverables

- Expert Group on Chemical Partitioning.
  - State-of-the-art report on national programmes in partitioning.
  - Report on flowsheet studies.
  - Report on separation criteria.
- Expert Group on Fuel Cycle Transition Scenarios Studies.
  - Status report on fuel cycle transition scenarios studies.
  - Regional study related to the potential implementation in Europe of advanced fuel cycle.
  - Benchmark report on scenario codes performances.
- Expert Group Lead-Bismuth Eutectic (LBE) technology.
  - LBE Handbook – Version 1.
  - Benchmark on thermal-hydraulic loop models for Lead-Alloy Cooled Advanced Nuclear Energy Systems (LACANES).
- Workshop on Utilisation and Reliability of High Power Proton Accelerators.
  - Proceedings of the fifth workshop (HPPA5).
- Information Exchange Meeting on Actinide and Fission Product Partitioning and Transmutation.
  - Proceeding of the 10th meeting (10IEMPT).

Mandate of the Working Party on Nuclear Criticality Safety (WPNCS)

Chair:	Jim Gulliford (UK)
Members:	All NEA Member countries
Observers	Representatives from the IAEA and the Russian Federation
Date of creation:	June 1996
Duration:	3 years starting in June 2007.
Mandate:	Agreed at the 7th Meeting of the Nuclear Science Committee (NSC) on 29-30 June 1996 [NEA/SEN/NSC(96)3], extended at the 11th meeting of NSC in June 2000 [NEA/SEN/NSC(2000)3], extended at the 15th meeting of the NSC in June 2004 [NEA/SEN/NSC(2004)3], extended at the 18th meeting of the NSC in June 2007 [NEA/SEN/NSC(2007)3].

SCOPE

Under the guidance of the Nuclear Science Committee, the Working Party will deal with technical and scientific issues relevant to criticality safety. Specific areas in interest include, but are not limited to investigations concerning static and transient configurations encountered in the nuclear fuel cycle such as fuel fabrication, transport and storage. Areas of activities include:

- Evaluation of available experimental data;
- Assessment of experimental needs;
- Code and data inter-comparison;
- Development of codes and models;
- Development of criticality methodologies and data;
- Establishment of technical basis for the application of burn-up credit.

OBJECTIVES

- Exchange of information on national programs in the area of criticality safety.
- Guide, promote and co-ordinate high priority activities of common interest to the international criticality safety community, establish co-operations.
- Monitor the progress of all activities and report to the NSC.
- Publish databases, handbooks, and reports.
- Facilitate communications within the international criticality safety community through relevant Internet sites.
- Co-ordinate the ongoing series of International Conferences on Nuclear Criticality Safety (ICNC), to be held every four years.
- Co-ordinate WPNCS activities with other working groups within the NEA and in other international frameworks to avoid duplication of activities.
- Provide a technical basis for other international activities (e.g. ISO, IAEA).

DELIVERABLES

- New editions of the International Handbook of Criticality Safety Benchmark Evaluation Project (2007, 2008 and 2009).
- Report of a study on the effect of axial burn-up profile asymmetry on criticality calculation (2007).
- Report summarising the findings of the Expert Group on Burn-up Credit and lessons learned (2008).
- Report on the analysis and benchmarking of ISTC 2670 project (Assay data for VVER440 fuel) (2009)
- Report summarising the findings of the Expert Group on the study of source convergence issues (2008).
- Report summarising findings of the Expert Group on the modelling of criticality transient experiments (2007, 2008).
- Activity plan for Experts Group on Assay data for Spent Nuclear Fuel and report on current state-of the art in measurement techniques and uncertainty analyses (2008)
- Updated version of the Spent Fuel COMPOsition (SFCOMPO) database including recent data sets and new review structure of the database (2008,2009)
- Web-based information resources on burn-up credit, criticality excursions, source convergence issues and PIE data.
- Status reports of the progress of ICNC 2011

Annex 4

Report to the Nuclear Science Committee from the Sixteenth Meeting of the Executive Group

13 June 2007
Pierre D'Hondt

Introduction

1. Apologies for not attending the meeting were received from T. Lefvert (Sweden), E. Nonboel (Denmark), J. Katakura (Japan), P. Vaz (Portugal), J. Pena Gutierrez (Spain), R. Chawla (Switzerland), M. Moss (UK), N. Ramamoorthy (IAEA), J. Coadou (EC) and W. Wiesenack (OECD Halden).

2. The agenda was adopted without any changes.

3. Thierry Dujardin informed the Executive group about the interest of Poland to participate in some of the NEA activities. He also informed the Executive Group that Akira Hasegawa, Japan, has taken the position of head of the Data Bank since July 2006.

4. The summary record of the fifteenth meeting was approved.

Progress report and programme of work

Computer program and integral data services

5a. Enrico Sartori gave an overview of the computer program and integral data services. It was noted that the new arrangement on distribution of codes and benchmark data with the US-DOE has been in place since February 2007. So far, 10 codes have been received already, and 52 copies have been distributed. The computer code distribution statistics was give to each member relative to his country. It was suggested to also distribute a table comparing contributions from and distribution to all member countries.

The upgrade of the dispatching system, DBAIS-2, was presented including the increased control demands requested for certain codes.

During 2006, a total of 64 codes were acquired and 71 were tested, of which 26 originated from non-OECD countries. Also to be mentioned are the 41 new or revised compilations of integral measurements in the databases SINBAD, IFPE and IRPhE. The number of codes and benchmarks received and tested are well in line with the objectives.

The Data Bank training courses on the use of selected computer programs continue to be popular and attract many participants. Several courses are planned, such as a training course on MCNPX in 2007.

Ivo Kodeli presented the Data Bank computer program services to non-OECD countries. In total, 726 packages were distributed to 32 non-OECD member states and the IAEA in 2006.

Nuclear data services and the JEFF project

5b.i. Hans Henriksson presented the nuclear data services. He informed the Executive Group that the compilation of experimental data into the EXFOR database had progressed as planned with 79 new neutron induced data sets and 108 new charged-particle induced data sets. The CINDA database, containing bibliographic information, has been updated and will be published in book format autumn 2007. The high priority request list for nuclear data had also been updated and contains now five high priority requests and six general requests.

The Janis nuclear data display software has been upgraded and a beta version was released in April 2007. Janis-3 is planned to be released soon. It is now a much appreciated tool for nuclear data users, with over 25000 accesses per month to the database.

5b.ii Yolanda Rugama presented the work in the JEFF project. A validation report, JEFF Report 22, is being prepared and the structure of the report has been decided. The plan for the next nuclear data library, JEFF-3.2, was outlined, with new evaluations being prepared on ^{235,238}U, ^{239}Pu, Cr, Mn, Ta and W, as well as a new activation data library. The new library is planned to include more covariance data as well as photonuclear data. A revision of the decay data library, JEFF-3.1.1, was also agreed within the JEFF working group for the autumn 2007.

The Thermochemical Database (TDB) project

5b.iii. Federico Mompean presented the status of the Thermochemical Database (TDB) project. There are now 9 volumes in the series of reviews and the work in phase III of the TDB project is concentrated on finalising four reviews on Iron, Tin, Thorium and solid solutions. It was planned to have all the reviews published by early 2008.

The current phase of the TDB project has been prolonged until 1 February 2008, and the plans for a fourth phase were outlined. The Radioactive Waste Management Committee endorsed the programme in March 2007, and the tentative start is February 2008. The NSC Executive Group endorsed the TDB-IV programme of work and renewed the Data Bank support for the TDB project.

Provision of expertise to other parties of NEA

5c. Apart from the TDB project and the preservation and dissemination of integral data on behalf of the NSC and the CSNI Data Bank staff is involved in a few other NEA projects, such as the Information System on Occupational Exposure (ISOE) within the Committee on Radiation Protection and Public Health.

In-house computer system

5d. Pierre Nagel presented recent and on-going software and database development activities undertaken by the Data Bank computing staff. He also highlighted the recent hardware upgrades to the Data Bank computer system.

Looking at the future of the Data Bank

Topical Presentation on Integral Experimental data

6. Blair Briggs gave a thorough presentation of the "anatomy of an evaluation" that encompassed a description of what the evaluation and review principles are in the IRPhE and ICSBEP benchmark collections. A discussion followed on how new benchmarks are chosen. The issue of making effective use of these data for inter-comparison of different data libraries was discussed and the opinion was expressed that it would be of interest to have validated MCNP input decks to be used for comparison purpose.

Discussion on the future of the Data Bank

7a. Enrico Sartori asked a few questions to the delegates to consider for the next Executive Group meeting concerning the evolution of the Computer Program services. It was for example discussed how the liaison officer system should be modified to better coping with the demands from both users and providers of for example computer codes. A workshop on Next Generation Computer Codes for Nuclear Engineering was proposed to be held in 2008.

7b. Hans Henriksson gave a short overview of the different services that the Data Bank could provide regarding basic nuclear data. Several proposals were given, such as the improvement of the experimental database EXFOR and increased scope towards nuclear structure and decay data. A discussion followed if

the NEA could provide expertise in the field of new nuclear data evaluations, or processing and benchmarking of nuclear data.

7c. Federico Mompean presented some reflections on the importance of incorporating more material science into the Data Bank activities. He gave examples of two thermochemical databases, namely on high temperature actinide bearing systems and on high ionic strengths and non-aqueous solvents. He also suggested stronger interaction between the standing committees within the NEA and continued feedback from member countries.

7d. The importance of Integral data and the need for high standards in the databases (SINBAD, IFPE) were presented.

7e. **Isao Yamagishi presented the Research and Test Facilities Database (RTFDB) for the** delegates as an example of a database where the Data Bank could carry out the maintenance.

7f. Pierre Nagel gave some views on the future concerning the in-house computer systems by looking back to see what was expected ten years ago. He envisaged increased interest in electronic conferencing and further development in computer security.

7g. Some general questions of the role of the Data Bank and knowledge preservation and transfer were posed by Akira Hasegawa. The work on giving training courses was discussed.

7h. Some comments were given by the delegates, but in principle the Data Bank was found to be running very well. A detailed questionnaire should be prepared for the delegates during the next few months, where the different proposals can be given priority, as the budget is not unlimited. Suggestion came up on providing "seed funding" for certain research of importance for the Data Bank activities. The system of Liaison officers for computer codes and integral data was debated. Although different views were expressed by the delegates, it was agreed that it works well and it should be kept.

Adjustment of work programme and proposed budget for 2008

8. No specific adjustments of work were proposed.

9. The Data Bank budget document was introduced by Akira Hasegawa. Some explanations were needed regarding the overhead costs to the OECD, as well as the modifications to the budget lines on operating costs, staff and publications.

The Executive Group endorsed the proposed Data Bank programme of work and budget for 2008.

International Conference on Nuclear Data for Science and Technology 2007
DOI:

Mono-energy neutron testing of single event effects

J. Blomgren[1,a], S. Pomp[1], J.-C. Bourselier[1], M. Österlund[1], A. Prokofiev[2], and A. Koning[3]

[1] Uppsala University, Dept of Neutron Research, Box 525, SE-75120 Uppsala, Sweden
[2] Uppsala University, The Svedberg Laboratory, Box 535, SE-75121 Uppsala, Sweden
[3] Nuclear Research and consultancy Group, P.O. Box 25, Petten, the Netherlands

Abstract. The role of mono-energy neutron testing for SEE is outlined. Recent improvements in nuclear reaction theory of relevance to computation of single-event effects from fundamental physics is reported. Older data, as well as recent results obtained with mono-energy neutron testing are well described. Future options of extremely intense mono-energy neutron sources are discussed.

1 Introduction

Neutron testing of SEEs in memory devices is performed with two major methods. White beam testing, performed at spallation neutron sources, has the advantage of simplicity, in that the facility spectrum resembles the spectrum of atmospheric neutrons, and only a single measurement is needed. A drawback is that these two spectra are not identical. Moreover, different test sites provide different neutron spectra. Thus, corrections have to be estimated if precise results are required, or if data from different white beam facilities should be compared. Unfortunately, accurate corrections are in general very difficult to determine, because the fundamental requirement for such a correction to be determined is knowledge about not only the neutron spectra involved, but also the energy dependence of the SEE sensitivity. The latter cannot even in principle be determined in a white beam, and therefore the corrections have to be estimated from very crude assumptions, resulting in limited precision in the results.

Mono-energy testing has the advantage of being able to overcome these obstacles. By measuring the energy dependence of the SEE sensitivity (i.e. the SEE cross section) at a number of energies, the total SEE sensitivity can be obtained by simply multiplying the SEE sensitivity and the neutron flux versus energy. In principle, this method allows more precise data to be produced than with white beam testing, but with the drawback that measurements have to be performed at several energies (which often is time-consuming). Moreover, the term *mono-energy* is a truth with qualification. Typically, about half the neutrons are found in a narrow energy interval at maximum neutron energy, while the remaining 50 % constitute a structure-less tail from maximum down to zero energy. The effects of this tail can, however, be corrected for.

A major advantage of using mono-energy testing is that the energy dependence of the SEE sensitivity can provide deep insights into the nuclear reaction mechanisms ultimately causing these effects. This is of great value for the development of computational tools allowing the SEE sensitivity to be estimated already before a new circuit design is taken into production.

[a] Presenting author, e-mail: jan.blomgren@tsl.uu.se

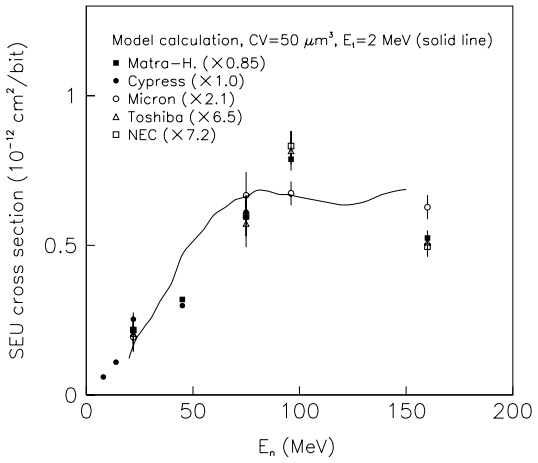

Fig. 1. The SEU cross section for a few memory devices produced in the late 1990s versus neutron energy, reprinted from ref. [5]. The line refers to a model calculation of the SEU cross section using the GNASH code [7] with a similar methodology as TALYS, described elsewhere in the present paper.

The present paper gives a few examples of how previous and recent measurements of the energy dependence of the SEE sensitivity can shed light on the underlying nuclear physics. Recent advances in relevant nuclear theory are described, and the possibilities to develop computational tools for pre-manufacturing SEE sensitivity estimations are outlined.

2 Fundamentals on neutron testing

The ultimate goal of all neutron SEE testing is to establish the sensitivity to the natural neutron flux. In principle, devices could be tested by subjecting them to the natural flux, but this is so time-consuming that it is generally not a realistic option [1]. Naively, one might assume that the ideal testing method would be to have a neutron flux with an energy spectrum identical to the natural flux, but with significantly larger intensity.

In reality, this is difficult to achieve. This is not just a problem related to testing methods, but also to the natural flux itself. The latter is not constant, but depends on a variety of natural parameters, like altitude, latitude or weather. In addition, man-made effects play a role. For instance, the presence of shielding material, like buildings or ship hulls, can modify the flux of cosmic particles. Thus, testing in one single neutron field supposed to be identical with the "natural flux" is ultimately impossible. There is no single "natural flux", but many.

If demands on accuracy are modest, white beam testing can be employed. In such facilities, neutrons are created by protons impinging on (most often also stopping in) a target of heavy nuclei, resulting in a strong neutron flux. The energy distribution resembles natural fluxes, but far from perfectly. If normalizing a given artificial and a given natural flux at a single energy to each other, the neutron flux can differ by a factor two in another energy region.

This is also true when comparing different white beam facilities. Different production techniques (i.e. different energy of the incoming beam and different target construction) can result in fairly different energy distributions. Thus, results obtained at two different white beam facilities can be significantly different, up to about a factor two. The standard approach in physics would be to establish correction factors to allow comparisons from, e.g., different facilities, but this is impossible unless information is available on the energy distribution both on the neutron fluxes involved and the energy dependence of the device sensitivity. Since the latter cannot be obtained at white beams, mono-energy testing is required. It should be pointed out that when it comes to correction factors to correlate testing of two different white beam facilities, the correction factors are unique to each component, because the energy dependence of their sensitivity is individual. The sensitivity depends on technical parameters, like critical charge and cell dimensions. Moreover, a correction factor established for a certain device to correlate, e.g., single-bit upset rate, does not apply to other effects in the same device, like multi-bit upsets or latch-ups. This is because the energy dependences of the sensitivities to different types of errors are different.

It can be concluded that if the result should be reliable to about a factor two, white beams can be used, but for better accuracy, mono-energy testing has to be used. Thus, the first added value of mono-energy testing is the potential to reach better accuracy. As will be discussed below, this is not the only reason.

3 Mono-energy neutron testing

If accuracy better than what can be obtained at facilities resembling the natural flux (i.e., white beams) is desired, mono-energy testing is the only alternative. Mono-energy testing is presently based on techniques in which a beam of charged particles hit a stationary target. Only a small fraction of the incident beam causes neutron production, and the remaining beam is bent and dumped in a way not to create unmanageable background. The neutrons are primarily produced in the forward direction, but the angular distribution is rather wide, and therefore collimators are required. Due to the fact that neutrons are very penetrating, these collimators have to be thick, of the order of meters, which is one unavoidable limitation of any neutron production technique.

The ideal production reaction should have a large probability (cross section) and as good mono-energy character as possible, i.e., a large fraction of the neutrons should appear in a narrow energy interval. Moreover, the incoming charged particle should preferably be easily accelerated, which in reality means protons. Three suitable reactions are available, proton-induced neutron production on deuterium (^{2}H) and the two stable lithium isotopes, ^{6}Li and ^{7}Li. Deuterium produces a nice spectrum, but requires expensive handling of liquid deuterium. The two lithium isotopes give comparable performance, but ^{6}Li is of strategic importance (it is an important ingredient in thermonuclear weapons) making it difficult to obtain. Thus, ^{7}Li has become the choice at essentially all present mono-energy neutron facilities.

The presence of a low-energy tail is unavoidable with neutron production on a fixed target for neutron energies above about 25 MeV, the limit determined by the maximum binding energy difference between the initial and final nuclear systems involved. Since testing has to be performed at higher energies, methods to correct for these tails have to be developed. Such corrections are routinely used in, e.g., nuclear physics research, and a large number of de-convolution codes exist. The most important limiting factors in the final result is a combination of the statistical uncertainty in the raw data, knowledge of the neutron energy spectra, systematic errors in the de-convolution methods (de-convolution is a poorly conditioned mathematical problem, with no single unique solution), and assumptions about the energy dependence of the real cross section.

The latter deserves a special discussion. For a higher nominal neutron energy, a larger fraction of the neutrons are found in the tail. If the real SEE cross section rises with energy all the way to the highest energy point, the correction factors become smaller than if the cross section peaks at a relatively low energy and then decreases. In the latter case, a smaller fraction of the events at the highest nominal energy are due to the full-energy peak, resulting in a larger correction factor, with a correspondingly larger uncertainty.

Thus, the final uncertainty is different for different cases. In general, a final uncertainty of the order of 10 % should be possible to reach with state-of-the-art methods. It is not likely that the final uncertainty can be significantly reduced in a foreseeable future. One ultimately limiting factor is monitoring of the neutron beam flux, which is very difficult to perform to better than 5 % uncertainty in these types of measurements.

4 Added value of mono-energy testing

As has been discussed above, the first added value of mono-energy testing is the possibility to suppress the final uncertainty from about a factor two to about 10 %. In the discussion of neutron testing, one important aspect often overlooked is the usefulness of large intensity at high energies. White beams can in principle be designed to yield a larger total number of neutrons, but the large majority of the neutrons have low

energy. The spectrum typically peaks around one or a few MeV, and falls off approximately as 1/E. This means that the intensity at high energies is much lower than at mono-energy facilities. In fact, the low-energy tail of the high-energy fields at intense mono-energy facilities contains more neutrons than the presently most intense white beam. A consequence of this is that testing of effects caused only by high-energy neutrons becomes very time-consuming at white beams. For instance, latch-up effects seems to require at least about 100 MeV in recent devices, and their sensitivity increases rapidly with neutron energy. This means that the testing to reach the same accuracy in the results would require at least an order of magnitude longer irradiation at LAMPF than at TSL (180 MeV field).

This is also needed when considering other types of effects more complex than standard single-bit SEU in memory devices. Multi-bit upsets (SMU) have been shown to have different energy dependence than single-bit SEU [2], with SMUs becoming more important at high energies. No measurement of energy-resolved SMU cross sections has been published recently, but the general trend of the pioneering paper in 1999 could be well described using fundamental nuclear physics theory, and using the same nuclear theory and modern device parameters results in a similar picture.

Testing is presently often carried out until a preset total number of upsets have been logged. If this is carried out at a white beam, this means that the risk - or chance - that complex errors appear is smaller than in mono-energy testing. Obviously, there is then a risk that the device later shows effects not observed in the testing. Up to now, the discussion has focused on commercial testing. Another advantage of mono-energy beams is their usefulness for research. For instance, mono-energy neutron beam results can in some cases be directly compared with proton beam results (which are inherently of mono-energy character), allowing improved insight into the underlying reaction mechanisms.

5 Results and discussion

In the present work, computations with TALYS [3] have been used to calculate energy and angular distributions of all ions created in neutron-induced nuclear reactions on silicon. For reasons described below, not all released reaction products induce upsets. Therefore, a separate post-analysis program has been developed that uses the output from TALYS and converts it to SEE probability, taking only relevant emitted ions into account [4].

In figure 1, the results of the first energy-resolved measurement of neutron-induced single-event upsets (SEU), published in 1998 [5], are presented. Five different memory devices were tested, and it was found that the energy dependence was very similar for all of them, but the absolute sensitivity differed by up to almost an order of magnitude. The oldest components showed lower sensitivity than more recent ones. As can be seen, the sensitivity showed a slow rise from low energy up to about 100 MeV, where it saturated or possibly even decreased.

In figure 2, the results of a recent similar test, published in 2005 [6], are shown, however for one device only. It can be seen that the uncorrected result, i.e., raw data before correction

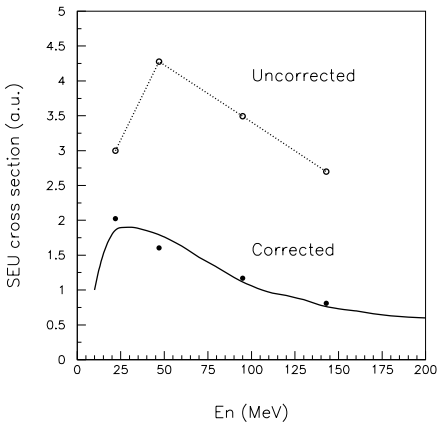

Fig. 2. The SEU cross section for a recent memory devices versus neutron energy, reprinted from ref. [6]. The two data sets are before and after correction for the low-energy tail. The figure is modified by the inclusion of a prediction by the nuclear reaction code TALYS of the cross section. The cross section scale is arbitrary. See the text for details.

for the low-energy neutron tail, partly resembles the results in figure 1, but with a maximum at a much lower energy and a significant decrease of the SEU cross section at high energies. The corrected result, however, shows a steady decrease already from the first datum point at 22 MeV.

All these results can be understood from fundamental nuclear physics point of view. These effects are caused by neutrons that induce nuclear reactions, releasing charge via emitted ions. (The neutron itself makes no effect, neither do emitted gamma rays.) Whether the released ions cause an upset or not primarily depends on the total charge released, that has to be larger than the critical charge of the component, and on the specific energy loss (dE/dx), i.e., the amount of energy transferred to the critical volume per length unit of the ion propagation. The latter is important because even if a large total energy in the form of a specific ion is released, but that particular ion does not deposit sufficient energy in a single bit, no upset will result.

All components shown in figure 1 required a rather large critical charge for a bit flip. This had the consequence that relatively exotic nuclear reactions were primarily responsible for the upsets. The cross section for those reactions has a threshold around 10–20 MeV and it increases slowly with energy up to about 50–150 MeV (depending of ion) after which it begins to decrease. Thus, the dependence in figure 1 is in line with expectations from well-known nuclear physics.

Recent components have a much smaller critical charge, but also smaller dimensions of the critical volume. These two effects go in opposite directions when it comes to sensitivity, but it seems as the leading effect is the former, i.e., modern devices require less specific energy loss to cause an SEU. This opens the possibility that other, more common, reaction channels come into play. The dominating neutron-induced

nuclear reaction is always elastic scattering. In fact, it is a fundamental quantum mechanics property that elastic scattering must constitute at least half the total neutron cross section. In elastic scattering, the neutron is deflected, leaving the nucleus in its ground state, but with a recoil due to the transferred momentum. This recoiling nucleus has a low energy, resulting in a large specific energy loss. Elastic scattering has no energy threshold, so the lowest energy in which it can induce an SEU is primarily determined by the critical charge of the device. As soon as the neutron energy is large enough to cause an upset via the recoils of elastic scattering, this can be expected to be the dominant mechanism, because the cross section is large. In addition, the effect can be expected to peak rather near to the threshold, and then the cross section should slowly decrease with energy.

This is in agreement with the dependence in figure 2. The solid line shows the prediction by TALYS, presuming reasonable dimensions of the critical volume and charge. The line and the data are normalized to each other, i.e., TALYS describes the trends well, but to get the absolute scale right, also unavailable detailed information on device parameters is needed.

6 Future facilities

Until recently, it has been an implicit truth that mono-energy facilities always has a low-energy tail, and that white beams in principle can be made more intense (although at present the leading mono-energy and white facilities actually produce about the same total number of neutrons per second). These presumptions are based on the boundary condition of neutron production on fixed targets. Recently, completely different neutron production techniques have been proposed, in which very intense mono-energy neutron beams can be envisioned.

Two production techniques have been proposed. The first is to use a proton beam of about 1–2 GeV impinging on a combined target and ion source to produce beta-decaying nuclei, which in turn are accelerated and inserted into a storage ring of race-track geometry [8]. Some beta-decaying nuclei emit neutrons immediately after the beta decay[1]. This neutron has a low energy relative to the decaying nucleus. This means that if the nucleus decays in flight, the neutron will be emitted along the direction of motion of the decaying nucleus, with the same velocity. As a consequence, intense mono-energy fluxes will be produced along the straight sections.

It has been estimated that fluxes of 10^{11} n/s could be achieved, compared with 10^6 today, i.e., a factor 100 000 (!) more intense than today. Even if the technique would be a factor 100 less efficient than the design implies, it would still be a factor 1000 more neutrons than presently. Moreover, with such a technique all neutrons would appear in a narrow (few MeV) energy range with no low-energy tail. This concept is a spin-off from a conceptual program at the particle physics laboratory CERN, in which similar techniques would be used to produce intense neutrino fluxes for particle physics and cosmology research. The proposed scheme requires infrastructure of the type only CERN can provide, e.g., several coupled high-energy accelerators. Thus, the realization of this technique depends on the realization of the proposed neutrino facility.

A second technique would be to use a similar production as above (1–2 GeV protons on a combined target-ion source) to produce the radioactive nuclide ^{6}He, which in turn would be accelerated to hit a target [9]. Roughly, ^{6}He can be described as an alpha particle with two loosely attached neutrons. When hitting a target, the two neutrons are dissociated with a large probability, and continue along the direction of the incident beam with the incident velocity. The charged particles (the remaining ^{6}He and residual ^{4}He) is bent by a magnet system and a clean neutron beam is produced. This latter technique does not have the potential to produce as intensive fluxes as the beta-decay in flight, but on the other hand it requires much less advanced accelerators. This technique could possibly be installed at existing CERN facilities after some upgrades. Initial estimates indicate a factor a hundred to a thousand larger neutron fluxes than for present facilities to be within reach.

[1] This effect is of major importance for the stability of nuclear power reactors

This work was financially supported by the Swedish Nuclear Fuel and Waste Management Company, the Swedish Nuclear Power Inspectorate, Ringhals AB, Barsebäck Power AB, Forsmark Power AB, the Swedish Defense Research Agency, the Swedish Natural Science Research Council, the Swedish Nuclear Safety and Training Centre, and the European Union.

References

1. J.F. Ziegler and H. Puchner, SER – History, Trends and Challenges, Cypress (2004).
2. K. Johansson, M. Ohlsson, N. Olsson, J. Blomgren, and P.-U. Renberg, IEEE Trans. Nucl. Sci. **46** (1999) 1427.
3. A.J. Koning, S. Hilaire, and M.C. Duijvestijn, AIP Conf. Proc. **769** (2005) 154.
4. J.-C. Bourselier, Uppsala University Neutron Physics report 05/07 (2005).
5. K. Johansson, P. Dyreklev, B. Granbom, N. Olsson, J. Blomgren, and P.-U. Renberg, IEEE Trans. Nucl. Sci. **45** (1998) 2519.
6. M. Olmos, A.V. Prokofiev, and R. Gaillard, 2005 IEEE International Reliability Physics Symposium Proceedings, 43rd Annual, San Jose, California, April 17-21, 2005, pp. 696-697.
7. M.B. Chadwick, H.H. Barschall, R.S. Caswell, P.M. DeLuca, Jr., G.M. Hale, D.T.L. Jones, R.E. MacFarlane, J.P. Meulders, H. Schuhmacher, U.J. Schrewe, A. Wambersie, and P.G. Young, Med. Phys. **26** (1999) 974; and ICRU Report **63** (International Commission on Radiation Units and Measurements, Bethseda, MD, 2000).
8. CERN beta beam project, http://beta-beam.web.cern.ch/beta-beam/
9. I. Tanihata and M. Lindroos, private communication.